Modeling MPN Pathogenesis and the IFNα Signaling Pathway in Murine Bone Marrow Cells and Patient Derived iPS Cells

Von der Fakultät für Mathematik, Informatik und Naturwissenschaften der RWTH Aachen University zur Erlangung des akademischen Grades einer Doktorin der Naturwissenschaften genehmigte Dissertation

vorgelegt von

M.Sc. Caroline Küstermann

Aus Halle/Saale

Berichter: Prof. Dr. rer nat Martin Zenke

Prof. Dr. med Steffen Koschmieder

Prof. Dr. rer nat Geraldine Zimmer-Bensch

Tag der mündlichen Prüfung: 05.09.2019

Diese Dissertation ist auf den Internetseiten der Universitätsbibliothek verfügbar

Table of Contents

Table of Contents

Zusammenfassung

Myeloproliferative Neoplasien (MPN) sind klonale Stammzellerkrankungen, die, wenn sie nicht behandelt werden, ein Versagen des hämatopoetischen Systems zur Folge haben. Ein Durchbruch in der MPN-Forschung war die Identifizierung von Treibermutationen, wie zum Beispiel BcrAbl in der chronisch myeloischen Leukämie (CML) und JAK2V617F in Polycythemia vera (PV). Ein weiterer Durchbruch, diesmal in der MPN-Behandlung, war die Entwicklung von Tyrosinkinase-Inhibitoren (TKI). Jedoch verursachte das Absetzen der TKI-Behandlung häufig ein Wiederauftreten der Leukämie, da die Leukämie induzierenden Stammzellen durch die TKI-Behandlung nicht beseitigt wurden. Interferonα (IFNα) wurde verwendet, bevor die TKI-Behandlung die First-In-Line-Therapie war. Studien an PV-Patienten zeigten eine Verringerung der JAK2V617F-Allelbelastung aufgrund der IFNα-Therapie. Der Signalweg im malignen Klon ist jedoch noch nicht gut verstanden. Im Gegensatz zu TKI zeigte die IFNα-Behandlung nach Absetzen der Therapie längere Remissionsphasen. Die Behandlung mit IFNα bei CML-Patienten zeigte jedoch schlechte Ergebnisse, während PV-Patienten sofort ansprachen. Untersuchungen an Knock-out-Mäusen und induzierten pluripotenten Stammzellen (iPSC) zeigten, dass der Interferon regulatorische Faktor 8 (IRF8) in CML herunterreguliert wird. Darüber hinaus wird davon ausgegangen, dass niedrige IRF8-Transkripte eine schlechte Prognose für die IFNα-Behandlung in der CML darstellen.

Zunächst untersuchte ich den Einfluss von IRF8 auf die Pathogenese von CML und PV. Außerdem untersuchte ich den IFNα-Signalweg in PV und CML in Bezug auf IRF8 Expression. Zu diesem Zweck isolierte ich IRF8$^{+/+}$ und IRF8$^{-/-}$ Knochenmarkszellen (BM) aus Mäusen und transduzierte diese Zellen mit BcrAbl oder JAK2V617F-Retroviren. Ich habe BcrAbl$^+$ Zellen als Einzeltherapie *in vitro* mit Imatinib oder IFNα behandelt. Analysen per Durchflusszytometrie zeigten, dass BcrAbl$^+$ Zellen unabhängig von Wachstumsfaktoren sind. Darüber hinaus zeigen IRF8$^{-/-}$ BcrAbl$^+$ Zellen eine höhere Expansion und reagieren nicht auf die Imatinib-Behandlung. Überraschenderweise war der IFNα-Effekt IRF8 unabhängig, da das

Wachstum von BcrAbl$^+$ Zellen sowohl in IRF8$^{+/+}$ als auch in IRF8$^{-/-}$ BM Zellen gehemmt wurde. BM Zellen, die mit JAK2V617F transduziert wurden, zeigten keine ausreichend hohe Transduktionseffizienz, um den IFNα Signalweg in diesem Zellsystem weiter zu untersuchen. Aus diesem Grund habe ich für spätere Experimente iPSC eingesetzt.

Zur Untersuchung des IFNα Signalweges generierte ich JAK2V617F und JAK2 iPSC-Klone aus PBMNC von 3 PV Patienten und differenzierte diese in hämatopoetische Zellen. Während der hämatopoetischen Differenzierung von JAK2V617F und JAK2 iPSC-Klonen beobachtete ich einen Anstieg der CD34$^+$ und CD235a$^+$ Zellpopulation in JAK2V617F$^+$ Zellen. Bei einer gerichteten Differenzierung mit Erythropoetin (EPO) konnte ich einen Anstieg der CD235a$^+$ roten Blutkörperchen nachweisen und so die klinischen Merkmale des PV-Phänotyps *in vitro* modellieren. Um den IFNα-Signalweg aufzuklären, verifizierte ich zunächst, dass IFNAR1, IFNAR2, IRF7, IRF9 und STAT1 in iPSC abstammenden hämatopoetischen Zellen exprimiert wurden. In Genexpressionsanalysen wurde jedoch keine Hochregulierung von IFNα-Zielgenen wie IRF7 oder IRF9 beobachtet. Darüber hinaus schien die IFNAR1-Präsentation auf der Oberfläche von iPSC abstammenden hämatopoetischen Suspensionszellen zu fehlen. Bemerkenswerterweise zeigten Zellen aus der EB-Schicht einen höheren Prozentsatz an IFNAR1$^+$ Zellen. Western Blot Analysen zeigten niedrige STAT1-Proteinspiegel. Zudem zeigten alle von iPSC abstammenden hämatopoetischen Zellen niedrige pSTAT1-Proteinspiegel nach IFNα Stimulation.

Abstract

Myeloproliferative neoplasms (MPN) are clonal stem cell disorders and when left unchecked cause failure of the hematopoietic system. A breakthrough in MPN research was the identification of driver mutations, such as BcrAbl for chronic myeloid leukemia (CML) and JAK2V617F for polycythemia vera (PV). Another breakthrough, this time in MPN treatment was the development of tyrosine kinase inhibitors (TKI). However, discontinuation of TKI treatment often caused relapses as leukemic stem cells were not eradicated by TKI treatment. Interferon α (IFNα) was used before TKI treatment was first-in-line therapy. Studies in PV patients showed a reduction of JAK2V617F allele burden due to IFNα therapy. Yet, the signaling pathway in the malignant clone is still not well understood. In contrast to TKI, IFNα treatment showed longer phases of remission after discontinuing therapy. However, IFNα treatment in CML patients showed poor outcomes while PV patients show immediate responses. Research in knock out mice and induced pluripotent stem cells (iPSC) showed that the interferon regulator factor 8 (IRF8) is downregulated in CML. Moreover, low IRF8 transcripts are thought to be a poor prognosis for IFNα treatment in CML.

First, I investigated the influence of IRF8 on the pathogenesis of CML and PV. Furthermore, I studied the IFNα signaling pathway in PV and CML in relation to the presence of IRF8. To this end, I isolated murine IRF8$^{+/+}$ and IRF8$^{-/-}$ bone marrow cells and transduced these cells with BcrAbl or JAK2V617F retrovirus. I treated BcrAbl^{+} cells with Imatinib or IFNα as single therapy *in vitro*. Flow cytometry analyses showed that BcrAbl^{+} cells are independent of growth factors. Additionally, IRF8$^{-/-}$ BcrAbl^{+} cells show a higher expansion and are unresponsive to Imatinib treatment. Surprisingly, IFNα effect was independent of IRF8 as BcrAbl^{+} cell growth was inhibited in both IRF8$^{+/+}$ and IRF8$^{-/-}$ BM cells. JAK2V617F transduced BM cells did not show a high transduction efficiency to continue to investigate the IFNα signaling pathway. Therefore, I switched to patient derived iPSC.

Second, to investigate the IFNα signaling pathway I generated JAK2V617F and JAK2 iPSC clones from PBMNC of 3 PV patients and differentiated them into hematopoietic cells. During hematopoietic differentiation of JAK2V617F and JAK2 iPSC clones I observed an increase of the percentage of CD34$^+$ and CD235a$^+$ cell populations for JAK2V617F$^+$ cells. In a directed red blood cell differentiation I was able to model the clinical features of the PV phenotype *in vitro* with an increase in the CD235a$^+$ red blood cells. To elucidate the IFNα signaling pathway I verified that IFNAR1, IFNAR2, IRF7, IRF9 and STAT1 are expressed in iPSC-derived hematopoietic cells. However, upregulation of IFNα target genes, such as IRF7 or IRF9 was not seen in gene expression analyses. Moreover, IFNAR1 expression on the surface of iPSC-derived hematopoietic suspension cells seemed to lack. Notably, cells from the EB layer showed a higher percentage of IFNAR1 expression. Western Blot showed low total STAT1 protein levels and following activation low pSTAT1 protein levels in all iPSC-derived hematopoietic cells

1 Introduction

1.1 Hematopoiesis

Hematopoiesis is the process in which all cells from the blood are formed throughout embryonic development and adult life. Most studies on hematopoiesis were done in mouse or zebrafish models, especially as ethical concerns limit the study of human embryonic hematopoiesis (Schmitt et al. (2014), Hsia and Zon (2005)). Hence, the mouse hematopoietic system is probably the best characterized system and often serves as a model systems for other vertebrate organisms or used in disease studies (Kohnken et al., 2017). Results on mouse systems, especially surface marker expression of hematopoietic stem and progenitor cells are now the basis of studies in human hematopoiesis and there are efforts to apply surface markers found in mice to the human system (Challen et al., 2009). In recent years the discovery of embryonic stem cells (ESC) and induced pluripotent stem cells (iPSC) has helped to capture part of the human hematopoietic development (Zambidis et al. (2005), Kennedy et al. (1997), Slukvin (2016), Lacaud and Kouskoff (2017)). All studies are aimed at identifying the most primitive cell in the hematopoietic system which might be the breakthrough for clinical applications, like stem cell transplantation (Ng and Alexander, 2017). Another aim is to study where the disease causing mutations occurs in the hierarchical hematopoietic tree. Consequently, clinicians have a cell target for analyzing whether the disease is cured or not.

1.1.1 Anatomical origin of hematopoietic stem cells (HSC)

From the onset of fetal development hematopoiesis is restricted in time and place (Palis et al. (2001), Lacaud and Kouskoff (2017)). First, the vascular development needs to take place followed by the actual hematopoietic system. The earliest hematopoietic cells that can be seen are in the yolk sac (Figure 1). The yolk sac is

an extraembryonic tissue and consists of a double layer of mesodermal and endodermal cells. The endoderm is part of the epithelium and adopts liver and intestine functions. In the mesodermal layer the first visible blood cells are observed at embryonic day 7.0 (E7.0) for the mouse system and in the first 3 weeks after gestation in the human system (Ditadi et al., 2017). The mesodermal layer forms primitive nucleated erythroblasts. They are distinguished by their retention of their nucleus, their larger size and their expression of ε-globin (Ditadi et al., 2017). The primary function of these cells is the support of oxygen transport to the tissue as this undergoes rapid growth and differentiation (Jagannathan-Bogdan and Zon, 2013). Furthermore, it was shown that these cells occur in blood islands (Palis et al. (2001), Lacaud and Kouskoff (2017)). In addition to primitive erythroblasts the yolk sac forms primitive megakaryocytes and macrophages (Tober et al. (2007), Ditadi et al. (2017)). All 3 cell types belong to the primitive hematopoiesis. Studies have shown that cells from the primitive hematopoiesis are derived from the hemangioblast whose existence has been suggested *in vitro* (Kennedy et al. (1997), Medvinsky et al. (1993)). The existence of the hemangioblast *in vivo* still needs to be verified, especially for higher vertebras (Lacaud and Kouskoff, 2017). The *in vitro* model suggests that the hemangioblast gives also rise to the vascular structure, thus is made out of bi-potent progenitor cells. The hemangioblast was characterized through the expression of Brachyury and KDR by Huber et al. (2004). However, the presence of these cells is transient and brief within the York sac. Afterwards, it rapidly differentiates and expands into hematopoietic and vascular progenitors. On E8.25 another wave of hematopoiesis is derived in the yolk sac. Erythro-myeloid progenitors (EMP) emerge from the endothelial cells of the yolk sac which give rise to definitive erythrocytes and most myeloid lineages (McGrath et al., 2015).

The intra-embryonic hematopoiesis has the most important role in establishing the hematopoietic system. Models provided clues of the existence of hemogenic endothelial (HE) cells which give rise to multipotent hematopoietic stem cells (HSC) that reside in the dorsal aorta. The main region in which definitive HSC are produced

is the endothelium of the aorta-gonad-mesonephros (AGM) region of the developing embryo around E8.25 in the mouse system (Figure 1, Swiers et al. (2013), Zovein et al. (2008), Eilken et al. (2009)). HSC that develop in the human AGM region are seen from day 27 to day 40 of development (Ditadi et al., 2017). Long-term adult repopulating HSC that can give rise to all blood cell lineage can only be found from E10.5 onwards in the mouse system. Then HSC emerge from the dorsal aorta, the vitelline, and umbilical arteries (Lacaud and Kouskoff, 2017).

Embryonic stage			
	E7	E8.25	E9	E10.5
Wave 1	Primitive erythroid progenitors macrophages megakaryocytes	Primitive erythroid progenitors macrophages megakaryocytes	Primitive macrophages	Primitive macrophages
Wave 2		EMPs	EMPs B lymphoid cells T lymphoid cells	EMPs (yolk sac) B lymphoid cells (AGM, yolk sac) T lymphoid cells (AGM, yolk sac)
Wave 3				Hematopoietic stem cells (AGM)

Figure 1. Anatomical origin of hematopoiesis in the mouse system

Hematopoiesis in the mouse environment is shown. Hematopoiesis occurs in 3 waves. The first wave emerges on embryonic day 7.0 in the yolk sac of the mouse embryo. In the yolk sac primitive nucleate erythroblasts, macrophages and megakaryocytes are formed. The second wave of hematopoietic cells is marked by the emergence of erythroid-myeloid progenitors (EMP) from the endothelial cells of the yolk sac. Additionally, definitive hematopoiesis takes place in the AGM region on E9 of the mouse embryo. T and B cells emerge from hemogenic endothelial cells in the AMG region. The third wave continues on E10.5 where B and T cells simultaneously emerge with EMP from the AGM and the yolk sac. Hematopoietic stem cells (HSC) are produced

in the umbilical cord and the placenta. HSC from all sides will migrate towards the fetal liver and eventually towards the bone marrow where they establish the hematopoietic system during adult life (taken from Yoder (2014)).

Multiple studies have demonstrated that hematopoietic stem and progenitor cells (HSPC) emerge from HE cells through endothelial-hematopoietic transition (EHT) (Rafii et al., 2013). These studies have shown that cells undergoing EHT are CD45$^+$ KDR$^-$ (Jaffredo et al., 1998). During EHT multipotent progenitors bud off of HE cells (Eilken et al. (2009), Swiers et al. (2013)). However, HE cells are still transient during development. EHT occurs in a specific window of time of embryonic development. Cells that have emerged from HE cells move to the fetal liver, and then to the adult bone marrow later on (Zovein et al., 2008). In recent years, studies by Beaudin et al. (2016) showed the existence of developmental restricted HSC (drHSC) that occur right before birth and until postnatal day 14 and have self-renewal potential in transplantation assays and produce B and T cells. However, these drHSC fail to continue their existence into adult life. They are thought to provide the first line of defense against pathogens to the developing organism (Beaudin et al. (2016), Waas and Maillard (2017)).

1.1.2 HSC hierarchy

Studies suggested that the hematopoietic system is organized in a hierarchical structure. Flow cytometry with the help of mouse models and functional assays like transplantation and colony forming assays helped in identifying each blood cell population. Functional and genetic assays helped to identify their potential and their biology. Consequently, a schematic overview of the hematopoietic hierarchy for mouse and human was developed (Figure 2).
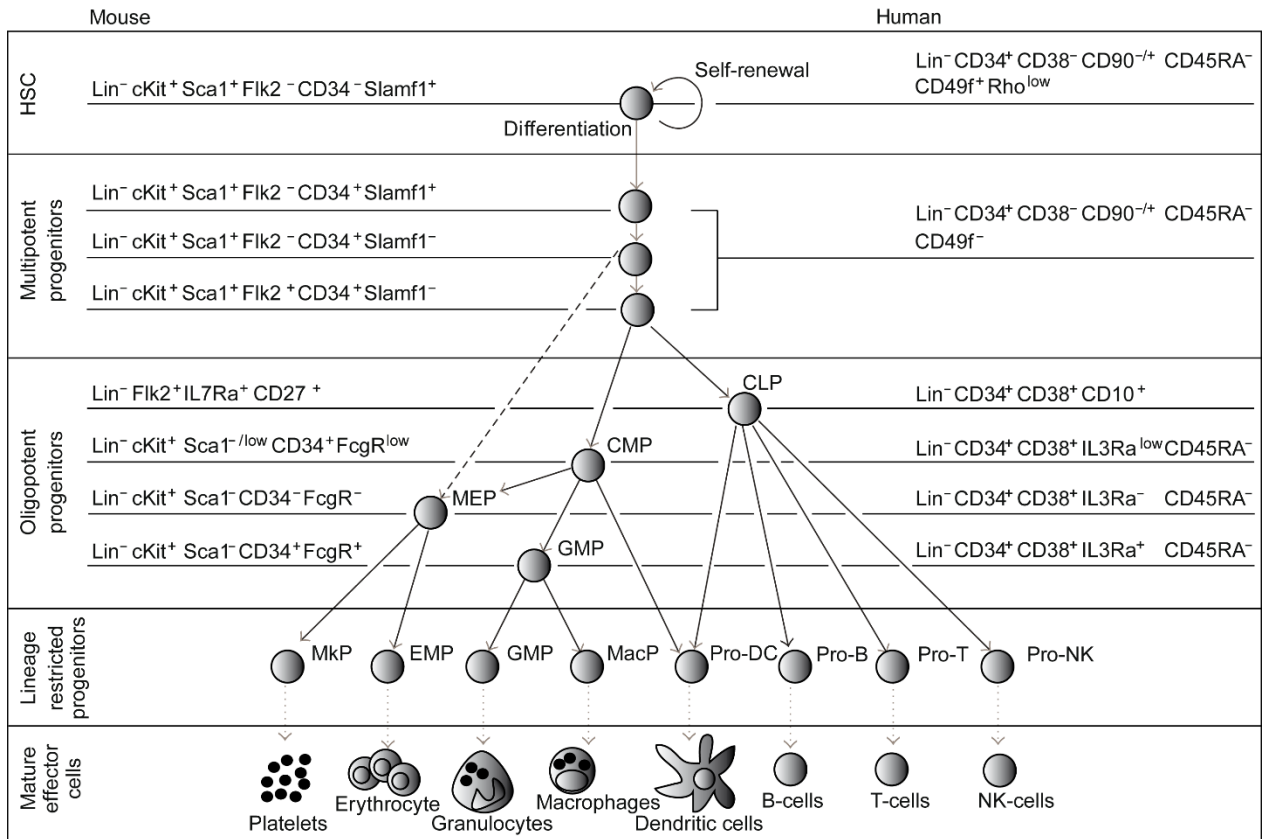
Figure 2. HSC hierarchy for human and mouse

Hierarchy of the mouse and human hematopoietic system is shown. Phenotypic surface markers for each cell population are shown on the sides. CLP, common lymphoid progenitor; CMP, common myeloid progenitor; DC, dendritic cell; EP, erythrocyte progenitor; GMP, granulocyte/macrophage progenitor; GP, granulocyte progenitor; HSC, hematopoietic stem cell; MacP, macrophage progenitor; MEP, megakaryocyte/erythrocyte progenitor; MkP, megakaryocyte progenitor; NK, natural killer; Lin, lineage markers (taken from Chotinantakul and Leeanansaksiri (2012)).

It was suggested that the origin of all hematopoietic cells are a pool of hematopoietic stem cells (HSC) which have self-renewal capacity and give rise to multipotent progenitors (MPP). These HSC are a rare cell population within the bone marrow and are mostly in their quiescent state, meaning that they do not proliferate. It is suggested that the HSC pool only enters cell cycle when the need for a replenishment of blood cells is required. When entering the cell cycle HSC give rise to multipotent progenitors (MPP). After giving rise to enough MPP it is suggested that HSC re-enter their quiescent state. Thus, the hematopoietic system can be replenished again and not be exhausted prematurely. For the isolation of HSC

CD34 is the most widely used surface marker. However, even with this specific marker the isolated HSC population is still heterogeneous (Chotinantakul and Leeanansaksiri, 2012).

To replenish blood cells MPP lose their self-renewal capacity. They are able to differentiate into all lineages of the blood. MPP give rise to 2 types of oligopotent progenitor cells, (i) the common lymphoid progenitor (CLP) and (ii) the common myeloid progenitor (CMP) which differentiate into their restricted lineages. First, CLP can give rise to all the cells of the lymphoid lineage, such as T, B and NK cells. Notably, CLP can also give rise to dendritic cell (DC) progenitors which are cells belonging to the myeloid lineage. These DC progenitors can further differentiate in to $CD8\alpha^+$ and $CD8\alpha^-$ DC and plasmacytoid DC (pDC). Second, CMP can give rise to the all the cells in the myeloid lineage. Therefore, CMP differentiate in multiple steps where different progenitors branch off into more restricted cells. In the myeloid lineage there are the (i) megakaryocyte/erythroid progenitors (MEP), (ii) granulocyte/macrophage progenitors (GMP) and (iii) DC progenitors. These progenitors differentiate further into megakaryocytes and red blood cells, granulocytes and monocytes/macrophages and DC, respectively (Chotinantakul and Leeanansaksiri (2012), Seita and Weissman (2010)). However, recent studies have suggested that there is a direct shortcut from HSC to megakaryocytic progenitors (Notta et al. (2016), Haas et al. (2018)).

Studies on HSC hierarchy are still undertaken as there are still stet backs with isolating completely pure cell populations. Due to the chosen isolation method like flow cytometry gates for surface markers are chosen subjectively and pre-determined on previous studies. Consequently, transitioning stages cannot be identified easily and are often overlooked. Recent studies challenge the pre-existing model shown in Figure 2. For example, Velten et al. (2017) and Karamitros et al. (2018) suggested that the HSPC compartment (Lin⁻ $CD34^+$ $CD38^-$ cells) gradually

acquire a lineage committed transcriptional program and do not jump from one multipotent cell type to another more restricted cell type. Only in the Lin⁻ CD34⁺ CD38⁺ cells Velten et al. (2017) were able to distinguish defined cell populations.

1.2 Interferon Regulatory Factor 8 (IRF8) in hematopoiesis

The Interferon regulatory factor 8 (IRF8) was originally named as interferon consensus sequence-binding protein (ICSBP) and was clone first in 1990 as IFNγ inducible nuclear protein (Driggers et al., 1990). IRF8 belongs to the family of Interferon regulatory factors (IRF) and acts as a homodimer as a transcription factor that has activating and repressing functions. Binding partners of IRF8 are PU.1, Id2 or Baft3 during DC differentiation, and Krüppel-like factor 4 (KLF4) in monocyte differentiation (Kanno et al., 2005). Furthermore, IRF8 acts with other IRF transcription factors like IRF1 and IRF2 to repress target genes of IFN-stimulated response elements (ISRE). It was shown that the amino acid structure of IRF8 genes between mice and human are highly conserved (Tamura et al. (2015), Yáñez and Goodridge (2016)).

With the discovery of IRF8 as a transcription factor in 1990 experiments with knock-out mice followed (Holtschke et al., 1996). These experiments established a role of IRF8 in hematopoietic differentiation (Iwasaki and Akashi (2007), Geissmann et al. (2010)). Studies found that IRF8 expression is absent in early HSC, multipotent progenitors and LMPP (Figure 3, Tamura et al. (2015), Lee et al. (2017)). When lineage restriction is established in GMP and CDP a graded expression of IRF8 was detected (Wang et al., 2014a). It was shown that IRF8 is essential for the development of pDC, CD8α⁺ and CD103⁺ cDC (Tsujimura et al. (2003), Edelson et al. (2010)). pDC are the major producers of type I IFN upon infection. CD8α⁺ and CD103⁺ cDC induced a cytotoxic T cell response via cross-presentation and produce IL12 to promote cellular immunity. Consequently, the lack of IRF8 results in the loss

of these cell populations and in an immunodeficiency (Hambleton et al., 2011). In other lineage tracing experiments it was shown that IRF8 is essential for the development of monocytes (Sichien et al., 2016). In IRF8$^{-/-}$ mice Ly6C$^+$ inflammatory monocytes lack completely while Ly6C$^-$ monocytes show reduced numbers (Kurotaki et al., 2013).
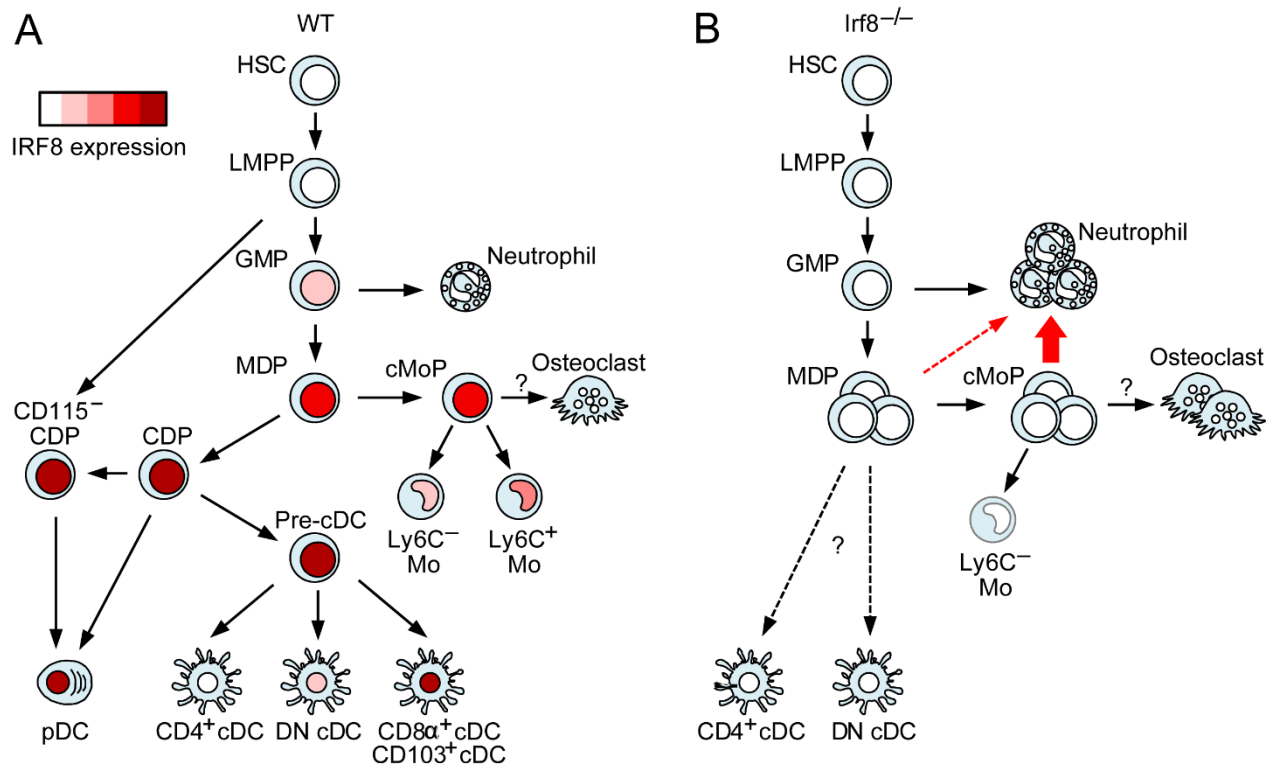
Figure 3. Expression of IRF8 during myeloid development

(A) IRF8 is not expressed in HSC and LMPP. IRF8 expression is upregulated in the differentiation for the first committed myeloid progenitors, GMP and CDP. However, terminal granulocyte differentiation is not dependent on IRF8 expression. In contrast, DC development, especially pDC, CD8α$^+$ and CD103$^+$ cDC depend on IRF8 expression. Monocyte differentiation has moderate IRF8 levels. (B) Lack of IRF8 results in loss of pDC, CD8α$^+$ and CD103$^+$ cDC differentiation. Moreover, IRF8$^{-/-}$ mice accumulate monocyte progenitors (MDP and cMoP) and show an overproduction of granulocytes. This is reminiscent to human CML. DN, double negative; cDC, classical dendritic cells; pDC, plasmacytoid dendritic cells; HSC, hematopoietic stem cells; Mo, monocytes; cMoP, common monocyte progenitors (taken and abbreviated from Tamura et al. (2015)).

As mentioned previously IRF8 also acts as repressor in certain cell types, such as neutrophils. This was stressed in experiments in IRF8$^{-/-}$ mice. As IRF8 is essential for monocyte differentiation IRF8$^{-/-}$ mice fail at terminal monocyte differentiation and

in turn accumulate MDP and common monocytes progenitors (cMoP). In the absence of IRF8 MDP and cMoP are able to differentiate into neutrophils as C/EBPα is no longer repressed by IRF8 resulting in overproduction of neutrophils in IRF8$^{-/-}$ mice (Kurotaki et al., 2014). This phenotype is reminiscent of patients suffering from CML and one patient with a homozygous mutation in IRF8 resulting in the loss of the IRF8 protein.

1.3 Myeloproliferative neoplasms (MPN)

Myeloproliferative neoplasms (MPN) are clonal stem cell diseases and are now characterized by the increased proliferation of erythrocytes, megakaryocytes or granulocytes and their progenitors. William Dameshek first introduced the term "myeloproliferative disorders" (MDP) in 1951 as he recognized the similarities in clinical patterns in different human blood diseases (Dameshek, 1951). He hypothesized that these diseases were caused by the proliferation of bone marrow cells *en mass* due to an unknown stimuli. However, during that time only chronic myeloid leukemia (CML), polycythemia vera (PV), essential thrombocythemia (ET) and primary myelofibrosis (PMF) were listed under the term of MDP.

The first attempt to establish a streamlined classification system of hematologic malignancies was done by the world health organization (WHO) in 2001. Since then this system is revised and refined due to new molecular findings in research and pathological findings in clinics. The current classification system was established in 2008 (Figure 4) as a new mutation in the Janus kinase 2 (JAK2) differentiated PV, ET and PMF from the BcrAbl$^+$ CML (Vannucchi et al., 2009). Furthermore, in 2008 the WHO changed the term of MDP to MPN to classify CML, PV, ET and PMF. Additionally, due to advances in understanding the molecular mechanisms underlying hematopoietic malignancies the WHO expanded the term of myeloid malignancies to include other forms of malignancies that have their origin due to a mutation in the hematopoietic stem cell pool. Malignancies like mastocytosis, acute myeloid leukemia (AML), chronic neutrophilic leukemia and chronic eosinophilic

leukemia were included in the current classification system, too (Tefferi and Vainchenker, 2011).

In 2016 the WHO updated the classification of myeloid malignancies again based on new revelations in recent research of biomarkers, results from next generation sequencing (NGS) approaches and gene expression analyses (Arber et al., 2016). However, the disease groups defined in 2008 stayed the same.
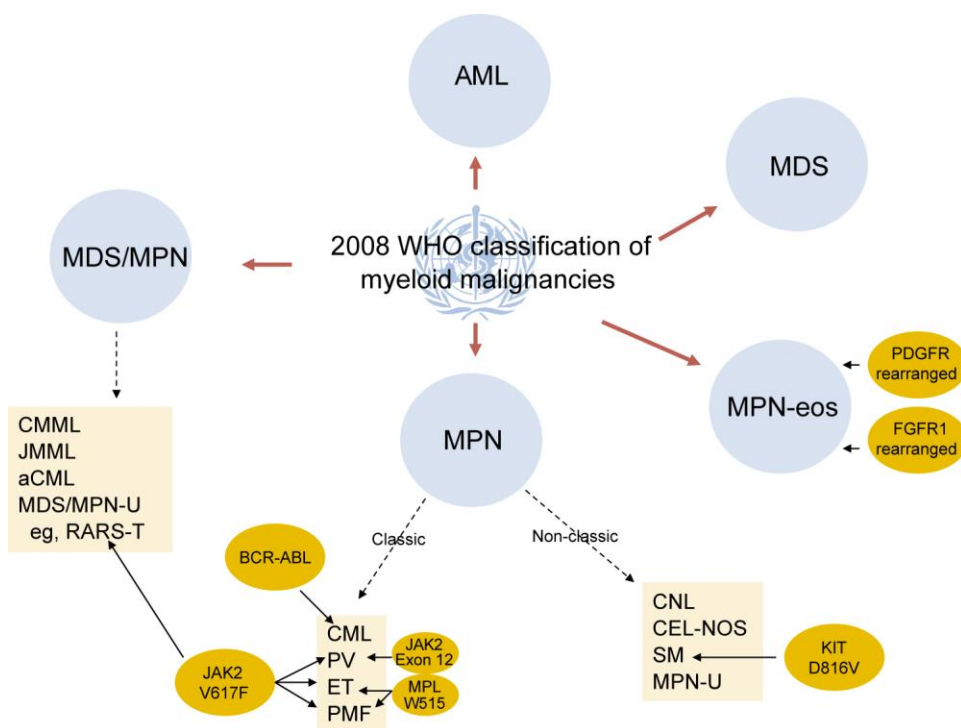
Figure 4. WHO classification of myeloid malignancies from 2008

The MPN category is split into classical and non-classical MPN. The classical MPN are chronic myeloid leukemia (CML) which is characterized by the occurrence of BcrAbl. The other 3 classical MPN are the JAK2V617F$^+$ forms of polycythemia vera (PV), essential thrombocythemia (ET) and primary myelofibrosis (PMF). In the non-classical MPN category are diseases like systemic mastocytosis (SM) which is characterized by the KITD816V mutation. MPN – myeloproliferative neoplasms; MDS – myelodysplastic syndromes; AML - acute myeloid leukemia; CMML – chronic myelomonocytic leukemia; JMML - juvenile myelomonocytic leukemia; CNL - chronic neutrophilic leukemia; CEL-NOS – chronic eosinophilic leukemia–not otherwise specified; MPN-U – MPN unclassifiable; PDGFR - platelet-derived growth factor receptor; FGFR1 - fibroblast growth factor receptor (taken from Tefferi and Vainchenker (2011)).

1.3.1 Chronic Myeloid Leukemia (CML)

To this day CML is the best studied form of MPN. The clinical features of CML were first described in 1845, as the cause for the splenomegaly could not be attributed to the predominant tuberculosis at that time. The underlying molecular cause was then identified in 1960 and termed by Nowell and Hungerford as the Philadelphia chromosome. Later, it was shown that the Philadelphia chromosome resulted from a translocation involving chromosome 9 and 22. The discovery of the fusion gene BcrAbl that is encoded on the Philadelphia chromosome is now believed to be the cause of CML (Goldman and Melo, 2003). CML has 3 phases: chronic phase (CP), accelerated phase (AP) and blast phase (BP). It was found that the aggressiveness and the disease progression rate is dependent on the expression level of BcrAbl as low level expression lead to a leukemia only after a long latency (Barnes et al., 2005).

Nowadays, CML is classified as a one of the classical MPN according to the 2008 WHO classification of hematological malignancies (Figure 4, Vannucchi et al. (2009)). It is believed that a multipotent progenitor acquired the BcrAbl mutation and gives rise to BcrAbl$^+$ progeny. BcrAbl in turn gives that progenitor and its progeny a proliferative advantage over normal hematopoiesis. In the accelerated phase BcrAbl blocks differentiation confers an expansion of peripheral blood cells, primarily the granulocytic cell lineage and an increase in spleen size (Ren, 2005).

1.3.1.1 The Philadelphia Chromosome (BcrAbl) as molecular basis of CML

The classic BcrAbl fusion gene stems from the ABL kinase on chromosome 9 and the BCR gene on chromosome 22 (Figure 5). ABL and BCR are expressed in all cell types. The physiological functions of the ABL kinase are complex. It is thought to be involved in the regulation of the cell cycle, the genotoxic stress response and the transmission of the microenvironment via the integrin pathway. However, these

studies were only performed in fibroblasts and studies that aimed at the role of ABL in hematopoietic cells in mouse models failed to deliver a conclusive model (Deininger et al., 2000). The BCR signaling protein contains several structural motifs. However, the true biological function of the BCR protein has not been discovered. Only a single study showed that neutrophils from BCR$^{-/-}$ mice produced an increased amount of oxygen metabolites (Ren, 2005).
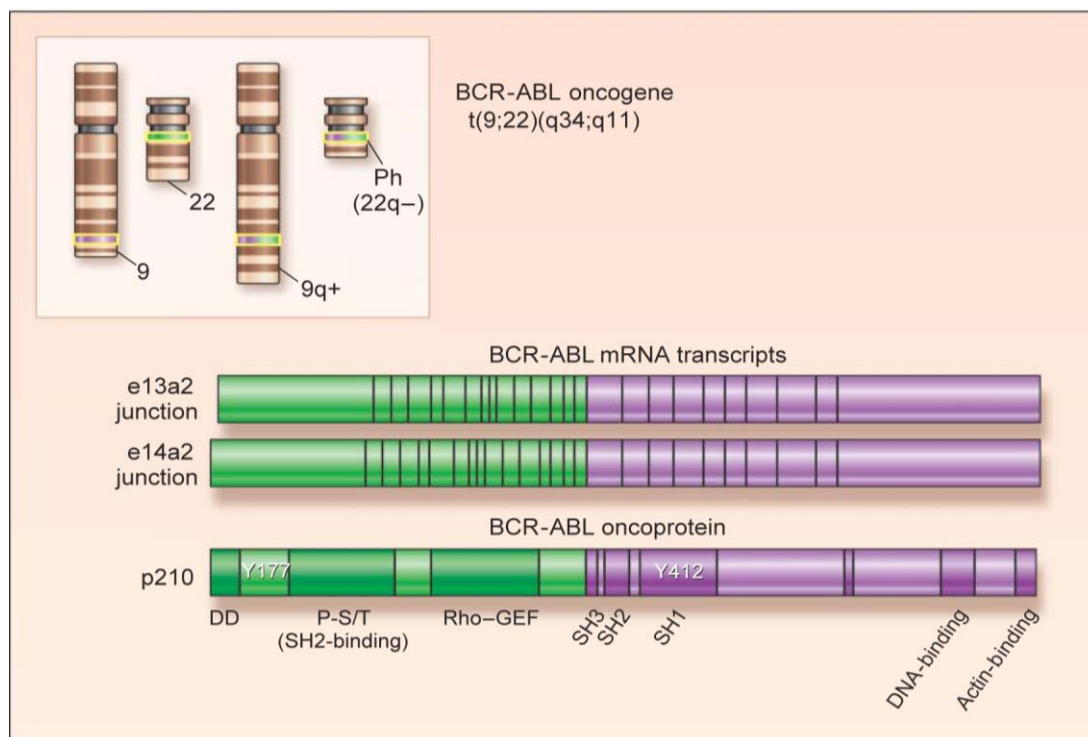
Figure 5. Scheme of the BcrAbl protein

The BcrAbl oncogene is a fusion gene of the N terminus of the BCR protein (green) and the C terminus ABL kinase (purple). There are two isoforms of the mRNA, (i) the e13a2 junction and (ii) the e14a2 junction. These junctions contain slightly different versions of where the fusion of BCR and ABL gene happened. The predominant version of the BcrAbl is transcribed into a protein with a size of 210 kDa (taken from Goldman and Melo (2003)).

The break that leads to the formation of the BcrAbl fusion gene occurs in the exon a2 of the ABL kinase and in the breakpoint region in the BCR gene. This is followed by the fusion of the 5' end of BCR to the 3' end of ABL on the chromosome 22. There are 2 types of junctions in the newly formed BcrAbl gene, (i) the e13a2

junction and (ii) the e14a2 junction. This depends on where the break happened in the BCR gene. From one of the junction types the mRNA for BcrAbl is transcribed. Due to the juxtaposition of BCR the ABL kinase is constitutively active. BCR promotes the dimerization of BcrAbl proteins leading to an auto-phosphorylation of BcrAbl. The predominant variant of BcrAbl forms a 210 kDa protein that is essential for the growth and survival of leukemic stem cells (Daley et al., 1990). The resulting signaling of BcrAbl replaces the physiological functions of the ABL kinase as a variety of effector proteins are affected (Goldman and Melo, 2003). The aberrant signaling results in the deregulation of cell proliferation, reduction of apoptosis and the reduction of interaction with the stroma cells of the hematopoietic niche (Goldman and Melo (2003), Diaz-Blanco et al. (2007)).

1.3.1.2 Downstream targets of BcrAbl

BcrAbl has a multitude of downstream signaling targets via tyrosine phosphorylation (Figure 6). One downstream target of BcrAbl is the signal transducer and activator of transcription 5 (STAT5) which is essential for BcrAbl induced CML. It was shown that deletion of one STAT5 allele decreased the formation of the CML phenotype. Moreover, a null mutation of STAT5a/b prevented the formation of CML. However, STAT5a/b$^{-/-}$ mice developed a B cell lymphoblastic leukemia as BcrAbl was still active in the cells showing that BcrAbl acts on more than one signaling pathway (Walz et al., 2012). Moreover, STAT5 signaling seems to be responsible for the anti-apoptotic signaling of BcrAbl. It was shown by de Groot et al. (2000) that BcrAbl activates the anti-apoptotic gene BCL-XL via STAT5 axis.

Another feature of BcrAbl signaling is the downregulation of IRF8 via STAT5 (Waight et al. (2014), Hjort et al. (2016)). CML patients show reduced or absent transcript numbers of IRF8 (Schmidt et al., 1998). Moreover, studies in IRF8$^{-/-}$ mice and IRF8$^{-/-}$ induced pluripotent stem cells (iPSC) showed features of human CML (Holtschke et al. (1996), Sontag et al. (2017a)). These studies showed an increase in the granulocytic lineage and an absence of dendritic cell subsets (Sontag et al., 2017a).

It was further shown that overexpression of IRF8 in BcrAbl^{+} cells reduced BcrAbl induced CML pathogenesis in mice suggesting that IRF8 acts as a tumor suppressor in CML (Hao and Ren, 2000). Another study showed that the tumor suppressor activity of IRF8 is mediated by IRF8 dependent repression of key target genes of BcrAbl, like the anti-apoptotic gene BCL-2 (Neubauer et al., 2004). It was also shown that IFNα treatment upregulated IRF8 gene expression in CML patients (Schmidt et al., 1998). Recent studies by Scheller et al. (2013) and Huang et al. (2010) also established a link between IRF8 and β-catenin, as the latter is activated by BcrAbl.

BcrAbl influences a multitude of signaling pathways (Figure 6). Among these pathways is the WNT/β-catenin pathway. The WNT/β-catenin pathway promotes self-renewal in stem cells and by downregulation of this pathway differentiation is initiated. Usually, by binding to its receptor, WNT ligand induces the inhibition of β-catenin phosphorylation by glycogen synthase kinase 3β (GSK3β) followed by β-catenin translocation into the nucleus and activation of several transcription factors. However, a study by Coluccia et al. (2007) showed that BcrAbl can interact with β-catenin directly and phosphorylate β-catenin in BcrAbl^{+} cells lines and primary CML cells. Furthermore, in a murine mouse model it was shown BcrAbl inhibits GSK3β by activating the PI3K/AKT pathway (Elena et al., 2018). Consequently, β-catenin again accumulates in the cytoplasm and translocates into the nucleus increasing the leukemic burden and promoting the progression to AML. Additionally, Scheller et al. (2013) suggested a model in which IRF8 expression is inhibited by BcrAbl and while BcrAbl enhanced β-catenin stabilization. Consequently, disease progression is promoted.

The second pathway that is deregulated by BcrAbl is the RAS/ERK pathway. BcrAbl is able to phosphorylate itself at the tyrosine residue Y177. The phosphorylation provides docking sides for proteins with an SH2 domain, such as GRB-2. Via a GRB-2/SOS complex the RAS protein is stabilized in its active form and thus promotes the CML phenotype. Moreover, GRB-2 is able to recruit of GAB2 which is phosphorylated and can bind the p85 subunit of phosphoinositide 3-kinase (PI3K).

JUNB, an antagonist of the RAS target JUN, is involved in the negative regulation of cell proliferation. Additionally to IRF8, JUNB was identified as tumor suppressor as JUNB$^{-/-}$ mice develop a CML-like phenotype. Primary CML cells were shown to downregulate JUNB (Ren, 2005).
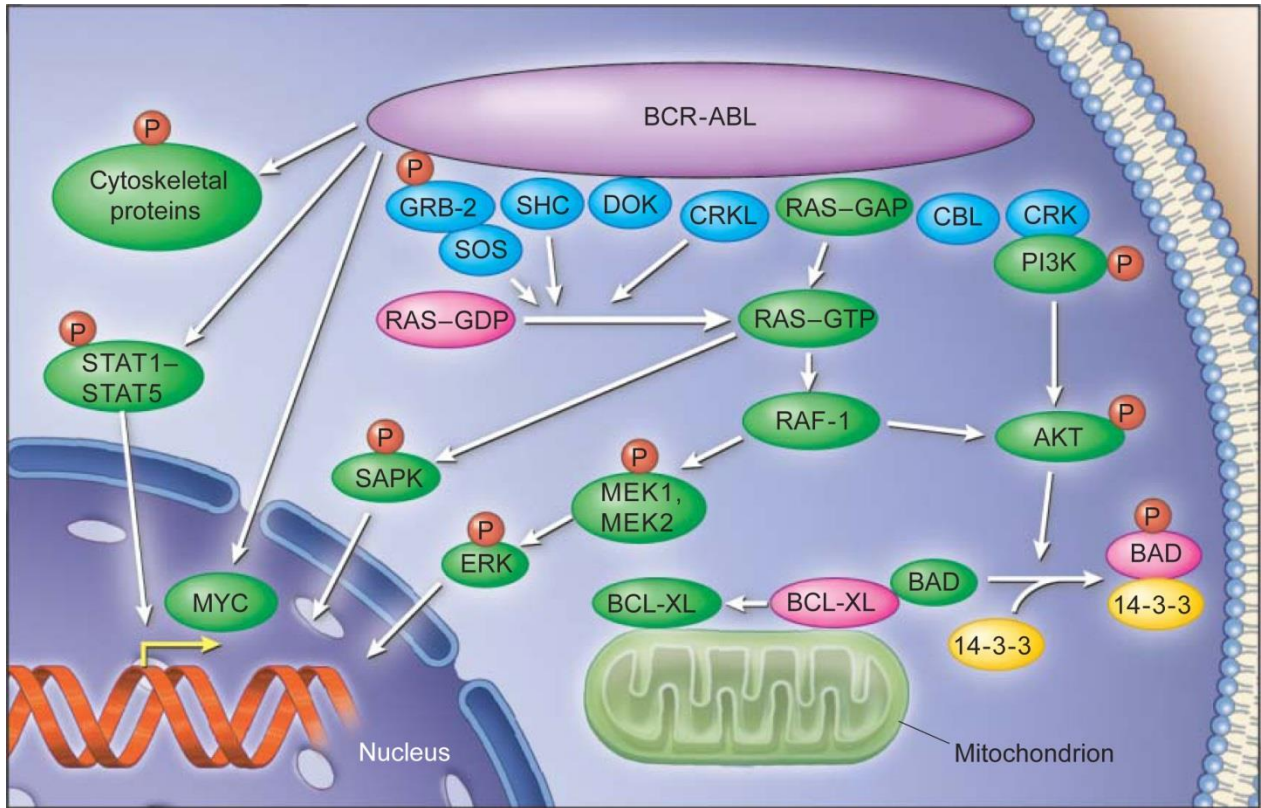
Figure 6. BcrAbl's influence on multiple signaling pathway

BcrAbl affects multiple signaling pathways by interaction and tyrosine phosphorylation of adapter proteins. The most prominent pathways are the mitogen-activated kinase (MAPK) pathway, PI3K pathway and the RAS/MEK pathway. Additionally, BcrAbl phosphorylates STAT proteins, predominantly STAT5, to induce gene expression of anti-apoptotic genes or downregulate tumor suppressor genes (taken from Goldman and Melo (2003)).

It is suggested that the PI3K pathway in BcrAbl$^+$ cells is used to promote proliferation. BcrAbl forms a complex with CRK, CRKL, PI3K and CBL. Consequently, PI3K kinase is activated. The next essential target that is activated in this signaling pathway is the AKT kinase. AKT in turn phosphorylates the pro-apoptotic protein BAD. Consequently, BAD cannot bind to the anti-apoptotic gene BCL-XL anymore and pro-survival signaling is promoted. Interestingly, AKT kinase is used in the physiological IL3 signaling pathway. It seems that BcrAbl mimics this

pathway and consequently conveys an IL3 independence in BcrAbl⁺ cells (Deininger et al., 2000).

1.3.2 Polycythemia Vera (PV)

Polycythemia vera is a clonal stem cell disease affecting elderly people. According to the 2008 WHO classification (Figure 4) PV is classified as classical MPN. Clinically, it is characterized by an expansion of the red blood cell lineage together with high hemoglobin levels, the presence of the JAK2V617F mutation and subnormal levels of serum erythropoietin (EPO) levels. Other features include an enlarged spleen, genetic markers that define clonal hematopoiesis and the formation of endogenous erythroid colonies (EEC) (Tefferi and Barbui, 2017). *In vitro* studies showed that PV CD34⁺ cells develop into erythroid colonies, so called EEC, independent of the presence of EPO via JAK2/STAT5 signaling pathway (Garçon et al., 2006). Other mutations in PV also include a mutation in the exon 12 of JAK2. Yet, this mutation in only found in a minority (about 3%) of PV patients. PV is mostly an indolent disorder with a modest reduction of life span for the patients. This reduction in life span is mostly attributed due to complications associated with the disease, such as thrombotic events, stroke or myocardial infarction, rather than progression to AML (Vannucchi et al. (2009), Tefferi and Barbui (2017)). At diagnosis the first line of treatment are usually low doses of aspirin and phlebolomies to drain the excess of red blood cells and decrease the risk of thrombotic events. Other drug treatments involve hydroxyurea and tyrosine inhibitor (TKI) treatment (chapter 1.4.1). Additionally, in recent years IFNα treatment came into the focus of treating JAK2V617F⁺ MPN again (chapter 1.4.2) (Tefferi and Barbui, 2017).

1.3.2.1 The point mutation V617F in the Janus Kinase 2 (JAK2)

An important progress in the identification of BcrAbl negative MPN was done by the discovery of the JAK2V617F mutation. The JAK2V617F mutation was found in 95% of patients with PV and 60% of patients with ET or PMF in 2005 (Jones et al. (2005), James et al. (2005)). At first it was unknown how a single mutation causes 3 disease phenotypes. Yet, current research hypothesized that the dose of JAK2V617F is linked to the disease phenotype (Campbell et al., 2005). It was shown that cells from PV patients show a predominant JAK2V617F homozygous subclone whereas in ET patients there rather is a dominant JAK2V617F heterozygous subclone present (Godfrey et al. (2012), Jones et al. (2005)). Furthermore, other mutations play into the disease phenotype and progression. Therefore, other insights in research showed that the mutation order had an distinct effect on clinical features and therapy methods (Ortmann et al., 2015).
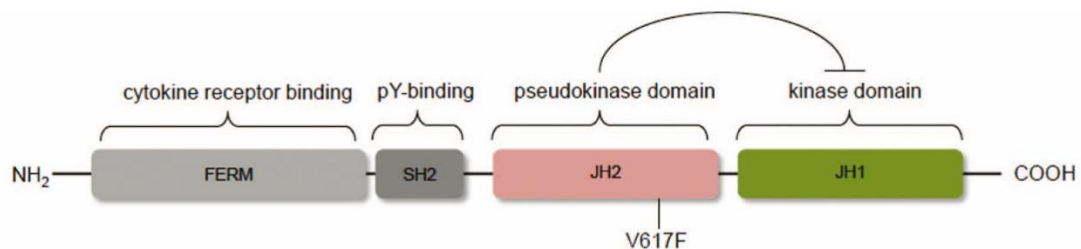
Figure 7. Scheme of JAK2 protein

The JAK2 protein consists of 4 major domains. First, the FERM domain that binds to cytokine receptors, like EPOR and TPOR. Second, the SH2-like domain that provides phospho-tyrosine residues as docking stations for effector molecules that have an SH2-domain. Third, the pseudokinase domain that creates a negative feedback loop to inhibit the kinase domain. Finally, the kinase domain that phosphorylates effector molecules (taken from Chen and Mullally (2014)).

JAK2V617F is a somatically acquired point mutation in the Janus kinase 2 (JAK2). It is a single nucleotide shift from a G to a T which results in a substitution of a valine (V) residue by a phenylalanine (F) residue. The mutation side is situated in the pseudokinase domain of the protein (Figure 7). This domain of JAK2 is postulated to

inhibit the kinase activity of JH1 domain via a negative feedback loop. Yet, due to G to T shift the inhibiting function of pseudokinase domain is disrupted and the kinase domain is constitutively active (Vainchenker and Constantinescu, 2013). Expression of JAK2V617F *in vitro* confers a hypersensitivity to cytokines and IL3 independent growth in hematopoietic cells and cell lines, such as 32D and Ba/F3 cells. Yet, this is most effective when JAK2V617F is co-expressed with the erythropoietin receptor (EPOR) or thrombopoietin receptor (TPOR) (Lu et al. (2005), Levine et al. (2007)). Transplantation of JAK2V617F^{+} cells into mice or mice expressing JAK2V617F in the hematopoietic lineage due to knock-in models show a disease phenotype reminiscent of human PV (Wernig et al. (2008), Lacout et al. (2006)).

1.3.2.2 Downstream signaling of JAK2V617F

JAK2 belongs to the family of Janus kinases and is mostly bound to cytokine receptors lacking an intrinsic kinase activity. These receptors are type I homodimer receptors and are usually for cytokine receptors from the hematopoietic system, like interleukins (IL), colony stimulating factors (CSF), interferon (IFN), erythropoietin (EPO) or thrombopoietin (TPO) (Lu et al. (2005), Vannucchi et al. (2009)). These receptors are usually used in the myeloid lineages therefore, due to coupling of these receptors to JAK2; there is a myeloproliferation when JAK2 is mutated. Usually, JAK2V617F activates STAT proteins, however, the exact STAT proteins that are activated largely depends on the receptor JAK2V617F is coupled to. For example, the EPOR signals via STAT5 while MPL uses STAT1, STAT3 and STAT5.

It was shown that STAT5 is essential for JAK2V617F signaling in MPN as the deletion of STAT5 normalized blood counts and abrogated MPN in mice (Walz et al. (2012)). Another study focused on the relevance of STAT1 in JAK2V617F signaling. It showed that deletion of STAT1 restrained erythropoiesis, yet enhanced thrombocytosis which resulted in an ET like phenotype in mice (Duek et al., 2014). Thus, due to the difference in STAT1 levels different phenotypes can be observed (Chen et al., 2010). STAT3 has a tumor suppressing influence on JAK2V617F[+]

MPN. It was shown that STAT3 deletion slightly reduced red blood cell counts and hematocrit parameters. However, STAT3$^{-/-}$ JAK2V617F^{+} mice showed a significantly increased the neutrophil counts/percentages and markedly reduced the survival of mice expressing JAK2V617F. Thus, deletion of STAT3 increases the severity of MPN induced by JAK2V617F (Yan et al., 2015).

In a receptor model it was hypothesized that, in the absence of a ligand the cytokine receptor is kept in an inactive state in which the JAK proteins are bound together (Figure 8, left) (Chen and Mullally, 2014). The pseudokinase domain of one JAK2 protein interlocks with the kinase domain of the opposing JAK2 protein and vice versa. Hence, the pseudokinase domain exerts its inhibiting function. When a ligand binds to the appropriate cytokine receptor it results in a physical separation and bringing the kinase domains of the JAK2 molecules closer together (Figure 8, center).
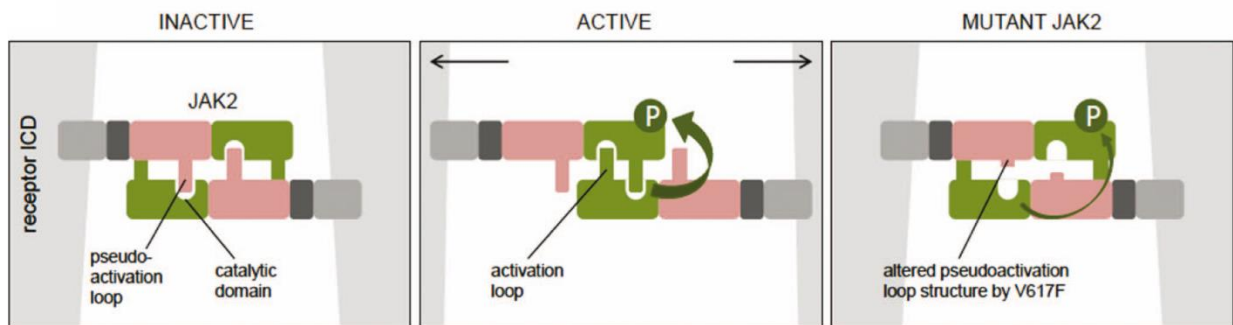
Figure 8. The influence of the V617F mutation of the receptor conformation

A schematic model for the interaction of the different JAK2 domains of a cytokine receptor is shown. Left - In the inactive form the pseudokinase domain and the kinase domain are locked tightly. Center - When a ligand binds to its receptor there is movement of the receptor and in turn brining the kinase domains of the JAK2 dimers together which results in phosphorylation. Right – JAK2V617F alters this model by altering the pseudokinase domain (taken from Chen and Mullally (2014))

In the active conformation of the cytokine receptor there is an activation of the JAK2 kinase by auto-phosphorylation followed by cytokine receptor phosphorylation (Figure 9A). This provides docking stations for effector molecules like STAT proteins. STAT proteins are phosphorylated by JAK kinases and can in turn activate

downstream signaling proteins and multiple signaling pathways like the PI3K or MAPK pathway (Levine et al., 2007). Negative control mechanisms are carried out by SOCS proteins. This mechanism is perturbed by the JAK2V617F mutation which inhibits the interlocking of the pseudokinase domain of one JAK2 molecule with the kinase of the opposing JAK2 molecule (Figure 8, right) and keeps the receptor partially active(Figure 9B) (Skoda, 2010). Therefore, low cytokine concentrations are needed to fully activate the signaling cascade rendering the cells hypersensitive to cytokines. Furthermore, it was shown that JAK2V617F can inhibit SOCS3; hence it can interfere with the negative feedback loop of the JAK/STAT pathway (Hookham et al., 2007).
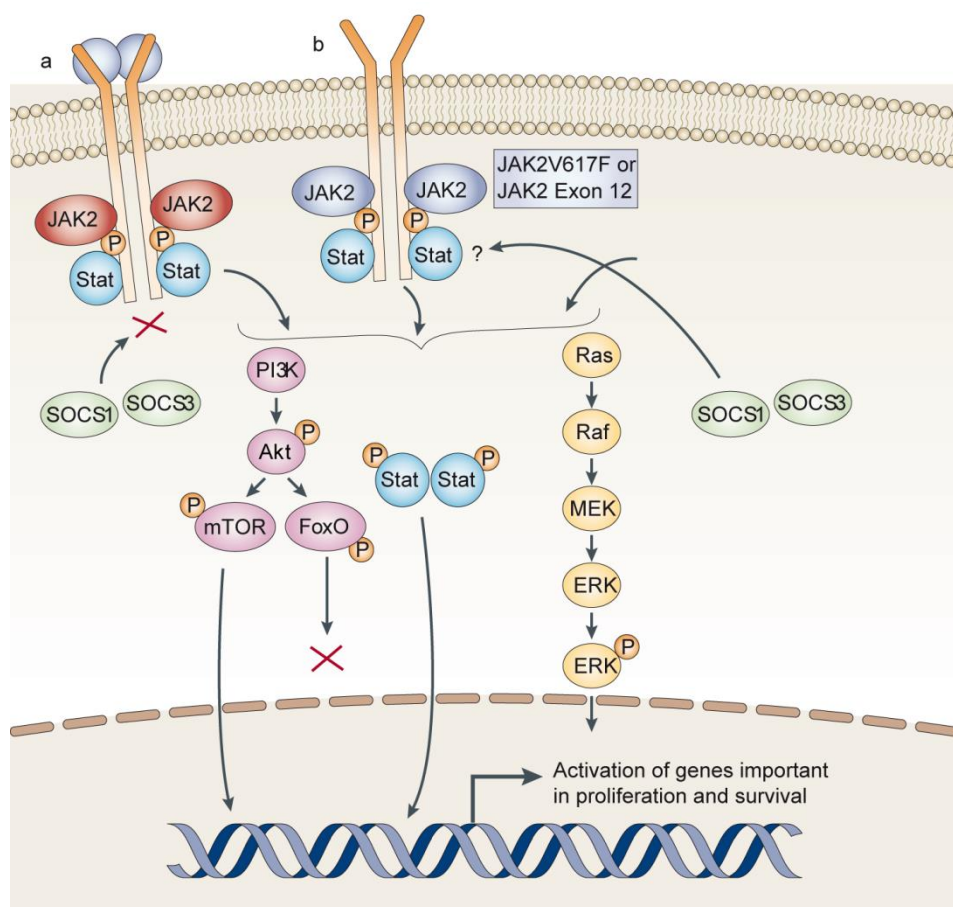
Figure 9. JAK/STAT pathway

(A) Cytokines usually bind to their respective receptors which in turn results in an auto-phosphorylation of JAK2. JAK2 recruits effector proteins like STAT proteins, MAPK or PI3K, and phosphorylates tyrosine residues these

effector proteins. This results in propagation of cytokine signaling into the nucleus and activation of gene expression. (B) Mutations in JAK2, like JAK2V617F, bind to the cytokine receptor and are phosphorylated in the absence of a bound cytokine and leading to cytokine independent signaling (taken and abbreviated from Levine et al. (2007))

1.4 Treatment in MPN

The most effective and long-term treatment option for any myeloid malignancy is an allogenic stem cell transplantation (Garcia-Manero et al., 2003). However, there is a low frequency of matches between patients and donor which limits this option to patients that develop resistances towards pharmacological treatments. Furthermore, allogenic stem cell transplantation has a high risk of mortality and is only used for patients that show good organ functions which also limits the application of this option to a good overall health of the patient (Elias and Hagop, 2018). Hence, for the management of CML and PV in those patients that are unfit for allogenic stem cell transplantation different pharmacological treatment options are needed.

1.4.1 Tyrosine Kinase Inhibitor (TKI) Treatment in MPN

The deregulated kinase activity of the mutated proteins is essential for the development of CML and PV *in vivo*. Thus, ideas were developed to design small chemical compounds to compete with the ATP at the binding side of the kinase domains. Hence, kinase activity is blocked and the entire downstream signaling of the oncogene is blocked as well. Consequently, the oncogene addicted cells are inhibited. These compounds are tyrosine kinase inhibitors (TKI).

The development of Imatinib and second generation TKI therapy to block the activity of BcrAbl was a breakthrough in CML management. Studies showed a molecular response in chronic phase CML patients after Imatinib treatment (Kantarjian et al., 2002). Others showed that there was no evidence of BcrAbl messenger RNA (mRNA) six months after treatment with Imatinib and that 90% of CML patient

showed a long term survival (Barbany et al., 2002). Furthermore, for some patients in accelerated or blast phase Imatinib treatment showed a response (Talpaz et al., 2002). Compared to other therapy forms Imatinib was easily administered as is was applicable orally. Moreover, Imatinib showed low toxicities compared to IFNα, hydroxyurea or other chemotherapeutical drugs (Kujawski and Talpaz, 2007). However, point mutations in BcrAbl during Imatinib therapy occur which renders BcrAbl^{+} cells resistant to Imatinib therapy (Branford et al., 2002).

Ruxolitinib, a JAK1/JAK2 inhibitor, also brought a breakthrough in the management of JAK2 mutated MPN forms and for patients that showed an inadequate response to hydroxyurea treatment (Vannucchi et al., 2015). Yet, there were still differences of the efficacy of Ruxolitinib in the different JAK2V617F[+] MPN forms. Studies showed a modest reduction of JAK2V617F allele burden in PV and ET patients with Ruxolitinib treatment with only few patients achieving a complete molecular remission (Pieri et al., 2015).

However, a study by Rousselot et al. (2007) showed that even though BcrAbl was undetectable in 12 patients after Imatinib treatment following discontinuation 6 patients showed a relapse with detectable BcrAbl transcripts. The standing hypothesis is that Imatinib and other TKI aim at fast proliferating cells while slow proliferating or quiescent leukemic stem cells remain untouched by TKI therapy. After TKI discontinuation these leukemic stem cells proliferate again causing relapses (Figure 10).

1.4.2 IFNα treatment in CML and PV

Before Imatinib and second generation TKI therapy was implicated CML patients were treated with unspecific agents like IFNα or hydroxyurea. In mouse experiments it was shown that IFNα activates dormant HSC indirectly via the disruption of HSC interaction with the BM cell niche (Trumpp et al., 2010). Furthermore, Essers et al. (2009) showed that due to JAK/STAT activation mouse HSC and their progenitors

proliferate *in vivo*. Pietras et al. (2014) and Essers et al. (2009) showed that in acute IFNα treatments dormant HSC exit their G0 phase and enter cell cycle within a few hours of IFNα treatment. However, HSC dormancy is reacquired after 5 days. Thus, the stem cell pool is not exhausted (Pietras et al., 2014). In contrast, chronic IFNα treatment has a negative effect on HSC self-renewal. In competition experiments IFNα pre-treated HSC were outcompeted by the host hematopoiesis (Essers et al., 2009). The exit of stem cells from their dormancy by IFNα is used in treating CML and PV either as single treatment or in combination with TKI treatment (Figure 10).
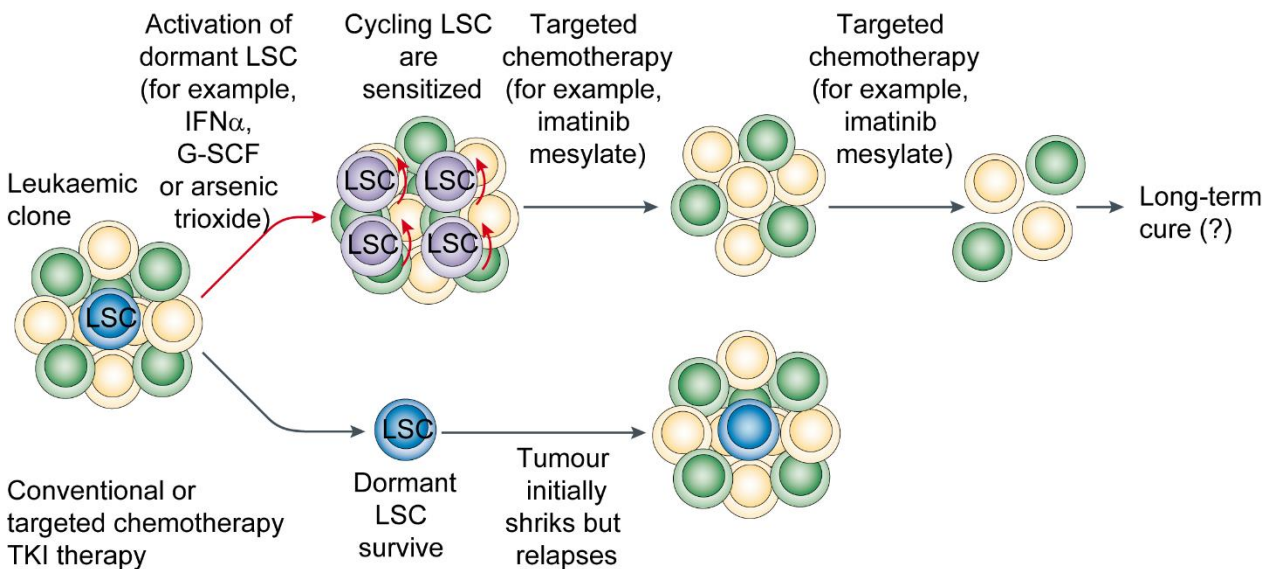
Figure 10. IFNα treatment to eradicate leukemic stem cells in MPN

A mutation in acquired in the stem cell pool with in an organism. Leukemic stem cells (LSC) exist in their dormant state within the stem cell pool and give rise to proliferation progeny. In conventional chemotherapy mutated proliferating cells are eradicated while leaving LSC untouched. When chemotherapy is discounted LSC exist their dormant state again and cause relapses. With IFNα therapy, LSC are activated to exist their dormant state and enter cell cycle. Cycling LSC can then be targeted with Imatinib to potentially cure the disease (taken from Trumpp et al. (2010)).

IFNα therapy for CML patients was initially studied in the early 1980's and produced a hematological (reduction of white blood cell counts), long lasting cytogenic (reduction of BcrAbl+ cells in the bone marrow) responses and an improved survival rate compared to hydroxyurea (Kujawski and Talpaz, 2007). However, response

rates for IFNα therapy in CML patients were long. IFNα therapy took up to 16 months to induce a complete molecular response with a normalization of white blood counts and no detectable BcrAbl$^+$ cells (Kantarjian et al., 2003). Moreover, only newly diagnosed CML patients benefitted from IFNα therapy. CML patients in late chronic phase showed a modest to low response to IFNα. Patients in accelerated phase lacked an IFNα response (Kujawski and Talpaz, 2007). This was linked to low IRF8 transcripts (Schmidt et al., 2001).Toxicity effects of IFNα led to discontinuation in a high percentage of CML patients (Elias and Hagop, 2018). Yet, with the development of pegylated IFNα (PegIFNα) the tolerability improved while toxicity effects decreased. Furthermore, the pegylated IFNα formulations needed less frequent applications and together with TKI treatment studies showed a higher response in CML patients than with TKI alone (Preudhomme et al., 2010). Combination of TKI and IFNα show promising results in first trials as they reduced the spleen size and reduced the JAK2V617F allele burden faster than monotherapy would have done (Bjørn et al., 2014).

In PV patients IFNα therapy has led to a great success in disease management, especially with the development of PegIFNα. Studies by Quintas-Cardama et al. (2009) and Kiladjian et al. (2006) showed a reduction of the JAK2V617F allele burden over the time course of IFNα therapy for both ET and PV patients whereas PV patients showed a more dramatic decrease of JAK2V617F allele burden. Later, it was suggested that the pathway that was activated by IFNα in JAK2V617F$^+$ cells is the MAPK pathway and that through that signaling JAK2V617F$^+$ cells were eradicated (Lu et al., 2010). A study by Kiladjian et al. (2010) also found hematological responses in 80% of PV patients after IFNα therapy. However also in JAK2V617F$^+$ MPN forms the outcome of IFNα therapy is dependent on additional mutations. It was shown that patients having the JAK2V617F mutation and a mutation in the TET2 gene have resistances towards IFNα treatment. Furthermore, Ishii et al. (2007a) showed that relapses could occur even in PV patients after IFNα treatment.

1.5 Type I Interferon (IFN)

Type I Interferons (IFN) have been described more than 60 years ago. They were the first proteins that have been purified, cloned and produced in a recombinant manner to be used for human therapy. Notably, this was achieved without the help of cDNA libraries, hence making the process costly and labor intensive.

In humans type I IFN consists of 5 classes: IFNα, IFNβ, IFNε, IFNκ and IFNω. Moreover, IFNα can be further subdivided into 13 subclasses and hematopoietic cells, especially plasmacytoid dendritic cells (pDC) are the main producers of IFNα. (Platanias, 2005). Generally, IFN are proteins that are secreted by infected cells. Binding of microbial products to pattern recognition complexes (PPR) induces type I IFN production. Moreover, cytokines like tumor necrosis factor (TNF), macrophage colony stimulating factor (M-CSF) and NF-κB can induce type IFN production. (Yarilina et al., 2008). Type I IFN have 3 major functions. First, they possess antiviral effects in response to viral infection of cells or double stranded RNA. IFN act in a cell intrinsic manner and affect neighboring cells to limit the spread of the infection. Second, IFN modulate innate immune function by promoting antigen presentation NK cell function. IFN also inhibit cytokine production and pro-inflammatory signaling pathways. Third, IFN activate the adaptive immune system and promote the development of antigen specific T and B cell responses (Ivashkiv and Donlin, 2014).

Because of their anti-proliferative effect and the effect on NK cells type I IFN have also been used for their antitumor effect in therapy since the 1980s. First approvals were for hairy cell leukemia and Kaposi's sarcoma (Paredes and Krown, 1991). Nowadays it is approved of for the treatment of CML and metastatic malignant melanoma (Talpaz et al., 2013). Next to cancer therapy IFNα, in particular, has been approved for viral infections like hepatitis C and chronic hepatitis B therapy (Roffi et al. (1995), Mazzella et al. (1999)).

1.5.1 Canonical IFNα signaling pathway

Type I IFN, such as IFNα and IFNβ have the same receptor to which they bind – the IFNα receptor (IFNAR). It is a heterodimeric transmembrane receptor and made out of 2 subunits: IFNα receptor 1 (IFNAR1) and IFNα receptor 2 (IFNAR2) (Figure 11). The receptor itself has no tyrosine kinase activity, hence, the subunits are associated with 2 tyrosine kinases, TYK2 and JAK1 (Velazquez et al., 1992). TKY2 is bound to the IFNAR1 subunit. JAK1 is bound to the IFNAR2 subunit. All of these components are widely expressed in cells. Thus, most cell types are competent to respond to type I IFN signaling (Ivashkiv and Donlin, 2014).

In the canonical IFN signaling pathway type I IFN binding activates TYK2 and JAK1 followed by phosphorylation of STAT1 and STAT2. Phosphorylated STAT1 and STAT2 dimerize to form a heterodimer and translocate into the nucleus. In the nucleus STAT1-STAT2 heterodimer binds IRF9 which results in a complex called IFN-stimulated gene factor 3 (ISGF3). Finally, ISGF3 binds to DNA sequences that are known as IFN-stimulated response elements (ISRE) and activates gene expression of IFN-stimulated genes (ISG) (Levy et al., 1989). The predominant signaling is the activation of STAT1 and STAT2, there are also studies that state that IFNα and IFNβ can activate STAT3, STAT5 or directly active interferon regulatory factors (IRF) (Su and David, 2000).

STAT proteins can also form homodimers when phosphorylated. After translocation into the nucleus these homodimers bind DNA elements known as IFNγ-activated sites (GAS). GAS elements were originally defined as a requirement for the rapid transcriptional induction of genes in response to IFNγ which is a type II IFN. However, IFNα can also activate genes that have GAS elements. Notably, some ISG have only GAS or ISRE elements in their promotors meaning that they are selectively induced by type I or type II IFN. These are genes like IRF1 or hypoxia inducible factor 1 (HIF1) (Der et al., 1998). However, other genes have both ISRE and GAS elements in their promotors and the combination of different STAT dimers

activates gene expression (Nguyen et al., 2002). Suppression of type I IFN signaling is done either by downregulation and internalization of the receptor on the cell surface or induction of suppressor of cytokine signaling (SOCS) 1 and SOCS3 proteins or miRNA (Ivashkiv and Donlin, 2014).
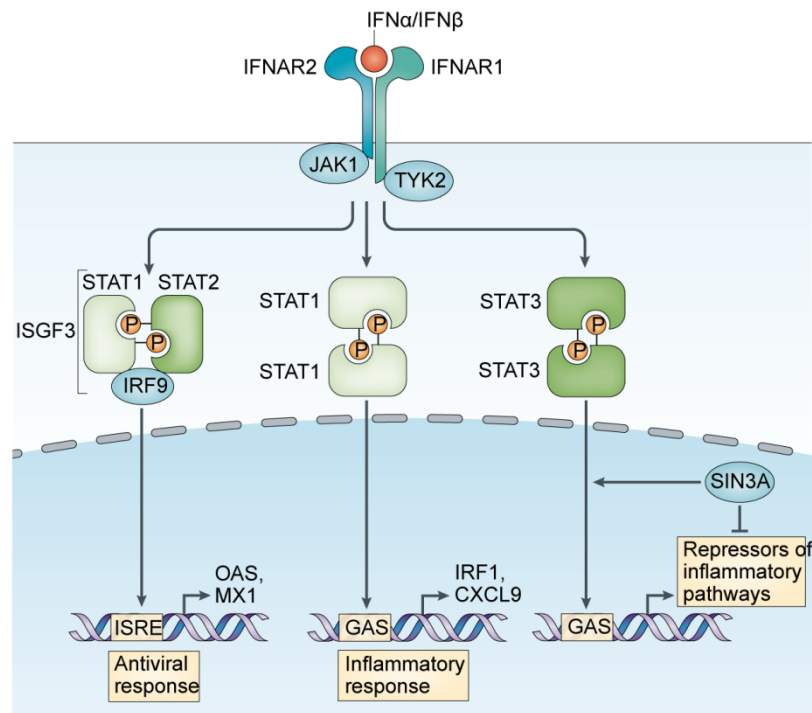
Figure 11. Canonical IFNα signaling pathway

The IFNα-Receptor (IFNAR) is composed of 2 subunits, IFNAR1 and IFNAR2, which are associated with JAK1 and TYK2. Due to ligand binding the receptor get phosphorylated by these 2 kinases and in turn provides docking stations for STAT proteins. The kinases phosphorylate STAT1 and STAT2 which form a heterodimer and bind IRF9 in the ISGF3 complex. This complex translocates into the nucleus, bind to ISRE elements in promotor regions and activates ISG. Activates STAT1 can also form homodimers and translocate into the nucleus and activates gene expression as a homodimer. Here it binds to GAS elements in the gene promotors to activate gene transcription (taken from Ivashkiv and Donlin (2014))

It is clear that the IFN signaling pathway involves the JAK/STAT pathway; however the downstream events are not well defined. Furthermore, the detailed mechanisms of IFN signaling are not well defined in most cases. Mechanisms vary from species to species and even within an organism IFN signaling varies in different cell types. Additionally, it was shown that other JAK/STAT independent pathways play a role in

type I IFN signaling. Platanias et al. (1999) showed that CRKL can be activated by TYK2 in response to IFNα and IFNβ. This pathway is in part related to the growth inhibitory effect of IFNα in primary hematopoietic cells. Mitogen activated protein kinases (MAPK) are also activated by type I IFN. Studies by Mayer et al. (2001) and Lu et al. (2010) showed that the p38 signaling cascade has an important role in IFN signaling, especially in malignant cells. Another pathway that is also activated by type I IFN is the PI3K pathway in a STAT1 independent manner. Instead of STAT1 phosphorylation, type I IFN phosphorylate tyrosine residues in IRS1 forming docking stations for the p85 subunit of PI3K (Uddin et al., 1995). Due to PI3K activation STAT1 is phosphorylated at the serine 727 (Ser727) by PKC-δ. Studies showed that phosphorylation at Ser727 mediates the chemotherapy induced apoptosis (DeVries et al., 2004).

Due to the multitude of signaling pathways activated by type I IFN there are multitude of side effects and toxicities when IFN is used therapeutically. Consequently, it is making the study of the IFN signaling pathway in each cell type all the more necessary to limit the side effects on bystander cells.

1.6 Induced pluripotent stem cells (iPSC)

1.6.1 Pluripotent, totipotent and multipotent cells

During mammalian development, the potential of cells becomes more and more restricted as cells fully differentiate to fulfill their specialize functions in tissues. Therefore, cells can be classified as totipotent, pluripotent, multipotent and unipotent (Kelly, 1977). Totipotent cells are zygotes and blastomeres. They can give rise to all embryonic and extraembryonic tissues, like the placenta. The most stringent test under experimental conditions for totipotent cells is the generation of a fully formed organism from a single cell. Pluripotent cells are cells of the inner cell mass (ICM) of blastocysts. They can give rise to all embryonic tissues, however, not all

extraembryonic tissues. Multipotent cells reside in the adult tissue as adult stem cells. These can give rise to all cells within their cell lineage, for example hematopoietic cells. When more than one developmental option within their lineage is possible, for example all cells from myeloid and lymphoid hematopoietic lineage, then cells are multipotent. Unipotent cells have only one option within their lineage, for example they can give rise to all cells within the myeloid lineage. Upon terminal differentiation cells lose their developmental potential and become somatic cells (De Los Angeles et al., 2015).

1.6.2 History and generation of iPSC

The first experiments in the field of pluripotency and generation of pluripotent cells for *in vitro* cultures were done by Briggs and King (1952). They established the method of nuclear transfer to study the potential of nuclei from late embryonic cells that were injected into enucleated oocytes. Gurdon et al. (1958) used the method of nuclear transfer in the late 1950 and showed the method of generating cloned eggs from the same species using nuclei of differentiated amphibian cells and injecting these into frog eggs. The results show the development of frogs from these eggs. Over the years nuclear transfer has been used to clone various animals (Wilmut et al. (1997), Inoue et al. (2005)). However, these animals have abnormalities in their phenotype and gene expression suggesting that nuclear transfer is still faulty (Hochedlinger and Jaenisch, 2002).

However, the establishment of pluripotent stem cells *in vitro* was first performed by Evans and Kaufman (1981) who isolated cells from ICM of mouse blastocysts. Thus, mouse ES cells were established. Thomson et al. (1998) generated the first human pluripotent cell line by isolating cells from the ICM of human blastocysts and culturing these cells on mouse embryonic fibroblasts (MEF). The generated cells had distinct properties. First, cells grew in dense colonies and cells within these colonies showed a high ratio of nucleus to cytoplasm. Second, cells showed indefinite proliferation potential without any differentiation. Third, cells expressed

stage specific embryonic markers, like SSEA-4, SSEA-3 and TRA 1-60. Lastly, cells displayed teratoma formation when injected into severe combined immunodeficiency (SCID) mice. Furthermore, when analyzed these teratomas showed structures from all 3 germ layers; mesoderm, ectoderm and endoderm. As the origin of these cells came from a developing embryo the generated cells were termed moue and human embryonic stem cells, mESC and hESC respectively (Thomson et al., 1998). However, when using ES cells in research there are always ethical and legal issues to be taken into account, especially when hESC are used.

In the late 1980s a study by Davis et al. (1987) already showed the importance of master regulators in cell fate decisions. Davis et al. (1987) ectopically expressed MyoD in fibroblasts and converted these cells into myoblasts. However, a breakthrough in stem cell technology was achieved only in 2006. Takahashi and Yamanaka (2006) reported that by the ectopic expression of OCT4, KLF4, SOX2 and c-MYC in mouse embryonic or adult fibroblasts can reprogram somatic cells into cells with properties of ESC cells. As Yamanaka and colleagues used somatic cells as origin material they termed the generated cells as induced pluripotent stem cells (iPSC). However, these iPSC were again generated from mouse cells. One year later, Takahashi et al. (2007) and Yu et al. (2007) reported the first generation of iPSC from human somatic tissue (human fibroblasts). Due to the breakthrough in stem cell technology of Yamanaka by using only 4 transcription factors for reprogramming KLF4, OCT4, SOX2 and c-MYC were termed OSKM or Yamanaka factors. Since the first description of iPSC generation from human tissue iPSC have been shown to be a powerful and versatile tool for regenerative medicine and basic research at the same time.

1.6.3 Reprogramming methods to generate iPSC

Several methods are available for the generation of iPSC. First, there are integrating methods, like the use of retroviruses, lentiviruses or transposons (Bellin et al., 2012). Up until now the method of choice in most research laboratories is still the reprogramming with retroviral vectors which has higher efficiencies than non-integrative methods (Aoi et al. (2008), Okita et al. (2007)). Retroviruses deliver the genes into the genome of proliferating cells and the added genes are usually silenced during reprogramming (Stewart et al., 1982). However, every iPSC clone has multiple integration sides. Therefore, no iPSC clone is exactly the same as the viral vectors integrate at random which could pose a problem when comparisons of iPSC clones are needed (Takahashi and Yamanaka, 2006). Furthermore, Okita et al. (2007) also showed that 20% of chimeric animals suffered from tumors because of reactivation of c-MYC suggesting that the use of retroviruses in iPSC generation is not suitable for clinical applications of iPSC.

Instead of using retroviruses another delivery system are lentiviruses (Yu et al., 2007). The advantage is that also non-proliferating cells are transduced with the Yamanaka factors thus making them more efficient (Sommer et al., 2009). However, the previous observed problems in using retroviruses are even more pronounced when using lentiviruses to generate iPSC (Brambrink et al., 2008). Notably, the use of inducible transgenes with doxycycline or transgenes coupled with Lox/P sides have been shown to circumvent or diminish the problems of continuous expression of transgenes (Sommer et al., 2010). However, the issue with multiple integration sites still existed. Furthermore, for clinical applications lentiviruses were not suitable. The last method of for reprogramming is the use of transposons (Woltjen et al., 2009). They have the advantage that they are not viral. However, when excision of the transposon is done the transposase can leave footprints. Within the footprints regions inserted or deleted sequences might change the genome of the cells suggesting that mutagenesis can occur.

To counteract the possible reactivation of integrated transgenes and the resulting mutagenesis newer methods for iPSC generation needed to be developed. Especially when using iPSC technology for clinical and therapeutic applications, integration free methods are needed. These methods express the OSKM factors transiently to induce pluripotency. One of the first attempts of integration free generation of iPSC was done by Stadtfeld et al. (2008) who used replication-defective adenoviruses on mouse fibroblasts and fetal liver cells. F-deficient sendai viruses which are (–) strand RNA viruses, are another method to generate integration free iPSC from a wide range of somatic cells. For example, Fusaki et al. (2009) effectively generated functional iPSC from human fibroblasts and showed that the reprogramming only needs a transient expression of transgenes. However, the generation and purification of sendai virus particles is difficult in a standard research laboratory set and commercial options are cost intensive. Therefore, other methods are episomal vectors, synthetic mRNA or mature miRNA (Bellin et al., 2012). Moreover, there have been studies with small molecules that promote and enhance the efficiency of integration free reprogramming methods (Li and Ding, 2010). Within this search a study was published by Hou et al. (2013) stating that a combination of small molecules can be used to substitute the OSKM factors and be used to generate iPSC on their own.

1.6.4 Using iPSC in clinical applications

In recent years efforts to improve integration free methods to generate iPSC have increased as these approaches proved to pave the way for iPSC use in a range of clinical applications (Figure 12).

One potential application for iPSC in clinics is the modeling of human diseases *in vitro*. In human disease like leukemia the affected cell type can be rare and hard to access. The advantage of iPSC for researchers is that the affected cell type can be

differentiated from iPSC and depending on the protocol of iPSC differentiation in large quantities. Thus, studies with patient derived iPSC can model the stages of human disease with a focus on either one specific mutation, for example a driver mutation in leukemia like BcrAbl or JAK2V617F or with multiple mutations influencing the disease (Figure 12A). There have been multiple reports that generated iPSC from multiple patients suffering from diseases, like ALS, Parkinson's disease or Fanconi anemia (Bellin et al., 2012). Proof of principle in disease modeling was done by Ye et al. (2014) and Kumano et al. (2012) who recapitulated the pathological features of JAK2V617F[+] and BcrAbl[+] MPN, respectively, *in vitro*. Moretti et al. (2010) generated iPSC from patients suffering from multiple heart conditions which could be recapitulated *in vitro*. Furthermore, patient derived iPSC are suitable for finding of new drug targets, the development of new drugs for human disease and toxicity tests on different cell types (Figure 12B and C).
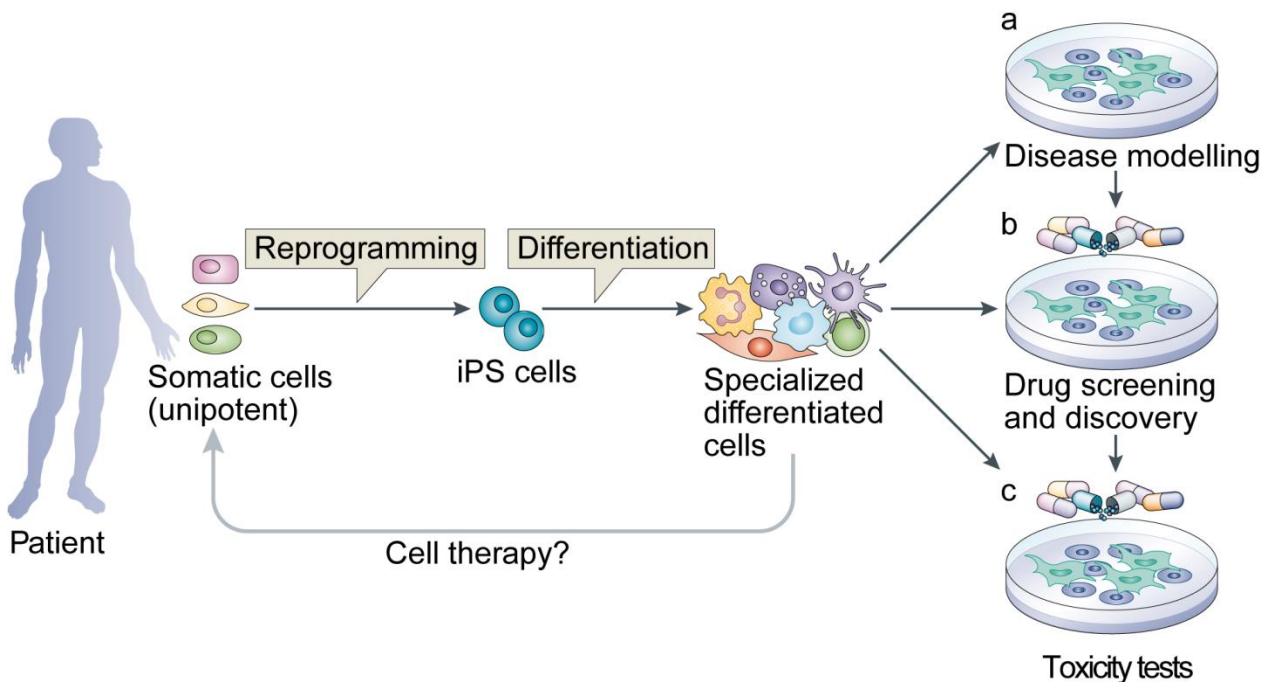
Figure 12. Scheme for potential clinical applications of patient derived iPSC

Somatic cells, like peripheral blood mononuclear cells (PBMNC) or fibroblasts are taken from a diseased patient and reprogrammed into iPSC. Patient derived iPSC will be differentiated into the cell type affected by the supposed driver mutation. (A) The iPSC-derived cell types can be used for disease modeling or the study of the

influence of a certain mutation on the cell type. (B) Another application is the screening for new drugs that inhibit the disease causing mutation. (C) Finally, the discovered drugs can be used in first toxicity tests on the desired cell type (taken and abbreviated from Bellin et al. (2012)).

As gene editing techniques are getting more suitable to use in iPSC the ultimate goal is to repair the disease causing mutation in iPSC, differentiate patient specific iPSC into the preferred cell type and transplant cells into the host to cure the disease. Proof of principle has been done by Hanna et al. (2007) who generated iPSC from a humanized mouse model of sickle cell anemia. After correction of the mutation in iPSC followed by hematopoietic differentiation of these iPSC and autologous transplantation of hematopoietic progenitors the mice have been rescued (Hanna et al., 2007). Lachmann et al. (2015) published a protocol that generated iPSC derived terminally differentiated myeloid cells. Moreau et al. (2016) generated large quantities of iPSC-derived megakaryocytes that could produce functional platelets. These could be used in cell therapy approaches when produced in larger quantities. It remains to be seen if these techniques are feasible for generalized medicine.

1.7 Aims and objectives

This thesis aims at investigating (i) the role of IRF8 for MPN development and therapy (ii) the role of JAK2V167F on human hematopoiesis and (iii) elucidating the IFNα signaling pathway in MPN (Figure 13).

The first aim is to gain insight into the role of IRF8 in the pathogenesis of CML and the influence on MPN therapy. Therefore, IRF8$^{+/+}$ and IRF8$^{-/-}$ BM cell were isolated, transduced with BcrAbl and subjected to (i) cytokine withdrawal, (ii) TKI or IFNα single therapy and (iii) TKI/IFNα combinational therapy (Figure 13A). This will give insight into cytokine independence of BcrAbl$^+$ cells and the efficacy of TKI and IFNα therapy in the absence and presence on IRF8.

The second aim was to study the role of JAK2V617F on human hematopoiesis. The objectives were (i) to generate patient derived iPSC from PBMNC of 3 PV patients, (ii) to differentiate patient derived iPSC into iPSC-derived hematopoietic cells and further into red blood cells. Both differentiation steps were followed by flow cytometry. This gives in sight whether JAK2V617F has only an influence on mature differentiated cells or if JAK2V617F has also an influence on more primitive hematopoietic cells. The last aim was to study the IFNα signaling pathway in JAK2V617F⁺ HPC compared to JAK2 HPC. During IFNα treatment of iPSC-derived hematopoietic cells (i) cell survival, (ii) gene expression of IFNα target genes, (iii) expression of IFNAR1 and IFNAR2 on the cell surface and (iv) STAT1 activation was investigated (Figure 13B).

A Studying the role of IRF8 in MPN pathogenesis and TKI/IFNα therapy
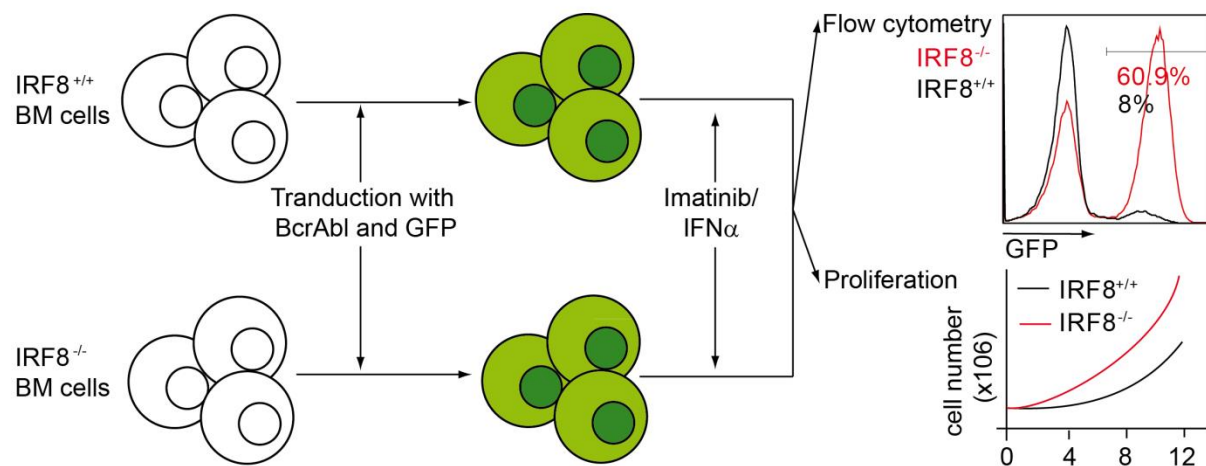
B Studying the PV pathogenesis and elucidating the IFNα pathway in JAK2V617F$^+$HPC
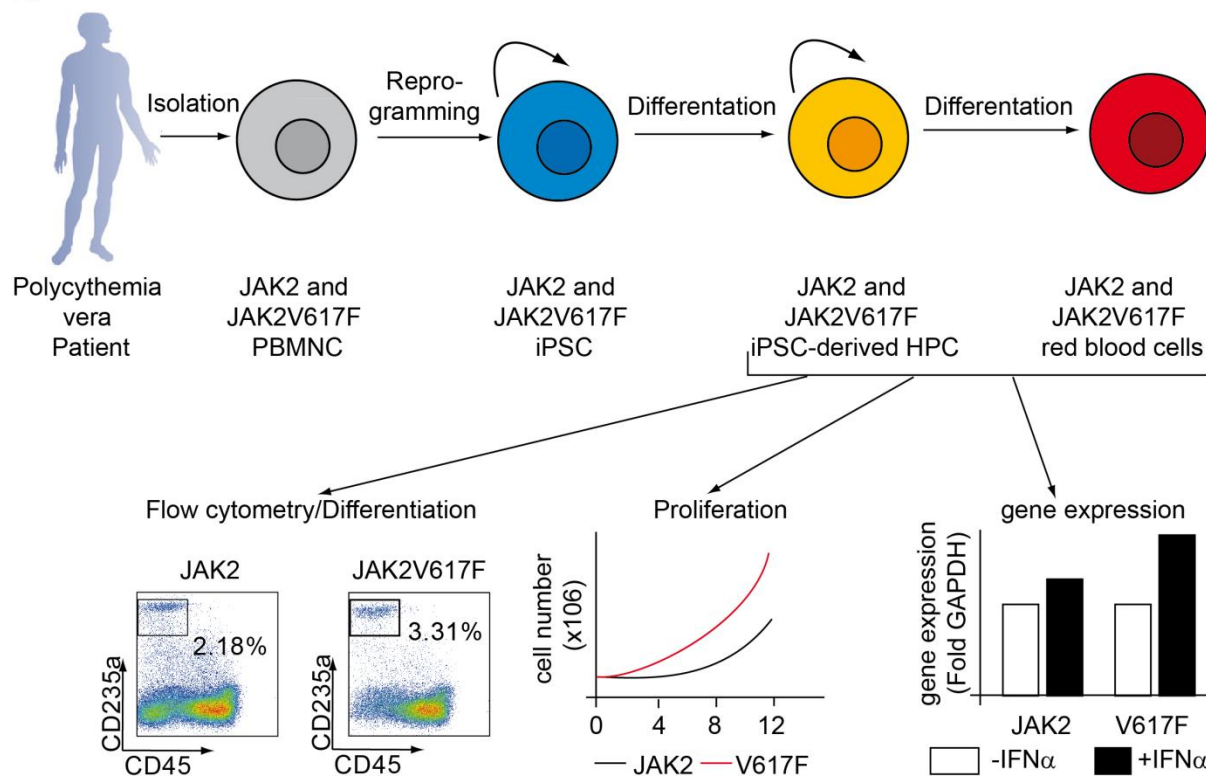
Figure 13. Schematic representation of aims and objectives

(A) To investigate the role of IRF8 on MPN pathogenesis and therapy IRF8$^{+/+}$ and IRF8$^{-/-}$ bone marrow cells were isolated, amplified and transduced with BcrAbl. BcrAbl$^+$ cells were treated with Imatinib and/or IFNα. BcrAbl$^+$ cells were followed via flow cytometry via their GFP expression. BcrAbl$^+$ cells were also analyzed for different cell population and their development during IFNα and Imatinib treatment was followed. (B) To study PV pathogenesis JAK2 and JAK2V617F iPSC generated by reprogramming patient PBMNC. iPSC were differentiated towards hematopoietic progenitor cells (HPC) and further into red blood cells. Both differentiation steps were followed via flow cytometry. Additionally, iPSC-derived HPC were analyzed for their proliferation capacity. To elucidate the IFNα signaling pathway, iPSC-derived HPC were treated with and without IFNα and gene expression for IRF7, IRF9 and STAT1 was analyzed (figure for experimental setup loosely adapted from Bellin et al. (2012)).

2 Materials and Methods

2.1 Materials

All centrifugation steps during cell culture were performed with a Hereaus Megafuge 16 (Thermo Scientific). For flow cytometry steps (chapter 2.2.2.3) or purification of amplified oncogene vector constructs (chapter 2.2.1.4.2) all centrifugation steps were performed with a Heraeus Multifuge 3L (Thermo Scientific). Cytospins (chapter 2.2.1.12) were performed with a Shandon 4 centrifuge (Thermo Scientific). For cell culture a Heracell incubator (Thermo Scientific) was used. Cell morphology was monitored with a Leica DM IL microscope (Leica Microsystems). For checking GFP expression and picking iPSC clones an EVOS microscope (Thermo Scientific) was used. Immunofluorescence images (chapter 2.2.1.9) were obtained with an Axiovert 200 microscope (Carl Zeiss). Histological stainings (chapter 2.2.1.12) were recorded with a Leica DMRX microscope and Leica Application Suite software (both by Leica Microsystems).

All serological pipettes used were supplied by Greiner. If not otherwise stated all tissue culture plates (TCP) were purchased from TPP. Gelatin was dissolved in distilled water and autoclaved at 121°C for 30 min. Gelatin coating of plates for MEF isolation (chapter 2.2.1.6), MEF seeding for iPSC culture (chapter 2.2.1.7.1) or hematopoietic differentiation (chapter 2.2.1.10) was done for 15 min at 37°C. FACS tubes were supplied by Sarstedt. Cytokines used for cell culture are listed in Supplemental Table 1. All media and cell culture components are listed in Supplemental Table 2 and Supplemental Table 3. Flow cytometry analyses of surface marker expression and cell sorting was done with a FACS Canto II and FACS Aria (BD Biosciences), respectively. SDS-PAGE (chapter 2.2.2.7) was performed with chambers supplied by BioRad. Furthermore, blotting of proteins from SDS gels onto nitrocellulose membranes was performed with a semi-dry blotting device from BioRad.

2.2   Methods

2.2.1 Cell Culture

2.2.1.1 Mouse strains

IRF8$^{+/+}$ and IRF8$^{-/-}$ mice were used for isolation of bone marrow cells. The mice were kept in a C57BL/6J background. Mice were kept under pathogen free conditions and bred in the central animal facility of the RWTH Aachen University Hospital, Aachen, Germany. Animal experiments were approved by local authorities (Landesamt für Natur, Umwelt und Verbraucherschutz Nordrhein-Westfalen – LANUV NRW) in compliance with the German animal protection law (Reference number 87–51–04.2010.A040).

2.2.1.2 Retroviral oncogene vectors

Retroviral vectors shown in Figure 14 were used in this thesis. Both vectors were obtained from Dr. Nicolas Chatain (Department of Hematology, Oncology, Hemostaseology, and Stem Cell Transplantation, Faculty of Medicine, RWTH Aachen University, Aachen, Germany). cDNA of BcrAbl and human JAK2V617F were cloned into the pMSCV vector (Daley et al., 1990). The pMSCV vector was used as control during transduction of murine bone marrow (BM) cells. The pMSCV vector contained the open reading frame (ORF) for the green fluorescent protein (GFP) and an ampicillin resistance. Cells that were transduced with retroviral vectors co-expressed GFP along with the oncogenes. GFP was used for tracing oncogene expressing BM cells in flow cytometry analyses.

For amplification of vector constructs, 100 ng of each vector construct was taken up and amplified by DH5α cells. DH5α cells were cultured over night at 37°C on LB agar or in LB medium that was supplemented with ampicillin. Only DH5α cells that

had taken up the vector were able to grow in the overnight cultures. Isolation of vector constructs was performed with the NucleoBond® Xtra Midi/Maxi kit (Macherey Nagel) according to the manufacturer's protocol.
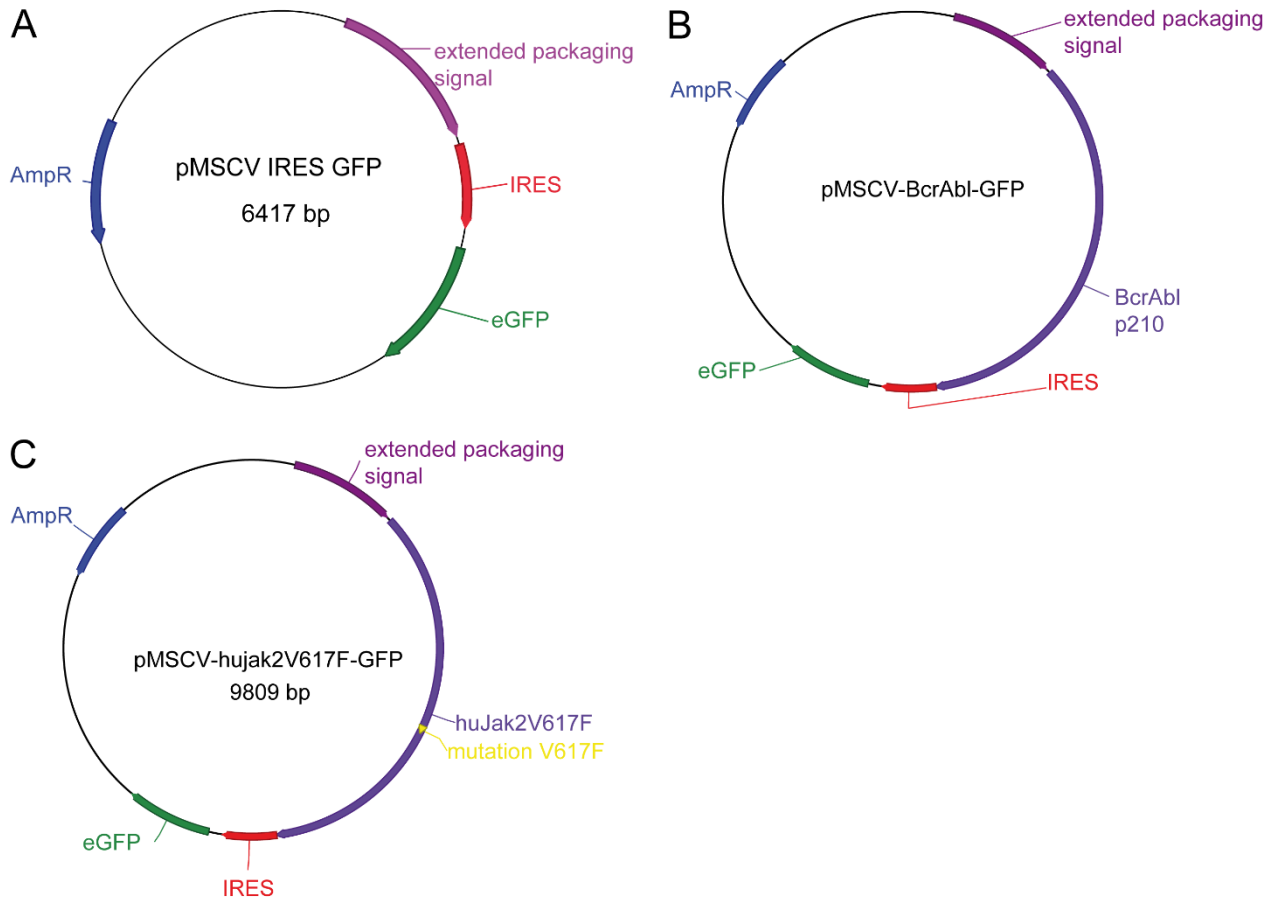
Figure 14. Vector maps used for retroviral transduction of BM cells

Shown are schematic maps for the (A) empty vector, (B) vector containing BcrAbl and (C) vector containing human JAK2V617F gene. For tracing transfection and transduction of cells all vectors contain GFP. AmpR, Ampicillin resistance; IRES, internal ribosome entry site.

2.2.1.3 Culture of HEK239T cells

HEK293T cells were cultured in high glucose Dulbecco's Modified Eagle Medium (DMEM) supplemented with 10 % FCS, 2 mM L-Glutamine, 100 U/ml Penicillin and 100 µg/ml streptomycin. Cells were grown on 10 cm tissue culture plastic (TCP)

plates for 2 – 3 days. Passaging was performed when a cell density of 70 – 85 % was reached. Cells were washed once with 1x phosphate buffered saline (PBS). 0.05 % Trypsin/EDTA was warmed to 37°C and added to the cells for 2 – 3 min at 37°C. Trypsin/EDTA was inactivated with culture medium and cells were split in a 1:5 to 1:20 ratio. For transfection with oncogene vectors, cells were passaged 24h before transfection. Cells were counted with an electronic cell counter (CASY, Schärfe System) and seeded at a density of $0.75 \times 10^6 – 2 \times 10^6$ cells per 10 cm plate.

2.2.1.4 Isolation and culture of mouse bone marrow (BM) cells

Mice were sacrificed and femur and tibiae were collected (Felker et al., 2010). Bone marrow (BM) cells were isolated by flushing the bones several times with BM cell medium (Table 1). Cells were passed repeatedly through a 1 ml syringe and a 23G needle to break up cell aggregates, thus forming a single cell suspension. The suspension was left untouched for 1 – 2 min, so the debris was able to sink to the bottom of the falcon tube. The supernatant was then transferred to a fresh tube. Following, the cell number was determined using an electronic cell counting machine. The rest of the suspension was centrifuged for 4 min at 1400 rpm. After determining the cell number the cells were seeded at 2×10^6 cells/ml using BM cell medium and cytokines were added accordingly (Table 2) to promote cell proliferation. Cells were incubated at 37°C and 5 % CO_2. On day 3 after BM isolation cells were subjected to a density gradient centrifugation. This serves to purify the hematopoietic progenitor cells from debris and dead cells. For this purpose, lymphocyte separation medium (LSM, 1.077g/ml, PAA) was transferred into a falcon tube and overlaid with the same amount of cell suspension. Centrifugation was carried out for 15 min at 2000 rpm with minimal break. A thin white ring containing the hematopoietic progenitors was visible between the LSM and the medium layer. The ring was harvested using a plastic pasteur pipette. Cells were then washed twice with PBS and subjected to cell counting using the CASY machine. Cell

numbers were adjusted to 1.5 x 10^6 cells/ml with cytokine supplemented BM cell medium and seeded into 6 well plates. Maximum cell number per well did not exceed 5 x 10^6 cells. Cells were cultured for 4h at 37°C. Afterwards, cells were transduced with oncogenes vectors (Figure 14) on day 3 and day 4 after BM isolation (Figure 15B).

Table 1. BM cell medium

Ingredient	Final Concentration
RPMI 1640	500 ml
FCS (heat inactivated)	10 % (50 ml)
Penicillin/Streptomycin (Pen/Strep)	100 U/ml (5 ml)
L-glutamine	2 mM (5 ml)
β-mercaptoethanol	50 µM (500 µl)

Table 2. Cytokines for proliferating murine BM cells

Ingredient	Final Concentration	Company/Origin
murine SCF	100 ng/ml (1:100)	produced by stably transfected CHO KLS C6 cell line
hyper-IL6	25 ng/ml (1:1000)	gift from Dr. Rose-John (Institute of Biochemistry, Medical Faculty, Christian-Albrechts-University, Kiel, Germany)
IGF-1	40 ng/ml (1:1000)	Sigma-Aldrich
Flt3L	25 ng/ml (1:1000)	PeproTech

2.2.1.4.1 Transfection of HEK293T cells with oncogene vectors

HEK293T cells were used to produce virus particles (Chen, 2012). To this end, HEK293T cells were seeded at a concentration of 0.75 x 10^6 - 2 x 10^6 cells/ml on 10 cm plates 24h before transfection. On the day of transfection, medium was refreshed and HEK293T cells were transfected with oncogene vectors (Figure 15A). To this end, a DNA-CaCl$_2$ mix was prepared. 10 µg per ongogene encoding vector was mixed with 2 packaging vectors (3 µg of pVpackGP and 7.5 µg of pVpackEco; both from Stratagene/agilent, Supplemental Figure 1). Next, 2xHBS buffer was added dropwise under constant mixing to the DNA mix. Finally, DNA-CaCl$_2$ mix was added dropwise to the HEK293T cells and incubated at 37°C. 18h after transfection medium was refreshed and cells were checked for GFP expression. Virus particles were secreted into the supernatant. Therefore, supernatant was harvested 48h and 72h after transfection and used for transduction of murine BM cells according to chapter 2.2.1.4.2.

2.2.1.4.2 Retroviral transduction of mouse BM cells with oncogenes

Transduction of IRF8$^{+/+}$ and IRF8$^{-/-}$ BM cells was performed on day 3 and 4 after BM isolation (Figure 15B). To this end, virus containing supernatant from transfected HEK293T cells was collected into Falcon tubes and medium for HEK293T cells was replaced by fresh medium. Supernatant was centrifuged for 5 min at 1400 rpm to separate possible dead cells from virus supernatant. Supernatant was filtered through a 0.45 µm CA filter (GE healthcare, Whatman) (Landázuri and Le Doux, 2006). 8 µg/ml Polybrene (Sigma, H-9268, Stock 80 mg/ml dissolved in distilled water) and 8 µg/ml Chondroitin Sulfate Sodium Salt (Sigma, C4384, Stock 80 mg/ml dissolved in distilled water) was added to the filtrate and incubated for 20 min at 37 °C. Next, filtrate was centrifuged for 20 min at 4000 rpm and supernatant was discarded. Virus containing pellet was dissolved and homogenized in 100 µL BM cell medium by pipetting up and down approximately 50 times. The homogenized pellet

was added to the BM cells drop wise and BM cells were incubated at 37 °C. A second density gradient centrifugation was performed 16 – 18h after the second round of transduction. A medium change was performed 36h later. BM cells were starved of growth factors for 2 days to select for oncogene expressing cells followed by TKI and IFNα treatment (2.2.1.17 and 2.2.1.18).
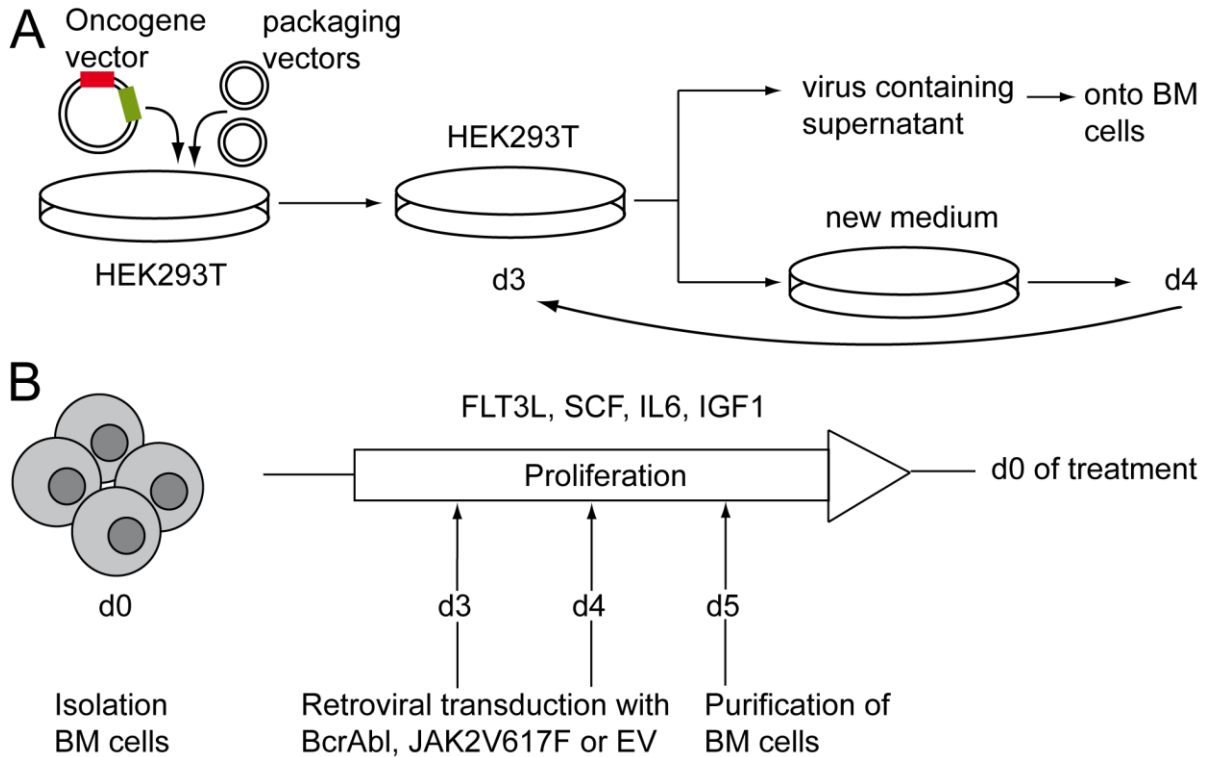
Figure 15. Schematic overview of retrovirus production by HEK293T and retroviral transduction of BM cells

(A) Schematic protocol for retrovirus production is shown. HEK293T cells were transfected with packaging vectors and the vector containing BcrAbl or JAK2V617F and a GFP cassette using CaCl$_2$ precipitation as described in chapter 2.2.1.4.1. (B) Murine BM cells were isolated from tibia and femur. BM cells were cultured with FLT3L, SCF, IL6 and IGF1 for 3 days. Then, BM cells were subjected to density gradient centrifugation and viable cells were enriched. After 4h of culture, the first retroviral transduction was performed as described in chapter 2.1.4.2. 24h later, a second retroviral transduction was performed. On day 5 post BM isolation cells were purified via density gradient centrifugation. Finally, cells were split into different conditions and used in subsequent experiments.

2.2.1.5 Generation of iPSC from peripheral blood of PV patients

For generation of patient specific iPSC, peripheral blood of 3 PV patients was taken and mononuclear cells were isolated via density gradient centrifugation (chapter 2.2.1.16). Mononuclear cells were cultured for 2 – 3 days in StemSpan supplemented with 100 ng/ml SCF, 20 ng/ml TPO, 50 ng/ml FLT3L and 10 ng/ml hyper-IL6 (Figure 16). Medium was refreshed 24h after thawing and right before reprogramming. For reprogramming, the Cytotune 2.0 kit (Thermo Scientific) was used according to the manufacturer's protocol and as published by Sontag et al. (2017a). In short, Sendai virus particles containing OCT4, SOX2, c-MYC and KLF4 were mixed 1:1. Mononuclear cells were counted via Neubauer counting chamber. 4×10^5 cells in 270 µl StemSpan^{TM} SFEM supplemented with cytokines were taken for reprogramming. 30 µl of Sendai virions were added to the cells, gently mixed and incubated for 48h with the cells. Next, cells were washed and resuspended in StemSpan^{TM} SFEM supplemented with cytokines. Medium was changed every 2nd day and cells were monitored for the formation of grape-like structures. Following the appearance of these grape-like structures, a medium change was performed; cells were counted and seeded on a mouse embryonic fibroblast (MEF) monolayer with 3 – 4 different cell concentrations. In the following 2 days StemSpan^{TM} SFEM medium was replaced stepwise with iPSC medium (Table 3). Cells were cultured for 2 – 3 weeks with a medium change every 24h. During that time cells underwent mesenchymal-to-endothelial transition (MET) and formed ES-cell like colonies. MEF were reseeded every 5 - 6 days. After 2 – 3 weeks, MEF were seeded in a monolayer into a 24 well plate. Single iPSC colonies were picked (1 Well = 1 colony) with an EVOS microscope under sterile conditions. iPSC colonies were expanded and DNA for allele specific PCR was isolated. iPSC clones that were not needed were frozen in FCS + 10% DMSO and stored in liquid nitrogen.
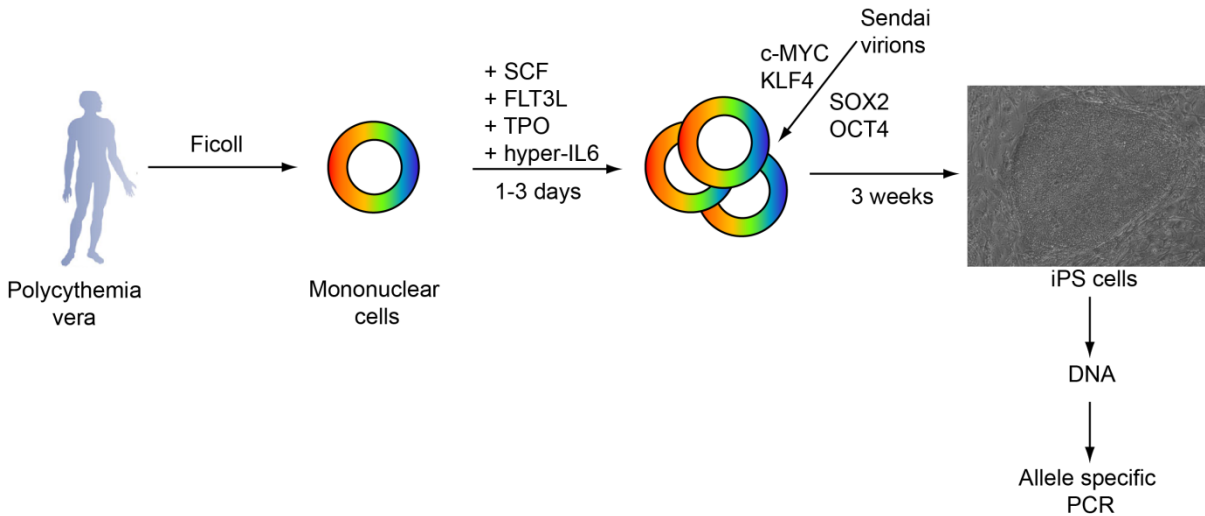
Figure 16. Generation of patient specific iPSC

Phlebotomies form 3 PV patients were used for generating patient derived iPSC. Mononuclear cells were isolated by density gradient centrifugation and cultured for 1 – 3 days with growth factors. PBMNC were infected with CytoTune 2.0 Sendai virus containing SOX2, OCT4, c-MYC and KLF4 and cultured for 2 days. Cells were seeded on MEF and after 3 weeks of culture individual iPSC colonies were picked, DNA was isolated and allele specific PCR for JAK2V617F was performed.

2.2.1.6 Culture and Irradiation of Mouse Embryonic Fibroblasts (MEF)

To isolate MEF for iPSC cell culture, pregnant mice were killed on embryonic day 13.5 and the uterus was opened (Durkin et al., 2013). Fetal bags (embryo + membrane + placenta) were extracted, washed with Penicillin/Streptomycin solution (in PBS) 3 times. Afterwards, fetal bags were washed 3 times with 1x PBS. Next, bags were opened and the embryo including placenta and membrane was taken out. The placenta and the attached membrane was removed. Next head, tail, legs, liver and inner organs from each embryo were removed. All carcasses were collected in a new Petri dish and minced with scissors until no big clumps remained and the suspension appeared homogenous. 8 ml of pre-warmed 1x Trypsin was added, minced carcasses were resupended with pipette up and down 2 – 4 times and collected in a 15 ml Falcon tube. Carcasses were incubated for 4 min at 37 °C. Big pieces had settled to the bottom, single cells stayed in the supernatant which therefore appeared milky. The milky supernatant was harvested and transferred

directly transfer to a 15 ml conical tube filled with 8 ml of MEF medium. Fresh Trypsin was added to the remaining carcasses. The procedure was repeated 4 – 5 times. MEF were centrifuged at 1000 rpm for 4 min and supernatant was discarded. MEF were cultured in high glucose DMEM supplemented with 10 % FCS, 2 mM L-Glutamine, 100 U/ml penicillin and 100 µg/ml streptomycin (later referenced to as MEF medium). Cells were resuspended in MEF medium and distributed onto 15 cm TCP dishes (2.5 embryos per 15 cm dish). A partial medium change was done every 2 days. MEF were expanded 2 times. To this end, medium was discarded and cells were washed 2 times with 1x PBS. Afterwards, 4 ml of 1x trypsin was added onto MEF and dishes were incubated for 4 min at 37°C. Trypsin was stopped with 6 ml of MEF medium. Cells were collected in Falcon tubes and centrifuged at 1000 rpm for 4 min. MEF were resuspended in fresh MEF medium. For further culture, cells were distributed equally in a 1:4 to 1:6 ratio over 15 cm TCP plates and incubated at 37°C. For inactivation, MEF were pooled in Falcon tubes and cells were kept on ice until irradiation. Cells were γ-irradiated with 30 Gy (3000 rads) and immediately put back on ice. MEF were centrifuged at 1000 rpm for 4 min and resuspended in freezing medium (FCS + 10% DMSO) at a cell concentration of 4×10^6 cell/ml. MEF were distributed over cryo vials (NUNC) and transferred into -80°C. For long term storage cryo vials were transferred into liquid nitrogen 24h after MEF harvest.

2.2.1.7 Culture of iPSC

2.2.1.7.1 Maintenance culture of iPSC on MEF

Patient derived iPSC were cultured on an inactivated MEF monolayer in iPSC medium (Table 3) (Sontag et al., 2017a). Medium was refreshed daily. Passage was performed every 4 – 5 days. To this end, MEF were thawed and seeded in 6 well TCP plates 24 h before passing iPSC. MEF were seeded at a cell density of 2.6×10^5 to 3×10^5 cells/cm^2 on gelatin (Sigma, #G-1890) coated 6 well plates. For passaging iPSC, old medium was discarded and 1 ml of collagenase IV (Gibco, #17104-019, 1 mg/ml dissolved in KO-DMEM) was added to each well. Cells were

incubated with collagenase IV for 60 min at 37°C. Progress of colony detachment was observed through the microscope. Collagenase treatment was stopped with 2 ml KO-DMEM per well when edges of colonies began to roll up. Wells were rinsed gently and cell clumps were collected in Falcon tube. Cells were centrifuged for 4 min at 1000 rpm, supernatant was discarded and cell clumps were resuspended in 1 ml iPSC medium. MEF medium was aspirated from MEF coated plates and each well was washed with 1x PBS. PBS was discarded directly and 2 ml iPSC medium per well was added. iPSC clumps were equally distributed over MEF coated plates and mixed gently by rocking the plate back, forth, left, right.

Table 3. Composition iPSC medium

Reagent	Volume
KO-DMEM	192 ml
KO-Serum replacement	50 ml
Penicillin/streptomycin	2.5 ml
L-Glutamine	2.5 ml
Minimal non-essential amino acids	2.5 ml
β-mercaptoethanol	500 µl
bFGF	25µl

2.2.1.7.2 Culture of iPSC on vitronectin for next generation sequencing (NGS) and immunofluorescence staining

To analyze iPSC clones for additional mutations next generation sequencing (NGS) analysis was performed. To this end, iPSC were cultured under feeder free conditions for 2 passages. For feeder free culture of iPSC, JAK2 and JAK2V617F iPSC had to be transferred from MEF coated onto vitronectin coated plates (Ludwig et al., 2006). To this end, 6 well plates were coated with 2 ml of vitronectin (Stemcell Technologies, 250 µl diluted in 12 ml 1x PBS, final concentration 5 µg/ml, 0.5

µg/cm^2) for 1h at room temperature. While coating was performed, iPSC were passaged with collagenase IV for 1h at 37°C and detached with KO-DMEM afterwards. To deplete MEF from detached iPSC, clumps were let to settle via gravity. Consequently, single MEF were left in the supernatant and iPSC clumps accumulated at the bottom of the Falcon tube. Supernatant was discarded up to 5 ml. This procedure was repeated twice. After the last washing step cells were centrifuged at 1000 rpm for 4 min and resuspended in iPSbrew. Excess vitronectin was discarded from the plate and 1.5 ml per well of iPSbrew was added. iPSC were distributed equally over the wells. Medium was refreshed every 24h. iPSC were cultured for 4 – 5 days until passaged again. For passages in feeder free conditions, supernatant was discarded and 1 ml of 0.5 nM EDTA was added. Cells were incubated for 2 – 3 min at 37°C. When colonies stared to disintegrate, EDTA was discarded completely, 1 ml per well iPSbrew was added and colonies were detached. Clumps were seeded onto a new vitronectin coated plate. After 2 passages in vitronectin iPSC lost most of the MEF. iPSC were detached with 1x trypsin/EDTA and gDNA was isolated with the NucleoSpin$^®$ Tissue Kit (Machery Nagel).

For immunofluorescence iPSC were seeded onto vitronectin coated glass slides in 4 well TCP after MEF depletion. iPSC were cultured for 4 – 5 days, depending on the cell density, with medium changes every 24h. Afterwards, cells were processed for immunofluorescence as described in chapter 2.2.1.9.

2.2.1.8 Embryoid body (EB) assay

The EB assays were done as described previously (Qin et al., 2014). Briefly, iPSC were cultured on MEF for 3 – 4 days. On the day of EB Assay (d0), iPSC were detached by adding 1 ml of collagenase IV per well of a 6 well plate and incubated at 37°C for 60 min. When colony edges started to roll up, 2 ml of KO-DMEM per well of a 6 well plate was added. Wells were rinsed gently and cell clumps were collected in a 50 ml conical tube. A sample of undifferentiated iPSC was taken (d0). MEF were

depleted from iPSC by letting big aggregates sediment for 10 min before carefully aspirating the supernatant up to 3 – 5ml. KO-DMEM was added and suspension was centrifuged at 900 rpm for 4 min. Supernatant was discarded and EB were resuspended in 10 – 12 ml EB medium (Table 4). EB suspension was transferred to an ultra-low attachment (ULA) plate (Corning). Medium was changed every second day starting with day 1. Therefore, EB suspension was collected in a 15 ml Falcon tube and EB were left to settle by gravity for 30 min. Supernatant was discarded up to 2 ml and fresh EB medium was added. EB were replated on the same ULA plate as before. EB were cultured in suspension for 7 days. On day 7, a medium change was performed as described. Cell suspension was divided into further culture and a sample for RNA isolation. For further culture EB were seeded onto a gelatin coated (0.1 % gelatin) tissue culture dish. Adherent EB were cultured for another 7 or 14 days. Medium changes were done every second day. Morphology was checked under the microscope and pictures were taken with an EVOS microscope. At the end of differentiation, cells were washed twice with 1x PBS. 0.05 % trypsin/EDTA solution was added and cells were incubated at 37°C for 2 – 5 min. Trypsinization was stopped with EB medium. Cells were collected in a Falcon tube and centrifuged at 900 rpm for 4 min. Supernatant was removed and pellet was processed for RNA isolation and RT-qPCR as described in chapter 2.2.2.5.

Table 4. Composition EB medium

Reagent	Volume
KO-DMEM	192 ml
FCS (LONZA)	50 ml
Penicillin/streptomycin	2.5 ml
L-Glutamine	2.5 ml
Minimal non-essential amino acids	2.5 ml
β-mercaptoethanol	500 µl

2.2.1.9 Immunofluorescence staining and microscopy

For immunofluorescence staining, iPSC were cultured on vitronection for 3 – 4 days (chapter 2.2.1.7.2). On the 1st day, iPSC were fixed with PFA for 20 min at room temperature followed by 3 washing steps with PBS for 5 min. Next, blocking was performed with goat serum for 30 – 40 min at room temperature followed by an overnight incubation with the primary antibodies (TRA 1-60, dilution in PBS, Table 5). On the 2nd day, cells were washed 3x for 10 – 15 min with PBS at room temperature. Next, cells were incubated with secondary antibodies for 1h at room temperature followed by another 3x washing step for 5 min with PBS. For intracellular staining, OCT4 antibody was diluted in in 0.1 % TritonX100 (in PBS) and cells were incubated overnight at 4 °C. On the 3rd day, cells were washed as described on day 2 with PBS and secondary antibody for OCT4 was diluted in 0.1 % TritonX100 (in PBS) and added to the cells for 1h at room temperature. Following 3x 5 min washing steps cells were stained with DAPI at a dilution of 1:400,000 (5 µg/ml) in 0.1 % TritonX100 (in PBS) for 15 min. Finally, cells were washed once for 1 min with PBS and 1 drop of mounting solution (Dako) was added onto a glass slide. Cover slip were removed carefully from the well, flipped upside down and put onto glass slide. Mounting solution was set to dry at room temperature for 10 – 20 min. Fluorescence was observed with an Axiovert 200 microscope (Carl Zeiss). Imaging processing was done using Image J 1.46r (National Institute of Health) and Adobe Photoshop CS2 (Adobe Systems Inc.).

Table 5. Primary antibodies used for immunofluorescence staining

Antigen	Clone	Species	Subtype	Company	Dilution
OCT-4	H-134	Rabbit	IgG	Santa Cruz	1:200
TRA 1-60		Mouse	IgM	Stemgen	1:200

Table 6. Secondary antibodies used for immunofluorescence staining

Antibody	Company	Dilution
Goat anti-mouse IgM Alexa 594	Invitrogen	1:200 in PBS
Goat anti-rabbit IgG FITC	Invitrogen	1:200 in 0.1 % Triton-X 100 in PBS

2.2.1.10 Hematopoietic differentiation of iPSC

The basis of the following protocol was the hematopoietic differentiation published by Kennedy et al. (2012). Furthermore, the detailed protocol for the hematopoietic differentiation used in this thesis was published by Sontag et al. (2017b). Suppliers and stock concentrations for every cytokine used in this differentiation are listed in Supplemental Table 1. In short, iPSC were expanded, cultured for 3 – 4 days and harvested via collagenase IV treatment when they reached 70 - 80 % confluency. iPSC colonies were collected in Falcon tubes. Suspension was left to stand for 10 min so that big EB settled via gravity while single MEF stayed in suspension. Supernatant was discarded and iPSC colonies were washed with KO-DMEM. Cells were centrifuged at 1000 rpm for 4 min and supernatant was discarded completely. For each differentiation day basal medium (Table 7) was supplemented with cytokines as shown in Figure 17. Cells were resuspended in 1 ml induction medium d0 containing 8 ng/ml bone morphogenetic protein 4 (BMP4). EB were resuspended thoroughly until EB contained 50 – 100 cells. If EB were in the desired range cells were transferred onto petri dishes and rest of induction d0 medium was added. Cells were cultured for 8 days at 37°C in a 5 % CO_2 and 5 % O_2 incubator (referred as hypoxic conditions). On day 1 of differentiation old medium was diluted 1:2 with fresh medium containing 8 ng/ml BMP4 and 10 ng/ml basic fibroblast growth factor (bFGF) (Figure 17). On day 2 of differentiation, EB were collected in 50 ml Falcon tubes and centrifuged at 800 rpm for 4 min. Supernatant was discarded completely. Cell pellet was resuspended gently in 10 - 15 ml induction medium d2 (10 ng/ml

bFGF, 8 ng/ml BMP4, 10 ng/ml vascular endothelial growth factor (VEGF), 10 ng/ml hyper-Interleukin 6 (hyper-IL6), 25 ng/ml insulin like growth factor (IGF1) and 100 ng/ml stem cell factor (SCF)) and transferred onto new petri dish. On day 4 of differentiation, medium change was performed as given on day 2 of differentiation and EB were resuspended in 10 - 15 ml induction medium d4 (10 ng/ml bFGF, 10 ng/ml VEGF, 10 ng/ml hyper-IL6, 25 ng/ml IGF1, 100 ng/ml SCF, 10 ng/ml Flt3L, 20 ng/ml thrombopoietin (TPO) and 30 ng/ml interleukin 3 (IL3)). On day 6 of differentiation, medium change was performed as given on day 4 of differentiation. EB were resuspended in 10 - 15 ml induction medium d6 (100 ng/ml SCF, 10 ng/ml Flt3L, 20 ng/ml TPO and 30 ng/ml IL3; later referred to as EHT medium) and transferred onto 6 well plates (coated with 0.1% gelatin). On day 8 of differentiation, most EB were adherent on the pate. Old medium was aspirated and replaced with new EHT medium and plates were transferred into normoxic conditions. Medium was changed until day 14 of differentiation every 2nd day as given on day 8. Afterwards, medium change was done every 3rd day. Hematopoietic progenitor cells (HPC) were harvested from day 14 of differentiation to day 30 of differentiation.
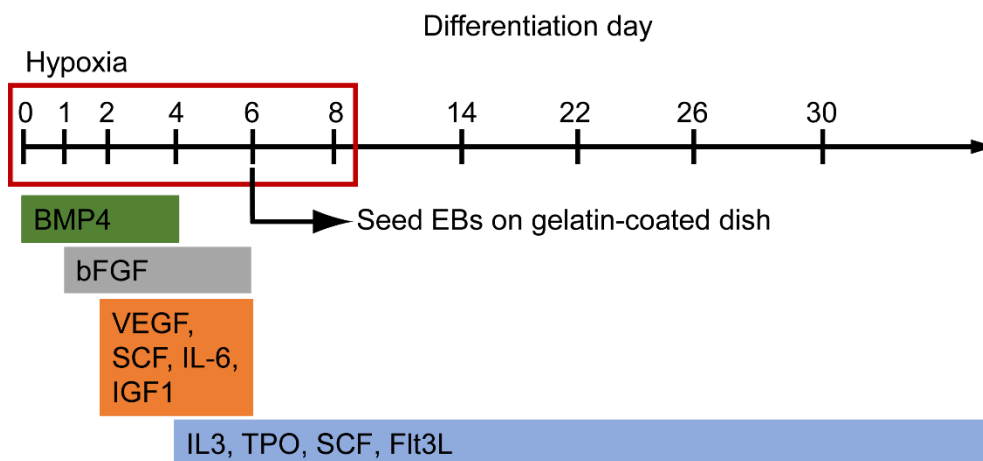

Figure 17. Scheme Hematopoietic Differentiation of iPSC

Differentiation time line and corresponding cytokine composition is shown (adapted from Kennedy et al. (2012) and Sontag et al. (2017b)). From day 6 of differentiation onwards cells are kept with FLT3L, TPO, SCF and IL3 (referred to as endothelial-to-hematopoietic transition (EHT) medium) to promote HPC development from the EB layer.

Table 7. Composition of basal medium for hematopoietic differentiation of iPSC

Reagent	Volume
StemPro34	250 ml
StemPro34 supplements	6.5 ml
Penicillin/streptomycin	2.5 ml
L-Glutamine	2.5 ml
Monothioglycerol (MTG)	1 ml
L-Ascorbic acid (L-AA)	250 µl

2.2.1.10.1   Digestion of EB layer

The EB layer of differentiating iPSC was used for magnetic activated cell sorting (MACS), cell cycle analysis by BrdU labeling or to analyze cells for IFNAR1 and IFNAR2 expression by flow cytometry. For these purposes, the EB layer was digested into single cells. The supernatant fraction was either discarded or used for IFNAR1/IFNAR2 analysis. 1 ml Accutase was added per well to the EB layer and incubated at 37°C for 20 min. Afterwards, 2 ml of KO-DMEM per well was added and used to detach EB layer fully from the TCP plate. Cell suspension was transferred into a fresh Falcon tube and thoroughly resuspended to fully isolate single cells from the layer. Cell suspension was passed over a 40 µm cell strainer (Greiner). Cell strainer and leftover tissue from the EB layer was discarded while single cell suspension was processed further.

2.2.1.11   Red blood cell differentiation

Red blood cell differentiation was done as described by Dorn et al. (2015). Briefly, iPSC-derived hematopoietic cells were harvested from hematopoietic differentiation cultures between day 22 and day 30 of differentiation. After passing the cells through

a 40 µm cell strainer (Corning), single cells were cultured in supplemented StemPro34. Cells were cultured with 100 ng/ml SCF, 30 ng/ml IL3 and 0.2 U/ml huEPO (human erythropoietin, cilag) according to the time range published by Dorn et al. (2015) and shown in Figure 18. Red blood cell differentiation was followed in time with flow cytometry analysis and cytospin preparations. During the first 8 days of red blood cell differentiation, cells were counted via Neubauer chamber and cell numbers were recorded for each condition.
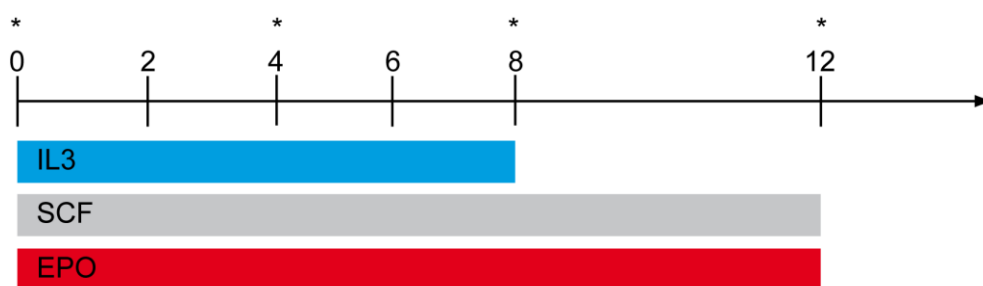
Figure 18. Scheme Red Blood Cell Differentiation

Red blood cell differentiation and time line is shown (adapted from Dorn et al. (2015)). Every 2nd day a partial medium. Change was performed and cells were expanded. Every 4th day medium was completely changed. Asterisks indicate time points when cells were used for flow cytometry and histological staining.

2.2.1.12 Cytospin and Histological Staining

After collection of iPSC-derived hematopoietic cells, cells were washed once with cold 1x PBS and counted via Neubauer counting chamber. Glass slides for cytospins were mounted with filter paper containing up to 6 holes, a corresponding cuvette was placed in a metal holder. First, 200 µl of PBS was added to each well of the cuvette and spun at 400 rpm for 4 min to wet the filter paper. Afterwards, 100.000 to 300.000 cells per well of the cuvette was added and spun at 400 rpm for 7 min. Slides were then extracted and air-dried for neutral benzidine/DiffQuik staining.

For the neutral benzidine/DiffQuik staining, cells were first fixed with methanol (Merck) for 4 min. Afterwards slides were placed for 2 min in a 1 % benzidine (Sigma, B-3503) solution following incubation for 1.5 min in a H_2O_2 solution. After washing with water, slides were transferred into the DiffQuik Red solution (Medion Grifols Diagnostics) and stained for 5x5 sec. Next, incubation with the DiffQuik Blue solution (Medion Grifols Diagnostics) was done for 30 sec. Slides were then transferred to water to wash off the excess staining solution und then dried. 1 drop of Entellan mounting medium (Merck #7960) was added onto each cytospin slide. Finally, cover slips were placed onto the mounting medium and air-dried. Cytospins were analyzed with a Leica DMRX microscope and the Leica Application Software suite v3.1.0.

2.2.1.13 Proliferation and cell cycle analysis

2.2.1.13.1 Carboxyfluorescein succinimidyl ester (CFSE) staining

For proliferation analysis iPSC-derived hematopoietic cells were labeled with CFSE. To this end, the supernatant fraction of differentiating iPSC was collected, stained with trypan blue and counted with a Neubauer counting chamber. iPSC-derived hematopoietic cells were washed twice with 1x PBS and afterwards cells were dissolved in 1 ml 1x PBS. CFSE (Stock 10 mM in DMSO) was diluted 1:10 in PBS followed by adding 1 µl (final concentration at 1 µM in medium) to the cells. Cells were incubated at 37°C for 5 min. Next, 30 µl FCS was added followed by a centrifugation step at 300xg for 4 min. Cells were washed 3 times with medium. Next, JAK2 and JAK2V617F iPSC-derived hematopoietic cells were seeded back onto the corresponding EB layer. A sample for 100 % CFSE labeled cells was taken after 2h of culture at 37°C. CFSE distribution over the daughter generations was analyzed after 3 days of culture by flow cytometry. Additionally, iPSC-derived hematopoietic cells were stained for additional surface markers as descried in chapter 2.2.2.3. Calculation of generations was done by FlowJo (V 7.8).

2.2.1.13.2   Bromodeoxyuridine (BrdU) staining

For cell cycle analysis APC BrdU Flow kit (BD, 552598) was used. BrdU pulse and staining was performed according to manufacturer's instructions. To this end, JAK2 and JAK2V617F EB layers were digested according to chapter 2.2.1.10.1 and seeded as single cells in EHT medium at a concentration of 1.5 x 10^6 cells/ml. Cells were pulsed with 10 µM BrdU and cultured for 1h at 37 °C. As control for BrdU incorporation, one part of the cells were kept without BrdU. Afterwards, cells were collected into FACS tubes and washed twice with FACS buffer (Table 12). Cells were stained for surface markers according to chapter 2.2.2.3. Afterwards, pellet was resuspended in 100 µl Cytofix/Cytoperm buffer (BD, 554722), vortexed and incubated for 30 min at room temperature. Cells were washed with 1 ml of 1x Perm/Wash buffer (BD, 554723) and spun at 400xg for 4 min. Next, pellet was resuspended in 100 µl Cytoperm Plus buffer (BD, 561651), vortexed, incubated for 10 min on ice followed by another washing step with 1 ml 1x Perm/Wash buffer. For re-fixation, cell pellet was resuspended in 100 µl Cytofix/Cytoperm buffer, vortexed and incubated for 5 min at room temperature. Following another washing step with 1 ml 1x Perm/Wash buffer, cell pellet was resuspended in 70 µl PBS/Mg (5mM MgCl$_2$), vortexed and 300 µg/ml DNase was added. Cells were mixed by pipetting up and down followed by and incubation at 37°C for 1h. Cells were washed with 1 ml 1x Perm/Wash buffer afterwards. Next, pellet was resuspended in 50 µl FACS buffer, containing 1:100 diluted anti-BrdU-APC antibody and incubated 30 min at room temperature. After another washing step with 1 ml 1x Perm/Wash buffer cells were stained with 10 µl 7AAD (BD) for 5 min on ice. 500 µl FACS was added and cells were analyzed by flow cytometry (FACS Canto II).

2.2.1.14   Magnetic activated cell sorting (MACS) for CD34$^+$ cells

For magnetic activated cell sorting (MACS) EB layer was digested as described in chapter 2.2.1.10.1. Cell number was determined manually by using trypan blue

staining and a Neubauer counting chamber. For CD34$^+$ cell isolation CD34$^+$ magnetic bead kit (Miltenyi, 130-046-702) was used according to manufacturer's protocol. In short, cell suspension was centrifuged at 1000 rpm for 4 min and supernatant was discarded. Pellet was resuspended in 300 µl MACS buffer (Table 8) and 100 µl FcR blocking reagent was added. 100 µl of CD34 microbeads were added to the cells, vortexed and incubated for 30 min at 4°C. Cells were mixed every 5 min to ensure optimal binding of beads to the cells. Following an addition of 10 ml of MACS buffer, cells were centrifuged at 1000 rpm for 4 min. Supernatant was discarded completely and cells were resuspended in 500 µl MACS buffer. Magnetic separation was done with LS columns (Miltenyi, 130-042-401). Columns were placed in a magnetic field and rinsed 3 times with 3 ml MACS buffer. Cell suspension was added onto column and flow through with unlabeled cells was discarded. Columns were washed 3 times with 3 ml MACS buffer. To elude cells, columns were removed from magnetic separator and placed in a fresh Falcon tube. Cells were flushed out by adding 5 ml of MACS buffer to the column and firmly pushing the plunger into the column. Cells were centrifuged again at 1000 rpm for 4 min and respuspended in EHT medium. Cells were cultured for 11 days. To monitor cell proliferation, medium was refreshed and cells were counted with a Neubauer counting chamber every 2 – 3 days. Analysis of cells by flow cytometry was done on day 0, 6 and 12 of culture.

Table 8. MACS buffer composition

Reagent	Volume
PBS (1x)	250 ml
FCS	12.5 ml
EDTA (0.5 M)	1 ml

2.2.1.15   Colony forming unit (CFU) assay

To evaluate the colony formation potential of iPSC-derived hematopoietic cells CFU assays were performed. Cells were harvested on day 18 of hematopoietic differentiation, passed through a 40 µm cell strainer, washed once with 1x PBS and then counted via Neubauer chamber. Cell number to be seeded was calculated according to the protocol given by manufacturer of MethoCult (Miltenyi). Cells were centrifuged (1000 rpm, 4 min) and resuspended in StemPro34 (without supplements) according to manufacturer's protocol. 300 µl of cell suspension was transferred into 3 ml of MethoCult (StemMACS$^{(TM)}$ HSC-CFU lite with EPO – human, Miltenyi, Order No. 130-091-281) and mixed via vortexing. Seeding of CFU assay was done in duplicates according to manufacturer's protocol. Analysis of CFU assays was done after 14 days of incubation at 37°C. Pictures of colonies were taken after 14 days of incubation. Individual colonies were picked and spun onto glass slides. Histological staining was performed afterwards.

2.2.1.16   Isolation of peripheral blood mononuclear cells (PBMNC) from healthy donors

Peripheral blood from healthy individuals was obtained from the department of transfusion medicine of the university hospital Aachen (UK Aachen). The samples were randomized and an ethical agreement with the healthy individuals was in place. Peripheral blood mononuclear cells (PBMNC) were isolated via a density gradient centrifugation with lymphocyte separation medium (LSM) using Miltenyi Biotech's protocol. In short, EDTA vails containing peripheral blood were first diluted with twice the blood volume with 1x PBS/EDTA. 15 ml LSM was transferred into a Falcon tube and overlaid with 35 ml diluted peripheral blood. Next, a centrifugation step at 2000 rpm for 20 min without brake was performed. At the interface of blood and LSM a white ring of mononuclear cells formed. Mononuclear cells were carefully aspirated

and transferred into a new Falcon tube. Cells were washed with 1x PBS/EDTA twice. Therefore, cells were centrifuged at 1000 rpm for 10 min and the supernatant was discarded. Next, PBMNC were resuspended in RPMI + 10 % FCS. Cells were stained with trypan blue and counted with a Neubauer counting chamber. Finally, PBMNC were cultured in RPMI + 10 % FCS without cytokines for 4h. During 4h of culture cells were stimulated with IFNα (chapter 2.2.1.17). Afterwards, samples were processed either for RT-qPCR (chapter 2.2.2.5) or Western Blot (chapter 2.2.2.7).

2.2.1.17 Interferon α (IFNα) treatment of BM cells, iPSC-derived HPC, patient and healthy PBMNC

Treatment of murine BM cells was done for 3 – 4 days with the indicated concentrations of murine IFNα (Miltenyi Biotech, 130-093-131, stock concentration 1×10^7 U/ml in 1x PBS). Untreated BM cells were used as control. Human IFNα (Immunotools, recombinant human Interferon-alpha 2 beta, stock concentration 2×10^7 U/ml in H_2O) was used to treat iPSC-derived hematopoietic cells and primary PBMNC. Samples for RT-qPCR were treated with 200 U/ml human IFNα for 4h in RPMI + 10 % FCS. Samples used for Western Blots were starved in RPMI for 4h followed by a pulse of 2000 U/ml human IFNα for 30 min.

2.2.1.18 Tyrosine kinase inhibitor (TKI) treatment of BM cells

Treatment of oncogene expressing murine BM cells with TKI was done for 3 – 4 days. TKI were refreshed with medium every 24h. BcrAbl$^+$ murine BM cells were treated with Imatinib (LC Laboratories, stock concentration 10 mM in DMSO). JAK2V617F$^+$ murine BM cells were treated with Ruxolitinib (LC Laboratories, stock concentration 10 mM in DMSO).

2.2.2 Biochemical assays

2.2.2.1 MTT assay

To evaluate the toxicity of IFNα and Ruxolitinib on iPSC-derived hematopoietic cells MTT assays were performed (Han et al., 2016). iPSC-derived hematopoietic cells were harvested and washed once with 1x PBS. Cells were diluted to a cell concentration of 2×10^5 cells in 90 µl in EHT medium. Measurements were performed in triplicates. IFNα or Ruxolitinib was diluted with serum free medium (SFM). 10 µl of IFNα or Ruxolitinib was added per well of a 96 well plate first, afterwards 90 µl of cell suspension was added to the each well. Cells were incubated at 37°C for 2 – 4 days. As blank SFM was used and incubated for the same time without any drug addition. Afterwards, 10 µl MTT was added and incubated for 4h at 37°C. Next, 100 µl Isopropanol-HCL was added to lyse the cells. Colorimetric analysis was done in a plate reader at 550 nm. The mean optical density from each concentration was calculated and blank was deducted from each value. The resulting values together with the mean standard deviation for each value were put into a graph with GraphPad Prism v6.

2.2.2.2 Allele specific Polymerase Chain Reaction (PCR) for JAK2V617F allele

To detect JAK2V617F in patient derived iPSC an allele specific PCR was performed in collaboration with Kristina Feldberg (Department of Hematology, Oncology, Hemostaseology, and Stem Cell Transplantation, Faculty of Medicine, RWTH Aachen University, Aachen, Germany). To this end, 2 PCR reactions were set up with the primers listed in Supplemental Table 5 (Jones et al., 2005). In a first PCR 10 µM of JAK2 forward and reverse primer were mixed with 10x RED Taq buffer and, 10 mM dNTP mix and RED Taq polymerase (Quiagen). In a second reaction, JAK2 and JAK2V617F primer were mixed with RED Taq buffer, dNTP mix and RED Taq

Polymerase. 200 ng of DNA was used per PCR. The PCR was run in a PCR cycler (Eppendorf) with the program shown in Table 9. PCR product was loaded onto a 3 % agarose gel and set to separate for 30 min at 100 V.

Table 9. PCR program allele specific PCR JAK2V617F

Temperature	Time	Cycles
94°C	5 min	1
94°C	30 sec	
58°C	30 sec	34
72°C	1 min	
72°C	5 min	1
10°C	∞	∞

2.2.2.3 Flow Cytometry and Sorting

To analyze the surface marker expression during hematopoietic differentiation of iPSC or monitor oncogene expressing cells during IFNα/TKI treatment, cultured cells were subjected to flow cytometry (Sontag et al. (2017a), Chauvistre et al. (2014)). The harvested cells were centrifuged for 4 min at 1400 rpm and washed once with PBS. Cells were stained with fluorochrome-conjugated antibodies (Table 10,

Table 11). Antibodies used for iPSC-derived hematopoietic cells were diluted 1:100 in 50 μl FACS staining buffer (Table 12). Antibodies used for murine BM cells were diluted 1:400 in 50 μl FACS staining buffer. Next cells were stained for flow cytometry for 30 min at 4°C followed by washing steps with FACS staining buffer. For flow cytometry cells were resuspended in 200 μl FACS staining buffer and measured on a FACS Canto II device (BD Biosciences). The obtained data were analyzed with FlowJo software (Tree Star, Inc.). As control, a part of the cells was stained with an IgG isotype control that was conjugated to the same fluorochrome as the specific antibody. This staining served as a control for unspecific binding. For

sorting iPSC-derived myeloid cell populations cells were resuspended in 500 µl FACS buffer. Additional FACS tubes with FACS buffer were prepared. Cells were sorted on a FACS Aria device (BD Biosciences). Sorted cells were spun on glass slides and stained for phenotypical analyses as described in chapter 2.2.1.12.

Table 10. Flow cytometry antibodies used for murine BM cell culture

Surface Marker	Fluorochrome	Clone	Company	Dilution used
Gr1	PerCPCy5.5	RB6-8C5	BD	1:400
ckit	PeCy7	ACK2	eBioscience	1:400

Table 11. Flow cytometry antibodies used for detection of human hematopoietic cells from human iPSC

Surface Marker	Fluorochrome	Clone	Company	Dilution used
CD3	PerCP-Cy5.5	UCHT1	BD	1:100
CD14	PE	MOP9	BD	1:100
CD14	PE	9F5	BD	1:100
CD19	PE-Vio770	AC145	Miltenyi	1:100
CD31	PE	WM59	BD	1:100
CD33	APC	AC104.3E3	Miltenyi	1:100
CD34	APC	581	BD	1:100
CD43	FITC	1G10	BD	1:100
CD43	Biotin	DF-T1	Miltenyi	1:100
CD45	APC-Vio770	5B1	Miltenyi	1:100
CD61	FITC	VI-PL2	eBioscience	1:100
CD66b	PE	G10F5	BD	1:100
CD66b	PerCPCy5.5	G10F6	BD	1:100
CD71	FITC	OKT9	eBioscience	1:100
CD117	APC	M5E2	BD	1:100
CD123	FITC	HIB19	BD	1:50
CD123	PE-Cy7	104D2	eBioscience	1:100
CD235a	PE	HIR2 (GA-	eBioscience	1:1000

		R2)		
FcεR	FITC	CRA1	Miltenyi	1:100
HLADR	PECy7	LN3	eBioscience	1:100
HLADR	FITC	LN3	eBioscience	1:100
IFNAR1	FITC	MMHAR-1	PBL Assay Science	1:10 (50 µl volume for staining)
IFNAR2	PE	MMHAR-2	PBL Assay Science	1:25 (50 µl volume for staining)

Table 12. FACS Buffer Composition

Reagent	Volume
PBS (1x)	500 ml
BSA	2.5 g
EDTA (0.5 M)	5 ml

2.2.2.4 Live/dead Staining for flow cytometry

Live/dead staining was performed for murine BM cells and iPSC-derived hematopoietic cells. To this end, cells were harvested and washed once with FACS buffer (Table 12). Cells were stained with Zombie Aqua (BioLegend, 1:400 in 1x PBS) for 30 min at room temperature in the dark. Next, cells were washed with FACS buffer and additional surface markers were stained according to chapter 2.2.2.3. Finally, cells were analyzed by flow cytometry.

2.2.2.5 RNA isolation and quantitative Real-Rime Polymerase Chain Reaction (qRT-PCR)

RNA isolation and RT-qPCR was performed as described previously (Chauvistre et al., 2014). To analyze the expression of IFNα target genes, RNA isolation was performed with a NucleoSpin RNA II Kit (Machery-Nagel). The RNA concentration was then determined using a Nanodrop device. According to the manufactures protocol cDNA synthesis was performed using a High Capacity cDNA Reverse Transcription Kit (Applied Biosystems). 5 ng of cDNA was applied as template for quantitative PCR (qPCR). To this end, Syber Green (Fast SYBR Green Master Mix, Applied Biosystems) and primers (Supplemental Table 4 and Supplemental Table 6) and 5 ng cDNA were mixed according to Table 13. Quantitative PCR was performed using a StepOnePlus Real Time PCR System (Applied Biosystems) and the standard program. The data was analyzed with the StepOnePlus Software v2.1 (Applied Biosystems) with Glyceraldehyde 3-phosphate dehydrogenase (GAPDH) for normalization. After normalization, the relative expression to GAPDH was plotted.

For normalization: $\Delta C_{T\ (sample)} = C_T\ Mean_{(Sample)} - C_T\ Mean_{(GAPDH)}$

For fold GAPDH: $2^{-\Delta CT\ (sample)}$

Table 13. qPCR Master Mix

Reagent	Volume
Syber Green	5 µl
PrimerPair	0.5 µl
Water	2.5 µl
cDNA	2 µl

2.2.2.6 Protein extraction and Bradford Assay

For protein extraction JAK2 and JAK2V617F iPSC-derived hematopoietic cells were harvested on day 26 – 34 of hematopoietic differentiation. Cell suspension was collected in a Falcon tube, cells were counted and centrifuged for 4 min at 1400 rpm at 4°C. Cells were washed once with 1x PBS followed by resuspension in 50 µl – 100 µl lysis buffer (Supplemental Table 3). Cells were vortexed until a homogeneous solution was obtained. Cell suspension was kept on ice for 45 – 60 min and vortexed every 10 min. Next, tubes were centrifuged for 10 min at 13000xg at 4°C (Sigma, 3K15). Supernatant was transferred into a fresh Eppendorf tube and kept at -80°C.

To calculate the protein concentration of harvested iPSC-derived hematopoietic cells a Bradford assay was performed (Bradford, 1976). Protein samples were diluted in distilled water. BSA (stock concentration 1 mg/ml) standards were prepared as shown in Table 14. Bradford solution (BioRad, 500-0006) was diluted 1:5 with distilled water. BSA standards (Table 14) and protein samples were diluted 1:1 with Bradford working solution and incubated for 1 min at room temperature. Absorption was measured at 595 nm with a photometer. Protein concentration was calculated with equation from linear regression of BSA standards.

Table 14. BSA protein standards

Standard	BSA stock solution	distilled water
Blank	0	1 ml
2.5 µg/ml	2.5 µl	997.5 µl
5 µg/ml	5 µl	995 µl
10 µg/ml	10 µl	990 µl
15 µg/ml	15 µl	985 µl
20 µg/ml	20 µl	980 µl
25 µg/ml	25 µl	975 µl

2.2.2.7 SDS-Page and Western Blot

SDS-PAGE was performed as described before (Chauvistre et al., 2014). Compositions of buffers used for SDS-PAGE (sodium dodecyl sulfate-polyacrylamide electrophoresis) are listed in Supplemental Table 8. Samples of iPSC derived hematopoietic cells for SDS-PAGE were taken on day 26 to 34 of hematopoietic differentiation. Total protein was extracted as described in chapter 0. Total protein amount was determined, mixed with 4x loading dye and boiled at 95°C for 5 min. 40 µg total protein were loaded per lane onto a 8 % SDS-gel (Table 17) and separated for 2h a 50 V per gel. A prestained protein ladder (PageRuler prestained Protein Ladder, Thermo Scientific) was used as marker. After SDS-PAGE the gels were soaked in 1x transfer buffer together with filter paper and the nitrocellulose membrane. Proteins were blotted onto a nitrocellulose membrane (45 µM, Thermo Scientific) for 2h at 60 mA per membrane using a semi-dry system (BioRad). Ponceau staining was used as loading control additional to the actin detection. The membranes were blocked after that with 10 % BSA in TBS-T for 2h at room temperature. For detection the primary antibodies are listed in Table 15 and secondary antibodies in Table 16. Membranes were incubated with primary antibodies over night at 4°C followed by 3 washing steps with TBS-T of 10 min each. Incubation with secondary antibodies was performed for 1h at room temperature followed by another 3x 10 min washing steps with TBS-T. Afterwards, membranes were incubated with ECL reagent (Super Signal West Pico Chemoluminescent Substrate, Thermo Scientific) for detection. Signal detection was performed with a LAS System. All antibodies were diluted in TBS-T containing 5 % BSA.

Table 15. List of primary antibodies for Western Blot

Antibody	Clone	Species	Company
STAT1	#9172	Rabbit	Cell Signaling
pSTAT1 (Tyr701)	#9171	Rabbit	Cell Signaling

Actin	AC-74	Mouse	Sigma

Table 16. List of secondary antibodies for Western Blot

Antibody	Clone	Species	Company
α-Rabbit IgG	NA934V	donkey	GE Healthcare
α-mouse IgG	NA931V	sheep	GE Healthcare

Table 17. Composition SDS-gels

	Reagent	Amount for 2 Gels
8 % Separation Gel	Distilled water	5.2 ml
	40 % acrylamide-mix	2.1 ml
	1.5 M Tris-HCl (ph 8,8)	2.5 ml
	10 % SDS	100 µl
	10 % APS	100 µl
	TEMED	6 µl
Stacking gel	Distilled water	3,61 ml
	40 % acrylamide-mix	620 µl
	1.0 M Tris-HCl (pH 8,8)	630 µl
	10 % SDS	50 µl
	10 % APS	50 µl
	TEMED	5 µl

2.2.2.8 Statistical analyses

Data is represented as mean ± standard deviation (SD). Statistical significance was analyzed by using a Mann-Whitney-U-Test or a two tailed, unpaired Student's t-Test (GraphPad Prism 6.0). Differences were considered significant (*) with p-values ≤ 0.05, very significant (**) with p-values ≤ 0.005 and highly significant (***) with p-values ≤ 0.001.

3 Results

3.1 Importance of IRF8 for the response to TKI and IFNα treatment in MPN

Among differentially expressed genes in CML patients vs. healthy patients, was the transcription factor interferon regulatory factor 8 (IRF8). In primary CD34^{+} cells from CML patients it was shown that IRF8 expression is low (Schmidt et al., 1998). Studies that overexpress IRF8 showed an inhibition of AML progression or BcrAbl induced MPN suggesting that IRF8 acts as a tumor suppressor gene in leukemia (Sharma et al. (2015), Hao and Ren (2000)). Indeed, low IRF8 expression seems to be the cause for the poor outcome of IFNα therapy (Schmidt et al., 1998). The open questions that remain are how IRF8 influences disease development and how IRF8 influences therapy outcome. Therefore, in the first part of the thesis the aim was to gain insight into (i) the efficacy of combined TKI and IFNα therapy in BcrAbl[+] and JAK2V617F[+] MPN and (ii) the importance of IRF8 for MPN development and therapy. BcrAbl induced CML has been exclusively studied in cell lines, like 32D cells or K562 cells (Barnes et al. (2005), Waight et al. (2014)). However, to better reflect the absence or presence of IRF8 on (i) BcrAbl^{+} cells and (ii) TKI or IFNα treatment murine bone marrow (BM) cells were retrovirally transduced with BcrAbl in this thesis.

3.1.1 Efficacy of combined therapy in CML

3.1.1.1 BcrAbl expression renders BM cells cytokine independent

32D cells transduced with oncogenes, like BcrAbl and JAK2V617F, lose their growth dependence on cytokines, mainly their dependence on IL3 (Barnes et al. (2005), Lu et al. (2005)). The first aim was to investigate whether the cytokine independence of BcrAbl overexpressing cells also applied to other hematopoietic cytokines in the

used culture system (Figure 15B). The second aim was to study whether primary BM cells overexpressing BcrAbl gained this cytokine independence.
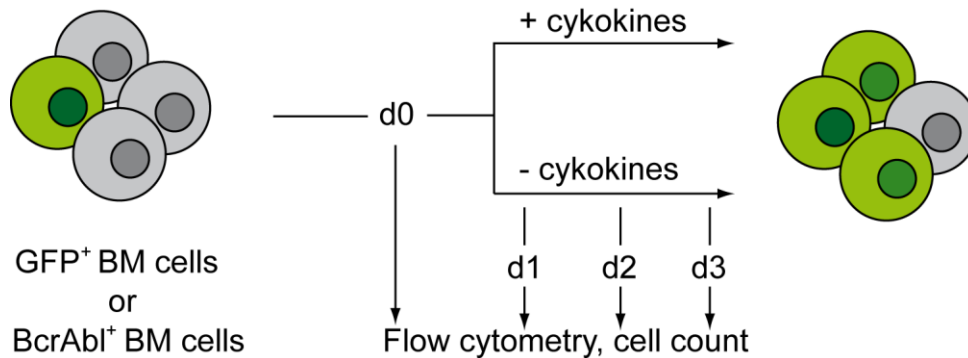

Figure 19. Cytokine independence of oncogene expressing cells

Murine BM cells were isolated, and retrovirally transduced as shown in Figure 15. After density gradient centrifugation on day 5 post BM isolation cells were seeded back and cultured further for another 3 days. Afterwards, cells were split (d0 of treatment) and cultured either with cytokines or without cytokines for 3 days. Every day medium was refreshed and cells were counted via an electronic cell counter. Transduced cells were quantified by flow cytometry as cells co-expressed GFP. Dead cells were excluded by staining cells with Zombie Aqua.

Murine BM cells transduced with BcrAbl or EV were split into cultures with and without cytokines (Figure 19). Cells were kept in culture for 3 days. Aliquots were taken daily to record cell counts quantify cell viability and GFP expression by flow cytometry. As shown in Figure 20A – B transduction efficiency of BM cells varied depending of the vector construct. Transduction efficacy for BcrAbl ranged from 26.5% of GFP+ cells in earlier experiments (Figure 20C, day 0 of culture) to 65% of GFP+ cells for later experiments. Transduction efficiency was between 10% of GFP+ cells and went up to 20% of GPF+ cells (Figure 20B).

Under cytokine supplementation the percentage of BcrAbl+ stayed constant during culture time (Figure 20C, blue). When cultured with cytokines empty vector also displayed a constant GFP expression level (Figure 20C, green). A live/dead analysis showed that the percentages of living and dead cells for BcrAbl and empty vector transduced BM cells stayed constant in the presence of cytokines (Supplemental

Figure 2). This suggests that the oncogene does not add an extra growth advantage of BcrAbl expressing cells over normal BM cells under cytokine supplementation.

In contrast, under cytokine withdrawal lead to an enrichment of BcrAbl⁺ cells after 24h of culture. On day 2 of culture the percentage of BcrAbl⁺ cells further enriched which was highly significant when compared to cytokine supplemented culture conditions (Figure 20C, red). The percentage of BcrAbl⁺ cells continued to increase until the end of the culture. Yet, without cytokines BM cells transduced with EV died during culture (Figure 20C, purple). Analysis of living and dead cells revealed that the increase BcrAbl⁺ cells was due to a severe drop of living cells (Supplemental Figure 2) suggesting that BcrAbl⁺ cells rather displayed a survival advantage in cytokine deprived culture. Only after 3 days of cytokine withdrawal, living cells for BcrAbl⁺ cells increased suggesting an outgrowth of BcrAbl⁺ cells (Supplemental Figure 2).
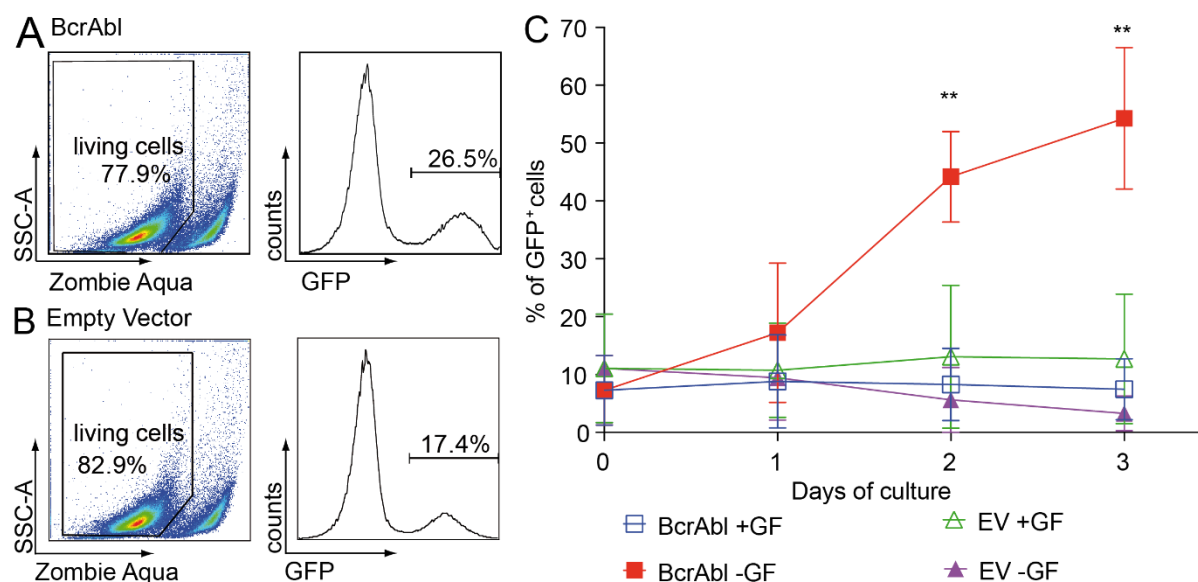

Figure 20. Overexpression of BcrAbl renders murine BM cells cytokine independent

Primary murine BM cells were isolated and cultured and transduced as shown in Figure 15 and Figure 19. Overexpression of BcrAbl in murine BM cells was done by retroviral transduction. As control, BM cells were transduced with an empty vector. Expression of BcrAbl was detected by GFP expression. (A – B) Live/dead staining was performed with Zombie Aqua. Living (Zombie Aqua⁻) cells were analyzed for their GFP expression to track transduced cells. Representative flow cytometry analyses on day 0 of treatment for (A) BcrAbl and (B) Empty vector are shown. (C) GFP⁺ cells were recorded for 3 days of cytokine withdrawal. The percentages of GFP⁺ cells for BcrAbl and empty vector with and without cytokines are shown. Per experiment one data point

was recorded. 3 independent experiments were performed (n = 3). For statistical analyses a Mann-Whitney-U-Test was performed. For each vector construct +GF and -GF were compared. Data points indicated with (*) show p-values ≤ 0.05, data points indicated with (**) show p-values ≤ 0.005.

Taken together, BcrAbl⁺ cells showed a survival advantage compared to control cells when cultured without cytokine supplementation. Only after 3 days of cytokine deprived culture showed BcrAbl⁺ cells a growth advantage. This could suggest that cytokine starvation might be one signal that oncogene expressing cells need for transformation and outgrowth in MPN pathogenesis. Thus, growth of BcrAbl rendered primary BM cells independent to other cytokines, not only IL3 as previous reports for cell lines overexpressing BcrAbl showed (Barnes et al., 2005). Notably, transduction rates for BcrAbl varied during experiments. Thus, for further experiments, the cytokine independence of BcrAbl⁺ cells was taken advantage of to increase BcrAbl⁺ cells before treatment with Imatinib or IFNα was performed.

3.1.1.1 Impact of Imatinib on BcrAbl expressing cells

Imatinib was the first drug in CML therapy that specifically reduced BcrAbl expressing cells without affecting healthy cells. Furthermore, Imatinib treatment showed fast responses and few side effects in CML patients (Kantarjian et al., 2003). For CML therapy, 5 µM is the clinically applied Imatinib concentration which aims at eradicating BcrAbl⁺ cells (Gotta et al., 2014). However, for combined treatment with IFNα later on, an Imatinib concentration needed to be determined were cells were inhibited, yet do not completely go into apoptosis. Therefore, Imatinib concentration for *in vitro* BM culture was titrated.

To this end, murine BM cells were transduced with BcrAbl as shown in Figure 21A. BcrAbl displayed an increased survival in cytokine deprived cultures (Figure 20C). Therefore, the survival properties of BcrAbl⁺ cells were taken advantage of to increase the percentage of BcrAbl⁺ cells by removal of cytokines for 2 days of culture (Figure 21A). Afterwards, BcrAbl⁺ BM cells were cultured with increasing

concentrations of Imatinib (Figure 22A). Imatinib was refreshed every 24h. Furthermore, cells were analyzed daily by counting with an electronic cell counter and were analyzed for GFP$^+$ cells via flow cytometry. Again, cells were stained with Zombie Aqua to exclude dead cells. Notably, starvation previous to Imatinib treatment increased the percentage of dead cells on day 0 of treatment (Supplemental Figure 3).
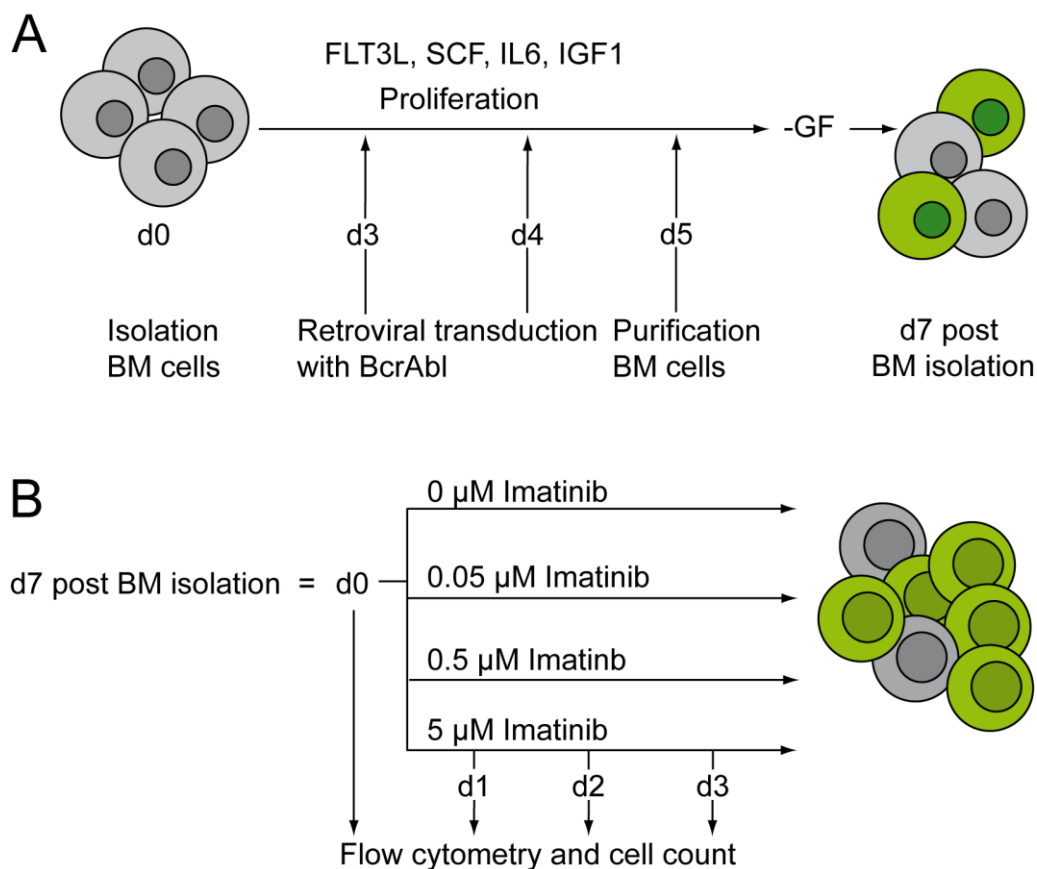

Figure 21. Schematic overview of Imatinib treatment

(A) Primary BM cells were isolated and cultured for 3 days with IL6, SCF, FLT3L and IGF-1. A density gradient centrifugation was performed on day 3 post isolation. BM cells were transduced with BcrAbl retrovirally on day 3 and 4 post isolation as shown in Figure 15. To enrich for BcrAbl expressing cells, BM cells were starved of cytokines for 2 days (-GF). (B) BcrAbl$^+$ BM cells were cultured without cytokines and treated with 0.05 μM, 0.5 μM and 5 μM Imatinib or were left untreated as control. Cells were counted with an electronic cell counter. Medium and Imatinib was refreshed daily. BcrAbl$^+$ cells were tracked via flow cytometry by recording GFP$^+$ cells. Dead cells were excluded via Zombie Aqua staining.

In line with previous experiments (Figure 20) untreated BcrAbl^{+} BM cells showed a cytokine independent survival as the percentage of BcrAbl^{+} cells increased from around 20% to 90% in 4 days of cytokine free culture (Figure 22A – B, 0 µM). Furthermore, the number of BcrAbl^{+} cells increased over time (Figure 22C) which would suggest that BcrAbl also conveys a growth advantage. This was also suggested by previous experiments as the percentage of BcrAbl^{+} living cells increased on day 3 of culture (Supplemental Figure 2A).

However, with Imatinib treatment BcrAbl^{+} cells displayed a dose dependent reduction of living cells (Supplemental Figure 3A). This was accompanied by a dose dependent decrease in the percentage of BcrAbl^{+} cells over time (Figure 22A and 5B). In detail, 0.05 µM Imatinib showed a minor inhibition of BcrAbl^{+} cells over time whereas 0.5 µM Imatinib showed a serve reduction of the percentage of BcrAbl^{+} cells compared to untreated cells. Furthermore, when treated with 5 µM Imatinib the percentage of BcrAbl^{+} cells was kept at the same level over time (Figure 22B). Notably, 5 µM Imatinib treatment is the only Imatinib concentration out of the tested concentrations with a significant reduction in BcrAbl^{+} cells compared to untreated cells.

Taken together, 5 µM Imatinib is the only concentration that reduced BcrAbl[+] cell number *in vitro*. However, to study the effect of IRF8 on TKI in combination with IFNα treatment 5 µM Imatinib is too strong. Thus, the Imatinib concentration for further *in vitro* studies was adjusted to 0.5 µM. 0.5 µM showed an inhibition of both cell growth and percentage of BcrAbl^{+} cells, which was not as pronounced as with 5 µM Imatinib.

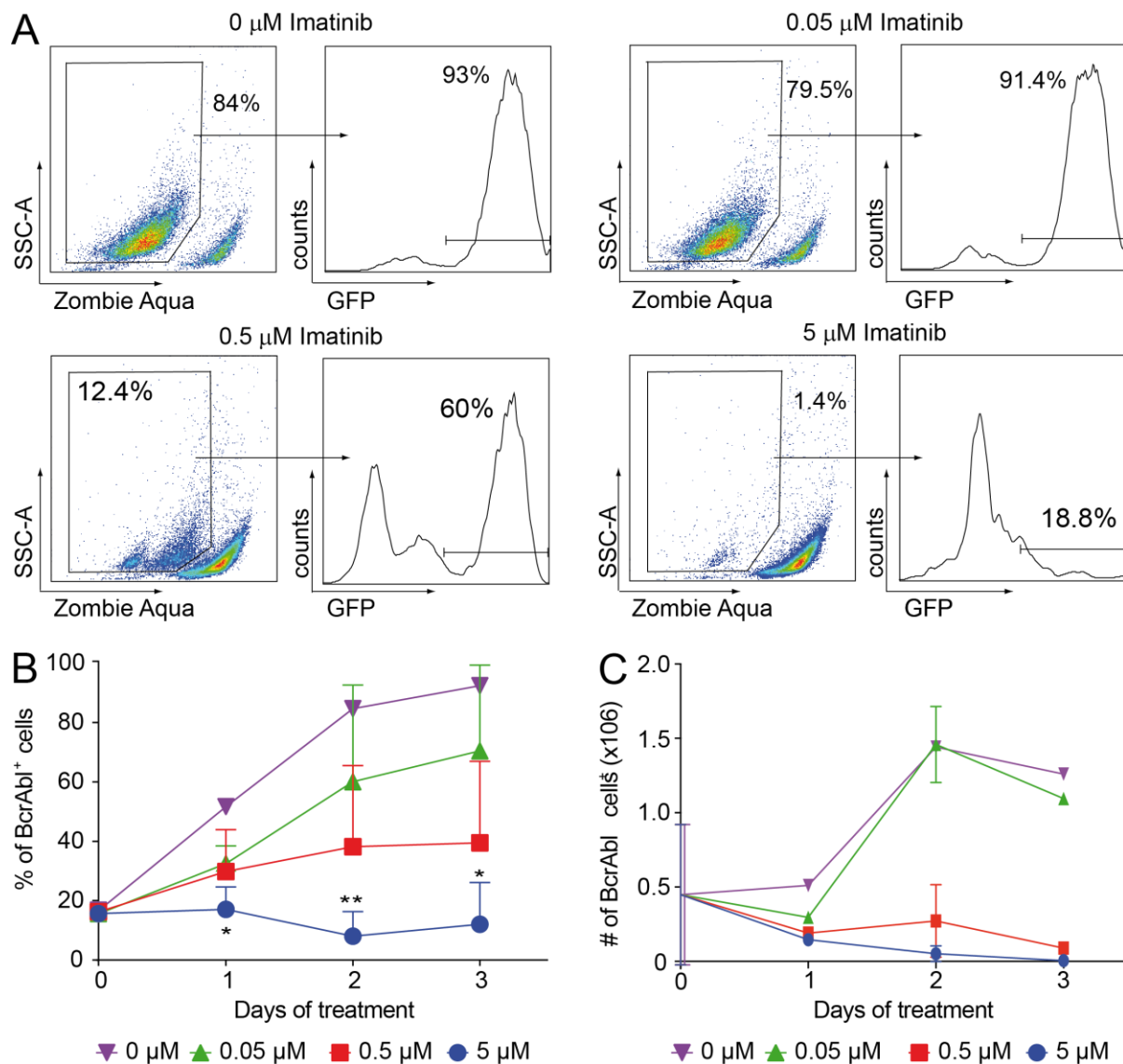Figure 22. 0.5 µM Imatinib inhibits BcrAbl+ cells *in vitro*

Transduced BcrAbl+ BM cells were treated with 5 µM, 0.5 µM and 0.05 µM Imatinib or left untreated. (A) Representative flow cytometry analyses from day 3 of Imatinib treatment. (B) The percentage of BcrAbl+ cells was analyzed by flow cytometry every day. (C) Number of BcrAbl+ cells was calculated by taking cell counts, % of living cells and % of GFP+ cells that was measured by flow cytometry in C into account (n = 3). Unpaired Student's T-test was used to determine significant decrease of BcrAbl+ cells by comparing Imatinib treatments to untreated (0 µM). Data points marked with (*) indicate samples with p-values ≤ 0.05; Data points marked (**) indicate samples with p-values ≤ 0.005.

3.1.1.2 Impact of IFNα treatment on BcrAbl expressing cells

In previous studies it was shown that IFNα treatment in CML patients have poor outcomes (Kantarjian et al., 2003). It was suggested that poor IFNα response is due to the low IRF8 expression. However, the signaling pathway of IFNα in CML and the role of IRF8 in IFNα signaling is still not completely understood. To study the impact of IFNα therapy in CML *in vitro* IFNα concentration for BcrAbl$^+$ cells needed to be determined first. As for Imatinib, this concentration should inhibit BcrAbl$^+$ cell growth *in vitro*, while not eradicating all proliferating cells and leaving a therapeutic window for Imatinib to act on cells for a combined treatment.

To this end, BM cells were isolated and retrovirally transduced with BcrAbl as shown in Figure 21A. Afterwards, BcrAbl$^+$ cells were treated with the indicated IFNα concentrations of 2 days (Supplemental Figure 4A). Additionally, cells were left untreated or were treated with 0.5 µM Imatinib. Medium change was performed daily. TKI and IFNα was refreshed along with the medium change. Cell counts were recorded with an electronic cell counter and BcrAbl$^+$ cells were quantified via flow cytometry over time. Zombie Aqua staining was used as live/dead staining.

When cells were left untreated BcrAbl$^+$ cells increased to 80% while Imatinib treated cells only showed 60% of BcrAbl$^+$ cells after 2 days of culture (Supplemental Figure 4B). These kinetics were in line with previous experiments (Figure 20 and Figure 22). All single treatments of IFNα displayed a minor and dose dependent reduction of the percentage of BcrAbl$^+$ cells compared to untreated cells on day 2 of treatment (Supplemental Figure 4B). When analyzing the total BcrAbl$^+$ cell numbers TKI treatment stunted BcrAbl cell growth slightly compared to untreated cells (Supplemental Figure 4C) which is in line with previous experiments (Figure 22C). 10^2 and 10^3 U/ml IFNα as single treatment rather increased BcrAbl$^+$ cell numbers compared to untreated (Supplemental Figure 4C). In contrast, 10^4 U/ml IFNα decreased the number of BcrAbl$^+$ cells compared to untreated cells. Surprisingly, when combining 0.5 µM Imatinib with 10^2 U/ml IFNα BcrAbl$^+$ cell numbers did not

change with the addition of Imatinib. Yet, combining Imatinib and 10^3 U/ml IFNα BcrAbl⁺ cell numbers decreased compared to untreated or single 10^3 U/ml IFNα treatment (Supplemental Figure 4C).

Taken together, IFNα dose was lowered to 10^3 U/ml for *in vitro* culture as this concentration showed a slight decrease in the percentage of BcrAbl⁺ BM cells as single treatment.

3.1.1.3 Impact of combined IFNα and Imatinib treatment on BcrAbl expressing cells

In clinics it is seen TKI induced faster responses in CML patients compared to IFNα. However, there are also studies that show that discontinuation of single TKI treatment results in relapses while IFNα showed longer remission times after discontinuation (Jabbour et al., 2011). Therefore, there are approaches of combining TKI and IFNα in CML therapy (Bunimovich-Mendrazitsky et al. (2018), Zhu et al. (2016)). It is hypothesized that TKI treatment eradicates proliferating BcrAbl⁺ cells. Additionally, IFNα would push quiescent BcrAbl⁺ initialing stem cells into cell cycle where IFNα or TKI can eradicate these cells (Essers et al., 2009).

To assess whether a synergistic effect of IFNα and Imatinib can be seen *in vitro,* the BcrAbl⁺ cells were cultured with both IFNα and Imatinib and the impact of the combined treatment was studied in comparison to single treatment (Figure 23A). To this end, BM cells were isolated, cultured and retrovirally transduced with BcrAbl as shown in Figure 21A. After enrichment of BcrAbl⁺ cells for 2 days BM cells were treated with 0.5 µM Imatinib or 10^3 U/ml IFNα as single treatment under cytokine withdrawal (Figure 23A). Furthermore, BcrAbl⁺ cells were treated with a combination of 0.5 µM Imatinib and 10^3 U/ml IFNα for 3 days. As control BcrAbl⁺ cells were left

untreated. Medium, IFNα and Imatinib were refreshed daily. Additionally, cells were counted via an electronic cell counter and samples for flow cytometry were taken. For flow cytometry cells were stained with Zombie Aqua to exclude dead cells.

Again, untreated BcrAbl$^+$ cells expanded without cytokine supplementation over the course of 3 days of culture (Figure 23B). In contrast, when treated with 0.5 µM Imatinib BcrAbl$^+$ cells were kept at initial levels in the first 24h of culture. In line with previous experiments (Figure 22) 0.5 µM Imatinib reduced BcrAbl$^+$ cells after 3 days of Imatinib treatment. Compared to untreated cells BcrAbl$^+$ cells showed a highly significant reduction of cell numbers for all the tested time points. Single IFNα treatment showed a slight increase in BcrAbl$^+$ cell number compared to day 0 of treatment. However, IFNα still significantly reduced BcrAbl$^+$ cells over the culture time (Figure 23B). The combination of TKI and IFNα treatment did show the same trend as for the single treatments, however reduction of cell numbers was stronger than for IFNα treatment alone at the endpoint of the culture. Notably, 0.5 µM Imatinib inhibited BcrAbl$^+$ cells too strong. Therefore, an adjustment of the Imatinib concentration was made (Supplemental Figure 5). For subsequent experiments Imatinib concentration was adjusted to 0.3 µM.
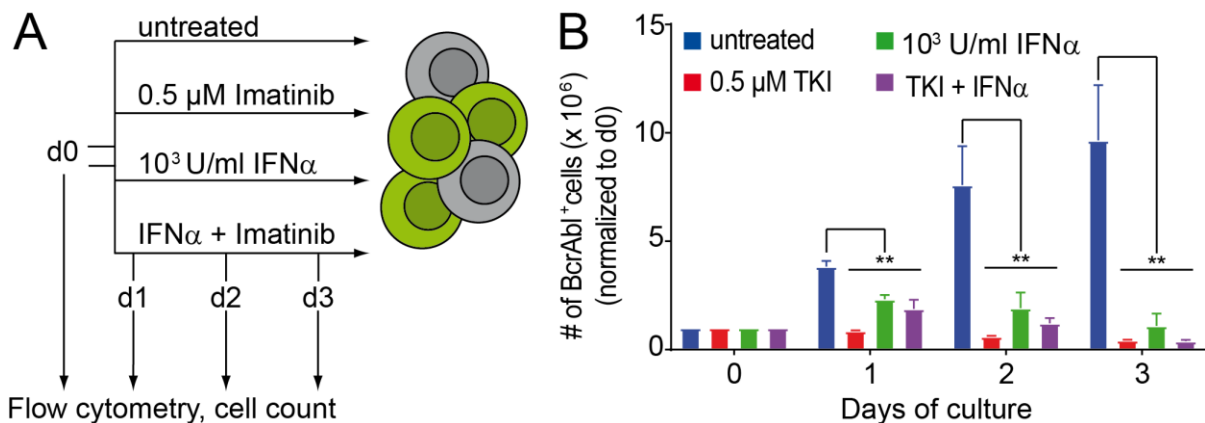

Figure 23. Imatinib and IFNα alone inhibit BcrAbl$^+$ cell growth too strongly

(A) Primary BM cells were isolated and cultured with FLT3L, IL6, SCF and IGF-1 for 3 days. After density centrifugation cells were transduced with BcrAbl in day -5 and -4 of culture. BcrAbl$^+$ cells were enriched by cytokine withdrawal for 2 days followed by treatment with 0.5 µM Imatinib and/or 10^3 U/ml IFNα for another 3 days under cytokine withdrawal. Untreated cells were used as control. Medium along with Imatinib and IFNα was refreshed daily. Cells were counted with an electronic cell counter and analyzed for GFP expression via flow

cytometry. Additionally, cells were stained with Zombie Aqua to exclude dead cells. (B) The number of BcrAbl$^+$ cells normalized to day 0 of culture is shown. To this end, cell counts for each day were multiplied by the percentage of GFP$^+$ cells from flow cytometric analyses. Afterwards cells were normalized to day 0 of culture. Data represent mean ± standard deviation (n = 3). For statistical analysis Mann-Whitney-U test was performed. TKI, IFNα and combined treatment was compared to untreated. Data points marked with (*) indicate samples with p-values ≤ 0.05; Data points marked (**) indicate samples with p-values ≤ 0.005.

In summary, IFNα significantly inhibits BcrAbl$^+$ cells as single treatment. 0.5 µM Imatinib strongly inhibited the number of BcrAbl$^+$ cells. However, for studying the combined effect of Imatinib and IFNα 0.5 µM Imatinib does not leave a wide enough therapeutic window for IFNα to act. Therefore, Imatinib concentration needed to be lowered again to 0.3 µM Imatinib for *in vitro* culture.

3.1.2 IRF8 and CML therapy

3.1.2.1 Lack of IRF8 amplified CML phenotype

Previous studies investigated CML pathogenesis solely in cell lines. Mouse models have the added advantage that KO mice can be generated the influence of transcription factors on disease pathogenesis can be investigated. Therefore, in a first step, the importance of IRF8 as a tumor suppressor was investigated in BcrAbl$^+$ cells. To this end, IRF8$^{+/+}$ and IRF8$^{-/-}$ BM cells were isolated and transduced with BcrAbl as shown in Figure 21A. Cells were cultured without cytokines and BcrAbl$^+$ cells were analyzed daily with flow cytometry. Cells were counted daily with an electronic cell counter (Figure 24A). Again, dead cells were excluded via Zombie Aqua staining in flow cytometry.

In line with previous experiments (Figure 20), IRF8$^{+/+}$ BM cells gained a cytokine independence when overexpressing BcrAbl (Figure 24B). Additionally, IRF8$^{-/-}$ BM cells also gained cytokine independence when overexpressing BcrAbl. Interestingly, IRF8$^{-/-}$ BcrAbl$^+$ cells displayed a significantly higher expansion in comparison to their IRF8$^{+/+}$ counterpart (Figure 24B) suggesting that IRF8 regulates the proliferation in BM cells. Therefore, it is suggested the IRF8 acts as a tumor

suppressor in murine BM cells. The absence of IRF8 in combination with BcrAbl overexpression deregulates the proliferation of BM cells.
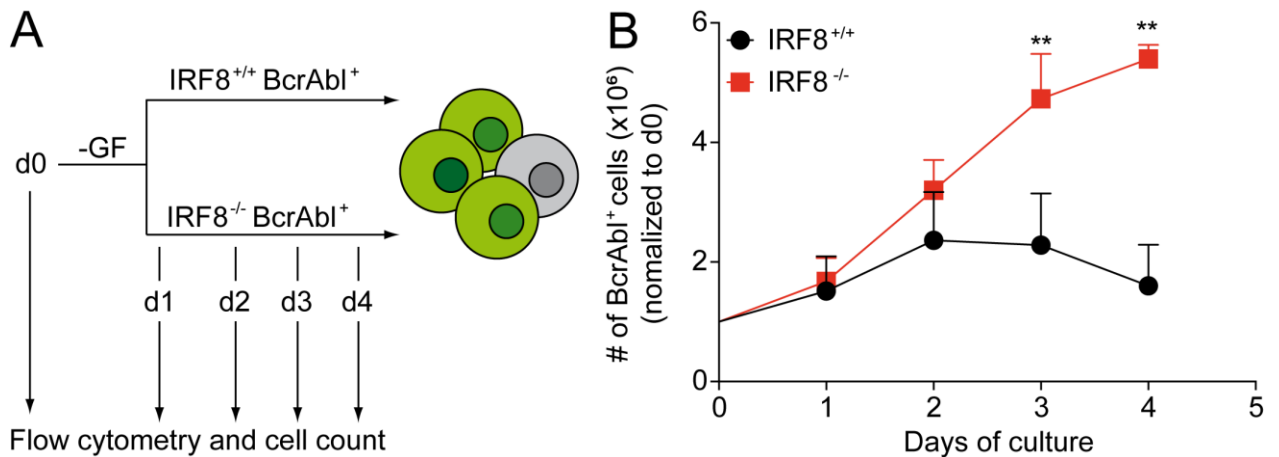

Figure 24. IRF8$^{-/-}$ BcrAbl$^+$ cells display a higher expansion than IRF8$^{+/+}$ BcrAbl$^+$ cells

BM cells of IRF8$^{+/+}$ and IRF8$^{-/-}$ mice were isolated and transduced with BcrAbl as shown in Figure 21A. (A) Afterwards, cells were deprived of cytokines (-GF) and cultured for 4 days. Medium was refreshed daily. Cells were counted with an electronic cell counter. During culture samples for flow cytometry were taken. Cells were stained with Zombie Aqua and analyzed by flow cytometry. (B) Shown is the BcrAbl$^+$ cell number for IRF8$^{+/+}$ and IRF8$^{-/-}$ BM cells over 4 days of culture (n = 3). Cell numbers are normalized to day 0. Statistical analyses were done with Mann-Whitney-U test by comparing IRF8$^{+/+}$ to IRF8$^{-/-}$ BM cells. Data points marked with (*) indicate samples with p-values ≤ 0.05; Data points marked (**) indicate samples with p-values ≤ 0.005.

3.1.2.2 Combination of TKI and IFNα therapy

It was shown that the lack of IRF8 had an impact on IFNα therapy outcome in CML patients. Therefore, in a second step, the importance of IRF8 for Imatinib and IFNα therapy in CML was investigated. To this end, IRF8$^{+/+}$ and IRF8$^{-/-}$ BM cells were isolated and transduced with BcrAbl as shown in Figure 21A. After cytokine starvation for 2 days, IRF8$^{+/+}$ BcrAbl$^+$ and IRF8$^{-/-}$ BcrAbl$^+$ BM cells were cultured either with 0.3 µM Imatinib or 10^3 U/ml IFNα or a combination of Imatinib and IFNα for 4 days (Figure 25A). Medium, Imatinib and IFNα was refreshed daily and cells were counted with an electronic cell counter. Again, BcrAbl$^+$ cells were monitored by flow cytometry over time.

As shown in previous experiments (Supplemental Figure 5) 0.3 µM Imatinib inhibited IRF8^{+/+} BcrAbl[+] cell growth. Interestingly, TKI was not able to reduce IRF8^{–/–} BcrAbl[+] BM cell numbers (Figure 25B). 10^3 U/ml IFNα inhibited both IRF8^{+/+} and IRF8^{–/–} BcrAbl[+] BM cell numbers (Figure 25C) suggesting that the IFNα effect might be independent of IRF8. Notably, IRF8^{–/–} BcrAbl[+] cell numbers increased in the first 2 days of IFNα treatment and were reduced only on day 3 and 4 of culture. One possible explanation might be that secondary signaling pathways are activated that are independent of IRF8. Finally, a combination of Imatinib and IFNα also reduced IRF8^{+/+} and IRF8^{–/–} BcrAbl[+] BM cell numbers (Figure 25D) showing again an IRF8 independent effect of treatment.
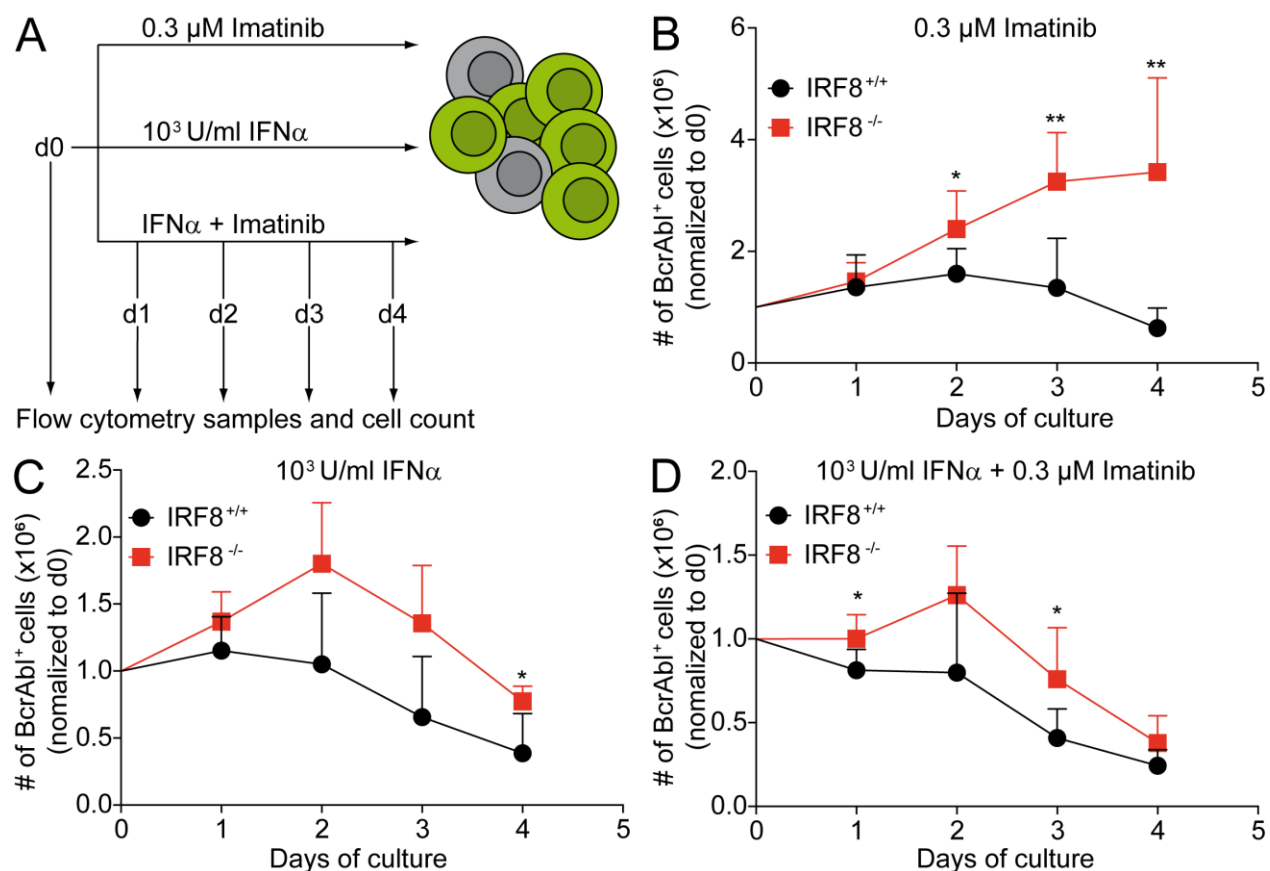
Figure 25. Reduction of BcrAbl^{+} cells by Imatinib is IRF8 dependent whereas IFNα effect is IRF8 independent

BcrAbl was overexpressed in IRF8^{+/+} and IRF8^{–/–} mouse BM cells by retroviral transduction as shown in Figure 21A. (A) BM cells were treated with 0.3 µM Imatinib, 10^3 U/ml IFNα or 10^3 U/ml IFNα + 0.3 µM Imatinib. Shown are the BcrAbl[+] cell number for (B) 0.3 µM Imatinib, (C) 10^3 U/ml IFNα and (D) 10^3 U/ml IFNα + 0.3 µM Imatinib. Data is represented as means ± standard deviation of three independent experiments (n = 3). Statistical

analyses were done with Mann-Whitney-U test by comparing IRF8$^{+/+}$ to IRF8$^{-/-}$ BM cells. Data points marked with (*) indicate samples with p-values ≤ 0.05; data points marked (**) indicate samples with p-values ≤ 0.005.

In clinics CML patients show an increased granulocyte population. Furthermore, it is hypothesized that the relapse of CML patients after discontinuation of Imatinib treatment is due to the lingering BcrAbl$^+$ immature progenitors that Imatinib does not eradicate (Figure 10). It is been proposed that immature leukemic progenitors have a low turnover rate, therefore Imatinib therapy is unable to eliminate immature cells.

To investigate which cell population is diminished by which treatment IRF8$^{+/+}$ and IRF8$^{-/-}$ BcrAbl$^+$ BM cells from Figure 24 and Figure 25 were further analyzed by flow cytometry. To this end, cells were stained for ckit, as a marker for immature progenitors, and for Gr1 as a marker for mature granulocytes (Figure 26A and Supplemental Figure 6). First, the percentages of Gr1$^+$ and ckit$^+$ cells were compared. At the start of treatment, Gr1$^+$ cell percentage was increased in IRF8$^{-/-}$ BcrAbl$^+$ cells compared to IRF8$^{+/+}$ BcrAbl$^+$ cells (Figure 26A) which is in line with primary CML cells. However, after 4 days of cytokine depleted culture percentages of Gr1$^+$ cells were decreased in IRF8$^{-/-}$ BcrAbl$^+$ cells compared to IRF8$^{+/+}$ BcrAbl$^+$ cells (Figure 26B).

Second, the total cell numbers for each population at day 4 of treatment were calculated. Notably, although IRF8$^{-/-}$ BcrAbl$^+$ cells display a lower percentage of granulocytes in comparison to IRF8$^{+/+}$ BcrAbl$^+$ cells after 4 days of culture (Figure 26B) the increased expansion under cytokine withdrawal (Figure 24B) also increased total granulocyte cell numbers for IRF8$^{-/-}$ BcrAbl$^+$ cells when left untreated. Hence, IRF8$^{-/-}$ BcrAbl$^+$ cells displayed a highly significantly increased number of mature granulocytes (Figure 26C) compared to IRF8$^{+/+}$ BcrAbl$^+$ cells. Interestingly, loss of IRF8 resulted in low response of mature granulocytes towards Imatinib treatment while IRF8$^{+/+}$ granulocytes were eliminated. Surprisingly, granulocytes in both IRF8$^{-/-}$ BcrAbl$^+$ and IRF8$^{+/+}$ BcrAbl$^+$ cells were eliminated by single IFNα treatment or combined with TKI.
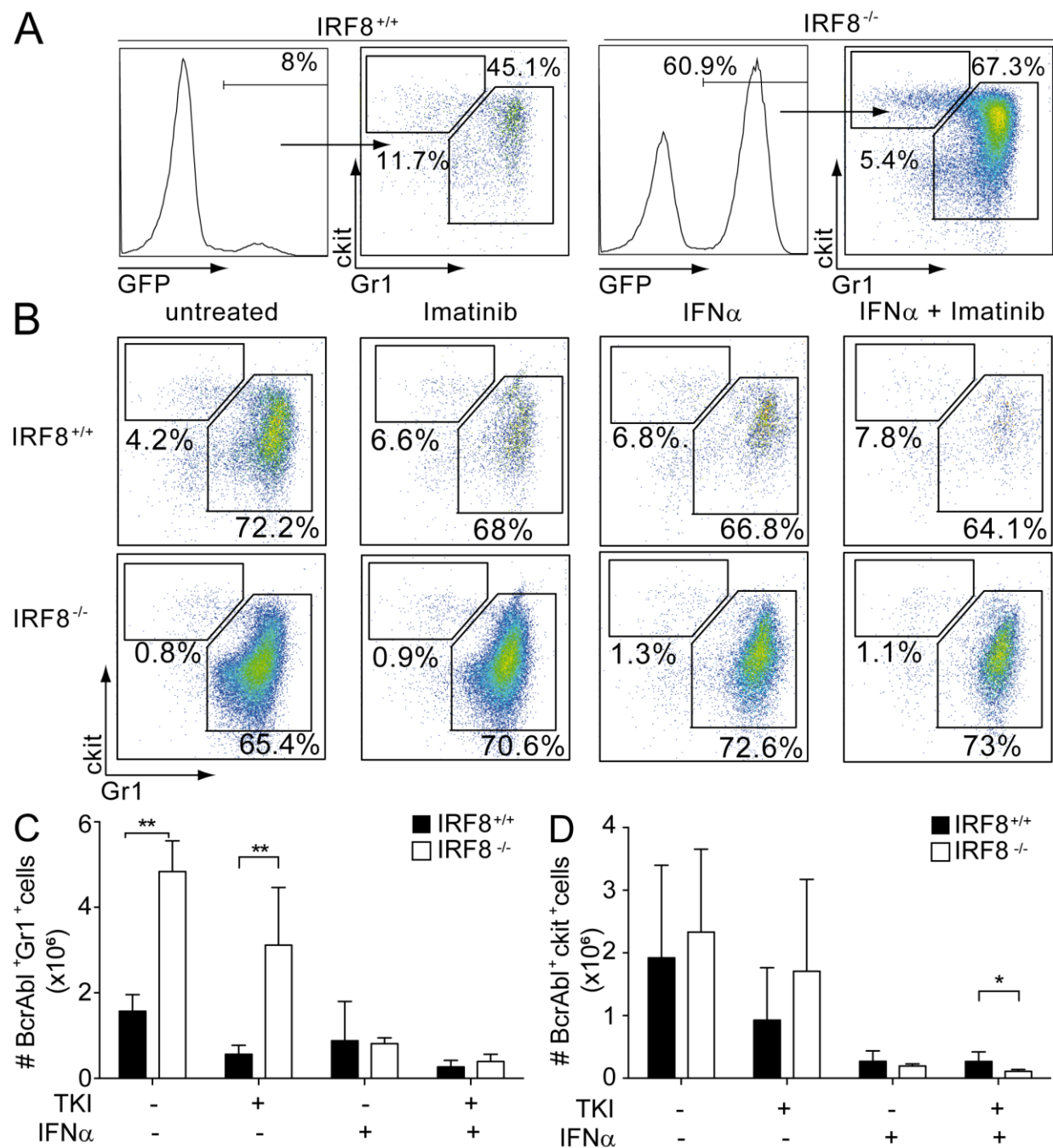
Figure 26. Impact of IFNα is independent of IRF8 on Gr1+ and ckit+ cells

BcrAbl was overexpressed in IRF8+/+ and IRF8–/– mouse BM cells by retroviral transduction and treated with 0.3 µM Imatinib (TKI), 10^3 U/ml IFNα or left untreated as shown in Figure 24. Start of treatment is day 0. Gr1+ and ckit+ cell populations form data in Figure 25 were analyzed by flow cytometry. Gating was performed according to Supplemental Figure 6. (A – B) A representative flow cytometry analysis for IRF8+/+ and IRF8–/– on (A) day 0 and (B) day 4 of treatment is shown. (C – D) Quantification of (B) Gr1+ and (C) ckit+ cells after 4 days of treatment is depicted. Data in represent means ± standard deviation of three independent experiments. Statistical analyses were done with Mann-Whitney-U test by comparing IRF8+/+ and IRF8–/– BM cells. Data points marked with (*) indicate samples with p-values ≤ 0.05; data points marked (**) indicate samples with p-values ≤ 0.005.

Finally, ckit$^+$ cells were analyzed after 4 days of Imatinib and IFNα treatment. The cell number of BcrAbl$^+$ ckit$^+$ cells was unaffected by the loss of IRF8 (Figure 26D). The absence of IRF8 did not affect the response of ckit$^+$ cells towards Imatinib or single IFNα treatment. However, combining Imatinib and IFNα treatment showed a significant inhibition of ckit$^+$ in the absence of IRF8 (Figure 26D).

Taken together, BcrAbl$^+$ cells display a higher expansion in the absence of IRF8 suggesting a role of IRF8 in the regulation of proliferation and in the context of leukemia as a tumor suppressor. Cell analysis showed a higher granulocytic cell population which reflected the CML phenotype *in vitro.* This is in line with previous studies in mice and cell lines (Holtschke et al. (1996), Sontag et al. (2017a)). Imatinib primarily reduced IRF8$^{+/+}$ BcrAbl$^+$ cells, yet this is due to eradicating mature granulocytes while leaving immature ckit$^+$ cells untouched. The leftover immature ckit$^+$ could likely be the cause for relapses in CML patients as these could differentiate again into mature BcrAbl$^+$ Gr1$^+$ cells. Moreover, TKI treatment does not affect BcrAbl$^+$ cell numbers when IRF8 is absent. This suggests there is a BcrAbl independent survival mechanism. Surprisingly, IFNα decreased BcrAbl$^+$ cell number independent of IRF8. IFNα reduced both mature Gr1$^+$ granulocytes and immature ckit$^+$ cells independent of the loss of IRF8.

3.1.3 JAK2V617F expressing BM cells gain cytokine independence

IFNα therapy induces molecular remissions in a large cohort of JAK2V617F$^+$ patients (Quintas-Cardama et al., 2009). This is in contrast to BcrAbl$^+$ CML patients who have a poor response to single IFNα treatment (Kantarjian et al., 2003). To study the differences in JAK2V617F$^+$ and BcrAbl$^+$ cells in response to IFNα murine BM cells were retrovirally transduced with JAK2V617F. JAK2V617F$^+$ BM cells were treated with IFNα and the IFNα response in JAK2V617F$^+$ cells was studied and compared to BcrAbl$^+$ BM cells. As for BcrAbl$^+$ cell lines reports show that due to the

overexpression of JAK2V617F coupled with the erythropoietin receptor (EPOR) or thrombopoietin receptor (TPOR) in cell lines, like 32D or Ba/F3 cells, oncogene expressing cells lose their IL3 dependent cell growth and become IL3 independent (Lu et al., 2005). Additional to a IL3 independence murine BcrAbl^{+} cells showed also a survival advantage to cytokines like SCF, FLT3L, IGF-1 or IL6 in previous experiments (Figure 22).

To investigate whether cytokine independence also applied to JAK2V617F[+] murine BM cells primary murine BM cells were isolated and transduced twice with a vector containing the cDNA for human JAK2V617F (Figure 15). Included in the vector construct was a GFP cassette that was co-expressed with JAK2V617F. Next, cells were split into 2 conditions as shown in Figure 19 and cultured in the absence or presence of SCF, IL6, FLT3L and IGF-1 for 3 days. Medium was refreshed every day and cells were counted with an electric cell counter. JAK2V617F^{+} cells were monitored by tracking the GFP expression via flow cytometry. To exclude dead cells, JAK2V617F^{+} BM cells were stained additionally with Zombie Aqua.

First, overexpression of JAK2V617F in murine BM cells resulted in very low transduction efficiency which was as low as 1% of GFP^{+} cells (Figure 27). Notably, the low transduction rates could not be increased in later experiments.
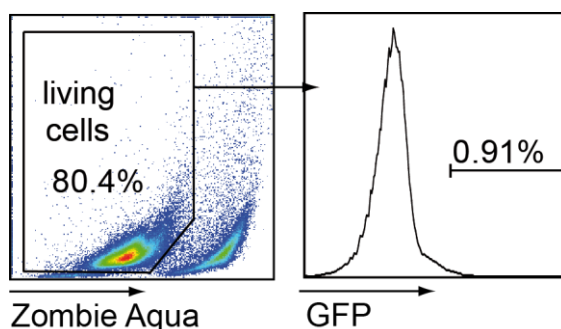

Figure 27. Transduction of murine BM cells with JAK2V617F resulted in low transduction rates

BM cells were isolated, cultured and transduced as shown in Figure 15. After transduction BM cells stained with Zombie Aqua to exclude dead cells. BM cells were analyzed for their GFP expression that substituted for oncogene expressing cells. A representative flow cytometry analysis is shown.

Second, as seen for BcrAbl^{+} BM cells (Supplemental Figure 2), cytokine supplemented culture did not decrease the percentage of living cells (Zombie Aqua^{−} cells, Figure 28A). However, without cytokines, the percentages of living cells decreased drastically (Figure 28A).

In the presence of cytokines the percentage of JAK2V617F^{+} cells stayed on the initial transduction level suggesting that JAK2V617F[+] has no advantage in comparison to JAK2V617F^{−} cells under these conditions (Figure 28B). In contrast, without cytokines the percentage of JAK2V617F^{+} cells increased after 2 days of culture slightly in comparison to cytokine supplemented culture. More importantly, JAK2V617F^{+} cells showed a major increase of GFP^{+} cells after 3 days of culture (Figure 28B) suggesting that in cytokine low or deprived cultures JAK2V617F shows a survival advantage in comparison to JAK2V617F^{−} cells probably giving the cells the boost for an outgrowth in later stages of the disease.

Taken together, JAK2V671F can render murine BM cells independent of cytokines like SCF and FLT3L which is also in line with previous results for 32D cells and their IL3 independence (Lu et al., 2005). Notably, JAK2V617F yielded suboptimal transduction efficiencies in most experiments.
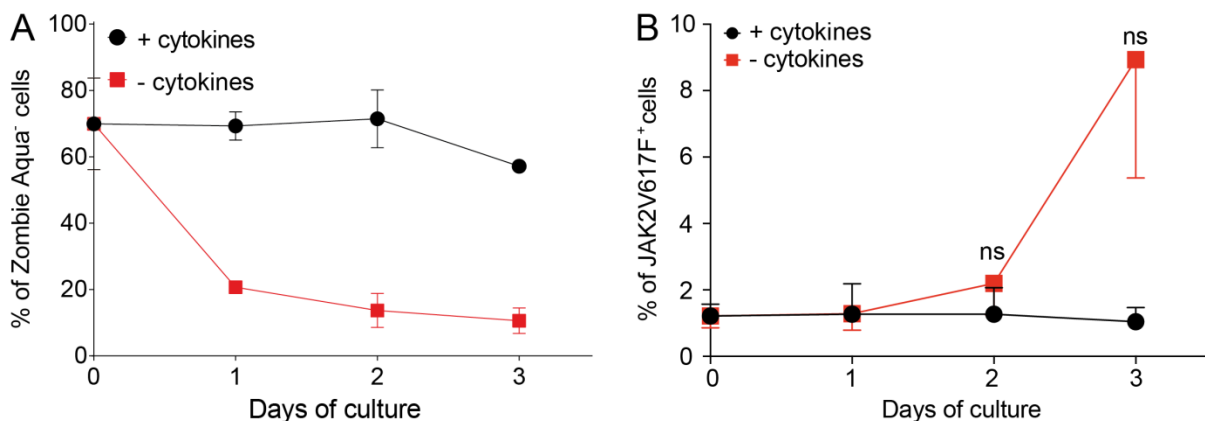

Figure 28. JAK2V617F^{+} BM cells gain cytokine independence

BM cells were isolated, cultured and transduced as shown in Figure 15. After medium change was performed, BM cells were either cultured with or without cytokines as shown in Figure 19. Medium was refreshed daily and

cells were counted with an electronic cell counter. JAK2V617F$^+$ cells were quantified by flow cytometry as cells co-expressed of GFP. Cells were stained additionally with Zombie Auqa as a live/dead staining. (A) Shown is a representative flow cytometry analysis on day 0 of cytokine starvation. Cells were first gated on Zombie negative cells, then JAK2V617F$^+$ cells were quantified by their GFP expression. (C) Living cells were quantified by their exclusion of the Zombie Aqua dye. Shown is the percentage of living cells during cytokine starvation (n = 3). (D) The percentage of JAK2V617F$^+$ cells during cytokine starvation is depicted (n = 3). For statistical analysis a Student's t test was performed by comparing –cytokines with +cytokines. ns = not significant.

3.1.3.1 Ruxolitinib inhibits JAK2V617F$^+$ BM cells *in vitro*

Ruxolitinib is a JAK1/JAK2 inhibitor and is used in JAK2V617F$^+$ MPN as therapy (Pieri et al., 2015). As for Imatinib *in vitro* experiments with JAK2V617F$^+$ BM cells might require a lower concentration than the concentration used for clinics or animal experiments. Therefore, BM cells were isolated, cultured and retrovirally transduced with JAK2V617F as shown in Figure 15. Afterwards, JAK2V617F$^+$ BM cells were treated with 0.01 µM, 0.1 µM and 1 µM Ruxolitinib (Figure 29A). Ruxolitinib and medium was refreshed daily and cells were counted with an electronic cell counter. Cells were cultured under cytokine starvation. JAK2V617F$^+$ cells were tracked via flow cytometry. JAK2V617F$^+$ BM cells were stained additionally with AquaZombie as a live/dead staining.

As cells were kept under cytokine withdrawal the percentage of living cells decreased during culture time (Figure 29B) which is in line with previous experiments (Figure 28A). The decrease in the percentage of living cells was independent of the applied Ruxolitinib concentration as the majority of cells did not express the JAK2V617F. Hence, JAK2V617F$^-$ cells displayed no cytokine independence. The few JAK2V617F$^+$ cells that survived the cytokine withdrawal could not increase the percentage of living cells so that flow cytometry could detect a difference for the various tested Ruxolitinib concentrations. As for BcrAbl$^+$ cells (Figure 22), treatment of JAK2V617F$^+$ BM cells with Ruxolitinib had a dose dependent effect (Figure 29C). In patients a plasma concentration of about 1 µM of Ruxolitinib is found (Heine et al., 2013). As shown 1 µM Ruxolitinib severely stunted the percentage of JAK2V617F$^+$ cells which is too drastic for *in vitro* culture (Figure

29C). When cells were treated with 0.1 µM Ruxolitinib the percentage of JAK2V617F$^+$ cells was inhibited too, yet not as drastic as for 1 µM Ruxolitinib. In contrast, 0.01 µM Ruxolitinib showed a minor reduction on JAK2V617F$^+$ cells as these cells were able to expand up to 4% of JAK2V617F$^+$ cells after 4 days of treatment.

In summary, 0.1 µM Ruxolitinib is sufficient to inhibit JAK2V617F$^+$ cells. However, due to the low transduction rate of murine BM cells with JAK2V617F retrovirus there is no reliable statement of the effect of Ruxolitinib on the living cell population. Additionally, transduction efficiency could not be increased in later experiments and JAK2V617F$^+$ cells could not be enriched sufficiently by cytokine starvation, thus making it insufficient to study the IFNα pathway in JAK2V617F$^+$ BM cells.

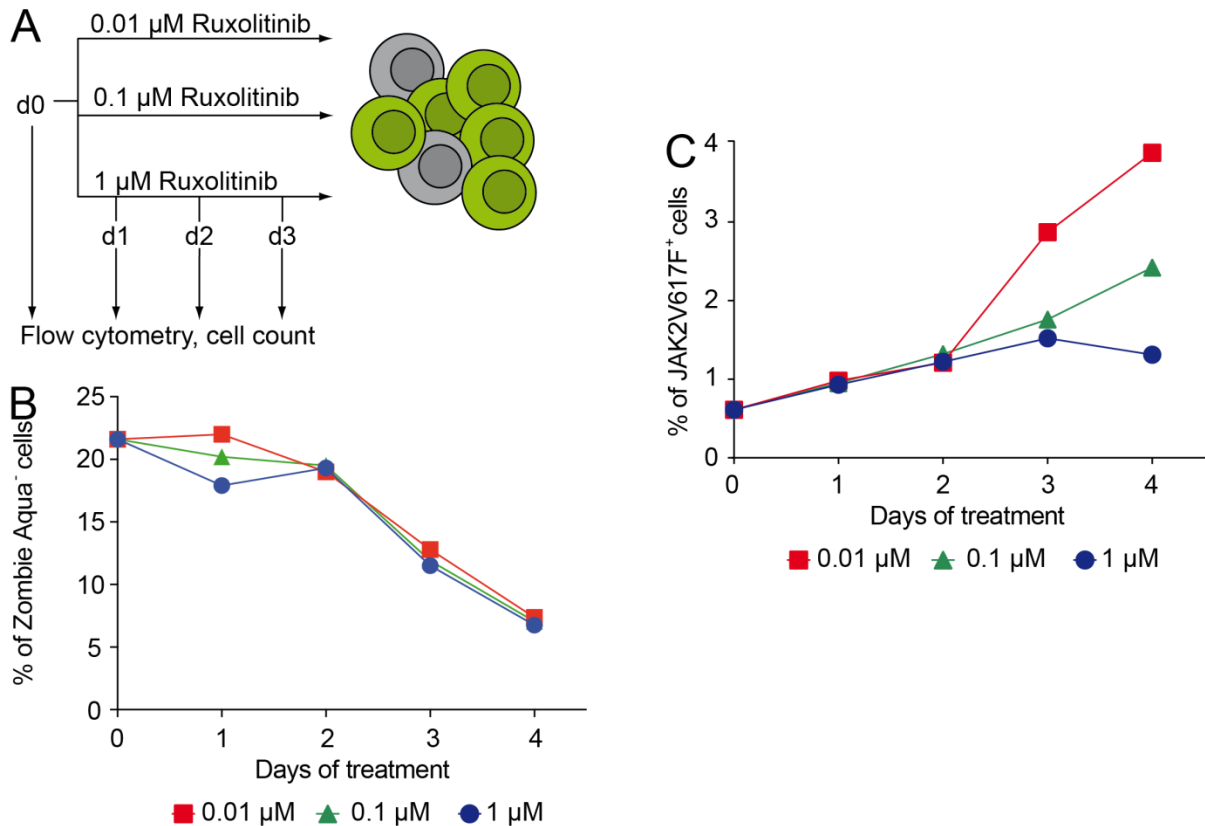Figure 29. Ruxolitinib is able to inhibit JAK2V617F$^+$ cells in vitro

BM cells were isolated, cultured retrovirally transduced with JAK2V617F as described in Figure 15. (A) Afterwards, BM cells were treated with 0.01 µM, 0.1 µM and 1 µM Ruxolitinib for 3 days. Medium and Ruxolitinib was refreshed daily. Every day cells were counted with an electronic cell counter and samples for flow cytometry

were taken. Cells were stained with Zombie to exclude dead cells. JAK2V617F$^+$ cells were quantified by their co-expression of GFP. (B) Shown is percentage of living cells (indicated as Zombie Aqua$^-$ cells) during culture time. (C) The percentage of JAK2V617F$^+$ cells during Ruxolitinib treatment was recorded and depicted here (n = 1).

Overall conclusion, in line with experiments in cell lines murine BM cells showed an oncogene dependent survival advantage in cytokine depleted cultures as TKI treatment of oncogene overexpressing cells was able to eradicate BcrAbl$^+$ and JAK2V617F$^+$ BM cells. BcrAbl also conferred a cytokine independent expansion of BM cells which was amplified in the absence of IRF8. Additionally, TKI treatment was insufficient to eradicate BcrAbl$^+$ cells in the absence of IRF8 highlighting the role of IRF8 as a tumor suppressor in BcrAbl$^+$ BM cells and in human CML. In contrast to clinical studies, IFNα was able to eradicated BcrAbl$^+$ cells independent of IRF8. The combination of TKI and IFNα treatment did not show an increase benefit in *in vitro* culture. JAK2V617F overexpression resulted in a low transduction rate. For this reason, the investigation of IFNα signaling pathway was done in patient derived iPSC.

3.2 Elucidating the IFNα signaling pathway in patient derived JAK2V617F⁺ iPSC

JAK2V617F was initially found in 2005 and was linked to the BcrAbl⁻ classical MPN forms of PV, ET and PMF then (James et al. (2005), Vannucchi et al. (2009)). The influence of JAK2V617F on the hematopoietic system and the modeling of PV has been initially done in mouse models. These results show an expansion of megakaryocytic, monocytic and erythroid lineages in the bone marrow with a skewering towards the erythroid lineage (Lacout et al. (2006), Mullally et al. (2010)). The discovery of iPSC and the generation of patient specific JAK2 and JAK2V617F iPSC the results from mouse experiments could be partially verified in the human system (Saliba et al. (2013), Ye et al. (2014)). To add to these studies, new JAK2 and JAK2V617F iPSC clones were derived from PV patients with varying JAK2V617F allele burden. Thus, the first aim of this thesis is to model human PV with these new iPSC clones *in vitro* using a directed hematopoietic differentiation protocol. Also, the influence of JAK2V617F dosage on hematopoiesis can be investigated side by side in the human system using these iPSC clones. It was shown that IFNα therapy is able to eradicate JAK2V617F expressing cells in PV patients. However, the IFNα pathway in JAK2V617F⁺ cells compared to JAK2 cells still remains largely unknown. Thus, the second aim in this thesis is to elucidate the IFNα signaling pathway in JAK2 and JAK2V617F iPSC-derived cells.

3.2.1 Generation of patient derived JAK2 and JAK2V617F iPSC

3 PV patients (PV1, PV2 and PV3) which were diagnosed with the JAK2V617F mutation were selected to generate iPSC (Table 18). The selected patients did not receive any IFN therapy before blood samples were taken. It is known that MPN therapies, such as TKI treatment, have the potential to select for a resistant subclone within the leukemic stem cell pool (Deshpande et al., 2011). Furthermore

TKI therapy frequently induces point mutations that render cells resistant to therapy, as known for Imatinib treatment of BcrAbl^{+} cells (Branford et al., 2002). It is hypothesized that these events favor relapses of the disease or even are the cause of the relapse (Tehranchi et al., 2010). By starting from blood samples of patients that did not receive IFNα treatment we aimed at preventing the generation of iPSC from selected subclones that are potentially resistant to IFNα or that acquired additional mutations due to treatment.

Table 18. List of polycythemia vera patient samples used for iPSC generation

Patient	Age	Gender	JAK2V617F	Allele burden	Received therapy?
PV1	43	f	yes	37%	No
PV2	47	m	yes	96%	Hydroxyurea
PV3	38	m	yes	Not determined	No

Peripheral blood of each patient was obtained via phlebotomies under an ethics approval (EK206/09 Biobank and 127/12 MPN bioregistry). Blood was subjected to density gradient centrifugation; mononuclear cells were isolated and frozen. To generate iPSC, peripheral blood mononuclear cells (PBMNC) were thawed (Figure 30A) and subjected to 3 round of centrifugation at 800 rpm to enrich for living cells. The remaining PBMNC were cultured with TPO, FLT3L, SCF and IL6 for 1 to 3 days. Then, PBMNC were collected, quantified and 3×10^5 cells were taken for reprogramming. The rest of the cells was frozen again.

Sendai virus particles coding for KLF4, OCT4, SOX-2 and c-MYC were added to the PBMNC for 2 days (Figure 30A, day 0). During the first 2 days cells were monitored for the formation of grape like clusters (Figure 30B, day 2). After 2 days of incubation with Sendai virus, medium and cytokines were refreshed. At day 4 of culture, cells were collected, breaking up the grape like clusters, and single cells were then transferred onto inactivated mouse embryonic fibroblasts (MEF) (Figure 30A, day 4). From day 4 to day 6, medium containing TPO, FLT3L, SCF and IL6 was replaced

gradually with iPSC medium containing bFGF (Figure 30A). Single cells started to proliferate and formed ES-like colonies from day 8 of culture (Figure 30B, day 8 and day 16).
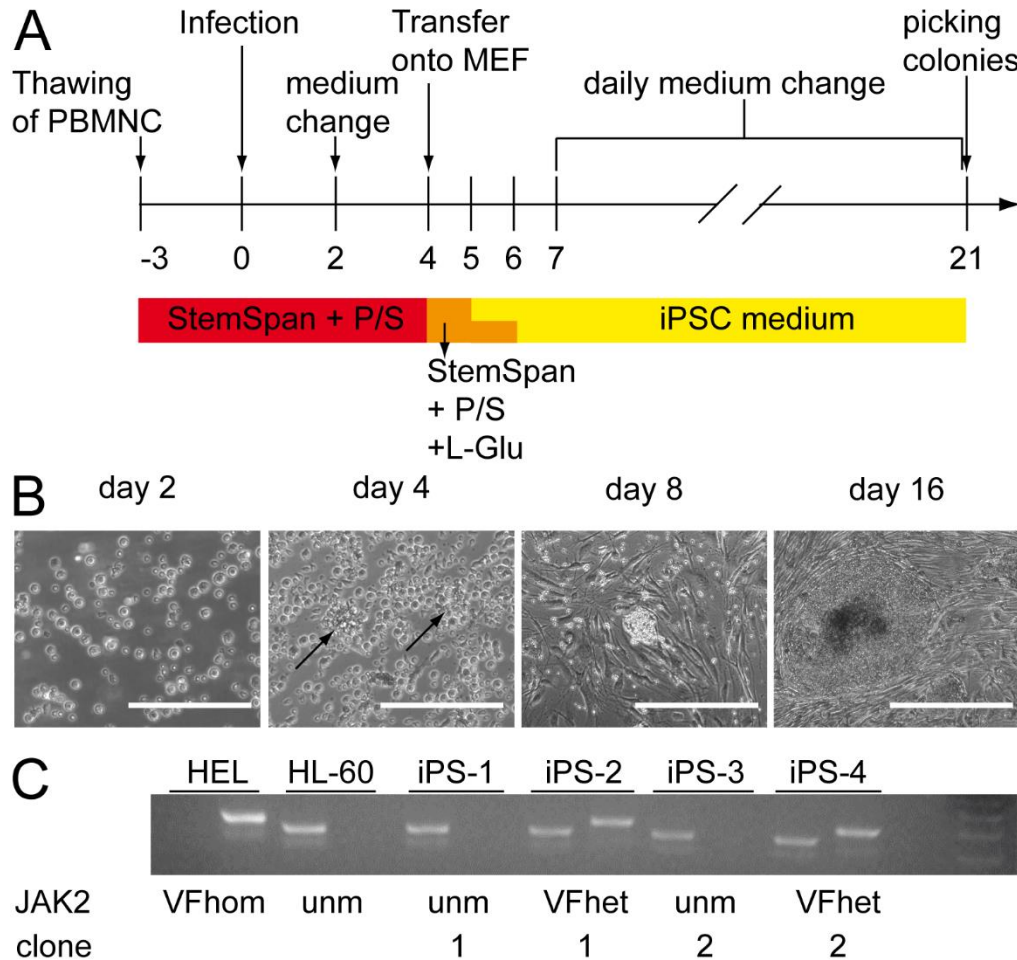

Figure 30. Reprogramming of PV patient PBMNC into iPSC

(A) Time line and scheme for reprogramming of patient PBMNC into iPSC. Patient PBMNC were thawed and cultured for 1 to 3 days in StemSpan containing TPO, FLT3L, IL6, SCF and P/S. Sendai virus particles coding for KLF4, OCT4, SOX-2 and c-MYC were added for 2 days. After formation of grape like clusters, cells were washed once and transferred onto MEF. On day 4, L-Glu was added to the StemSpan medium. The gradual switch to iPSC medium was performed on day 5 with a partial medium change followed by a full medium change on day 6 with iPSC medium. Cells were cultured for another 2 to 3 weeks until iPSC colonies formed. (B) Shown are representative phase contrast images during the reprogramming period. Arrows indicate grape like clusters. Scale bar for day 2 and 4 represents 200µm. Scale bar for day 8 and 16 represents 400µm. (C) Individual iPSC colonies were picked and DNA was isolated. Allele specific PCR for JAK2V617F was performed in collaboration with Kristina Feldberg - Department of Hematology, Oncology, Hemostaseology, and Stem Cell Transplantation, Faculty of Medicine, RWTH Aachen University, Aachen, Germany. HEL and HL-60 cells were used as control. Shown is a representative agarose gel for four iPSC clones for PV1. Unm, unmutated; VFhet, JAK2V617F heterozygous.

ESC-like colonies grew in size until 24 colonies for PV1 and 48 colonies for PV2 and PV3 were picked (Table 19). The presence of the JAK2V617F mutation for each iPSC clone was determined by allele specific PCR (Figure 30C). iPSC clones from PV1 were unmutated (JAK2) or heterozygous for the JAK2V617F mutation (JAK2VFhet) (Table 20). In contrast, iPSC clones from PV2 and PV3 were predominantly were homozygous for the JAK2V617F mutation (JAK2hom) while a minor fraction was JAK2VFhet (Table 20). Generation of patient derived iPSC lines was performed in collaboration with Dr. Stefanie Sontag (Department of Cell Biology, Institute for Biomedical Engineering, RWTH Aachen University Medical School, Aachen, Germany). Patient derived iPSC clones from PV1 were generated by Dr. Stefanie Sontag while iPSC clones of PV2 and PV3 were generated on my own. Allele-specific PCR for all iPSC clones was done in collaboration with Kristina Feldberg (Department of Hematology, Oncology, Hemostaseology, and Stem Cell Transplantation, Faculty of Medicine, RWTH Aachen University, Aachen, Germany).

Table 19. Overview of patient derived iPSC clones

Patient	# of clones picked	# of JAK2 unmutated clones	# of JAK2VF heterozygous clones	# of JAK2VF homozygous clones	Clones used in this thesis
PV1	24	11	7	0	PV007 PV009 PV015 PV020
PV2	48	0	2	34	PV2_021
PV3	48	0	4	39	PV3_026 PV3_031

For experiments reported in this thesis, 2 unmutated iPSC clones (JAK2_1 and JAK2_2) and 2 heterozygous iPSC clones (JAK2het_1 and JAK2het_2) of PV1 were selected, which were used for the majority of the experiments. Additionally, 1 iPSC clone from PV2 (JAK2hom_1) and 2 iPSC clones from PV3 (JAK2het_3 and JAK2hom_2) were chosen (Table 19 and Table 20). All iPSC clones were chosen because of good growth kinetics and overall good ESC-like morphology.

Table 20. iPSC clones and their genotype used in this thesis

Clone number	JAK2 Genotype	Nomenclature in figures
PV007	unmutated	JAK2_1
PV009	heterozygous	JAK2VFhet_1
PV015	unmutated	JAK2_2
PV020	heterozygous	JAK2VFhet_2
PV2_021	homozygous	JAK2VFhom_1
PV3_026	homozygous	JAK2VFhom_2
PV3_031	heterozygous	JAK2VFhet_3

3.2.2 Quality control of patient-derived iPSC clones

iPSC lines can be generated from every somatic cell in the human body using different reprogramming methods. Yet, the source of the generated iPSC line, the passage number of the iPSC line and culture conditions have an influence of the quality of the generated iPSC lines. Hence, a streamed lined quality assessment of the newly iPSC line is needed. Current assays for the quality assessment of iPSC lines were reviewed by Asprer and Lakshmipathy (2015) and some were used to assess the quality and functionality of PV patient derived iPSC clones for this thesis.

3.2.2.1 iPSC clones show phenotypical pluripotency characteristics

A first quality assessment of iPSC lines was the evaluation of morphology. During reprogramming and iPSC culture, morphology of the iPSC colonies was checked daily. Patient-derived iPSC cultured on MEF grew in tightly organized, round, flat colonies that displayed sharp edges. Cells within the colony grew in a single layer (data not shown). This is in line with the first generated human ES cell line by Thomson et al. (1998).
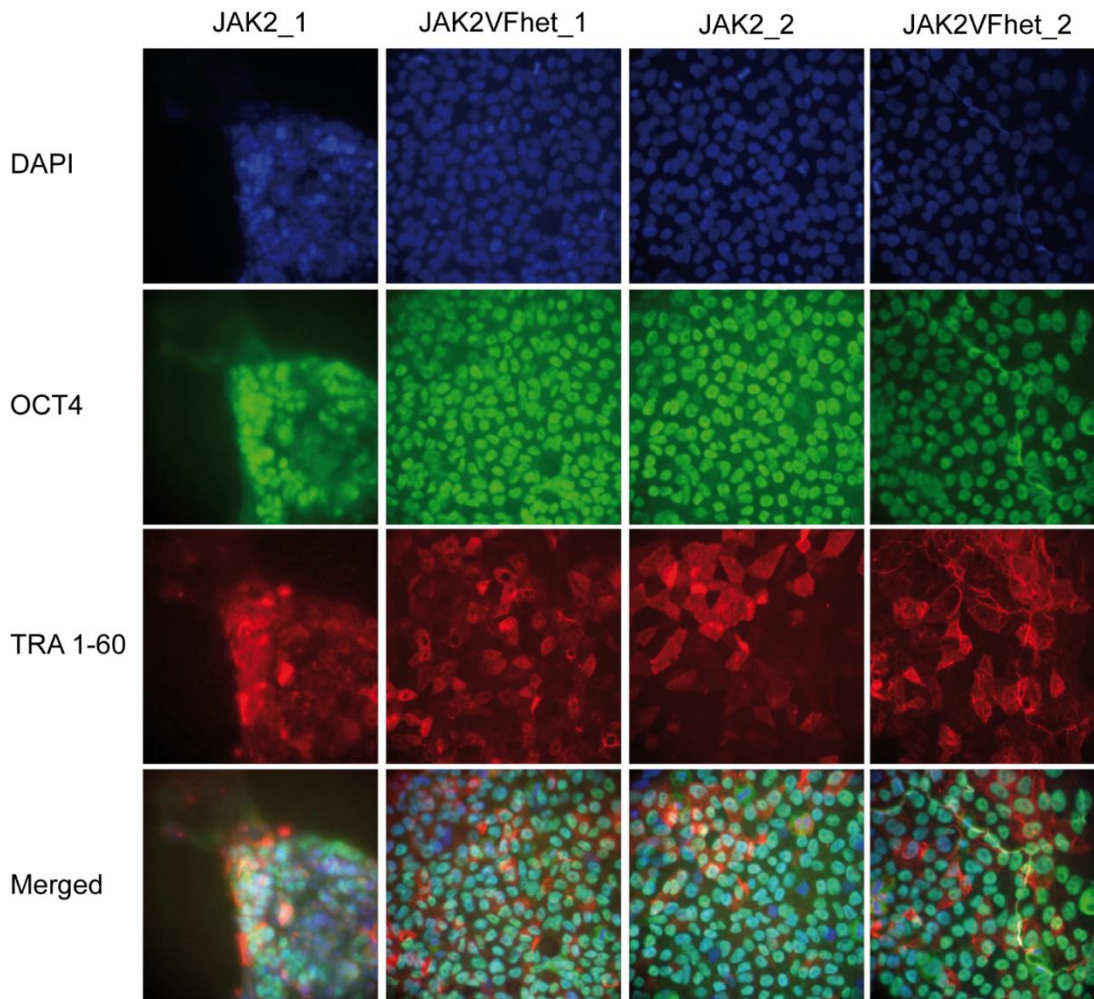

Figure 31. JAK2 and JAK2V617F iPSC express pluripotency markers

iPSC clones of PV1 were cultured vitronectin coated on glass slides for 4 day days. Afterwards, iPSC were fixed with 4 % PFA for 20 min. Next, cells were blocked with goat serum for 40 min followed by staining with

antibodies against Dapi (blue), OCT4 (green) and TRA 1-60 (red) as described in chapter 2.2.1.9. Representative immunofluorescence images are shown for the indicated clones (40x magnification; n =1).

A second quality assessment was the expression of pluripotency markers either via flow cytometry or via immunofluorescence (Asprer and Lakshmipathy (2015)). To this end, the selected iPSC clones were cultured on glass slides under MEF free conditions. After 4 days of culture, iPSC clones were fixed and stained for an immunofluorescence assay. Antibodies used in this assay were targeted against TRA 1-60 as a pluripotency marker on the cell surface of fully reprogrammed iPSC, and the transcription factor OCT4 as pluripotency and self-renewal marker present in the nucleus (Chan et al., 2009). DAPI was used to stain the entire nucleus. As shown in Figure 31 iPSC clones from PV1 showed expression of both pluripotency markers. OCT4 co-localized with DAPI staining thus showing that OCT4 is active in the nucleus.

3.2.2.2 iPSC clones possess three germ layer differentiation capacity

Expression of OCT4 and TRA 1-60 is not sufficient to functionally characterize newly generated iPSC lines as some genes have a secondary function in somatic tissue (Graham et al., 2003). Therefore, iPSC functionality needed to be verified. In an embryo pluripotent stem cells give rise to all cells of the human body and also iPSC have the capacity (Yu et al., 2007). To evaluate functional pluripotency of the newly differentiated iPSC clones, their capacity to differentiate into all 3 germ layers, mesoderm, ectoderm, endoderm was assessed (Asprer and Lakshmipathy (2015)). To this end, iPSC clones of PV1 (Figure 32), PV2 and PV3 were cultured without bFGF and in the presence of fetal calf serum (FCS) for 7 days. These culture conditions induce differentiation via the formation of suspended aggregates, so called embryoid bodies (EB) (Itskovitz-Eldor et al., 2000). This was followed by a culture period of 7 to 14 days in which EB attached to the plate and covered the tissue culture plastic (TCP) in a monolayer of tightly packed spindle shaped cells.
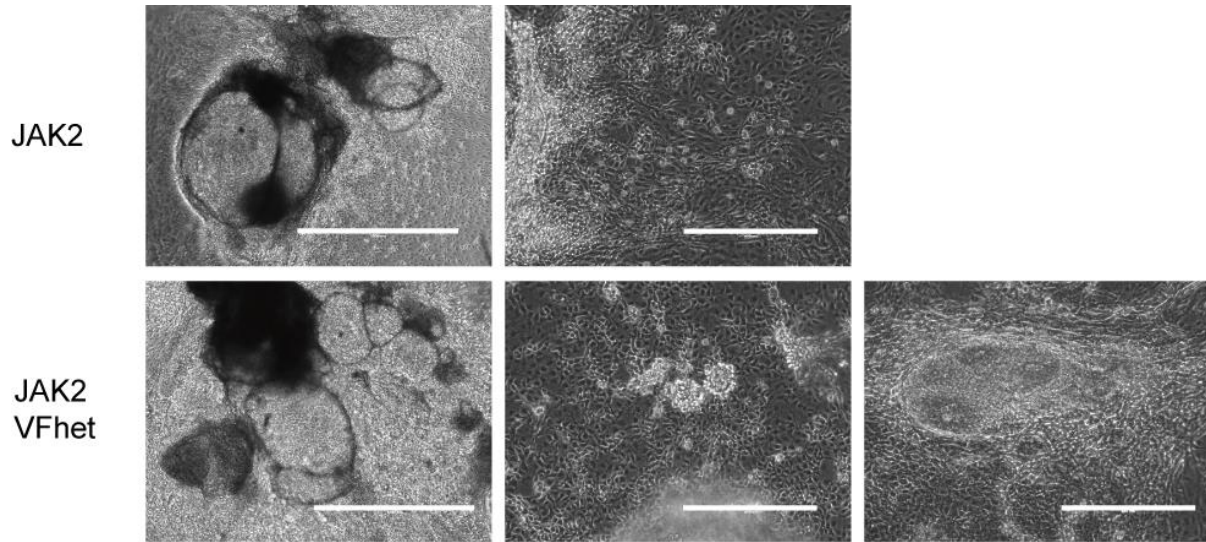
Figure 32. Differentiation of iPSC clones into three germ layers via embryoid body formation

iPSC clones of PV1 were induced to differentiate into all three germ layers. iPSC colonies were harvested via Collagenase IV treatment for 1h at 37°C. After MEF depletion EB were washed with KO-DMEM once. Finally, EB were resuspended in KO-DMEM supplemented with 10 % FCS, 1 % L-Glutamine, 1 % Penicillin/Streptomycin, 1 % minimal non-essential amino acids and 0.2 % β-mercaptoethanol in a ULA plate for 7 days. After 7 days, EB were transferred onto a gelatin-coated TCP and cultured for another 7 to 14 days. Medium changes were done every 2 days. Representative pictures were taken between day 9 and day 14 of germ layer differentiation. Shown are cystic structures of the attached EB (left column) and hematopoietic stem and progenitor cells (HSPC) together with the monolayer of tightly packed spindle shaped cells (center column) for JAK2_1 and JAK2VFhet_1. JAK2VFhet_1 showed differentiation into ectoderm by development of neuronal rosettes (right column). Scale bar for the left column represents 1000 μm, scale bar for center and right column represents 400 μm.

During the first 7 days, EB often formed cystic structures in suspension. These cystic structures were also seen when EB attached to the culture plate during later stages of germ layer differentiation (Figure 32, left column). Furthermore, light microscopic images showed the formation of distinct structures attributed to one germ layer. Mesodermal structures were observed in the form of beating areas and hematopoietic stem and progenitors (HSPC) that were budding off from the spindle shaped cells (Figure 32, center column). Ectodermal structures were seen in the formation of neuronal rosettes (Figure 32, right column) during differentiation.

Next, to monitor transition from pluripotency into the different germ layers the expression of genes associated with pluripotency or one of the germ layers was analyzed. On day 0, 7 and 14 of differentiation cells were harvested, RNA was isolated and cDNA was synthesized followed by qPCR with the appropriate primers (Supplemental Table 4). Loss of pluripotency was confirmed by downregulation of the pluripotency gene OCT4 over time (Figure 33). Undifferentiated iPSC clones showed a high expression of OCT4 whereas on day 7 and 14 OCT4 expression was strongly downregulated (Figure 33 and Supplemental Figure 7).

Next, Brachyury (T) and SOX17 show a transient upregulation fitting their function in early mesoderm and endoderm, respectively. Undifferentiated iPSC clones have low levels of brachyury. During differentiation brachyury is upregulated (Figure 33, d7; Supplemental Figure 7) which with previous studies (Kubo et al., 2004; Wilkinson et al., 1990). As differentiation proceeds, T is downregulated again (Figure 33, d14; Supplemental Figure 7). It was shown early on that Brachyury (T) has a distinct expression pattern in stem cell differentiation. It is first expressed in the primitive streak during gastrulation and is widely used as the earliest differentiation marker in human stem cell studies (Wilkinson et al., 1990). Brachyury is essential for mesoderm formation and definitive endoderm progenitors co-express Brachyury and SOX17 (Faial et al. (2015), Kubo et al. (2004)). SOX17 is a regulator in the development of human germ cells. As shown in Figure 33 and Supplemental Figure 7 patient derived iPSC upregulate SOX17 transiently with a peak at day 7 of differentiation. This is in line with previous studies and its function in early embryonic development (Kubo et al., 2004).

As each germ layer gives rise to a multitude of terminal differentiated cells various genes were selected to cover the different possible cell types during differentiation. As shown in Figure 33 and Supplemental Figure 7 JAK2 and JAK2V617F iPSC clones upregulated the glial fibrillary acidic protein (GFAP) and SOX1 as early as day 7 of differentiation showing ectoderm differentiation. SOX1 is expressed in the early stages of neuroectoderm development where cells of the spinal cord and brain

develop from (Genethliou et al. (2009)). GFAP is induced in cells of the central nervous system, like glial cells (Hol and Pekny, 2015).

Finally, genes used by lineage restricted cells late in differentiation were analyzed (Figure 33 and Supplemental Figure 7). Mesoderm differentiation was assessed by verifying the expression of CD31, CD34, CDH5 (gene for VeCadherin), NKX2.5 and MYH6. CD34 is an early hematopoietic marker define early hematopoietic stem cells (Baum et al., 1992). CD31 and CDH5 are used to define endothelial cells (Vestweber, 2008). MYH6 gene codes for the myosin heavy chain 6 expressed in development of cardiac muscles (England and Loughna, 2013). NKX2.5 is also expressed during heart development. Alpha-fetoprotein (AFP) was used as a second endodermal marker. AFP is produced by the yolk sac and the fetal liver, thus early embryonic development (Jones et al., 2001). Expression of the 5 mesodermal and 1 endodermal genes increased in time showing highest levels at day 14 and day 22 of differentiation. Moreover, expression was similar in JAK2 and JAK2VFhet iPSC clones (Figure 33).

Taken together, the new patient-derived iPSC clones express pluripotency markers when cells are kept in their undifferentiated state. Furthermore, they have the potential to differentiate into the 3 germ layers, hence resembling human embryonic stem cells. Importantly, the JAK2V617F mutation did not confer a bias towards one specific germ layer as JAK2, JAK2VFhet and JAK2VFhom clones show similar expression patterns for germ line specific genes. Thus, the iPSC clones display a good, stable morphology and are fully functional. Therefore, the chosen iPSC clones are reliable and will be used for subsequent experiments.
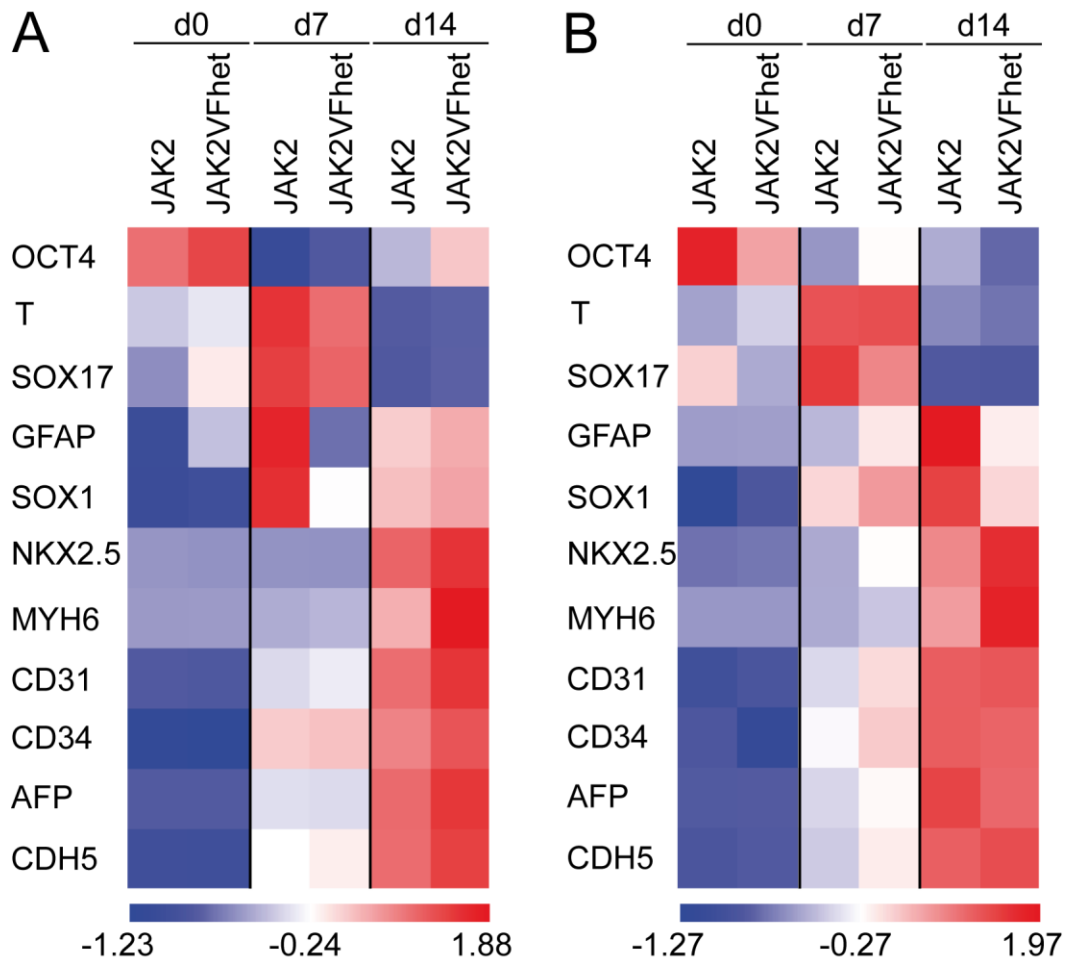
Figure 33. iPSC clones differentiate towards all 3 germ layers

PV1 iPSC clones were harvested via Collagenase IV treatment at 37°C for 1h. After MEF depletion, EB were washed with KO-DMEM once followed by culture in ULA plates in KO-DMEM supplemented with 10 % FCS, 1 % L-Glutamine, 1 % Penicillin/Streptomycin, 1 % minimal non-essential amino acids and 0.2 % β-mercaptoethanol for 7 days. Afterwards, EB were plated on gelatin-coated TCP and cultured for another 7 to 14 days. On day 0 (undifferentiated iPSC), 7 and 14 samples were harvested and RNA was isolated. RT-qPCR was performed. Data is shown in a heatmap format for (A) JAK2_1 and JAK2VFhet_1 and (B) JAK2_2 and JAK2VFhet_2 (n = 3). Z-Score represents expression levels: red, high expression; blue, low expression.

3.2.2.3 Patient derived iPSC clones do not show any major additional mutation

Patient derived iPS cells reflect the genome of the patient's cell that was reprogrammed with the Yamanaka factors. That means that next to the mutation of interest, e.g. JAK2V617F, additional mutations are reflected in that particular clone.

Additional mutations might have an influence on the stability of the generated iPSC clone or reflect the effect of certain therapy regimen on this particular cell type, e.g. resistances towards the applied drug which was done until now in mouse models or cells lines (Chen et al., 2015). Moreover, studies showed that point mutations could arise during reprogramming posing the question of their safety in clinical applications (Junfeng et al., 2012). To address the aforementioned concerns iPSC clones JAK2_1, JAK2_2, JAK2VFhet_1 and JAK2VFhet_2 from PV1 were screened for additional mutations by next generation sequencing (NGS). NGS is one of the most powerful methods developed in recent years (van Dijk et al., 2014). With this technique a larger number of samples from a disease cohort can be analyzed in a relative low amount of time. Furthermore, more genes associated with human diseases can be screened with higher sensitivity via NGS than the conventional PCR. To this end, iPSC were first cultured under MEF free conditions for 2 to 3 passages. Next, genomic DNA (gDNA) was isolated and an NGS run for further cancer associated genes, like TET2, KRAS, NRAS or KIT was performed (Kuo and Dong, 2015). During the sequencing short reads of sense and anti-sense DNA strands are created and matched to a reference genome. The sequencing records the number of amplifications. Afterwards, the number of mutated and unmutated reads are compared and converted into a ratio for each tested gene (Table 21). NGS analysis was performed in collaboration with the human medicine department of the Uniklinik Aachen, Germany. The cut off for positive hits in the NGS run was set at 25 %.

As shown in Table 21 NGS confirmed the presence of the JAK2V617F mutation in JAK2VFhet_1 and JAK2VFhet_2 iPSC clone. Furthermore, NGS detected 2 mutations in the TET2 gene, yet at different locations. NGS detected a missense and a frameshift mutation in the JAK2VFhet_1 and JAK2VFhet_2 iPSC clones, respectively. Moran-Crusio et al. (2011) showed that loss of TET2 resulted in an increased self-renewal of hematopoietic stem cells. Furthermore, co-expression of JAK2V617F and TET2 mutant variants showed a higher oncogenic ability of the

mutated clones compared to single mutations in MDS, MPN and AML patients (Chen et al., 2015; Delhommeau et al., 2009).

Additional to the JAK2V617F mutation, the NGS run showed another JAK2 mutation in JAK2VFhet_2 iPSC clone, yet to a very low percentage. In JAK2_2 NGS also detected a point mutation in the JAK2 gene other than the checked JAK2V617F mutation. However, up until now there are not studies referencing these particular mutations. Notably, all iPSC clones had one mutation in common, a complex mutation in the CBL gene (Table 21). Studies showed that mutations in the CBL gene promoted a hypersensitivity to IL3 (Aranaz et al., 2012).

Taken together, JAK2 iPSC clones have no mutation at the V617F side. Moreover, the additional mutations are clone specific, yet no influence of these additional mutations were detected during iPSC culture. All 4 iPSC clones did not show any instability in their undifferentiated state or were prone to differentiate spontaneously. The mutations in TET2 might be of concern as studies showed that TET2 mutations confer a resistance towards IFNα treatment (Kiladjian et al., 2010). For extended experiments with PV2 and PV3 iPSC clones the same NGS analyses will need to be done.

Table 21. NGS analysis of PV1 JAK2 and JAK2VFhet iPSC clones (in collaboration with the human medicine department of the Uniklinik Aachen, Germany)

iPSC were cultured for 2 to 3 passages in feeder-free conditions. Afterwards, gDNA was isolated and given to the human medicine department for NGS analysis. From left to right: Shown is the gene for which a mutation was detected. Next, the position of the mutation specifies the exon and the mutation which was detected. The reference alternative allele shows the nucleotide shift that has happened with the mutation (original nucleotide/detected nucleotide). The mutation feature shows the type of mutation. Last, the different iPSC clones are shown. The numbers per iPSC clone and mutation is the ratio between mutated allele versus unmutated allele.

Gene	Mutation Position	Reference Alternative Allele	Mutation Feature	JAK2_1	JAK2VFhet_1	JAK2_2	JAK2VFhet_2
JAK2	Exon 14, V617F	G/T	missense	-	0.2911	-	0.4712
TET2	Exon 3, N12S	A/G	missense	-	0.2727	-	-
TET2	Exon 11, P1829	GC/G-	frameshift	-	-	-	0.2821
JAK2	Exon 17, S755N	G/A	missense	-	-	0.3056	-
JAK2	Exon 19, E845E	A/G/T	missense	-	-	-	0.0325
CBL	Exon 9, Y455del	TATG/++++ ATG/T---	Non frameshift	0.3919	0.2532	0.0632	0.4585

3.2.3 Hematopoietic differentiation of JAK2 and JAK2V617F iPSC clones

Human hematopoiesis and hematopoietic stem cells have been studied for several decades. Due to ethnic concerns of using human embryos the hematopoietic system has been studied with models systems such as zebra fish, chicken, frogs or mice. 40 years ago it was shown that hematopoiesis occurs in the yolk sac and the embryo proper (Dieterlen-Lievre, 1975). Furthermore, in the last 10 years models showed that hematopoiesis has 2 waves: primitive and definitive hematopoiesis. However, studies also showed that the transition between developmental programs is fluid. The use of ESC and discovery of iPSC has helped to isolate various cell populations analyze their differentiation potential.

Reprogramming of patient mononuclear cells generated JAK2 and JAK2V617F iPSC clones (Figure 30C). Based on the previous analyses patient derived iPSC clones are stable (Figure 31, Figure 32, Figure 33) and mutations that have a possible influence on experiments are known (Table 21). JAK2V617F is the driver mutation in PV, a human disease affecting hematopoietic stem and progenitor cells. However, disease models for PV are limited to mouse models. Hence, the newly generated iPSC were used to evaluate the influence of JAK2V617F expression on the hematopoietic differentiation.

3.2.3.1 Hematopoietic differentiation of iPSC with an hypoxia based protocol

It was shown that the earliest hematopoietic cells originate from the haemangioblast (Ditadi et al., 2017). Further studies show that definitive hematopoiesis occurs in cells that have hematopoietic and endothelial differentiation potential, so call hemogenic endothelial cells (HE cells), that reside in the dorsal aorta. Studies have found that HE cells co-express CD31, CD34, and Flk-1 in human and mouse emrbryos (Oberlin et al., 2002). Furthermore, lineage trancing experiments show that HSC develop from HE cells via endothelial-to-hematopoietic transition (EHT)

(Boisset et al., 2010). These results have been used to establish various hematopoietic differentiation systems for ESC and iPSC. Protocols either use a co-culture system with stromal cells and serum containing media or EB based protocol with defined cytokines (Kennedy et al. (2012). However, most protocols solely produce primitive hematopoietic cells. In recent years, studies used small molecules like WNT activators to induced definitive hematopoiesis *in vitro* (Ditadi and Sturgeon, 2016).
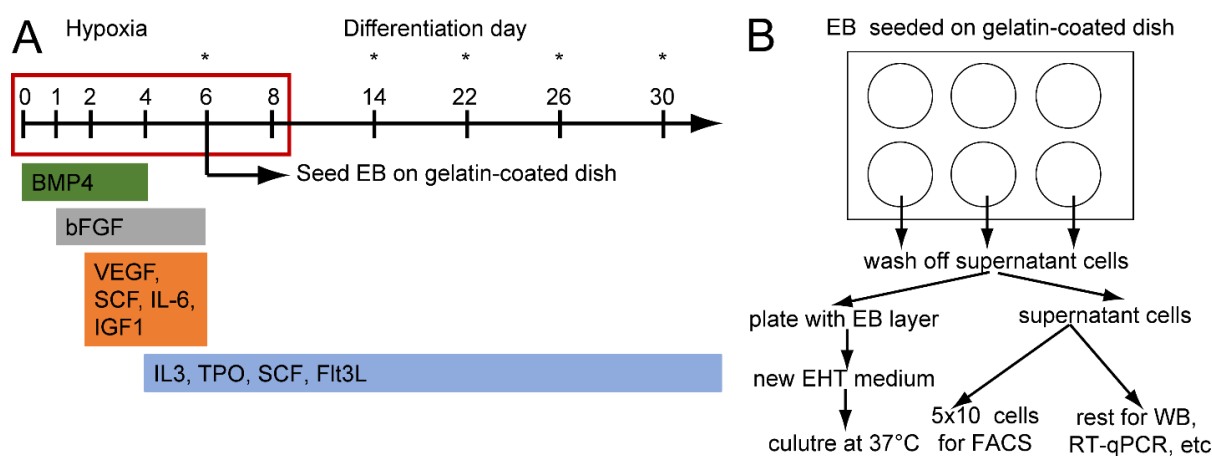

Figure 34. Scheme hematopoietic differentiation of patient derived iPSC

(A) iPSC were differentiated into hematopoietic cells via an EB based differentiation protocol published by (Kennedy et al., 2012). On differentiation day 0 iPSC were expanded for 4 days and harvested by Collagenase treatment for 1h at 37°C. After MEF depletion, EB were washed once with KO-DMEM. Afterwards, StemPro34 supplemented BMP4 were broken up into smaller EB and cultured under hypoxic conditions. As indicated in A, medium changes and supplementation with the indicated cytokines were done on day 1, 2, 4, 6, and 8 followed by cultured under hypoxic conditions. Asterisks (*) indicate time points of harvest and flow cytometry samples. (B) On day 6 of differentiation EB were seeded on a gelatin-coated plate (10 cm TCP or 6well plate). EB attached over the next few days and hematopoietic cells were released into the medium. Supernatant cells from each well were harvested and processed for flow cytometry, RT-qPCR and Western Blot (WB).

To assess whether patient derived iPSC differentiate into hematopoietic cells similar as *in vivo* stem cells a differentiation protocol by Kennedy et al. (2012) was adopted. In contrast to Kennedy et al. (2012) the time line of the stage-specific cytokines and growth factors was shortened in this differentiation protocol (Figure 34A). Furthermore, Kennedy et al. (2012) let the EB dissociate into single hematopoietic cells. In this thesis, however, EB were seeded onto gelatin-coated

plate on day 6 of differentiation (Figure 34B). The same approach was performed by Guibentif et al. (2017). Moreover, this lead to a continuous production of hematopoietic cells from and thus a culture time of 30 to 40 days. However, this is in contrast to the approach by Kennedy et al. (2012) where differentiation is finished after 15 days. One might hypothesize that HE cells are maintained within the EB layer and, consequently, upkeep the production of hematopoietic cells. However, after 30 days of culture the production of hematopoietic cells slowed down.

Patient specific iPSC were dissociated into small clusters and hematopoietic differentiation was induced as embryoid bodies by applying stage-specific combination of cytokines (Figure 34A and Figure 35, d0). EB were cultured under hypoxic conditions (5% O_2) to mimic the hematopoietic development in a human embryo. In the first 2 days of differentiation, cells underwent mesoderm commitment by the application of BMP4 and EB grew in size (Figure 35, d2). Cells that failed to undergo mesoderm commitment died in the first days of hematopoietic differentiation.

After 2 days hematopoietic and endothelial growth factors and cytokines were added, like VEGF, IL6 and SCF to induce hematopoietic and endothelial specification in EB. At day 4 of differentiation, BMP4 was washed out and replaced by hematopoietic growth factors (Figure 35, d4). At day 6 of differentiation EB were heavily diluted and seeded onto gelatin-coated plates (max. 50 EB per well) to support formation of an HE monolayer (Figure 34A and Figure 35, d6). From then on cells were cultured with medium containing SCF, FLT3L, TPO and IL3 (later called EHT medium). EB attached on the plate within the following 24h. From day 6 of differentiation onwards cells were cultured with SCF, FLT3L, TPO and IL3 (later called EHT medium). On day 8 of differentiation, cells were transferred into normoxic culture conditions and kept until the end of culture.
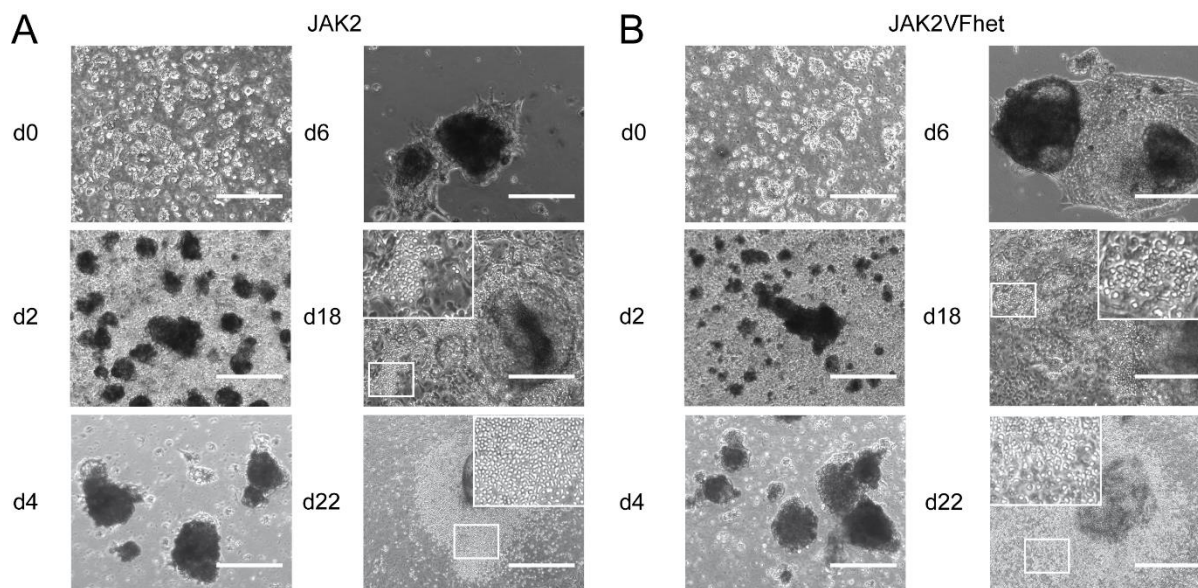
Figure 35. Light microscopic images during hematopoietic differentiation of iPSC

Patient derived iPSC were induced differentiate into hematopoietic cells as described in Materials and Methods. Briefly, iPSC colonies were disrupted into small embryoid bodies (EB) on day 0 of differentiation. During differentiation EB grew in size and debris was lost with medium changes every 2 days (d2, d4). On day 6 of differentiation a tight and dense network of endothelial cells developed trapping the EB on the plate. EB were seeded in low concentrations (50 EB per well) on gelatin coated TCP plates to promote the formation of a monolayer of HE cells. Hematopoietic cells were seen emerging from the formed HE layer and accumulated until day 18 of differentiation (d18). Representative phase contrast images of JAK2_1 (A) and JAK2VFhet_1 (B) during hematopoietic differentiation are shown. Scale bars for d0 to d18 represent 400 µm. Scale bar for d22 represent 1000 µm. Zoomed in images of single HSPC are displayed in the corner of d18 and d22 images. White squares in d18 and d22 images represent location where image was zoomed into for single HSPC.

During normoxia attached EB first gave rise to HE cells that covered the culture plate in a monolayer (later referred to as EB layer). In the following days, endothelial-to-hematopoietic transition (EHT) was observed as small round cells emerged from the EB layer and were released into the supernatant. The appearance of hematopoietic cells happened as early as day 10 up to day 49 of differentiation (Figure 35, d18 and d22). Hematopoietic cells that were released into the supernatant could be harvested for characterization via flow cytometry. Due to leaving the EB layer intact hematopoietic cells were harvested from the supernatant constantly for experiments every 4 days until day 30 of differentiation. JAK2 and JAK2V617F iPSC were differentiated in parallel. JAK2 iPSC were used to compare the influence of JAK2V617F on hematopoietic differentiation.

In conclusion, the newly generated iPSC line undergo hematopoietic differentiation as described in various publications from other pluripotent cells (Kennedy et al. (2012), Eilken et al. (2009), Lachmann et al. (2015)). The initial phenotypical characterization does not show a difference between JAK2 and JAK2V617F. Furthermore, it seems that the EB layer drives the hematopoiesis from day 14 to day 40 of differentiation leading to multiple harvests. One might hypothesized that HSC are rather trapped within the EB layer giving rise to hematopoietic cells to be released into suspension. Consequently, the EB layer might drive the hematopoiesis enabling multiple harvests *in vitro*.

3.2.3.1.1 Kinetics during hematopoietic differentiation of iPSC

Hematopoiesis and hematopoietic stem cells have been characterized in mice and human quite intensively due to constant use of mice in transplantation, disease modeling and general understanding of hematopoiesis (Challen et al. (2009), Schmitt et al. (2014), Lacaud and Kouskoff (2017)). Moreover, the use of iPS cells help to further understand the human hematopoietic system. Studies have been performed to analyze iPSC-derived hematopoietic cells and establish a reliable system for cell characterization and isolation (Karamitros et al., 2018). As in the initial phenotypical analysis showed the new iPSC line showed the same potential to differentiate into hematopoietic cells (Figure 35) as described in literature.

In a next step, patient iPSC were differentiated and iPSC-derived cells were analyzed by flow cytometry to assess whether the developing cell populations described by Kennedy et al. (2012) were similar despite the adjustment in culture conditions (Figure 34A). Therefore cell specific markers were recorded over time. To this end, on day 6 of differentiation EB were dissociated into single cells and single cells were analyzed by flow cytometry. On day 14 to 30 of differentiation hematopoietic cells from the supernatant were harvested every 4 days and analyzed

for their surface markers (Figure 36). Notably, cells that are analyzed with flow cytometry on day 6 of differentiation all cells inside the EB, i.e. cells that have not jet committed to the mesoderm or hematopoietic lineage. In contrast, cells analyzed on day 14 to day 30 are suspension cells and per definition represent hematopoietic cells.

As mentioned iPSC lines have been differentiated into hematopoietic cells *in vitro* in many studies which have shed light on different cells types during hematopoiesis. Kennedy et al. (2007), Rafii et al. (2013) and Rahman et al. (2017) showed a cell population that develops early during differentiation. These cells show co-expression of CD34, CD31 and ckit which were characterized these cells as HE cells. Indeed, early in the differentiation of the new JAK2 and JAK2V617F iPSC clones a small population of CD34$^+$ CD31$^+$ HE cells can be observed (Figure 36, Supplemental Figure 8A). Notably, hematopoiesis specific surface markers like CD43 and CD45 are absent on day 6 of differentiation. From day 14 onwards only a small population of suspension cells was identified as HE cells. As previously mentioned an EB layer developed after EB were seeded onto gelatin coated plates (Figure 34). It was hypothesized that the EB layer drives hematopoiesis *in vitro.* Here it is seen that only a small amount of HE cells are in the supernatant on day 14 of differentiation. This gives another suggestion that HE cells are enclosed within the EB layer itself and are responsible for hematopoiesis.

On day 14 of differentiation only suspension cells were harvested. More than half of suspension cells expressed CD31 compared to day 6 of differentiation. Most of CD31$^+$ cells also co-expressed CD43 rather than CD34 (Figure 36). This is in line with a previous study (Sontag et al., 2017a). CD31$^+$ CD43$^+$ cells have been characterized as hematopoietic progenitor cells (HPC). Previous studies show that at this point of differentiation suspension cells have already committed to the hematopoietic and even skewered to the myeloid lineage (Choi et al., 2009). Indeed, the majority of CD31$^+$ CD43$^+$ cells co-expressed the hematopoietic marker CD45 which is line with previous reports (Rahman et al., 2017). Following hematopoietic differentiation via flow cytometry (Figure 36, d18 to d30), from day 14 to day 30 the

percentage of CD31$^+$ CD43$^+$ HPC increased up to 85% of which all cells were CD45$^+$.

Kessel et al. (2017) showed that *in vitro* erythropoiesis starts from CD43$^+$ cells and that during red blood cell differentiation cells first lose their CD45 and CD43 expression but gained CD235a expression. Sturgeon et al. (2014) showed a small population of CD235a$^+$ cells which they defined as primitive red blood cells. In line with this observation, a small population of CD45$^-$ CD235a$^+$ cells was detected on day 6 of differentiation. These were defined as red blood cells (Ye et al. (2014), Yang et al. (2017)). On day 14 of hematopoietic differentiation of the new iPSC clones showed 12% of CD45$^-$ CD235$^+$ red blood cells (Figure 36). Notably, the population increased compared to day 6 of differentiation. However, from day 18 to day 30 of differentiation the red blood cell population decreased.

Previous iPSC experiments show that the EB layer ages and more committed myeloid cells, such as mast cells or granulocytes arise during longer differentiation time (Sontag et al., 2017a). Thus, terminal differentiated cells were monitored. Indeed, 2 % of CD45$^+$ ckit$^+$ mast cell progenitors developed over time (Figure 36) (Dahlin et al., 2015). Moreover, granulocytes accumulated from day 14 to day 30 of differentiation whereas no definite trend of CD61$^+$ megakaryocytes was observed.
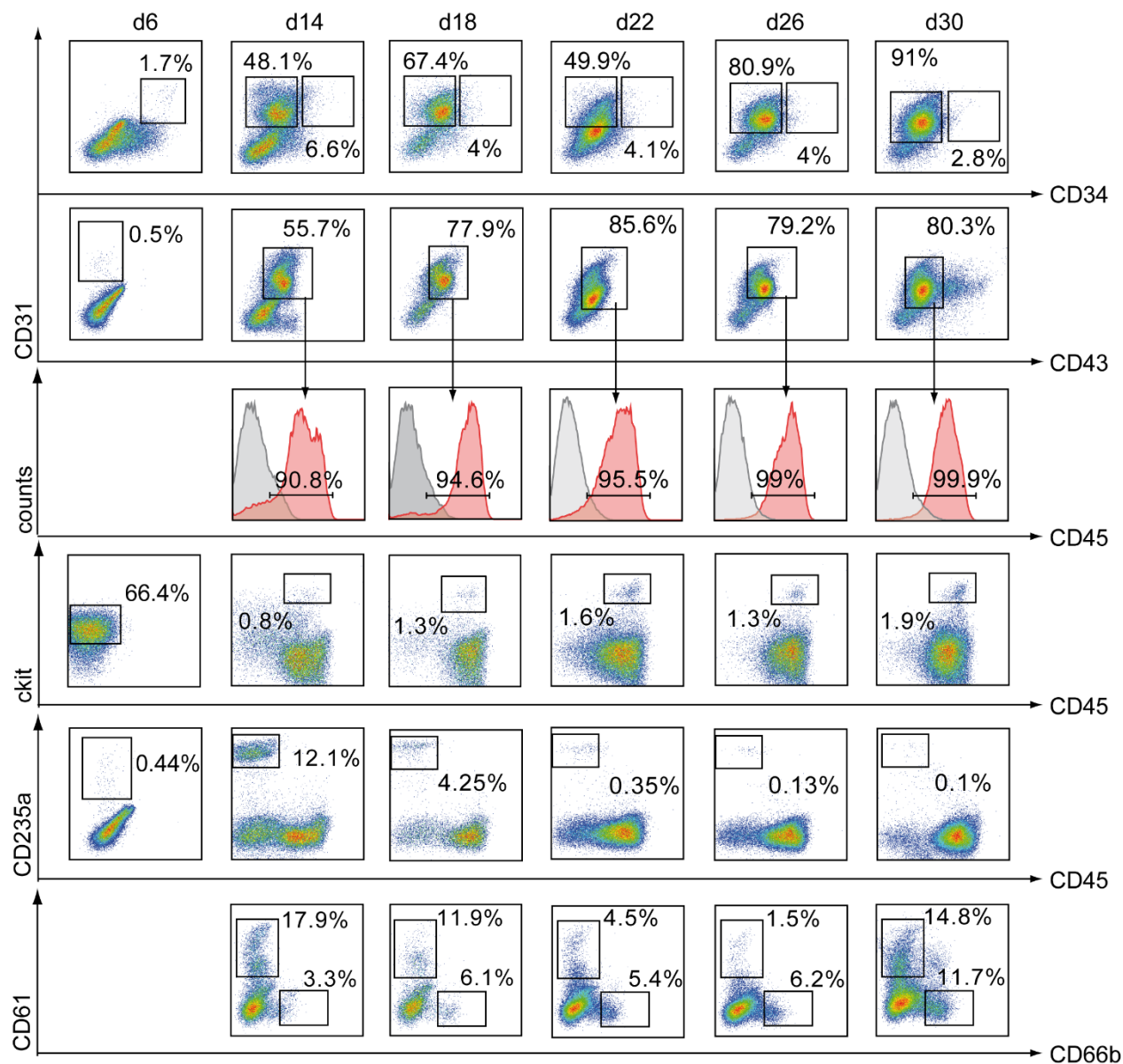
Figure 36. Surface marker expression during hematopoietic differentiation of iPSC

Patient derived iPSC were induced to differentiate towards hematopoietic cells as described in chapter 2.2.1.10. Surface marker expression was analyzed via flow cytometry and representative flow cytometry examples for JAK2_1 are shown for the indicated days. On day 6 of differentiation EB were treated with Accutase for 15 min at 37°C to obtain single cells which were passed through a 40 µm cell strainer. From day 14 of differentiation onwards suspension cells were harvested. Cells were stained with antibodies specific for CD34, CD31, CD45, CD43, ckit, CD235a, CD61 and CD66b and analyzed by flow cytometry. CD34+ CD31+ marks cells from the HE, CD31+ CD43+ represents HPC, CD45+ are mature hematopoietic cells, CD45− CD235+ are erythroid cells. The detailed gating is shown in Supplemental Figure 19. Statistical analysis of each cell population for independent experiments (n = 3-7) is shown in Figure 37 and Supplemental Figure 10.

Taken together, the first cells to emerge in hematopoietic differentiation are HE cells. Following differentiation it seems that HE cells are developing within the EB layer after seeding EB on gelatin-coated plates. Trapped HE cells then give rise to HPC which are released into suspension and commit to the myeloid lineage due to CD45 expression. A small portion of CD235a$^+$ red blood cells that decreases over time can be detected. These kinetic are in line with a studies (Rahman et al. (2017), Yang et al. (2017), Kennedy et al. (2012)).

3.2.3.2 JAK2V617F mutation has a minor effect on hematopoietic differentiation of iPSC

Based on previous results patient derived iPSC generated a small amount of HE cells and primitive red blood cell progenitors on day 6 of differentiation while other hematopoietic cells were absent (Figure 36). From day 14 of differentiation onwards cells committed to the myeloid lineage could be harvested every 4 days. Moreover, a small population of red blood cells was detected during differentiation. Finally, due to leaving the EB layer untouched multiple harvests were possible. Consequently, one might hypothesize that the EB layer drives hematopoiesis *in vitro*. The next step was to investigate the influence of JAK2V617F on hematopoiesis. To this end, multiple JAK2V617F and JAK2 iPSC clones were differentiated in parallel as described (Figure 34 and chapter 3.2.3.1). Hematopoietic differentiation was monitored via flow cytometry as described (chapter 3.2.3.1.1).

As expected and shown in previous experiments (Figure 36) on day 6 of differentiation EB contained CD34$^+$ CD31$^+$ HE cells (Figure 37A and Supplemental Figure 8A). Notably, with multiple independent experiments JAK2V617F iPSC show a higher population of HE cells on day 6 of differentiation (Figure 37A). This significance is lost over the course of differentiation. However, this might be due to

HE cells being trapped inside the EB layer and not being released into suspension from day 14 onwards (Figure 35A, d18).

In line with previous experiments (Figure 36) JAK2 and JAK2V617F iPSC generated a low amount of $CD31^+$ $CD43^+$ HPC on day 6 of differentiation. Also in line with previous results HPC population increased to a medium of 80% from day 14 of differentiation onwards (Figure 37B and Supplemental Figure 8C – D). However, HPC development as well as the development of $CD45^+$ committed progenitors seemed to be unaffected by the JAK2V617F mutation as there was no significant difference during hematopoietic differentiation between JAK2 and JAK2V617F (Figure 37B).

Next, the erythroid lineage was analyzed as JAK2V617F is documented to increase the number of red blood cells in PV patients and mouse models (Garçon et al., 2006). Furthermore, previous experiments showed that a $CD45^-$ $CD235a^+$ red blood cells population developed (Figure 36). Therefore, JAK2 and JAK2V617F iPSC-derived hematopoietic cells were analyzed for their spontaneous, EPO-independent red blood cell development. Flow cytometry showed that JAKV617F heterozygous cells gave rise to 4.5% and 2.5% of red blood cells (JAK2het_1 and JAK2het_2, respectively) compared to 2.5% and 1.14% for JAK2 cells on day 18 of differentiation (JAK2_1 and JAK2_2, respectively) (Figure 37C). On day 22 of differentiation red blood cell population decreased for both JAK2 and JAK2V617F cells, however JAK2V617F expressing cells still formed significantly more red blood cells (2- to 3-fold) than JAK2 cells suggesting a minor effect of JAK2V617F on the erythroid lineage (Figure 37C).
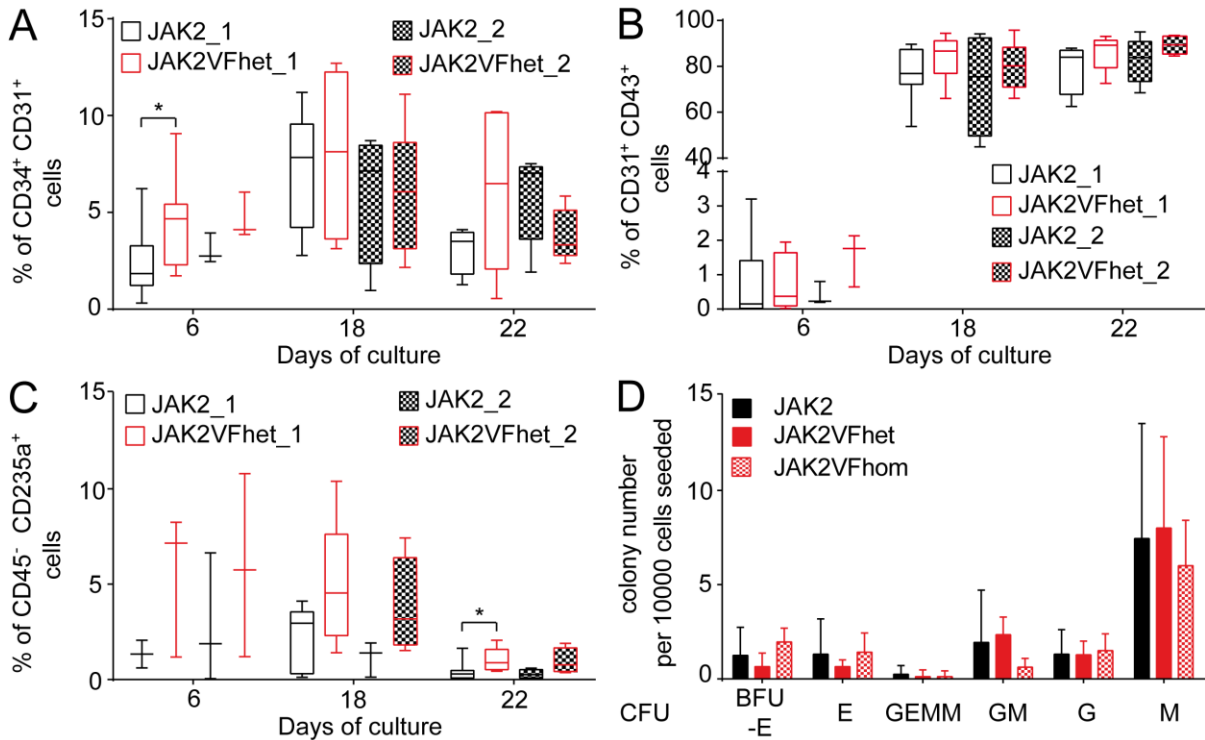
Figure 37. JAK2V617F expression has an impact on HE and red blood cell development

JAK2 and JAK2V617F iPSC were differentiated towards hematopoietic stem cells as described in chapter 3.2.3.1. Cells were harvested and stained with antibodies specific for CD31, CD34, CD235a, ckit, CD43 and CD45 followed by flow cytometric analyses. Summary of flow cytometric analyses of (A) CD34+ CD31+ HE cells, (B) CD31+ CD43+ HPC and (C) CD45− CD235+ red blood cells for all 4 iPSC clones from PV1 during hematopoietic differentiation (n = 3-7). Shown are the percentages of single cells for each cell type. A detailed gating strategy is shown in Supplemental Figure 19. (D) JAK2, JAK2V617F heterozygous and JAK2 homozygous iPSC-derived HPC were harvested on day 18 of differentiation. 20000 to 40000 HPC were seeded in semisolid medium. Per CFU assay duplicates were seeded. Colonies were scored after 14 days of culture (n = 3). Afterwards, colony number was normalized. CFU assays were done with iPSC-derived HPC from clones JAK2_1, JAK2VFhet_1 and JAK2VFhom_1. For statistical analysis Mann-Whitney-U-Test was used by comparing JAK2 with JAK2V617F. Data points marked with (*) indicate samples with p-values ≤ 0.05.

Already in the 1970s it was shown that primary cells from PV patients show an EPO independent emergence of red colonies, so called endogenous erythroid colonies (EEC) (Zanjani et al., 1977). Furthermore, when plated in semisolid medium primary cells from PV patients show an increased formation of erythroid colonies (Dai et al., 2005). To investigate whether this observation can be modeled with iPSC-derived hematopoietic cells JAK2 and JAK2V617F suspension cells were harvested on day 18 of differentiation. They were seeded in semisolid medium supplemented with cytokines for myeloid and erythroid development, such as SCF, GM-CSF, IL3 and EPO. Colony formation was evaluated after 14 days of culture. Evaluation was done

either by microscopy or by picking colonies and performing cytospins and H&E staining (Supplemental Figure 9). As shown iPSC-derived hematopoietic cells showed colonies of all myeloid cells and erythroid cells (Figure 37D). However, when normalized to 10.000 cells per assay CFU assays revealed no bias towards the erythroid lineage as there was an average of 2 and 3 BFU-E or CFU-E for either JAK2VF heterozygous and JAK2 iPSC-derived hematopoietic cells, respectively. Even JAK2VF homozygous iPSC-derived hematopoietic cells did not show an increase in erythroid colony formation (on average 3 CFU-E or BFU-E per 10000 cells seeded) compared to JAK2 or JAK2VF heterozygous iPSC-derived hematopoietic cells. Notably, JAK2 and JAK2V617F cells displayed a high bias towards macrophage colonies (CFU-M) (Figure 37D, Supplemental Figure 9). Furthermore, iPSC-derived cells barely formed CFU-GEMM. This suggested that iPSC-derived hematopoietic cells have already been restricted to one lineage when cells were seeded into the semi-solid medium.

In summary, JAK2V617F has a minor effect on hematopoietic differentiation impacting on the formation of CD34$^+$ CD31$^+$ HE cells during the first 6 days of differentiation. As shown for PV patients JAK2V617F had an impact on the erythroid lineage, conveying an increased percentage of CD45$^-$ CD235$^+$ red blood cells in the absence of EPO (Jamieson et al., 2006). However, this could not be seen in CFU assays. One could hypothesize that the EPO concentration (2 U/ml) which is used in the semisolid medium is negating the JAK2V617F influence on red blood cell formation and also providing optimal growth conditions for JAK2 cells. Hence, it might be that JAK2V617F is effective in growth conditions with low EPO concentrations.

3.2.3.3 JAK2V617F does not convey a bias towards a specific myeloid linage

It was shown that mice transplanted with JAK2V617F$^+$ BM cells showed a tri-lineage expansion of red blood cells, platelets and neutrophils (Lacout et al. (2006), Shimizu et al. (2016)). Yet, iPSC-derived hematopoietic cells showed only a trend towards an increased CD45$^-$ CD235a$^+$ cell population for JAK2V617F$^+$ cells (Figure 37C) and CFU assays revealed no difference differentiation potential (Figure 37D).

Even though the culture was supplemented with SCF, IL3, TPO and FLT3L, it was noted that during the longer periods of culture there was an accumulation of more differentiated cells at the expense of HSPC (Sontag et al., 2017a). This lead to the hypothesis that the EB layer produces additional cytokines and prompts the formed iPSC-derived hematopoietic progenitor cells in the supernatant to differentiate into myeloid cells. Furthermore, the hematopoietic cells inside or below the EB layer were also promoted to differentiate. So far the influence of JAK2V617F was analyzed on the iPSC-derived cells that have been released into the supernatant on early time points of hematopoietic differentiation. The next step was to determine whether there was a bias for a specific myeloid lineage in long-term differentiation culture.

To this end, hematopoietic differentiation was performed for 49 days as described (Figure 34). After 49 days, the EB layer was separated from the supernatant fraction. The EB layer was dissociated into single cells as described in chapter 2.2.1.10.1. Cells from the supernatant and EB layer were analyzed for the development of myeloid cells within the CD45$^+$ cell population by flow cytometry (Figure 38, Figure 39 and Supplemental Figure 11).

First, cells from supernatant and EB layer were analyzed for their presence of hematopoietic cells. To this end, CD45$^+$ cells were quantified (Figure 38). Independent of JAK2V617F more than 95% of supernatant cells were CD45$^+$ (Figure

38A). This percentage seemed stable when performed with multiple independent experiments (Figure 38B). Compared to suspension cells the CD45$^+$ cell population is less in the EB layer. This might be because the EB layer contains more immature cell that drive *in vitro* hematopoiesis. Notably, it seemed to vary more drastically within the EB layer. Multiple experiments showed a range from 80% CD45$^+$ cells to as low as 20% CD45$^+$ cells. This fluctuation might be because of technical difficulties when isolating single cells from the EB layer. At the end of differentiation the EB layer does not contain a monolayer of cells anymore but is comprised of multiple layers. Therefore, the digestion enzyme is not able to function optimally throughout all layers. And although a thorough resuspension followed digestion, EB layers were never fully digested into single cells using either Accutase or Collagenase IV or the combination of both.
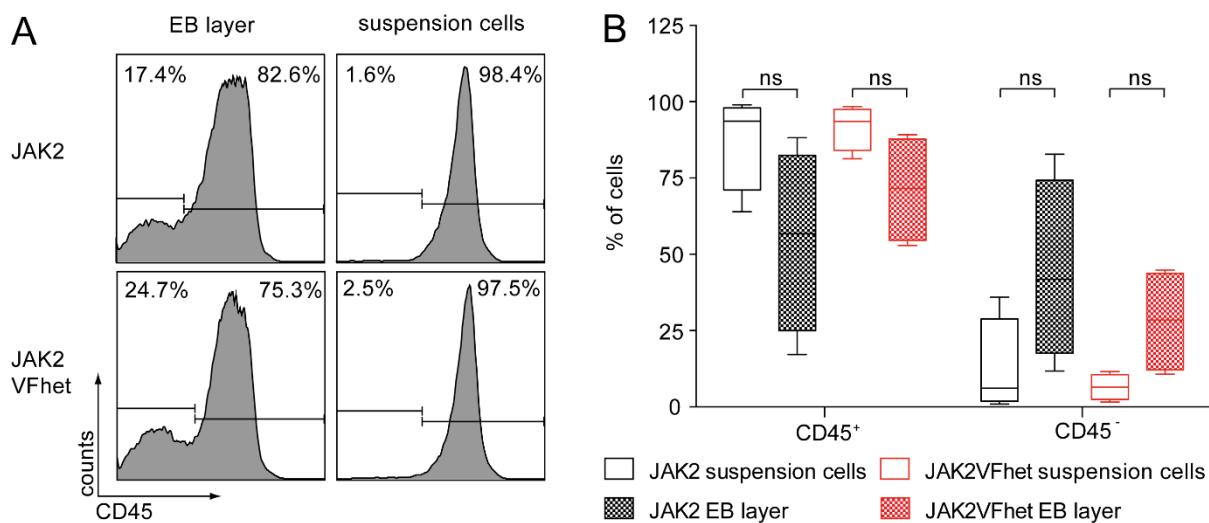

Figure 38. CD45$^+$ cells varies strongly within the EB layer

JAK2 and JAK2VFhet iPSC clones of PV1 were differentiated for 49 days as according to the protocol shown in Figure 34. EB layer was disrupted into single cells, stained with CD45 and analyzed with flow cytometry. Cells were gated according to Supplemental Figure 9. (A) Shown are representative flow cytometry analyses for JAK2_1 and JAK2V617F_1. CD45$^+$ cells are shown as a histogram. (B) Summary of CD45$^+$ and CD45$^-$ cells within EB layer and supernatant. For statistical analysis a Mann-Whitney-U test was performed. Per JAK2 genotype a comparison was done between suspension cells and EB layer (n = 4). ns = non significant.

Second, the CD45$^+$ cells were further analyzed for the presence of various myeloid subsets (Figure 39A – B). Additionally, for phenotypical analyses, iPSC-derived myeloid cells were sorted and cytospins were prepared. Previous studies show that neutrophils are CD66b$^+$ IL5R$^-$ while eosinophils were defined as CD66$^-$ IL5R$^+$ cells (Lachmann et al., 2015). Indeed, both granulocyte subsets were observed during hematopoietic differentiation (Supplemental Figure 12 and Supplemental Figure 11B). Flow cytometric analyses showed that the majority of cells differentiated into eosinophils (20% of CD45$^+$ cells). A small population of neutrophils was present in both JAK2 and JAK2VFhet iPSC clones. However, there was no difference between JAK2 and JAK2VFhet iPSC-derived cells (Figure 39C – D).

It was shown that CD61 is a marker for the megakaryocytes (Moreau et al., 2016). Indeed, JAK2 and JAK2V617F suspension cells showed about 12% of CD61$^+$ cells (Figure 39A – B and Figure 39E). Notably, this population was increased in the EB layer. JAK2V617F expressing cells showed a small decrease in the megakaryocytic population. However, due to variation no significance was detected. Therefore, JAK2V617F showed no bias towards the megakaryocytic lineage compared to JAK2. Yet, when supernatant fraction and EB layer were analyzed, megakaryocytes were enriched in the EB layer.

Mast cells were analyzed by the surface expression of ckit and FcεReceptor (FcεR) (Kovarova, 2013) (Figure 39A – B). Mast cells were further divided into immature (ckit$^+$ FcεR$^-$) and mature (ckit$^+$ FcεR$^+$) mast cells. H&E staining showed the absence of mast cell typical granules in immature mast cells while mature cells also showed irregular cell edges (Supplemental Figure 12A). As shown in Figure 39F – G the majority of iPSC-derived cells formed immature mast cells. Furthermore, immature mast cells accumulated in JAK2 and JAK2VFhet EB layers to the same degree (35% and 25% of CD45$^+$ cells, respectively). As for all other myeloid cell types, JAK2V617F did not show a bias towards toward the mast cell lineage either.

EB layer and suspension cells were also analyzed for dendritic cells by the surface expression of HLA-DR and cytospin preparations (Supplemental Figure 11C and Supplemental Figure 12B). As shown in Supplemental Figure 11C JAK2 and

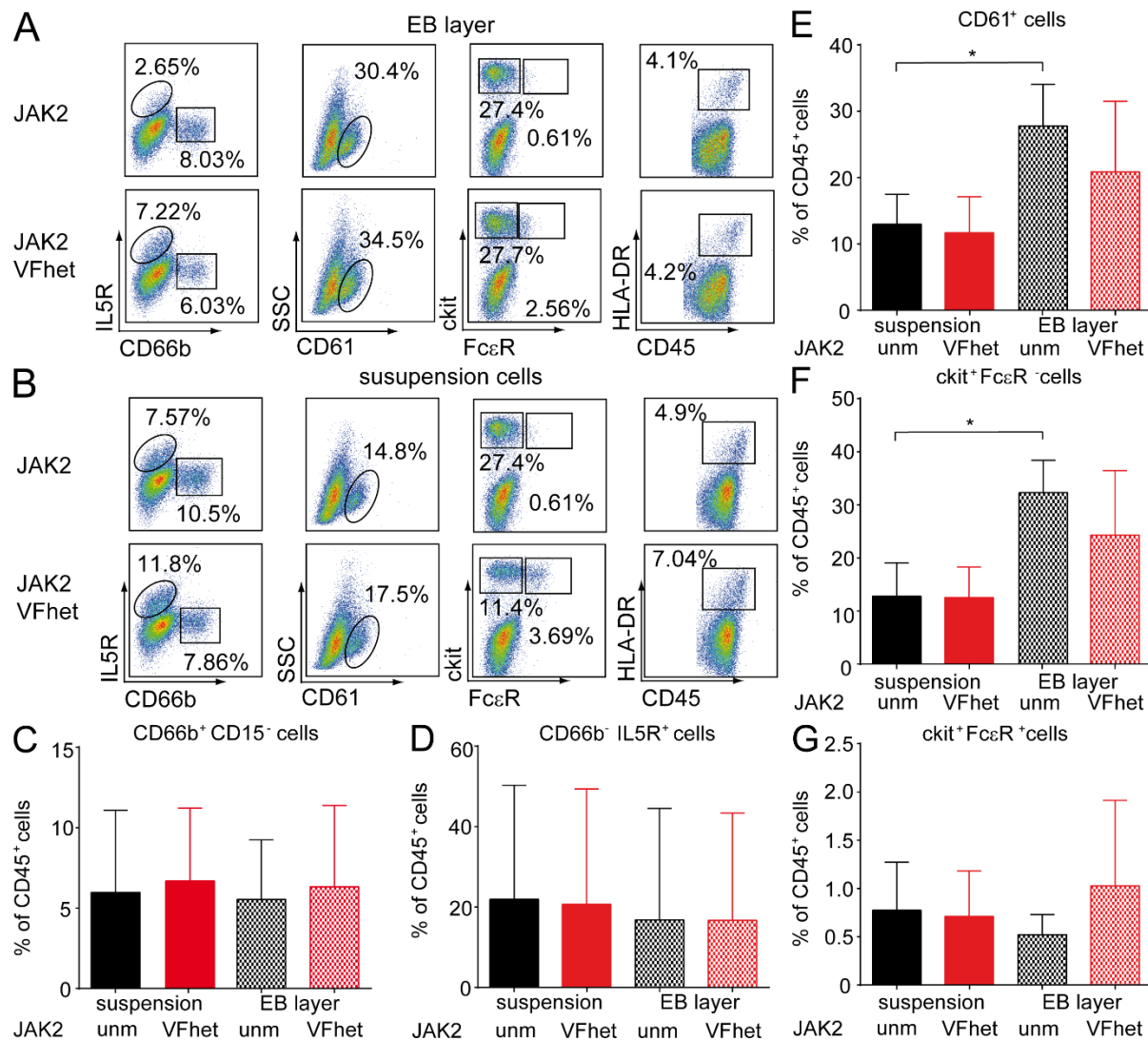JAK2VFhet iPSC clones differentiated into 7% of DC showing no bias towards the DC lineage.

Figure 39. JAK2V617F iPSC-derived hematopoietic cells do not show a bias toward a myeloid linage compared to JAK2 iPSC-derived hematopoietic cells

PV1 iPSC clones were subjected to hematopoietic differentiation for 49 days. Medium changes were done every 4-5 days. On day 49 of differentiation, supernatant fraction was harvested. EB layer was treated for 20 min with Accutase and thoroughly resuspended. Cells were stained with antibodies against CD45 and myeloid lineage markers. (A – B) Flow cytometry analyses of (A) supernatant fraction and (B) EB layer for JAK2_1 and JAK2VFhet_1 is shown as an example. Cells were first gated on living cells followed by gating on single cells. Next, cells were gated on CD45 followed by gating for myeloid. The detailed gating strategy is shown in Supplemental Figure 20. (C – G) Differentiated myeloid cells for all iPSC clones of PV1 is shown (n = 3). For statistical analysis a Mann-Whitney-U test was performed. Data points marked with (*) indicate samples with p-values ≤ 0.05; Data points marked (**) indicate samples with p-values ≤ 0.005. CD66b$^+$ CD15$^-$ cells, neutrophils; CD66b$^-$ IL5R$^+$ cells, eosinophils; CD61$^+$, megakaryocytes lineage; ckit$^+$ FcεR$^-$, immature mast cells; ckit$^+$ FcεR$^+$, mature mast cells. unm, unmutated; VFhet, JAK2V617F heterozygous.

118

Taken together, JAK2V617F does not impact the differentiation towards any specific myeloid linage. This is in contrast to studies in mice in which JAK2V617F conferred an expansion of neutrophils, red blood cells and platelets (Shimizu et al., 2016). Notably, the EB layer seems to have an impact on the localization of megakaryocytes and immature mast cells.

3.2.3.4 JAK2V617F[+] iPSC-derived hematopoietic cells show faster expansion without influencing cell cycle

As shown in Figure 35 (d18) JAK2 and JAK2V617F EB formed a layer of endothelial cells which was left undisturbed in the endothelial-to-hematopoietic-transition (EHT) medium. Therefore, iPSC-derived hematopoiesis is a continuous process. Hematopoietic cells accumulated over time and suspension cells could be harvested every 4 days between day 14 and 30 of differentiation. With each harvest cells were quantified via Neubauer chamber and trypan blue staining. Interestingly, differentiating JAK2V617F[+] iPSC yielded a significantly increased amount of supernatant cells during every harvest compared to JAK2 iPSC (Figure 40A). Furthermore, the number of harvested cells increased with each harvest independent of the genotype.

In leukemia oncogenes downregulate tumor suppressor genes or genes that are involved in regulating cell proliferation. For example, IRF8 loss in CML in mediated by BcrAbl and is associated with a more aggressive disease (Scheller et al., 2013) making IRF8 a tumor suppressor in CML. JAK2V617F was shown to activate PIM kinases, c-MYC and JUNB (Wernig et al. (2008), Funakoshi-Tago et al. (2013)). These genes are involved in stimulating proliferation. Notably, there are a number of controversial studies whether JAK2V617F conveys a proliferative advantage in the mutated cells. Hence, the first hypothesis for the increased cell numbers was that

the JAK2V617F mutation conveys an increased proliferation to hematopoietic cells. To test this hypothesis, cell proliferation of JAK2 and JAK2V617F iPSC-derived cells was analyzed.

First, suspension cells were harvested and stained with the proliferation dye CFSE. Labeled cells were seeded back onto the EB layer and further cultured under the same conditions. After 2h a sample was taken and analyzed via flow cytometry to determine the signal for undivided cells (100% CFSE). After 3 days, the rest of the cells was harvested and CFSE signal was analyzed by flow cytometry. Each cell that divided gave half of CSFE to its daughter cells thus lessening CFSE signal compared to undivided cells and marking the first generation. Depending on how often a labeled cell divided the fainted CFSE signal became in flow cytometric analyses. Consequently, proliferation was monitored and cell number per generation was calculated with FlowJo. The majority of JAK2 and JAK2VFhet iPSC-derived cells 3 to 5 times (Figure 40B). About 10% to 15% of CD45$^+$ cells divided 6 and 7 times. A small population remained undivided. Surprisingly, JAK2V617F had no significant effect cell proliferation in CD45$^+$ hematopoietic cells for each generation (Figure 40B). One hypothesis for this observation is that suspension cells have already committed to the hematopoietic and lineage their proliferation potential might be limited to a few cell divisions until these cells are terminally differentiated and that the JAK2V617F mutation has no effect on the already committed cells. Therefore, it might be beneficial to assess the cells where the suspension cells originate from, i.e. the EB layer.
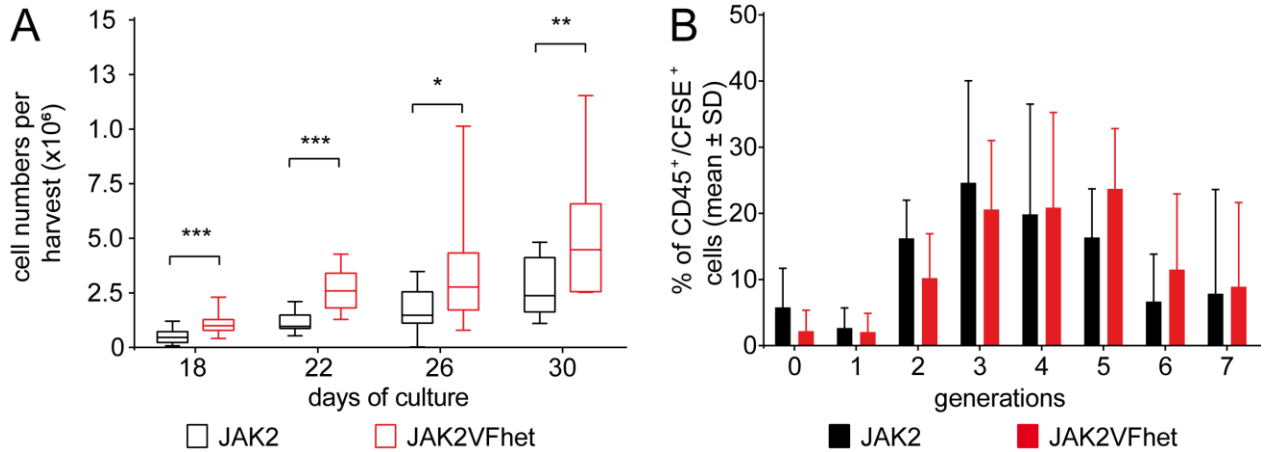
Figure 40. JAK2V617F show increased cell numbers on each harvest day during hematopoietic differentiation

JAK2 and JAK2VFhet iPSC clones of PV1 were differentiated as described in chapter 3.2.3.1. (A) iPSC-derived hematopoietic cells were harvested multiple times during hematopoietic differentiation of iPSC. Shown are the cell numbers per harvest on each harvest day for each iPSC of PV1 (n = 11). For statistical analysis a Mann-Whitney-U test was performed. (B) PV1 iPSC derived hematopoietic cells were harvested on day 18 or day 22 of differentiation and stained with 1 µM (final concentration) CFSE for 5 min, washed 3x with medium and seeded back onto the EB layer. A sample for undivided cells was taken after 2h of culture and CFSE signal of CD45$^+$ cells was analyzed by flow cytometry. After 3 days, cells were harvested and CFSE signal was analyzed by flow cytometry. Additionally, cells were stained with an antibody specific for CD45. Cell generation and cell number per generation was calculated with FlowJo. Shown is the percentage of cells in each generation for within the CD45$^+$ cell population. Data is represented as means ± standard deviation (n = 3). For statistical analysis a Student's t test was performed. Data points marked with (*) indicate samples with p-values ≤ 0.05; Data points marked (**) indicate samples with p-values ≤ 0.005. VFhet, JAK2V617F heterozygous.

Another study showed that JAK2V617F$^+$ cells displayed increased levels of Cyclin D2, a gene involved in the cell cycle (Walz et al., 2006). Accordingly, there might be a higher percentage of JAK2V617F$^+$ cells in S phase. Previous results showed that iPSC-derived hematopoietic cells developed in the EB layer and were released into the supernatant (Figure 35). Hence, another hypothesis was that JAK2V617F mediates a faster proliferation of cells from the EB layer. To label cells equally cells need to be as single cells. However, to achieve that for the EB layer said layer needs to be disrupted with a harsh process followed by subsequent culture. There is the chance that only a small portion of cells might survive this procedure. To circumvent problems with too stressed cells or not equally labeled cells JAK2 and JAK2V617F EB layers were subjected to Bromodeoxyuridine (BrdU) incorporation and subsequent cell cycle analysis. To this end, JAK2 and JAK2V617F EB layers were dissociated with Accutase into single cells. Cells were cultured in EHT medium

and pulsed with BrdU. As control, part of the cultured was left without BrdU. Subsequently, cells were stained for CD45 followed, fixed and permeabilized and probed with an antibody against BrdU incorporation. Finally, 7AAD was added.

First, cell cycle analysis of total cell population was done. As shown in Figure 41A 13.3% of JAK2 cells and 15.8% JAK2VFhet cells were in S Phase, therefore showing cell proliferation. Furthermore, the majority of cells, 72% of JAK2 and 69% of JAK2VFhet cells, did not enter the cell cycle and stayed in G0/G1 phase. Strikingly, cell proliferation was not altered in the JAK2V617F$^+$ EB layer (Figure 41C). Second, as the EB layer is made up by a multitude of cell types (Figure 39A – B), another focus was on the hematopoietic fraction (CD45$^+$ cells) of the EB layer (Figure 41B). Compared to total cells there was a higher percentage of CD45$^+$ cells that were in S phase. 33% of JAK2 cells and 30% and JAK2VFhet cells could be detected in S phase. However, CD45$^+$ cells also revealed no significant influence of JAK2V617F on the cell cycle (Figure 41D). Consequently, the increased expansion of JAK2VFhet cells does not have its origin in higher proliferation of CD45$^+$ cells or the EB layer.
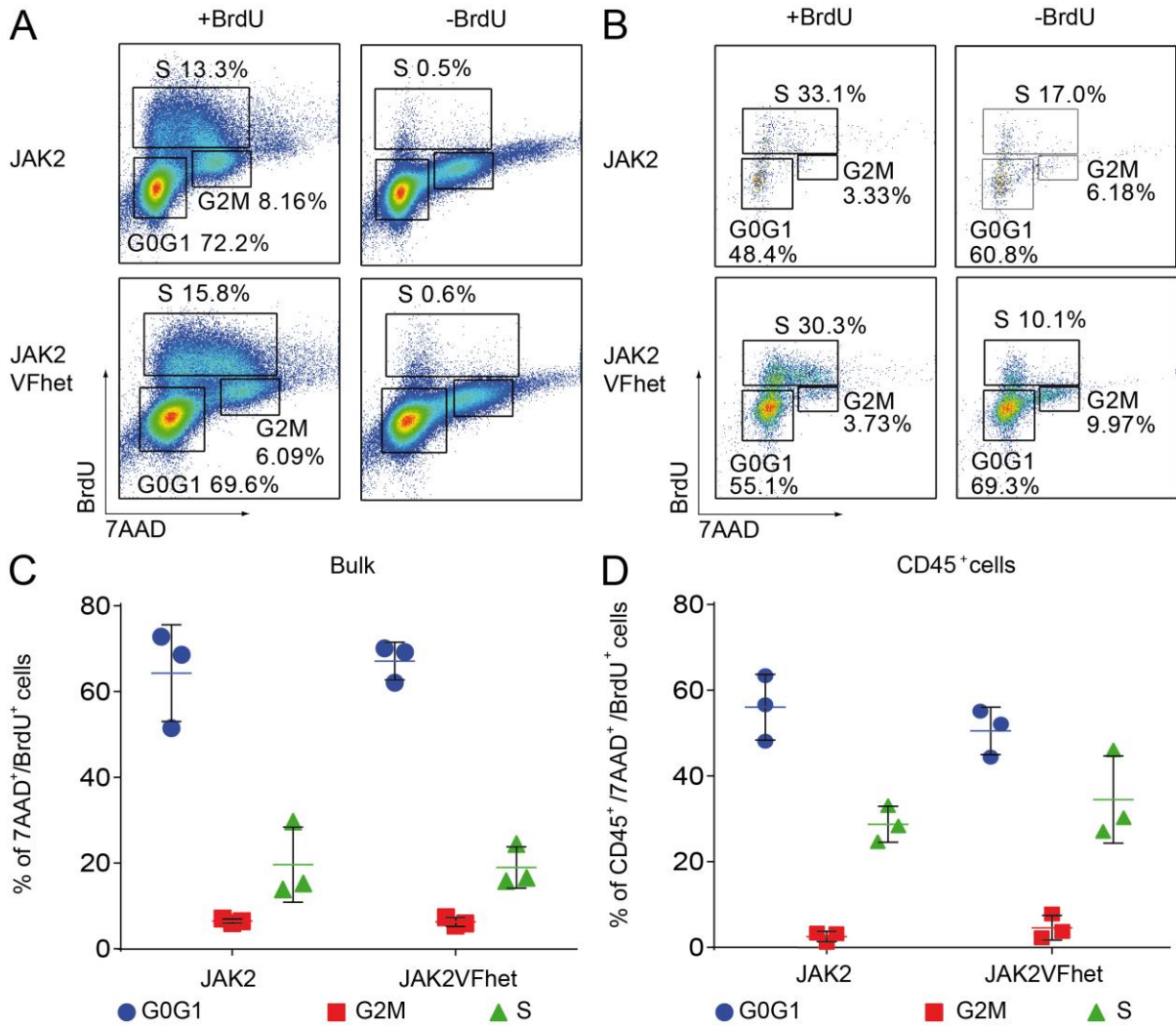
Figure 41. JAK2V617F does not influence the cell cycle in the EB layer

JAK2 and JAK2VF het iPSC clones from PV1 were subjected to hematopoietic differentiation. On day 14 of differentiation EB layers were harvested with Accutase and single cells were pulsed with or without BrdU for 1h. EB layer cells were stained for flow cytometry with CD45 prior to intracellular staining with an antibody against BrdU incorporation. Finally, cells were stained with 7AAD to analyze cell cycle. (A) Representative cell cycle analysis of total cells (bulk) in the EB layer from JAK2_1 and JAK2VFhet_1 is shown. (B) Cells from EB layer were pre-gated on CD45 before cell cycle analysis was done. Shown is a representative flow cytometry analysis of JAK2_1 and JAK2VFhet_1 for CD45+ cell population. (C – D) Summary of cell cycle analyses for (C) total (bulk) cells and (D) CD45+ cells in JAK2 (clone 1 and 2) and JAK2VFhet (clones 1 and 2) EB layer cells. Data is represented as means ± standard deviation (n = 3). For statistical analysis a Student's t test was performed. Data points marked with (ns) indicate samples with p-values that are not significant. VFhet, JAK2V617F heterozygous.

In conclusion, CFSE staining of supernatant cells showed no proliferative advantage for JAK2V617F+ cells (Figure 40B). Furthermore, BrdU incorporation and 7AAD staining showed no effect of JAK2V617F on the cell cycle of the EB layer in total or

CD45$^+$ cells of the EB layer (Figure 41). Consequently, the increased cell numbers per harvest does not seem to have the cause in increased proliferation of CD45$^+$ cells. These cells might be too committed to a certain cell lineage and have a limited proliferation capacity that the JAK2V617F mutation has any significant effect. The cause for the expansion seen during diffraction might be in the earliest hematopoietic cells that can be detected in this differentiation system.

3.2.3.5 Higher JAK2V617F cell numbers stem from higher expansion of CD34$^+$ cells in the EB layer

Previous experiments showed a higher percentage of CD34$^+$ CD31$^+$ HE cells on day 6 of differentiation for JAK2V617F heterozygous cells (Figure 37A). CD34$^+$ CD31$^+$ cells represent cells from the HE and, consequently, are the origin of all hematopoietic cells *in vitro* and *in vivo* (Boisset et al. (2010), Kissa and Herbomel (2010)). Lineage tracing has shown that HE undergo the process of EHT so that hematopoietic progenitors can be released (Eilken et al. (2009), Lam et al. (2010)).

The next hypothesis is that JAK2V617F has an effect on the development of the earliest hematopoietic cells. Therefore, the underlying cause for the higher JAK2V617F$^+$ cells might be located within the CD34$^+$ cell population that reside in the EB layers. It might be that the JAK2V617F mutation expands the HSC pool, consequently, HSC can give rise to more HPC. To assess this hypothesis, JAK2 and JAK2V617F EB layer was dissociated into single cells on day 18 of hematopoietic differentiation and CD34$^+$ cells were isolated from via magnetic activated cell sorting (MACS) (Figure 42A). All isolated CD34$^+$ cells were cultured in EHT medium. After 4 days a medium change was performed. Cells were gently washed off the plate as endothelial cells had attached to the plate while hematopoietic cells stayed in suspension. Afterwards, CD34$^+$ cells stayed in suspension and cells expanded for

another 7 days. Cell counts were recorded and cells were analyzed via flow cytometry over time.

First, an expansion of JAK2 and JAK2VFhet iPSC-derived CD34$^+$ cells over time was observed (Figure 42B). Interestingly, JAK2V617F expressing cells showed an increased CD34$^+$ cell number after MACS procedure (Figure 42B, d0 of culture). Additionally, JAK2V617F expressing cells showed a 70-fold higher expansion in comparison to JAK2 CD34$^+$ cells (Figure 42B). The high CD34$^+$ cell number was marked by an increased percentage of CD34$^+$ cells in the JAK2V617F$^+$ EB layer at day 18 of hematopoietic differentiation (Figure 42C). This suggested that the JAK2V617F mutation has an impact in the formation of CD34$^+$ hematopoietic cells and accelerates their expansion. Whether JAK2V617F also has an effect on the EHT remains to be determined. Flow cytometric analysis first indicated a 2-fold higher CD45$^+$ ckit$^+$ population (Figure 42C), yet multiple experiments showed no difference in development of CD45$^+$ ckit$^+$ cells. Additionally, the development of red blood cells was analyzed 11day post CD34 isolation. In line with previous experiments (Figure 37C) a small population of red blood cells developed in the absence of EPO. Moreover, JAK2V617F expressing cells showed a trend towards elevated CD45$^-$ CD235a$^+$ cells (Figure 42E). This is another hint of JAK2V617F affecting especially erythropoiesis and is in line with previous experiments (Figure 37C).
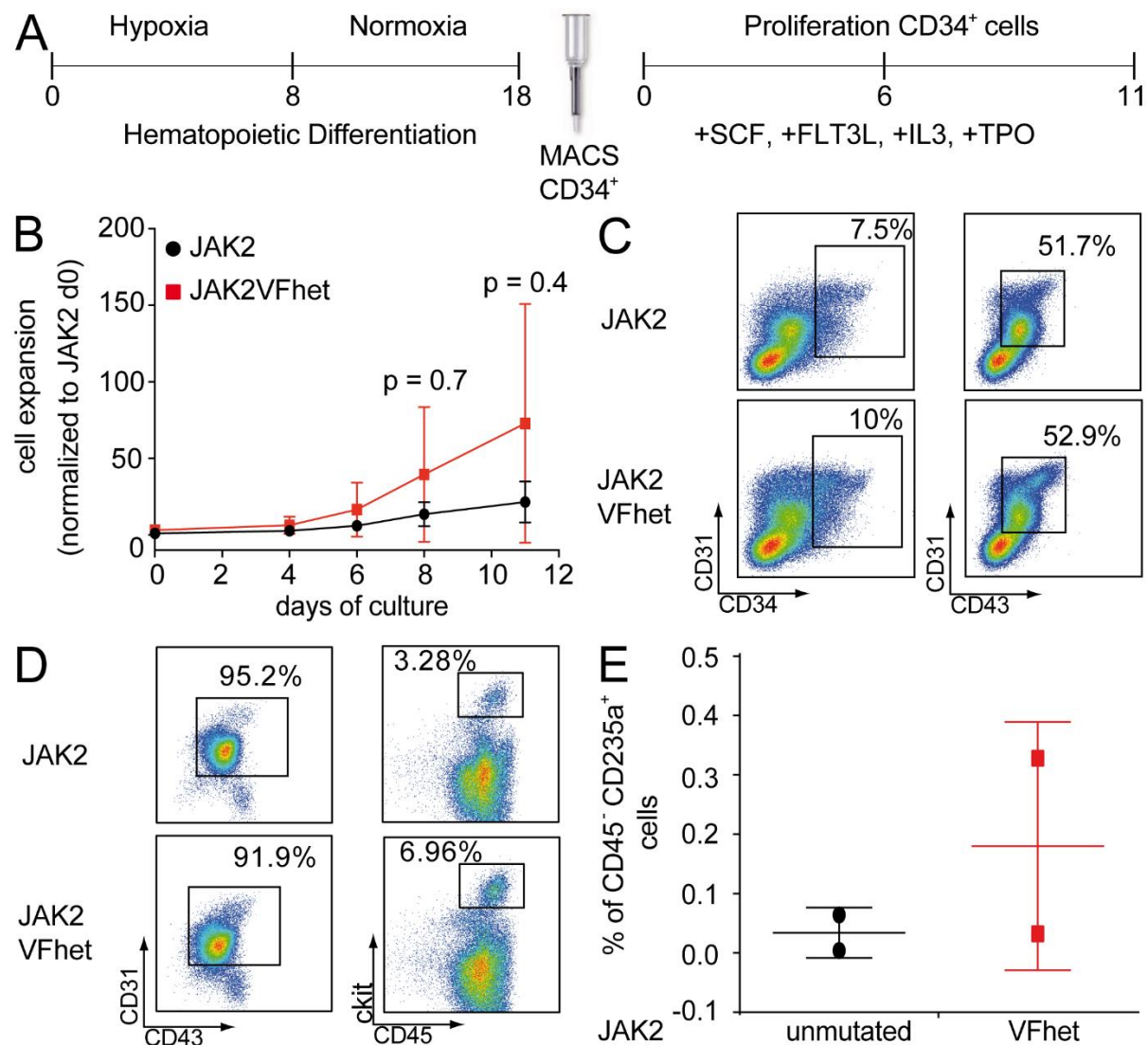
Figure 42. CD34+ JAK2V617F+ show increased CD34+ cells in the EB layer

JAK2 and JAK2VFhet iPSC clones of PV1 were subjected to hematopoietic differentiation as shown in Figure 34A. On day 18 of differentiation the EB layer was harvested, treated with Accutase to obtain single cells and CD34+ cells were isolated via MACS selection. CD34+ cells were cultured for 11 days with FLT3L, TPO, SCF and IL3. (A) Schematic representation of iPSC differentiation, MACS selection and subsequent CD34+ cell culture. (B) Cell counts were recorded with Neubauer counting chamber and trypan blue staining at indicated time points. Day 0 represents the day of MACS selection. A student's t-test was performed comparing JAK2V617F to JAK2 (n = 3). (C) On day 6 post CD34 isolation, cells were analyzed by flow cytometry. Shown is the flow cytometric analysis for JAK2_2 and JAK2VFhet_2 (n = 3). For statistical analysis a Student's t test was performed by comparing JAK2 and JAK2VF. P-values are indicated. (D) EB layer on day 18 of hematopoietic differentiation was analyzed. A representative flow cytometry analysis is shown from JAK2_1 and JAK2VFhet_1. (E) Summary of flow cytometric analysis for 2 independent experiments is shown. Percentage of CD45− CD235a+ cells is depicted (n = 2). Unm, unmutated; VFhet, JAK2V617F heterozygous.

In conclusion, JAK2V617F seems to rather have an effect on the number of CD34$^+$ cells in the EB layer. This suggests to be the case for the observed increase in cell numbers per harvest for JAK2 expressing cells (Figure 40A). There are more cells present in the EB layer that differentiate and, consequently, give rise to hematopoietic progenitors that are released into suspension. Additionally, JAK2V617F seems to convey an increased expansion towards CD34$^+$ cells. To support this hypothesis, BrdU incorporation in the CD34$^+$ cells could be done to see increased cell cycle activity. One might speculate that this the increase in CD34$^+$ cell number and their expansion might be more prominent in JAK2V617F homozygous cells as suggested in mice by Fink et al. (2013).

3.2.3.6 JAK2V617F confers hypersensitivity to EPO compared to JAK2

An increase in erythropoiesis and an overproduction of red blood cells is the major clinical feature in PV patients (Vannucchi et al., 2009). Indeed, transplantation and knock in studies in mice showed that an MPN phenotype mimicking human PV can be initiated from a single JAK2V617F$^+$ cell (Hasan et al., 2013; Lacout et al., 2006; Lundberg et al., 2014). Furthermore, the capacity to form erythroid colonies in the absence of EPO is also a phenomenon of JAK2V617F$^+$ primary cells (Dupont et al., 2007). Moreover, studies showed that an overexpression of JAK2V617F in cells co-expressing the erythropoietin receptor (EPOR) renders cell lines independent of IL3 signaling (Lu et al., 2005). Ye et al. (2014) showed that iPSC-derived hematopoietic cells with a JAK2V617F mutation are also independent of EPO signaling, however these iPSC clones were homozygous for JAK2V617F. Notably, the newly generated iPSC line from PV1 is heterozygous for JAK2V617F.

Previous experiments showed that *in vitro* differentiation of JAK2V617F iPSC showed only a trend towards elevated red blood cell production in the absence of EPO (Figure 37C). However, CFU assays of JAK2V617F iPSC-derived

hematopoietic cells failed to recapitulate the aspect of elevated erythroid colonies all together (Figure 37D). To investigate whether the trend towards higher erythroid cells in JAK2V617F expressing cells can be amplified JAK2 and JAK2VF iPSC hematopoietic cells were differentiated in to red blood cells. In case JAK2V617F expressing cells gave rise to increased red blood cells the new iPSC line can be used as an *in vitro* model system for human PV.

To this end, iPSC clones shown in Table 19 and Table 20 were first differentiated towards the hematopoietic lineage. Afterwards, JAK2, JAK2VFhet and JAK2VFhom iPSC-derived cells were harvested from suspension on day 22 of hematopoietic differentiation. Next, harvested cells were induced to differentiate further toward red blood cells with EPO, IL3 and SCF for 12 days according to the protocol published by Dorn et al. (2015). As control in the given culture conditions, cells were cultured in the absence of EPO. Red blood cell differentiation was monitored by flow cytometry analysis of CD235a, CD45 and CD43 expression with HPC defined as CD45$^+$ CD43$^+$, red blood cell progenitors as CD45$^-$ CD43$^+$ and red blood cells as CD45$^-$ CD43$^-$ or CD45$^-$ CD235a$^+$. In addition, cells were spun onto glass slides and stained with neutral benzidine and hematoxylin/eosin (H&E) to assess cell morphology.

Flow cytometry analyses showed that JAK2, JAK2VFhet and JAK2VFhom iPSC-derived cells gave rise to a low percentage of red blood cell progenitors (0.5%, 0.1% and 0.3%, respectively) in the absence of EPO (Figure 43A and Supplemental Figure 13A). Moreover, almost no CD45$^-$ CD43$^-$ red blood cells could be detected independent of the JAK2 genotype (Figure 43A, Figure 43C, Supplemental Figure 13C). It was shown that the majority of cells remained as CD45$^+$ CD43$^+$ HPC without EPO addition. A more direct gating on CD45$^-$ CD235a$^+$ red blood cells did not show any erythroid cell formation in the absence of EPO. Interestingly, JAK2V617F homozygous iPSC-derived hematopoietic cells produced a small population of CD45$^-$ CD235a$^+$ cells after 12 days of EPO differentiation (Figure 43A, left and center panels) in comparison to JAK2 and JAK2VFhet cells. Additionally, cytospin

and histological staining with neutral benzidine and H&E revealed no red blood cells (indicated as red color of the cytoplasm) were present (Figure 43A, right panels and Supplemental Figure 13A). Notably, JAK2, JAK2V617F heterozygous and JAK2V617F homozygous iPSC-derived cells developed into eosinophils and neutrophils after 12 days of culture without EPO. Total cell number of CD45$^-$ CD235a$^+$ stayed low in the absence of EPO (Figure 43D). The low CD45$^-$ CD235$^+$ cell population might indicate that cells with JAK2V617F are not as EPO or growth factor independent as for example BcrAbl$^+$ CML cells, thus identifying JAK2V617F as a mild oncogene. In previous experiments it was shown that physiological expression of JAK2V617F in mice results in a long latency of the MPN phenotype and that additional mutations lead to added characteristics, such as such as growth factors independence or an MPN phenotype *in vivo* (Shimizu et al., 2016).

In the presence of a low dose of EPO (0.2 U/ml), JAK2 iPSC-derived hematopoietic cells showed a small but detectable population of CD45$^-$ CD235a$^+$ cells. JAK2V617F heterozygous iPSC-derived hematopoietic cells initially produced a 6-fold higher CD45$^-$ CD235a$^+$ red blood cell population compared to JAK2 cells with low dose EPO (Figure 43B and Supplemental Figure 13B). This was even more increased when 3 independent experiment were performed (Figure 43C and Supplemental Figure 13C). Strikingly, the red blood cell population increased even more with JAK2V617F homozygous iPSC-derived cells (11-fold compared to JAK2 heterozygous cells) showing a hypersensitivity of JAK2V617F to EPO (Figure 43B, left and center panels). Neutral benzidine staining also showed an increase in normoblast formation with an increase in JAK2V617F allele (Figure 43B, right panels). Furthermore, with a low dose of EPO cell numbers of CD45$^-$ CD235a$^+$ also increased more dramatically with JAK2V617F$^+$ cells than with JAK2 cells (Figure 43E).
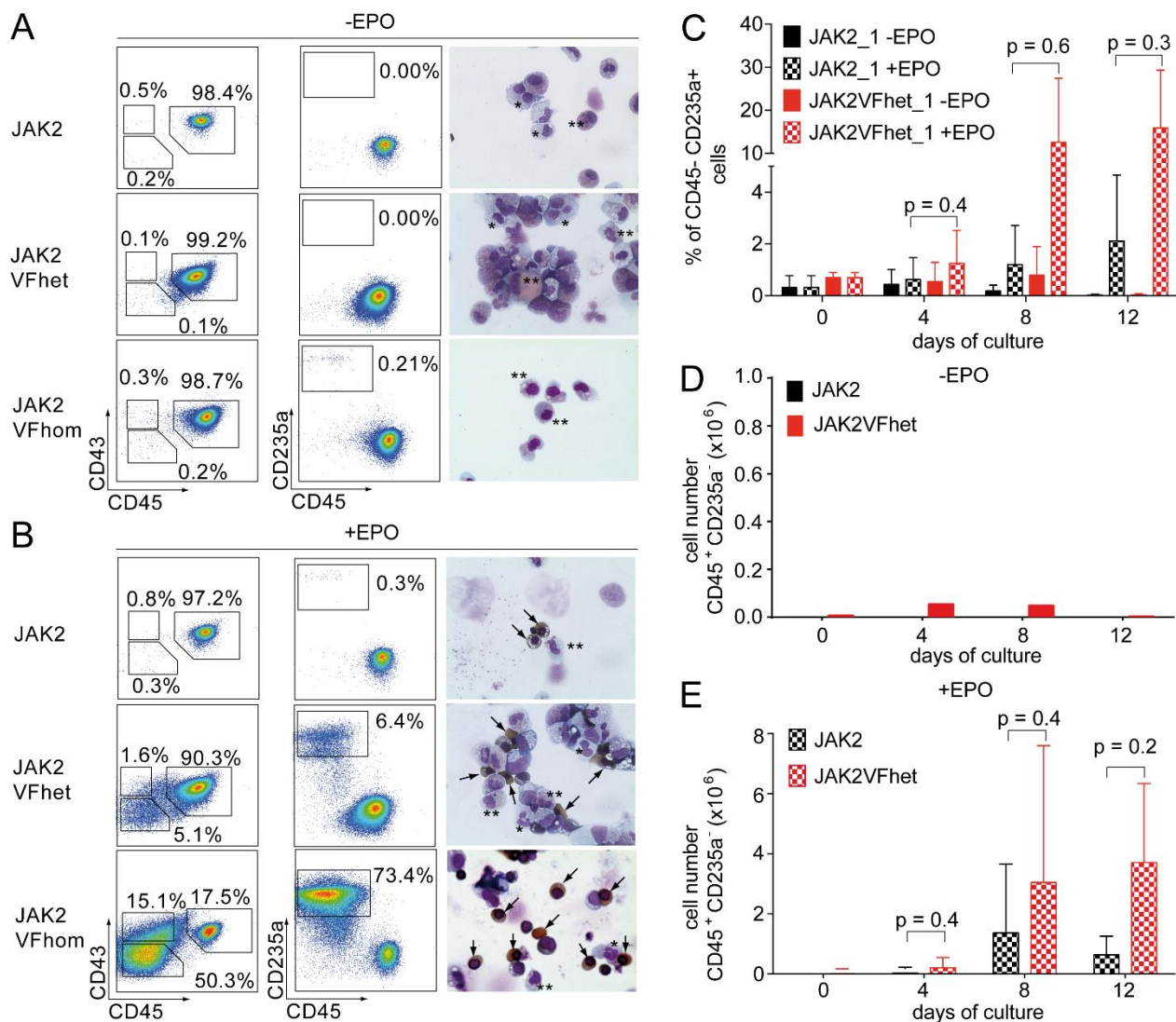
Figure 43. JAK2V617F$^+$ cells show a higher CD235a$^+$ cell population in response to EPO

JAK2 and JAK2VFhet iPSC clones from PV1 were induced to differentiate into hematopoietic cells as shown in Figure 34A. Next, iPSC-derived cells were harvested on day 22 of hematopoietic differentiation. Cells were cultured in StemPro34 supplemented with 100 ng/ml SCF, 30 ng/ml IL3 and 0.2 U/ml EPO. Red blood cell differentiation was induced according to the Figure 18. Cells were counted and analyzed by flow cytometry every 4 days. (A – B) Cells were stained with antibodies against CD43, CD45 and CD235a followed by flow cytometry analysis. Shown are representative analyses of JAK2_1, JAK2VFhet_1 and JAK2hom_1 on day 12 of red blood cell differentiation (A) in the absence and (B) presence of EPO. Additionally, cells were spun onto glass slides and neutral benzidine/H&E staining was performed. Arrows indicate normoblasts. Asterisks indicate neutrophils (*) and eosinophils (**). (C) Shown is the percentage of CD45$^-$ CD235a$^+$ cells for JAK2_1 and JAK2VFhet_1 during red blood cell differentiation. (D – E) The number of CD45$^-$ CD235a$^+$ cells (D) without EPO and (E) with EPO addition is shown (n = 3). Shown are the results from JAK2 (clone 1 and 2) and JAK2VFhet (clone 1 and 2). A student's t test was performed for statistical analysis. JAK2VFhet was compared to JAK2. For each differentiation day p values are indicated.

Taken together, JAK2V617F causes an overproduction of iPSC-derived red blood cells only in the presence of EPO. Notably, this is in contrast to previous studies in mice and studies with primary cells (Zaleskas et al., 2006). Furthermore, the overproduction is dependent on the JAK2V617F burden within the cells as JAK2V617F homozygous iPSC-derived hematopoietic cells generated a higher amount of CD45$^-$ CD235a$^+$ red blood cells compared to JAK2V617F heterozygous iPSC-derived hematopoietic cells. Consequently, JAK2V617F iPSC recapitulate the overproduction of red blood cells *in vitro* due to its hypersensitivity to EPO which is also seen in PV patients in clinics. Henceforth, JAK2V617F iPSC could be used as a model system for PV *in vitro*. Moreover, the overproduction of red blood cells can be analyzed in detail, i.e. signaling pathway of EPO in JAK2V617F expressing cell compared to JAK2 cells. This might add to results that have been done in cell lines, such as HEL, BaF3 cells (James et al. (2008), Zhao et al. (2005)).

3.2.4 IFNα signaling pathway in JAK2V617F$^+$ iPSC-derived hematopoietic cells

IFNα was used for the last 30 years as therapy for hepatitis C and in some cases for MPN therapy. In recent years, studies showed that patients with a JAK2V617F mutation (PV or ET) receiving IFNα therapy reached complete molecular or hematological responses. In these responses, JAK2V617F allele could not be detected with current detection methods. Yet, the signaling pathway of IFNα in the JAK2V617F malignant clone remained largely unknown (Kiladjian et al., 2016). The MAPK pathway was the only suggestion of the IFNα signaling pathway in JAK2V617F$^+$ cells (James et al., 2005). Therefore, the IFNα signaling pathway in JAK2V617F$^+$ cells was investigated in detail an compared to JAK2 cells. The second aim for this thesis is to obtain data on how IFNα eradicates JAK2V617F$^+$ cells while leaving JAK2 cells unharmed. This was done by comparing obtaining data from apoptosis assays to see whether JAK2V617F expressing cells are more sensitive to IFNα mediated apoptosis. Afterwards, gene expression and protein activation in

response to IFNα treatment will be analyzed in iPSC-derived JAK2 and JAK2V617F cells.

3.2.4.1 IFNα does not cause apoptosis in iPSC-derived hematopoietic cells

It was shown that human JAK2V617F$^+$ CD34$^+$ cells were induced to go into apoptosis by IFNα treatment (Lu et al. (2010), Mullally et al. (2013)). Other studies showed that IFNα depletes JAK2V617F expressing long-term stem cells, thus exhausting the stem cells pool of cells affected by the JAK2V617F mutation (Mullally et al., 2013). Consequently, IFNα lead to complete hematological remissions in mice and human. Other studies showed that murine HSC are induced to proliferate *in vivo* (Essers et al. (2009), Pietras et al. (2014)).

To investigate whether JAK2 and JAK2VFhet iPSC-derived hematopoietic cells showed similar kinetics as previous studies, iPSC-derived hematopoietic suspension cells were harvested on day 22 and 26 of differentiation. Cells were treated with varying concentrations of IFNα (50 to 1600 U/ml) or left untreated for 2 days followed by an MTT assay. As control of complete cell death cells were treated with puromycin. An MTT assay measures the metabolic activity of viable cells in an NADH-dependent manner as only viable cells are able to reduce MTT (3-(4,5-dimethylthiazol-2-yl)-2,5-diphenyltetrazolium bromide) to its insoluble form formazan.

As expected when treated with puromycin cells went into complete apoptosis independent of the JAK2 genotype (Figure 44A). Notably, JAK2 iPSC-derived cells did not show any reduction in viable cells. Surprisingly, JAK2VFhet iPSC-derived hematopoietic cells also showed no sign of apoptosis over the tested range of IFNα concentrations (Figure 44A). Furthermore, there was no difference in IFNα response when comparing JAK2V617F to JAK2 iPSC-derived hematopoietic cells.
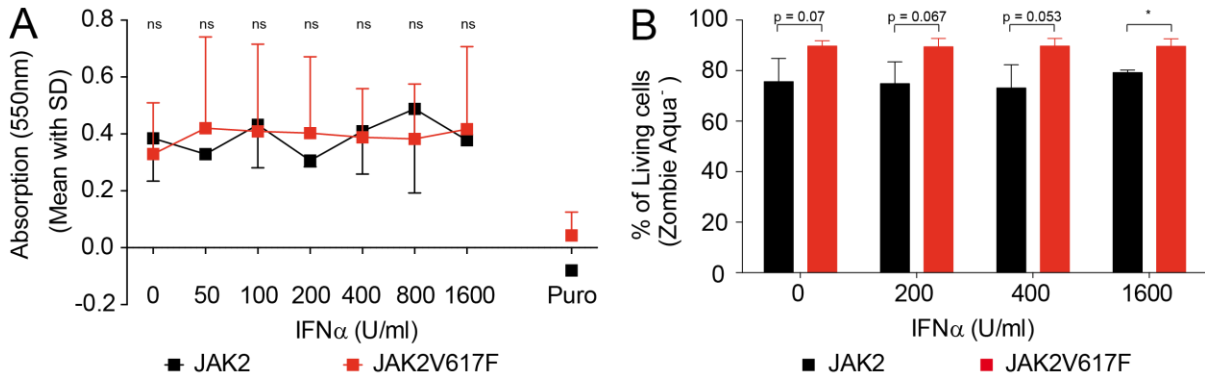
Figure 44. IFNα does not cause apoptosis in iPSC-derived hematopoietic cells

JAK2_1 and JAK2V617F_1 iPSC-derived hematopoietic cells were harvested on day 22 or 26 of differentiation. (A) An MTT assay was performed to quantify cell viability. After harvesting cells were washed once and diluted to 20000 cells per 90 µl with EHT medium followed by seeding into a microtiter plate. Next, 10 µl IFNα (50 to 1600 U/ml) were added per well followed by a 2 day culture period. Afterwards, 10 µl MTT was added and cells were cultured for 4h. Finally, 100 µl Isopropanol-HCL was added and absorption was measured at 550 nm. SFM was used as blank. A triple measurement per concentration was performed (n = 3). Puromycin (Puro) was used as positive control for complete cell death. (B) Live/Dead staining using Zombie Aqua of PV1 iPSC derived hematopoietic cells was performed. The percentage of living cells is shown (n = 3). A student's t test was performed for statistical analysis. JAK2VFhet was compared to JAK2. For each differentiation day p values are indicated. Data points marked with (*) indicate samples with p-values ≤ 0.05.

As there is a possibility to dilute responses to treatment when just looking at bulk cell responses like in an MTT assay. Therefore, another assay looking on single cell responses of IFNα treatment was performed to increase the sensitivity. To this end, JAK2 and JAK2VFhet iPSC-derived hematopoietic suspension cells were harvested on day 22 or day 26 of differentiation and cultured with chosen IFNα concentrations (200, 400 and 1600 U/ml) for 2 days. Cell viability was analyzed by flow cytometry using AquaZombie. However, even when analyzing apoptosis on single cell level IFNα treatment did not show a significant differences in the ratio of living and dead cells for JAK2 and JAK2V617F iPSC-derived hematopoietic cells (Figure 44B).

3.2.4.2 Gene expression of IFNα target genes in iPSC-derived hematopoietic cells and patient PBMNC

As iPSC-derived cells failed to respond in 2 apoptosis assays (Figure 44) it lead to 2 hypotheses. The first one was that IFNα does not induce an apoptotic response but a complex genetic response. The second hypothesis was that iPSC-derived suspension cells are unresponsive to IFNα which might be because of a defect in the IFNα signaling pathway. Therefore, the components of the IFNα signaling pathway (Figure 11) were further investigated in iPSC-derived cells to see where IFNα might be blocked.

It could be that RNA expression of IFNα signaling components, like IRF9, IRF7 or STAT1 is low or absent in iPSC-derived cells. Activation and level of the IFNα pathway can be evaluated by assessing the gene expression IFNα target genes, like IRF7 and IRF9 in response to IFNα (chapter 3.2.4.2). Another block can be in the phosphorylation of STAT1. With low STAT1 or pSTAT1 protein levels the response to IFNα is not optimal and, consequently, IFNα responses are decreased in iPSC-derived cells. Activation of the STAT1 can be evaluated by screening for pSTAT1 protein levels via immunoblotting after IFNα exposure (chapter 3.2.4.4). The last possible block of IFNα signaling is that iPSC-derived cells do not display IFNAR1 or IFNAR2 on their surface. Without the receptor being displayed on the surface there is no binding of the ligand and, consequently, no activation of the downstream signaling cascade. Therefore, iPSC-derived cells can be stained with IFNAR1 and IFNAR1 specific antibodies and analyzed with flow cytometry (chapter 3.2.4.3).

3.2.4.2.1 iPSC-derived hematopoietic cells do not upregulate IFNα target genes upon IFNα stimulation

First, JAK2 and JAK2V617F iPSC-derived hematopoietic cells were analyzed whether they express the genes to respond to IFNα. To this end, iPSC-derived

hematopoietic suspension cells were harvested on day 18 of differentiation and cultured for 4h in the presence and absence of 200 U/ml IFNα. RNA was extracted and cells were subjected to RT-qPCR. Expression of IFNAR1, IFNAR2, IRF7 and IRF9 was analyzed in response to IFNα.

In a first part, JAK2 and JAK2VFhet iPSC-derived hematopoietic cells were analyzed for their IFNα target gene expression in the presence and absence of IFNα. As shown in Figure 45A – B JAK2 and JAK2V617F iPSC-derived hematopoietic cells express both IFNAR subunits in the absence of IFNα. Notably, the expression levels of the receptor subunits seemed to differ. The maximal gene expression (Fold GAPDH) for IFNAR1 is 4x higher than that of IFNAR2. This pattern of higher IFNAR1 than IFNAR2 expression seems to be in line with studies from human cancer cell lines (Booy et al., 2014). In the presence of IFNα JAK2 and JAK2VFhet iPSC-derived hematopoietic cells upregulated IFNAR1 and IFNAR2. However, the increase in gene expression was not significant.

Next, gene expression of IRF7 and IRF9 was studied. As shown in Figure 45C – D RNA for both genes was detected in the absence of IFNα in JAK2 and JAK2V617F iPSC-derived hematopoietic cells. Notably, IRF7 and IRF9 expression levels for JAK2_2 iPSC-derived hematopoietic cells were lower than all the other iPSC-derived hematopoietic cells without IFNα treatment. In the presence if IFNα all iPSC-derived clones showed a slight upregulation of IRF7. Notably, upregulation was significant only for JAK2_2 iPSC-derived hematopoietic cells (5-fold, Figure 45C). However, the significance was not seen in IRF9 gene expression (Figure 45D). All iPSC-derived cells upregulated IRF9, however, there was no significance seen. As seen in Figure 45 high variations within the independent experiments might be the reason for the loss of significance.
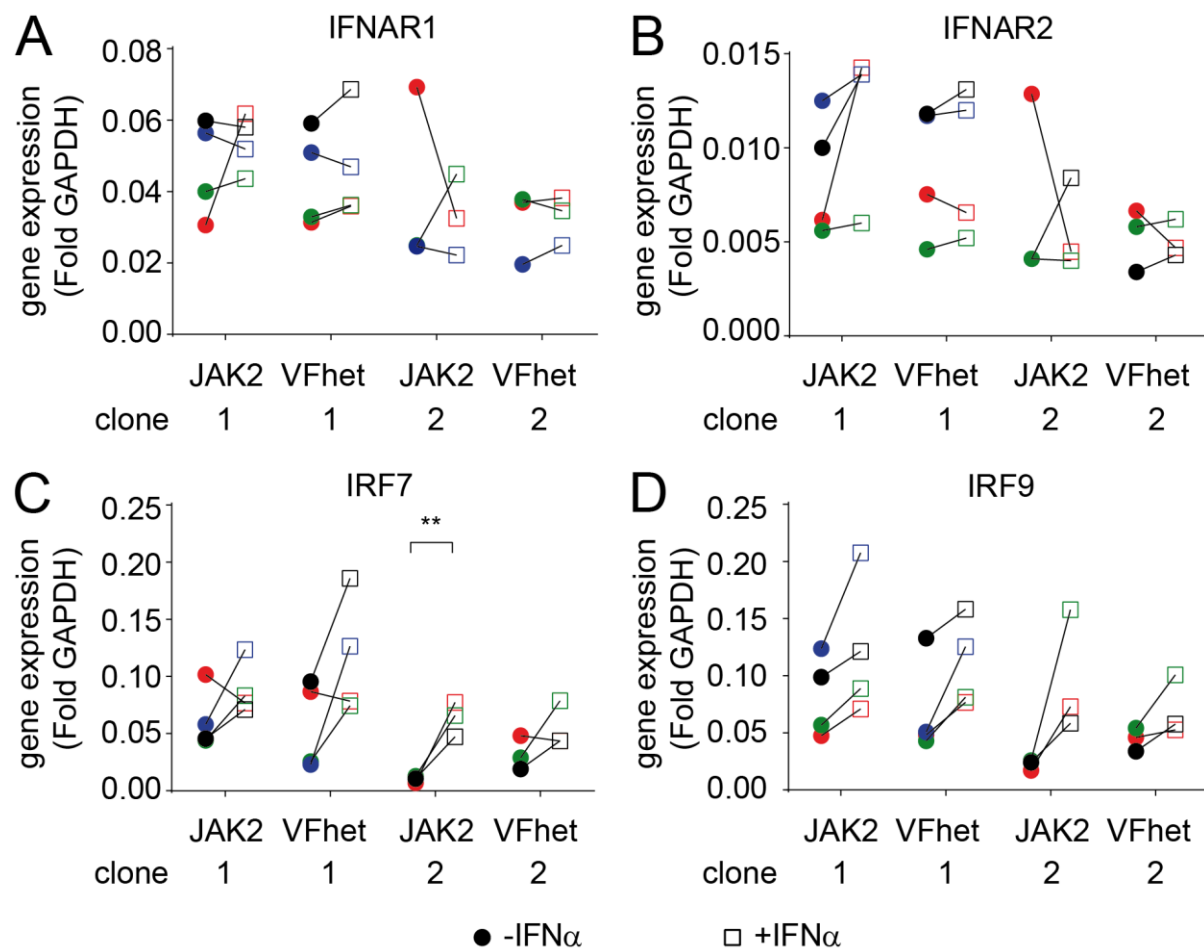
Figure 45. IFNα treatment of iPSC-derived hematopoietic cells does not upregulate IFNα target genes

iPSC clones of PV1 were subjected to hematopoietic differentiation as shown in Figure 34. On day 18 of differentiation iPSC-derived hematopoietic cells were harvested from the supernatant and cultured without cytokines in the presence or absence of IFNα (200 U/ml) for 4h. RNA was isolated and RT-qPCR for the indicated genes was performed (n = 4 for JAK2_1 and JAK2VFhet_1; n = 3 for JAK2_2 and JAK2VFhet_2). Circles represent samples that were cultured without IFNα. Squares represent samples that were treated with IFNα. Colors represent the independent experiments data was obtained from. For statistical analyses Student's t-test was performed. Data points marked with (*) indicate samples with p-values ≤ 0.05; Data points marked (**) indicate samples with p-values ≤ 0.005. Unm, unmutated; VFhet, JAK2V617F heterozygous.

In a second part, IFNα target gene expression was analyzed in JAK2VFhom iPSC-derived hematopoietic cells from PV2 and PV3 iPSC clones. The experimental setup stayed the same as for PV1 iPSC-derived hematopoietic cells. Surprisingly, iPSC-derived hematopoietic cells from JAK2VFhom_1 iPSC did not upregulate any of the selected IFNα target genes in the presence of IFNα (Supplemental Figure 14A). In contrast, JAK2VFhom_2 iPSC-derived cells showed an IFNα dependent increase in

gene expression for STAT1, STAT2 and IRF7 (Supplemental Figure 14B). In response to IFNα there was a 2-fold increase for STAT1 and STAT2 and a 2.5-fold increase for IRF7. Thus, JAK2VFhom_1 and JAK2hom_2 iPSC-derived cells seem to have a similar response to IFNα as iPSC-derived hematopoietic cells generated from PV1 iPSC (Figure 45).

Taken together, iPSC-derived hematopoietic cells from all 3 patients showed expression of IFNAR1, IFNAR2, IRF7 and IRF9 in the absence of IFNα. However, iPSC-derived hematopoietic cells from all 3 PV patients failed to significantly upregulate gene expression for IRF7 and IRF9 in iPSC-derived cells upon IFNα treatment. It might be that high variations were the cause for the loss of significant results. A more unlikely hypothesis was that all 3 patients were unresponsive to IFNα.

3.2.4.2.2 Patient PBMNC show IFNα target gene expression

To study whether the unresponsiveness is specific to the iPSC-derived suspension cells or is already seen in the cells used to generate the new iPSC lines, frozen PBMNC from all 3 PV patients were thawed. Afterwards, patient PBMNC were treated with and without 200 U/ml IFNα for 4h in the absence of cytokines. Next, RNA was extracted and RT-qPCR for IFNAR1, IFNAR2, IRF7 and IRF9 was performed. Peripheral blood from healthy blood donors of the transfusion medicine, Uniklink Aachen was taken to isolate healthy PBMNC which were used as a positive control for IFNα target gene expression (Figure 46).

Previous studies showed that IFNAR1 is highly expressed as its expression is almost at GPADH levels in PBMNC (Massirer et al., 2004). Indeed, patient PBMNC show the same relative expression in the absence of IFNα as described by Massirer et al. (2004) (Figure 46A). Interestingly, when comparing patient PBMNC with iPSC-derived cells IFNAR1 gene expression levels are 10x higher for patient PBMNC.

This might suggest that patient PBMNC have more IFNAR1 protein levels, consequently, a higher response to IFNα. As shown in Figure 45A – B and Supplemental Figure 14 iPSC-derived hematopoietic cells demonstrated a difference in IFNAR1 and IFNAR2 expression in the absence of IFNα. This expression pattern is confirmed in the corresponding primary PBMNC (Figure 46A – B) and in line with a previous study (Booy et al., 2014). RT-qPCR revealed also that IFNAR1 and IFNAR2 expression was not affected by the presence of IFNα confirming the results obtained from all iPSC-derived hematopoietic cells.

PV1 PBMNC showed expression of IRF7 which was in the range slightly higher than in healthy PBMNC in the absence of IFNα (Figure 46C). Notably, relative expression levels of IRF7 were at 4x to 10x higher in PV1 PBMNC compared to PV1 iPSC-derived hematopoietic cells (Figure 45C). IRF7 expression in primary PBMNC from PV2 and PV3 did not diverge from that of healthy PBMNC in the absence of IFNα either. Interestingly, IRF7 expression in PV2 and PV3 PBMNC was in the range of JAK2hom_1 and JAK2hom_2 iPSC-derived cells (Figure 46C). As expected healthy PBMNC upregulated IRF7 expression significantly (13-fold) in the presence of IFNα. Moreover, IRF7 expression increased significantly in primary PBMNC from all PV patients. Strikingly, PBMNC showed a much stronger IFNα dependent upregulation of IRF7 compared to iPSC-derived hematopoietic cells. For PV1 PBMNC a 3-fold increase in IRF7 was detected while PV2 and PV3 PBMNC showed a 6-fold and 3-fold increase, respectively (Figure 46C).

IRF9 expression in primary PBMNC (patient or healthy) was already highly expressed in the absence of IFNα (Figure 46D). As for IRF7, IRF9 basal expression of primary PBMNC was in the same range or even 2x to 10x higher than in iPSC-derived hematopoietic cells. When healthy PBMNC were stimulated with IFNα IRF9 expression was significantly upregulated (4-fold). For all 3 primary patient PBMNC expression of IRF9 was also increased in the presence of IFNα (1.5-fold for PV1 and PV3, 2-fold for PV2), yet this increase was not significant. However, there is a trend towards a higher expression of IRF7 and IRF9 in the presence of IFNα.
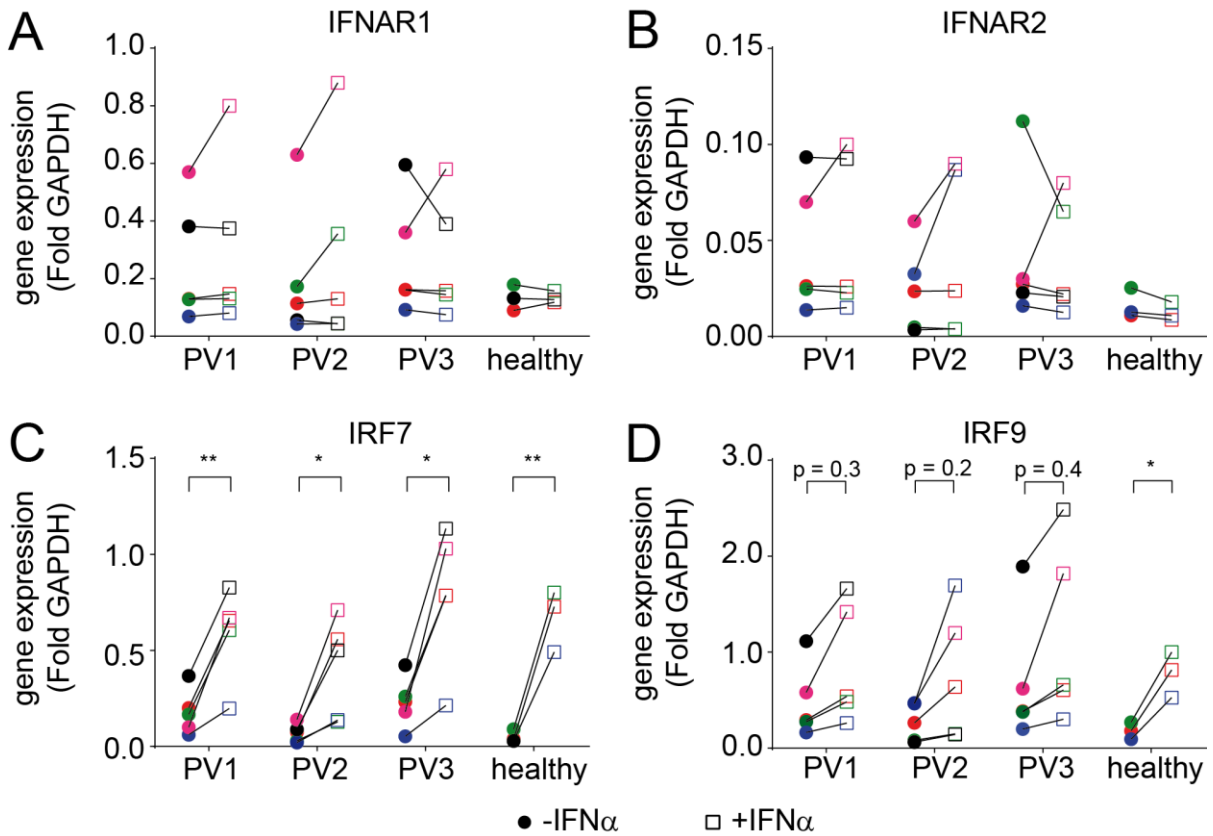
Figure 46. Patient PBMNC upregulate IFNα target genes in response to IFNα

PV patient PBMNC were thawed in RPMI + 10% FCS and living cells were enriched by 3x centrifugation at 800 rpm for 10 min. Fresh PBMNC were isolated from healthy donors via density gradient centrifugation and used as control. PBMNC were cultured in RPMI + 10% FCS without cytokines in the absence or presence of IFNα (200 U/ml) for 4h. RNA was isolated and RT-qPCR for the indicated genes was performed. Gene expression is shown as Fold GAPDH (n = 5). Colors represent the independent experiments data was obtained from. For statistical analyses unpaired Student's t-test was performed. Data points marked with (*) indicate samples with p-values ≤ 0.05; Data points marked (**) indicate samples with p-values ≤ 0.005.

Taken together, primary PBMNC upregulate IRF7 and IRF9 significantly in the presence of IFNα. Consequently, the unresponsiveness in iPSC-derived hematopoietic cells is not patient specific but specific for the iPSC-derived hematopoietic cells. There seemed to be an inconsistency in IFNα response between primary PBMNC and their corresponding iPSC-derived hematopoietic cells which needed to be investigated further.

3.2.4.3 IFNAR1 and IFNAR2 expression on the cell surface of iPSC-derived hematopoietic cells and patient PBMNC

Gene expression of IFNα target genes requires the binding of IFNα onto its receptor (Figure 11). Therefore, the receptor has to be displayed on the cell surface for a ligand, in this case IFNα to bind. RT-qPCR revealed that iPSC-derived hematopoietic cells expressed IFNAR1 and IFNAR2 (Figure 45, Supplemental Figure 14). However, receptor RNA expression was still 10x lower in iPSC-derived cells (Figure 45) compared to primary PBMNC (Figure 46). Furthermore, IFNα target genes were not significantly upregulated in iPSC-derived hematopoietic cells (Figure 45) while patient PBMNC displayed a robust upregulation of selected IFNα target genes (Figure 46). Consequently, the unresponsiveness of iPSC-derived cells towards IFNα stems from a mechanism that is specific to iPSC-derived cells. As RNA expression does not always correlate with protein levels, an in this case display of the receptor on the cell surface, the next step was to investigate the presence of IFNAR1 and IFNAR2 on the cell surface of the iPSC-derived hematopoietic cells and patient PBMNC.

3.2.4.3.1 A low percentage of iPSC-derived hematopoietic cells express IFNAR2 on their cells surface

JAK2 and JAK2VFhet iPSC-derived suspension cells were harvested on day 18 of hematopoietic differentiation. Cells were stained for IFNAR1 along with differentiation markers shown in Figure 36 and analyzed by flow cytometry. As mentioned *in vitro* hematopoiesis of iPSC stems from the EB layer that is developed in between day 6 and day 14 of differentiation (Figure 35). The EB layer seems to drive *in vitro* hematopoiesis and contained a multitude of differentiated myeloid cells (Figure 39) and immature CD34$^+$ cells (Figure 42B). Thus, along with hematopoietic suspension cells, JAK2 and JAK2VFhet EB layer was also harvested on day 18 of

hematopoietic differentiation, dissociated into single cells and stained for IFNAR1 along with the same differentiation markers as for suspension cells (Figure 36).

In line with previous experiments (Figure 36, Figure 37) iPSC-derived suspension cells showed their characteristic co-expression of CD31, CD43 and CD45 with more than 95% of cells CD45$^+$ (Figure 47A, Supplemental Figure 16A). Interestingly, multiple independent experiments showed that 1% to 10% of the CD45$^+$ cell population displayed IFNAR1 on their cell surface (Figure 47C). This suggests that the poor IFNα response stems from the inability of IFNα to bind to the cells as there is a low IFNAR1$^+$ population. The response that is seen in gene expression also suggests that the signal from the IFNAR1$^+$ cells is diluted by the IFNAR$^-$ cells. As there was a high variation seen in IFNAR$^+$ cells this might explain the high variation observed in gene expression (Figure 45). Notably, the low percentage of CD45$^+$ IFNAR1$^+$ cell population was iPSC clone independent.

In contrast, cells from the EB layer showed a lower CD31$^+$ CD43$^+$ HPC population compared to the cells in the supernatant. This is in line with previous experiments (Figure 42C). Out of the HPC population about 85% – 90% of the cells were committed progenitors. In comparison to suspension cells 8% to 17% of CD45$^+$ committed progenitors from the EB layer displayed IFNAR1 to a higher extent (Figure 47B – C, Supplemental Figure 16B). The higher IFNAR1 expression in CD45$^+$ committed progenitors of the EB layer seems to be clone independent, too, indicating that IFNα responsive cells might rather be in the EB layer than in suspension (Figure 47C). Consequently, suspension cells were unfit for IFNα signaling pathway analysis. Therefore, when investigating the IFNα signaling pathway one should isolated cells from the EB layer.
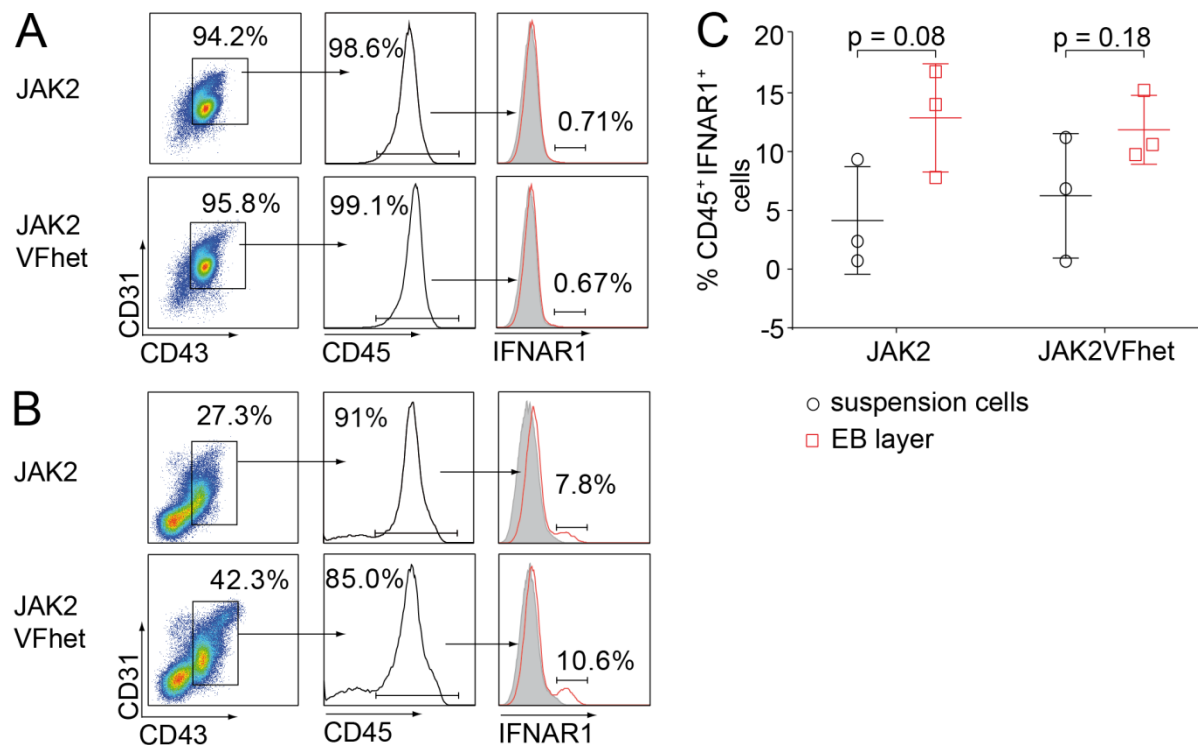
Figure 47. iPSC-derived hematopoietic suspension cells express IFNAR1 at low levels on the cell surface

JAK2 and JAK2V617F iPSC clones of PV1 were induced to differentiate into hematopoietic cells according to Figure 34. On day 18 of differentiation cells from the supernatant fraction were harvested by washing them off of the EB layer. EB layer was harvested by digestion with Accutase. (A) Suspension cells and (B) cells from the EB layer were stained with an IFNAR2-specific antibody and other surface markers followed by flow cytometry analyses. Shown is a representative analysis for JAK2_2 and JAK2VFhet_2. Gating strategy was done according to Supplemental Figure 23A. (C) Summary of IFNAR1+ cells in the CD43+/CD31+/CD45+ cell population for all PV1 iPSC clones (n = 3). For statistical analysis a Student's t test was performed by comparing EB layer and suspension cells per JAK2 genotype. P values are indicated.

IFNAR1 was detectable to a low degree on iPSC-derived hematopoietic cells. Yet, the overall identity of these cells was still unknown. To potentially know which cells would primarily respond to IFNα and upregulate IFNα target genes iPSC-derived hematopoietic cells were analyzed in more detail. To this end, iPSC-derived suspension cells and cells from the EB layer were gated first on CD43+ CD45+ cells, which are the committed hematopoietic cells. Further analysis was focused on the granulocytic (CD66b+) and the megakaryocytic (CD61+) lineage.

Granulocytes showed a low expression of IFNAR2 in supernatant and the EB layer (Figure 48A – C, Supplemental Figure 17). In contrast, megakaryocytes were the main cell type expressing IFNAR2 with a 10x higher percentage of CD61+ IFNAR2+

cells in comparison to CD66b^{+} IFNAR2^{+} cells (Figure 48A – B, D and Supplemental Figure 17). Notably, the EB layer accumulates megakaryocytic cells as shown in previous experiments (Figure 39E). Moreover, JAK2VFhet EB layer showed a slightly lower megakaryocytic cell population which is in line with previous experiments (Figure 39E). Hence, there are in total more cells in the EB layer that express the IFNAR2 and can bind IFNα and respond to is binding.
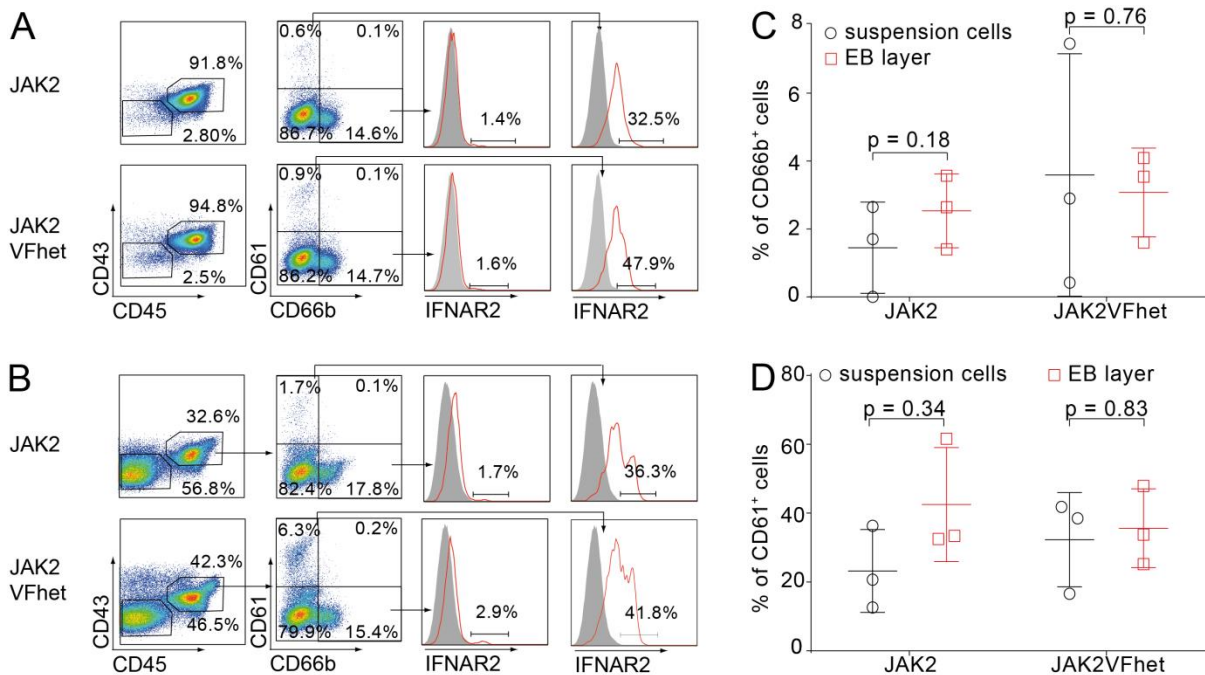

Figure 48. IFNAR expression is mainly found on CD61^{+} cells in iPSC-derived hematopoietic cells

JAK2 and JAK2V617F iPSC clones of PV1 were induced to differentiate into hematopoietic cells according to Figure 34. On day 18 of differentiation cells from the supernatant fraction were harvested by washing them off of the EB layer. EB layer was harvested by digestion with Accutase. (A) Supernatant fraction and (B) cells from the EB layer were stained with IFNAR1 and other surface markers followed by flow cytometry analyses. Shown is a representative analysis for JAK2_2 and JAK2VFhet_2. Gating was performed according to Supplemental Figure 23A. (C – D) Summary of IFNAR1^{+} cells in the (C) CD66b^{+} and (D) CD61^{+} cell population for 3 independent experiments for all PV1 iPSC clones. For statistical analysis a Student's t test was performed by comparing EB layer with suspension cells per JAK2 genotype. P values are indicated.

Taken together, CD45^{+} iPSC-derived hematopoietic cells from the suspension cells express low levels of IFNAR1 on their surface whereas the same cell population from the EB layer have a significantly higher percentage of IFNAR1^{+} cells. This could indicate that the EB layer might behave differently in response to IFNα than

cells in suspension. CD61$^+$ cells are the main cell type that expresses the IFNAR2 in both supernatant fraction and EB layer. As the EB layer accumulates CD61$^+$ cells there is another hint that the IFNα sensitive cells are rather in the EB layer than in the supernatant fraction. Thus suggests that the main cells that respond to IFNα might be megakaryocytes.

3.2.4.3.2 IFNAR1 and IFNAR2 is expressed on PV patient PBMNC

PBMNC contain different cell types with possible different levels of IFNAR 1 and IFNAR2 expression. Hence, IFNAR1 and IFNAR2 surface expression was analyzed on PV PBMNC to determine whether there is a differentiated cell type that has a very high surface expression of IFNAR1 and IFNAR2 thus is most likely to respond to a higher degree to IFNα thus mediating the IFNα effect in PV patients. To this end, PBMNC were thawed and living cells were enriched via 3 washing steps followed by centrifugation at 800 rpm. Healthy PBMNC were used as control (Figure 49 and Figure 50).
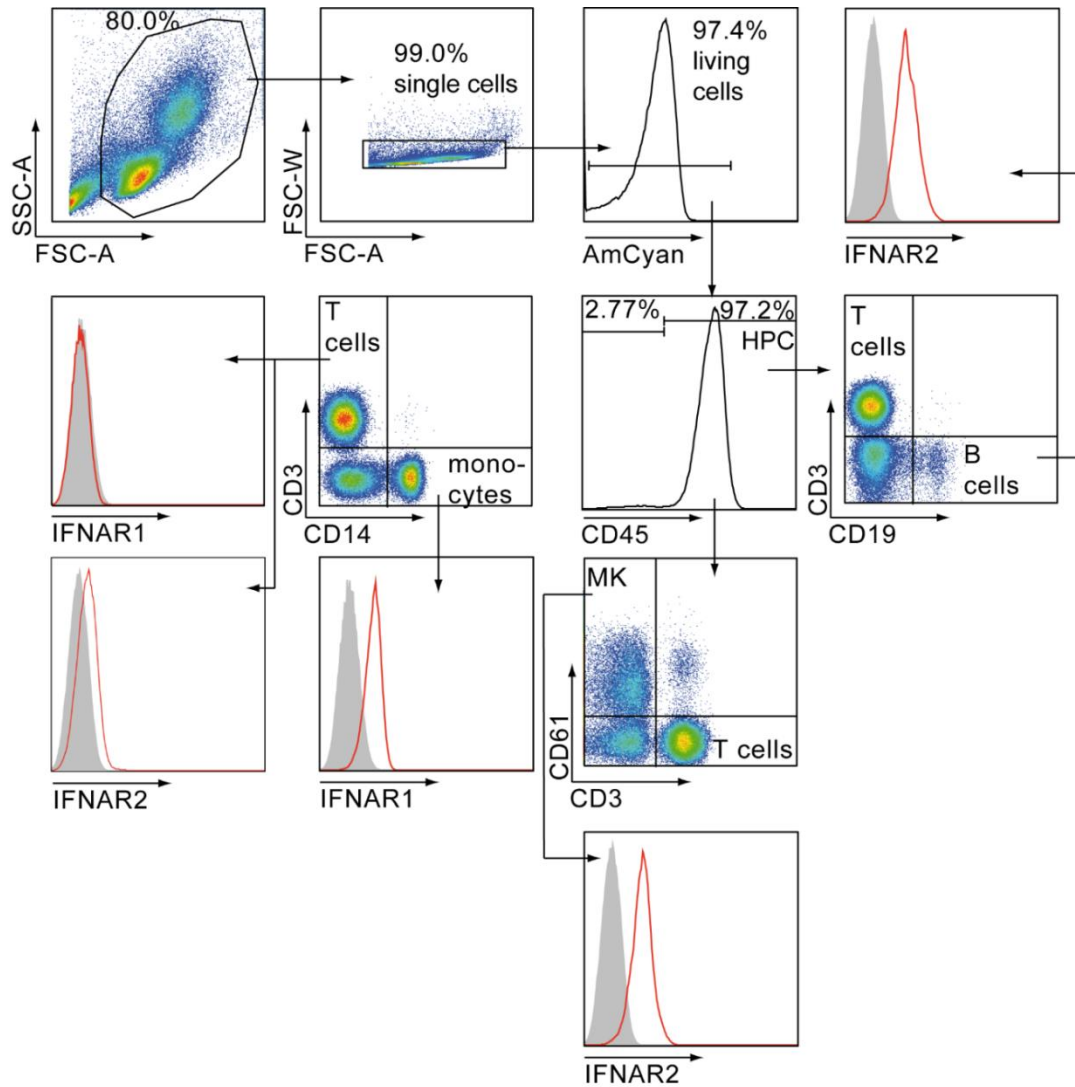
Figure 49. Patient PBMNC express IFNAR1 and IFNAR2 on myeloid cells and on B cells

Healthy PBMNC were isolated from whole blood via density gradient centrifugation. Patient PBMNC were thawed. Living and dead cells were separated by centrifugation at 800rpm. PBMNC were stained with CD3, CD19, CD45, CD61, IFNAR1 and IFNAR2 specific antibodies immediately after isolation/purification. Gating strategy of IFNAR1 and IFNAR2 analysis is shown. Grey histograms in the overlays show the signal for isotype stained sample. MK, megakaryocytes, HPC, hematopoietic progenitor cells.

First, the lymphoid cells were analyzed. T cells were defined as CD45$^+$ CD3$^+$ cells whereas the B cell lineage was determined as CD45$^+$ CD19$^+$ cells (Chungwen et al., 2011) (Figure 49). CD3$^+$ T cells from all 3 PV patients and from healthy individuals showed no detectable surface expression of IFNAR1 and IFNAR2 (Figure 50). CD19$^+$ B cells expressed IFNAR1 10x higher that the negative control (IgG).

Furthermore, there was no difference in expression level between PV patients and healthy individuals (Figure 50B, lower left panel).
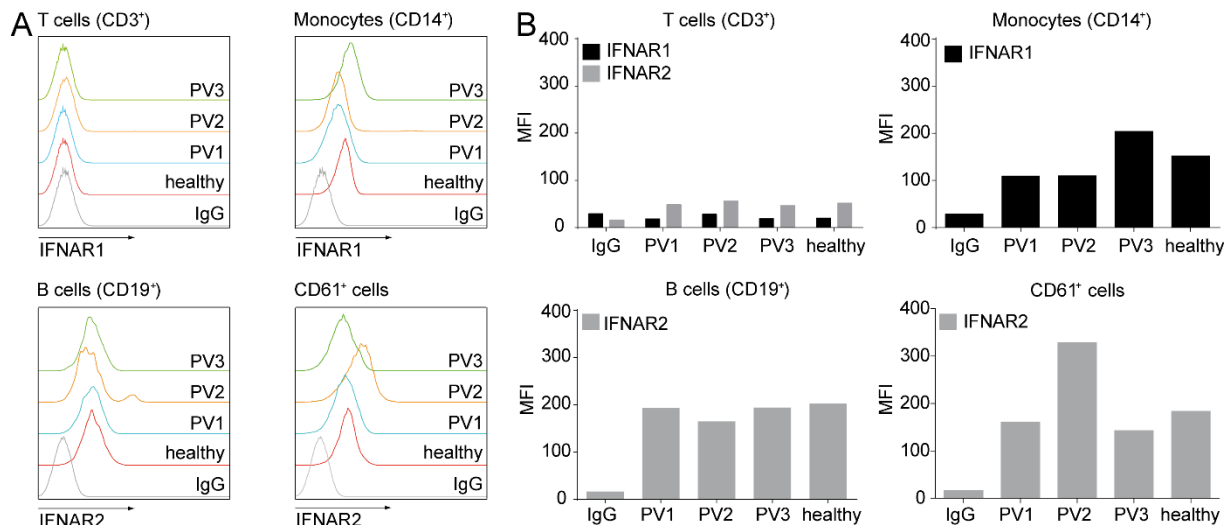

Figure 50. Primary PV patient PBMNC express IFNAR1 and IFNAR2 at the same levels as healthy PBMNC

PV patient PBMNC were thawed in RPMI + 10% FCS and living cells were enriched via 3 washing steps with 1x PBS and centrifugation at 800 rpm for 10 min. Healthy PBMNC were isolated form healthy donors via density gradient centrifugation. PBMNC were stained with antibodies for flow cytometry against myeloid and lymphoid lineage markers additionally to IFNAR1 and IFNAR2. Myeloid and lymphoid cells were analyzed for their IFNAR1 and IFNAR2 expression. Gating was done as shown in Figure 49. IgG staining was used as negative control. (A) Overlays of IFNAR1 and IFNAR2 surface expression per cell type is shown. (B) Mean fluorescence intensity (MFI) of IFNAR1 and IFNAR2 per cell type is depicted (n = 1).

Second, 2 subtypes from the myeloid cell lineage were analyzed. Monocytes were usually as CD14$^+$ cells and clearly showed IFNAR expression (Thomas et al., 2017) (Figure 50B, upper right panel). Depending of the heterodimer CD61 is bound in this surface marker defines megakaryocytes and platelets or monocytes and macrophages. Here, all CD61$^+$ cells were taken into account. Total CD61$^+$ cells in all conditions expressed IFNAR2, yet as shown in Figure 50B (lower right panel), to a different level. IFNAR2 surface expression in CD61$^+$ cell from PV patient 1 and 3 is in the same range as for healthy individuals. However, PV patient 2 has a very high expression of IFNAR2 in the CD61$^+$ cell population. Strikingly, this patient had an allele burden of 96% of JAK2V617F$^+$ cells (Table 18) and flow cytometry showed an

elevated CD61$^+$ cell population in peripheral blood. Thus, the higher IFNAR2 expression stems from the evaluated CD61$^+$ cell count.

In summary, all myeloid cells and B cells express IFNAR1 and IFNAR2, thus have can respond to IFNα. More importantly, patient PBMNC do not show any major differences in IFNAR1 and IFNAR2 expression level for myeloid cells or B cells compared to healthy individuals. The only striking difference is in the CD61$^+$ cell population which is elevated due to a high JAK2V617F allele burden in PV patient 2. The hematopoietic differentiation system shown in Figure 34 formed all myeloid cells that have been checked for IFNAR expression in PBMNC. Therefore, the IFNα signaling pathway can be explored for myeloid cells. Unfortunately, lymphoid cells could not be formed with the differentiation system.

3.2.4.4 iPSC-derived hematopoietic cells display low levels of STAT1 protein and show no phosphorylation of STAT1 in response to IFNα

Beside IFNAR1 and IFNAR2 expression on the cell surface, iPSC-derived hematopoietic suspension cells were also analyzed for other molecules of the IFNα signaling pathway. When IFNα binds to its receptor STAT1 and STAT2 are phosphorylated by TYK2 and JAK1 which dimerizes and is transferred into the nucleus to activate gene expression (Platanias, 2005) (Figure 11).

First, iPSC-derived hematopoietic cells were checked for STAT1 gene expression. To this end, suspension cells were harvested on day 18 of hematopoietic differentiation and subjected to RT-qPCR. In the absence of IFNα STAT1 gene expression is low in hematopoietic cells from all PV1 iPSC clones (Figure 52A). In the presence of IFNα STAT1 gene expression increases, yet, the level of upregulation seems to be clone-specific. iPSC-derived hematopoietic cells from

JAK2_1 and JAK2VFhet_1 upregulate STAT1 expression to the same extend (2-fold and 2.5-fold, respectively) whereas iPSC-derived hematopoietic cells from JAK2VFhet_2 show only a minor increase in STAT1 mRNA level. Moreover, iPSC-derived hematopoietic cells from JAK2_2 show a 5-fold upregulation in STAT1 expression when stimulated with IFNα (Figure 52A) which is significant as it was shown for IRF7 and IRF9 expression (Figure 46).

As PV patient PBMNC were responsive to IFNα and upregulated IRF7 and IRF9 quite strongly (Figure 46), patient PBMNC were checked for their STAT1 gene expression along with freshly isolated healthy PBMNC which were used as control. Moreover, STAT1 gene expression in patient PBMNC was also compared to STAT1 levels of PV1 iPSC-derived hematopoietic cells. STAT1 gene expression is in healthy PBMNC is low in the absence of IFNα (Figure 52B). Interestingly, in the absence of IFNα all patient PBMNC have higher STAT1 expression levels compared to healthy PBMNC. As shown in Figure 52B patient PBMNC express STAT1 2-fold higher than GAPDH. With IFNα stimulation STAT1 gene expression increased in patient (3.fold for PV1, 3.5-fold for PV2 and PV3) and healthy PBMNC (5.5-fold) increased strongly. Notably, expression levels for iPSC-derived cells were 10x lower than in their corresponding primary cells (Figure 52A – B) which is line with previous results (Figure 45 – Figure 46).

STAT2 is another component in the IFNα pathway (Figure 11). Gene expression analyzes of iPSC-derived hematopoietic cells showed a clone dependent expression pattern. Accordingly, in the absence of IFNα STAT2 gene expression is low in iPSC-derived hematopoietic cells. Surprisingly, when stimulated with IFNα STAT2 is not upregulated for all iPSC clones as STAT1 gene expression. For JAK2_2 and JAK2VFhet_2 STAT2 gene expression stayed at the same level as without IFNα treatment (Supplemental Figure 15A). JAK2_1 and JAK2VFhet_1 barely show a 2-fold upregulation of STAT2, yet without any significance. In contrast, primary patient PBMNC and healthy PBMNC upregulated 3 to 4.6-fold and 9-fold, respectively, (Supplemental Figure 15B). As shown for STAT1 (Figure 52) and IFNAR1 (Figure 45

– Figure 46) iPSC-derived suspension cells again showed 10x lower relative gene expression for STAT2 than patient PBMNC.
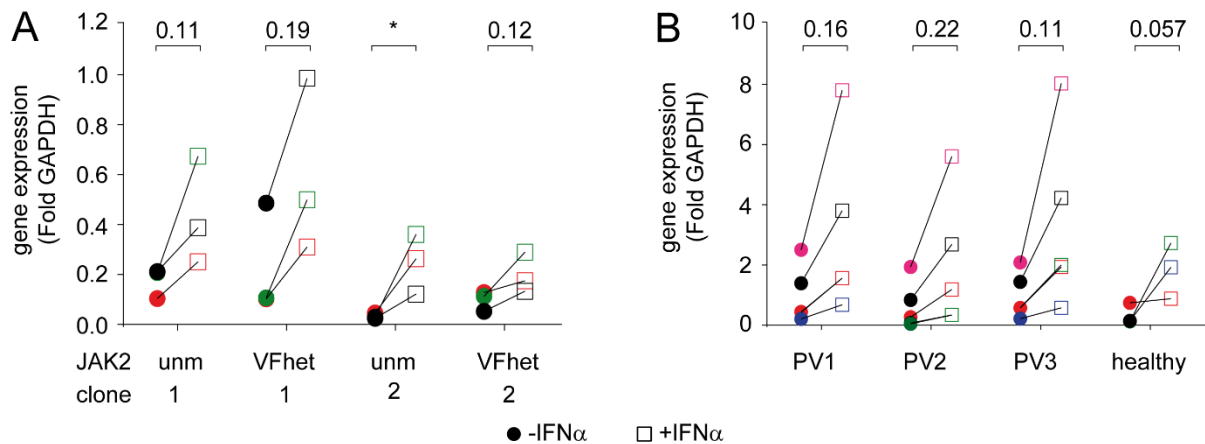

Figure 51. iPSC-derived hematopoietic cells upregulate STAT1 gene expression upon IFNα treatment

(A) iPSC-derived hematopoietic cells of PV1 were harvested on day 18 of differentiation and were cultured without growth factors in the presence or absence of IFNα (200 U/ml) for 4h. RNA was isolated and RT-qPCR for STAT1 was performed. Shown is the STAT1 gene expression normalized to GAPDH (n = 3). For statistical analyses Student's t-test was performed. (B) PV patient PBMNC were thawed in RPMI + 10% FCS and living cells were enriched by 3x centrifugation at 800 rpm for 10 min. Healthy PBMNC were isolated from healthy donors via density gradient centrifugation. Cells were processed for RT-qPCR as described in A. STAT1 gene expression normalized to GAPDH is shown (n = 5). Colors in A and B represent the independent experiments data was obtained from. Circles represent samples cultured without IFNα. Squares represent samples cultured with IFNα. For statistical analyses unpaired Student's t-test was performed by comparing untreated with IFNα treated samples. Data points marked with (*) indicate samples with p-values ≤ 0.05; Data points marked (**) indicate samples with p-values ≤ 0.005. Unm, unmutated; VFhet, JAK2V617F heterozygous.

Second, to investigate whether gene expression of STAT1 also reflects protein levels iPSC-derived hematopoietic cells were analyzed for total STAT1 protein. Furthermore, activation of STAT1 in response to IFNα was analyzed by pSTAT1 protein levels. To this end, JAK2 and JAK2VFhet iPSC were differentiated into hematopoietic cells. On day 26 to 34 of differentiation suspension cells were harvested, starved in RPMI to abrogate any cytokine signaling that would interfere with STAT1 and pSTAT1 detection followed by stimulation with IFNα. Freshly isolated healthy PBMNC were used as positive control for IFNα stimulation (Figure 52, Supplemental Figure 18). Additionally, HEK293T cells transfected with human JAK2V617F vector was used as control for protein size.

In healthy PBMNC total STAT1 protein could be detected in the presence and absence of IFNα (Figure 52A). Without IFNα stimulation healthy PBMNC do not show any pSTAT1 protein indicating that the starvation period was sufficient. As expected healthy PBMNC showed a strong phosphorylation of STAT1 in response to IFNα stimulation (Figure 52A). HEK293T cells overexpressing human JAK2V617F show a low STAT1 protein levels. However, JAK2V617F transduced HEK293T show high pSTAT1 levels without any IFNα stimulation (Figure 52A).

In contrast to healthy PBMNC, iPSC-derived hematopoietic cells showed low to undetectable levels of total STAT1 protein in the absence of IFNα (Figure 52B – C). Furthermore, STAT1 protein levels could not be increased with IFNα stimulation. As expected iPSC-derived suspension cells show no pSTAT1 protein levels in the absence of IFNα. With IFNα stimulation pSTAT1 levels were not detectable in iPSC-derived hematopoietic cells. This was also independent of iPSC clone (Figure 52B – C). This result is in line with the low IFNAR1 surface expression of iPSC-derived hematopoietic cells (Figure 47). There were very few cells to bind IFNα, consequently, there are few cells to activate STAT1. Thus, the low pSTAT1 levels were detected in Western Blot.

Taken together, STAT1 and STAT2 mRNA could be detected in iPSC-derived hematopoietic suspension cells and primary PBMNC. STAT1 mRNA levels increased with IFNα stimulation in patient and healthy PBMNC significantly, yet iPSC-derived hematopoietic cells showed only a trend towards higher STAT1 gene expression. STAT2 gene expression barley showed an upregulation in iPSC-derived hematopoietic suspension cells in response to IFNα while gene expression in PBMNC was significantly upregulated. Moreover, the level of upregulation of STAT1 expression seems to be clone-specific. However, STAT1 mRNA did not correspond to STAT1 protein in iPSC-derived hematopoietic cells. In comparison to primary healthy PBMNC iPSC-derived hematopoietic cells possess low STAT1 protein levels and undetectable pSTAT1 protein levels when stimulated with IFNα indicating that,

additional to the few CD45$^+$ IFNAR1$^+$ cells, iPSC-derived hematopoietic cells have too low STAT1 protein to transport IFNα signaling to the nucleus and activate gene transcription.
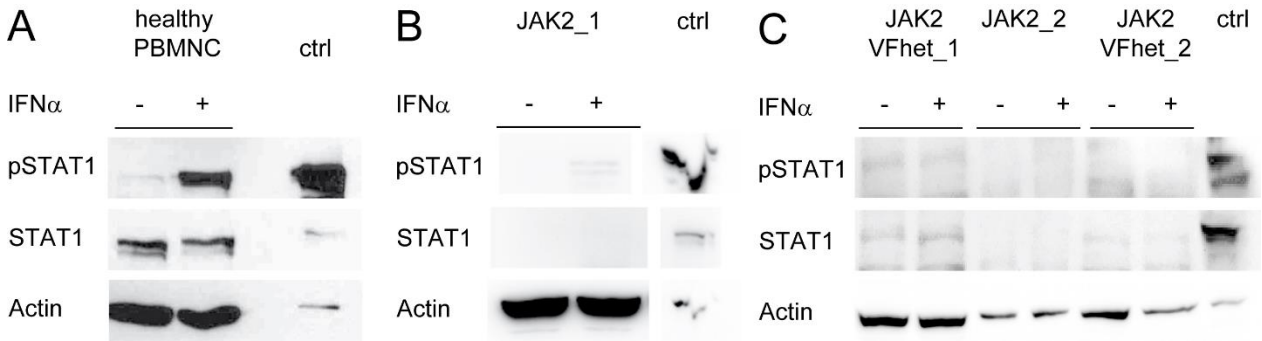

Figure 52. iPSC-derived hematopoietic cells show low STAT1 and pSTAT1 protein upon IFNα stimulation

(A) Healthy PBMNC were isolated as in Figure 51B. Cells were starved in RPMI for 4h followed by a pulse of IFNα (2000 U/ml) for 30 min. Afterwards, protein was isolated with RIPA buffer. Next, 40 μg protein per sample was loaded onto a 10% SDS gel and SDS-PAGE was performed for 2h at 25mA per gel. Proteins were blotted onto a nitrocellulose membrane for 2h at 80mA per membrane followed by a 2h blocking with 4% skim milk. Membranes were probed with antibodies against STAT1, pSTAT1 and Actin over night at 4°C. After washing membranes were probed with secondary antibodies for 1h at room temperature. After another washing step detection was done with ECL substrate. STAT1 and pSTAT1 detection was performed on separate membranes. HEK 293T transfected with JAK2V617F vector was used as control (ctrl) for STAT1 or pSTAT1 protein size. (B – C) iPSC derived hematopoietic cells were harvested from suspension on day 26 to 34 of hematopoietic differentiation. Afterwards, cells were starve and pulsed with IFNα as described in A. Protein isolation, SDS-PAGE and protein detection was done as described in A. Repeat experiments are in depicted in Supplemental Figure 18 (n = 3).

In conclusion, the newly generated JAK2 and JAK2V617F iPSC clones differentiated into hematopoietic cells. Notably, only myeloid cells and no lymphoid cells developed with the adapted differentiation system. JAK2VFhet iPSC clones recapitulate the increased red blood cell production *in vitro*, thus, these clones can be used as a model system for human PV and deregulated erythropoiesis. Furthermore, JAK2V617F expressing cells showed an increased expansion of CD34$^+$ cells including HE cells, resulting in higher yield during harvests. Independent of the JAK2 genotype suspension cells in iPSC hematopoietic differentiation show 10x lower gene expression of IFNα target gene in comparison to patient and healthy PBMNC. Moreover, iPSC-derived suspension cells showed low STAT1 protein levels in the absence of IFNα and pSTAT1 protein was barely detectable with IFNα

stimulation. As a result iPSC-derived cells showed a low IFNα response. The overall cause of the suboptimal activation of the IFNα pathway might be due to a low IFNAR1$^+$ cell population for iPSC-derived suspension cells. Interestingly, the EB layer had more IFNAR1$^+$ cells. Therefore, the EB layer could be used to isolate IFNAR1$^+$ cells and investigate IFNα signaling.

4 Discussion

The hematopoietic system and the consequences of mutations in hematopoietic stem cells have been studied in mouse and zebrafish models extensively. With the discovery and use of iPSC and ESC there have been various milestones in the modeling of human hematopoiesis. Other strategies have been implemented to define surface markers during certain stages of development (Pereira et al., 2016). The use of patient derived iPSC to model human diseases, such as cardiovascular diseases, ALS, Parkinson's disease or even CML has further shed light onto the disease pathogenesis (Yoshida and Yamanaka (2017), Ghaffari et al. (2018), Dimos et al. (2008), Badger et al. (2014), Kumano et al. (2012)). Additionally, model systems helped to identify potential drug targets or explored the used of iPSC derived cells in immunotherapy (Elitt et al. (2018), Zhu et al. (2018)).

One mutation that causes hematological diseases is BcrAbl, the driver mutation for CML. Studies for differential expressed genes in CD34$^+$ CML vs healthy cells show a downregulation of the transcription factor IRF8 (Hao and Ren, 2000). Furthermore, studies showed that BcrAbl downregulates IRF8 expression directly via STAT5 (Waight et al. (2014), Waight et al. (2013)). IRF8 is involved in many signaling pathways during hematopoiesis, especially the development of myeloid cells. It is the main transcription factor in the development of plasmacytoid DC (pDC) and CD8α$^+$ cDC and its lack results in immunodeficiency (Tsujimura et al. (2003), Bornstein et al. (2014), Schiavoni et al. (2002), Hambleton et al. (2011)). Increasing findings in IRF8$^{-/-}$ mice and primary CD34$^+$ CML cells has established IRF8 as a tumor suppressor gene (Tamura et al., 2015). While TKI like Imatinib are available to treat CML patients now, IFNα was used to manage CML before. However, results of IFNα treatment are mixed and studies linked low IRF8 expression with low response rates to IFNα (Lee et al. (1992), Talpaz et al. (1991)). But the mechanism of how IFNα exerts its anti-proliferative effect in CML cells has not been described. Moreover, the involvement of IRF8 in IFNα treatment is still unclear.

A second mutation that causes a hematological disease is JAK2V617F, a point mutation in JAK2 and a driver mutation in PV, ET and PMF. IFNα treatment in JAK2V617F$^+$ PV patients can be used as substitute for TKI treatment and its results are superior to those achieved in CML patients. There have been several studies investigating the influence of IFNα and its signaling pathway in JAK2V617F$^+$ hematopoietic cells. Studies found that IFNα treatment lead to a reduction in all blood parameters and JAK2V617F allele burden (Hasan et al., 2013). It was also shown that IFNα treatment caused an exit from G0 phase of murine HSC, a reactivation of the cell cycle and finally an exhaustion of the leukemic stem cell pool (Essers et al. (2009), Mullally et al. (2013)). However, these were only hints of a mechanism how IFNα acts in this disease causing stem cells. A direct mechanism has not been described yet.

4.1   The relevance of IRF8 in CML and for IFNα therapy

To examine the role of IRF8 in CML pathogenesis IRF8$^{+/+}$ and IRF8$^{-/-}$ hematopoietic cells were transfected with BcrAbl followed by culture in cytokine deprived conditions. Although BcrAbl$^+$ IRF8$^{+/+}$ hematopoietic cells expanded in these conditions (Figure 19) BcrAbl$^+$ IRF8$^{-/-}$ hematopoietic cells showed a higher expansion in these conditions than BcrAbl$^+$ IRF8$^{+/+}$ hematopoietic cells (Figure 24B). Moreover, BcrAbl$^+$ IRF8$^{-/-}$ hematopoietic cells acquired a TKI resistance (Figure 25B). This thesis also showed that TKI does not eradicate immature ckit$^+$ cells (Figure 26C – D).

The role of IRF8 and other Interferon regulators factors in CML pathogenesis has been studied in patient samples and mouse models alike (Watanabe et al. (2013), Manzella et al. (2016), (Tamura et al., 2015)). Early on research showed that murine IRF8$^{-/-}$ cells exhibited reduced apoptosis and enhanced proliferation (Gabriele et al. (1999), Burchert et al. (2004)). Later it was found that IRF8 controls

anti-apoptosis related genes, like BCL-2. BCL-2 is a key regulator of mitochondrial mediated apoptosis. In part this illustrates how IRF8 might act as a tumor suppressor (Neubauer et al. (2004), Danisz and Blasiak (2013)). A most recent study showed that the tumor suppressor function of IRF8 is conserved over the species, as lack of IRF8 in zebrafish showed the same overproduction of myeloid cells (Zhao et al., 2018). The growth advantage and TKI resitance of BcrAbl[+] IRF8^{−/−} hematopoietic cells seen in this thesis could be explained with a deregulated apoptosis mechanism due to the absence of the tumor suppressor IRF8 (Figure 24B). As BcrAbl also activates anti-apoptotic pathways on its own it seems that the lack of IRF8 and the expression of BcrAbl show synergism in leukemic stem cells. It has been shown that the lack of IRF8 can also synergize with other mutations in leukemia, such as AML1-ETO or MEIS1 and MEIS3 in AML (Schwieger et al. (2002), Hara et al. (2008), Sharma et al. (2015)). Also, BcrAbl is known to synergize with other mutations, such as JAK2 (Grundschober et al., 2014). This synergy between IRF8 deficiency and BcrAbl expression seems to render the cells resistant to TKI therapy. Weinstein (2002) showed early in CML research that mutated cells are oncogene addicted, i.e. transformation and signaling relies heavily on the acquired mutation overriding the normal cell signaling. Therefore, when set under cytokine starvation BcrAbl[+] IRF8^{+/+} cells expand (Figure 20). However, BcrAbl signaling is needed in cytokine deprived cultures thus when inhibited by Imatinib BcrAbl[+] IRF8^{+/+} cells lose their survival advantage in these conditions (Figure 22, Figure 23 and Supplemental Figure 5). As the lack of IRF8 results in the uncontrolled transcription of anti-apoptotic genes IRF8^{−/−} cells are not as oncogene addicted and are able to survive in cytokine deprived cultures in combination with Imatinib treatment (Figure 25B).

More recent studies have suggested that TKI resistance stems from nuclear β-catenin that acts independently of BcrAbl or its inhibition by TKI (Eiring et al., 2015). This might be a hypothesis as to why immature IRF8^{+/+} BcrAbl[+] ckit^{+} cells are not inhibited by TKI (Figure 26C – D). Although Imatinib therapy was a breakthrough in managing CML and eradicating BcrAbl^{+} cells patients still experience relapses due to BcrAbl[+] LSC that have not been eliminated by Imatinib treatment (Bocchia et al.

(2018), Hiwase et al. (2013), Schubert et al. (2017)). Corbin et al. (2011) proposed a model for relapses in Imatinib treated cells and the eventual relapse of the disease due to not eradicating LSC. A recent study by Carter et al. (2016) suggested that a combination of Imatinib treatment and a BCL-2 inhibitor inhibits BcrAbl and its downstream signaling. Moreover, Carter et al. (2016) showed that the combination eradicated CML stem cell numbers in mice and prolonged survival of the mice.

It is suggested that low IRF8 levels in CML patients are indicative of a poor outcome of IFNα therapy. However, experiments with IFNα in murine BcrAbl^{+} cells did not show a difference in reducing cell numbers (Figure 25C – D) or specific cell populations (Figure 26C – D) depending on IRF8.

As IFNα activates a multitude of signaling pathways it is possible that alternative mechanisms might act in these cells. Indeed, Yokota et al. (2017) suggested that IFNα induces C/EBPβ via STAT5 in primary Lin^{−} CD34^{+} CML cells and that this would exhaust leukemic cells in CML. Fish et al. (1999) and Platanias et al. (1999) suggested that IFNα can activate CRKL1 and CRKL2 proteins. A follow-up study by Grumbach et al. (2001) showed that IFNα induces the CRKL adapter proteins via STAT5 and the subsequent activation of PML and RAP1 in BcrAbl[+] cell lines. PML and RAP1 expression was followed by activation of anti-proliferative genes. As BcrAbl also binds CRKL for anti-apoptotic signaling pathways Grumbach et al. (2001) suggested a competition of BcrAbl and IFNα for the binding of CRKL protein. Mayer et al. (2001) and Verma et al. (2002) suggested the involvement of the p38 MAPK pathway. However, this only was true for an already IFNα sensitive cell line, KT-1 cells. K562 cells did not induce the p38 MAPK pathway upon IFNα signaling (Mayer et al., 2001). As this pathway was also suggested to be activated in JAK2V617F^{+} cells it would have been a good link between the 2 MPN forms (Lu et al., 2010).

4.2 Kinetics of hematopoietic differentiation of patient derived iPSC

Using iPSC to model human hematopoiesis specific protocols and specific cytokine compositions had to be applied to specifically induce the mesodermal germ layer and finally the directed differentiation into the hematopoietic lineage. To this end, the protocol published by Kennedy et al. (2012) was the basis for the hematopoietic differentiation protocol used in this thesis (Figure 17). CD34$^+$ cells were only detected in EB on day 6 of differentiation and low amounts of CD34$^+$ cells were released into the supernatant between day 14 and day 30 of differentiation (Figure 36, Figure 37, Supplemental Figure 8A). Otherwise, iPSC-derived hematopoietic cells co-expressed CD45, CD43 and CD31 (Figure 36).

Over recent years different protocols for the differentiation of iPSC into the hematopoietic lineage have been published (Kennedy et al. (2012), Kovarova et al. (2010), Salvagiotto et al. (2011), Li et al. (2017), Leung et al. (2018), Sontag et al. (2017b)). Early protocols were based on the formation of EB followed either by the stepwise application of specific transcription factors or the application of FCS for the induction of the mesoderm and eventual formation of HE cells. However, other approaches were also developed to seed single cells and treat these with cytokines like BMP4, VEGF, and bFGF to induce the formation HE cells (Salvagiotto et al., 2011). All hematopoietic differentiation approaches show the development of the same cell type – CD34$^+$ HE cells – either by EB dissolving into HSC or by EB attaching to the plate and continuously releasing HSC into the medium (Kennedy et al. (2012), Kovarova et al. (2010), Li et al. (2017)). As shown in Figure 35 the formation of HSC was more similar to the approach used by Kovarova et al. (2010) than the approach by Kennedy et al. (2012).

All mentioned approaches rely on the formation of CD34$^+$ HE cells, therefore the differentiation kinetics are greatly similar to the kinetics shown in this thesis (Figure 36). One difference is the lack of CD43$^+$ cells on day 6 of differentiation as shown by Kennedy et al. (2012), Sturgeon et al. (2014) or Kovarova et al. (2010). For JAK2

and JAK2V617F iPSC clones CD43 expression could only be detected on day 14 of differentiation. One might speculate that these differences have technical reasons depending on the activity of the used cytokines or the used antibody for CD43. However, Kovarova et al. (2010) showed that CD43$^+$ cells expressed CD34 which is in contrast to this thesis as CD43$^+$ cells co-expressed CD45 (Figure 36) and that the majority of CD34$^+$ cells was attached to the EB layer (Figure 42B). Another difference in published kinetics and the kinetics described in the thesis is the presence of CD235a$^+$ cells during differentiation even for JAK2 iPSC clones (Figure 36 and Figure 37C). While Salvagiotto et al. (2011) showed the emergence of CD235a$^+$ cells during differentiation, Leung et al. (2018) and Sturgeon et al. (2014) showed that these cells are a marker for primitive hematopoiesis early in hematopoietic differentiation. This suggests that the differentiation shown is this thesis is rather primitive hematopoiesis. Consequently, the higher percentage of CD235a$^+$ cells for JAK2V617F iPSC clones (Figure 36 and Figure 37C) suggests that JAK2V617F has also an influence on the primitive hematopoiesis.

As shown by Kovarova et al. (2010) and the results in this thesis (Figure 35 – Figure 39, Figure 40B) an EB layer developed during hematopoietic differentiation. This EB layer provided a constant replenishment of hematopoietic stem cells during differentiation. Furthermore, it was composed of endothelial like cells, HE cells and housed multiple hematopoietic cell types. These results provided a hypothesis that the EB layer is able to mimic the hematopoietic stem cells nice. It was shown that endothelial cells (EC) are an essential component of the hematopoietic stem cell niche (Asada et al., 2017). Notably, it was shown that EC of PV patients express JAK2V617F (Sozer et al. (2009), Rosti et al. (2013)). Therefore, this might suggest that EC expressing JAK2V617F and the microenvironment have an influence on hematopoietic differentiation (Pinho et al., 2018). The promotion of LSC by the altered microenvironment was already shown for BcrAbl$^+$ CML cells (Zhang et al., 2012). Recent studies showed that JAK2V617F$^+$ EC promoted JAK2V617F$^+$ HSC expansion at the expense of JAK2 HSC (Lin et al. (2016), Zhan et al. (2018)). Therefore, for future applications of the presented culture system (Figure 34, Figure 35) it might be advantageous to investigate the EB layer more closely as there might

be possible interactions of JAK2V617F[+] HSC with JAK2V617F[+] EC in *in vitro* culture of iPSC differentiation.

4.3 JAK2V617F oncogenic potential in human hematopoiesis

It this thesis, it was shown that heterozygous JAK2V617F iPSC are not entirely independent of cytokine signaling as in the absence of EPO no or very low CD45^{−} CD235a^{+} cells developed (Figure 43A and Figure 39C, respectively). Overexpression of JAK2V617F in murine BM cells resulted in low expression of JAK2V617F in murine BM cells (Figure 27). Moreover, even though JAK2V617F was expressed BM cells showed only a moderate cytokine independence (Figure 28B) suggesting that JAK2V617F has weak oncogenic abilities on its own. A study by Ishii et al. (2007b) confirmed that hint as they showed that JAK2V617F mutant CD34^{+} cells from ET and PV patients demonstrate relatively poor engraftment. Furthermore, there are several mouse models overexpressing JAK2V617F or in which JAK2V617F^{+} cells were transplanted in limiting dilution assays into host mice. Knock in models of JAK2V617F showed an MPN phenotype when only JAK2V617F was expressed (Grisouard et al. (2015), Lacout et al. (2006), Mullally et al. (2010)). However, limiting dilution experiments showed a long latency of the disease until MPN phenotype was visible or mice never showed an MPN phenotype at all (Shimizu et al., 2016).

JAK2 is usually coupled to type 1 homodimeric cytokine receptors that lack intrinsic kinase activity. These receptors are found in the myeloid lineage. Consequently, a gain of function mutation in JAK2, such as JAK2V617F has effects on the myeloid lineage. Already in 1976 a study of 2 PV patients showed that these patients show an expansion of erythrocytes, granulocytes and platelets which was confirmed 30 years later in mouse models (Adamson et al. (1976), Lacout et al. (2006), Shimizu et al. (2016)). This, however, is in contrast to the long-term differentiation of JAK2

and JAK2V617F iPSC (Figure 39E). Although, there was an increase in the megakaryocytic lineage this could only be seen between EB layer and supernatant cells. However, when JAK2 and JAK2V617F were compared there was no difference in the megakaryocytic lineage. It is tempting to assume that the contrast in mouse model and iPSC culture stems from the isolation technique of cells from the EB layer as there were high variations in the percentages of CD45$^+$ and CD45$^-$ cells (Figure 38). Meaning that due to a suboptimal isolation there is an underrepresentation of CD45$^+$ cells, consequently, a low representation of total cell populations in the EB layer. Therefore, the statistics would show no difference in JAK2 and JAK2V617F. However, it was already shown that JAK2V617F alone is a weak oncogene (Ishii et al., 2007b). Therefore, it might be possible that JAK2V617F iPSC cannot recapitulate all aspects of PV *in vitro*.

4.3.1 JAK2V617F confers an hypersensitivity to cytokines

The expansion of the red cell lineage is the most striking clinical feature of PV. During hematopoietic differentiation JAK2V617F had a minor effect on the CD45$^-$ CD235a$^+$ cell population (Figure 37C). However, directed differentiation of JAK2, JAK2V617F heterozygous and JAK2V617F homozygous iPSC derived hematopoietic cells resulted in an increased production on CD45$^-$ CD235a$^+$ cells that were later identified as normoblasts (Figure 43, Supplemental Figure 13C). Consequently, JAK2V617F displayed a dose/allele dependent hypersensitivity towards EPO in iPSC-derived cells.

This is in line with studies using JAK2V617F$^+$ primary cells or iPSC. Dupont et al. (2007) found that ET patients rather displayed JAK2 and JAK2V617F/WT colonies and displayed hypersensitivity at low doses of EPO in CFU assays. In contrast, PV patients displayed JAK2V617F heterozygous and a high amount of JAK2V617F homozygous colonies which were hypersensitive to EPO. Moreover, homozygous

colonies from PV patients grew independent of EPO. Another study by Ye et al. (2014) generated an iPSC line from a PV patient who was homozygous for JAK2V617F. In line with Dupont et al. (2007) the authors showed an EPO independence as CD235a$^+$ cells for JAK2V617F homozygous clone iPSC were observed in flow cytometry. However, both studies are in slight contrast to the results presented in this thesis. Only hematopoietic cells derived from JAK2VFhom_1 show a minor EPO independency (Figure 43A). However, Ye et al. (2014) use a 10x higher EPO concentration (2 U/ml) in their red blood cell differentiation than used in this thesis. It can be speculated that the higher EPO concentration might enhance the hypersensitivity effect of JAK2V617F. In contrast to Ye et al. (2014), a study by Saliba et al. (2013) that used a JAK2V617F heterozygous iPSC clone showed an independency towards TPO rather that EPO.

In combination with additional mutations JAK2V617F expressing cells also gain advantages over their wild type counterparts. For example, Grand et al. (2009) analyzed CBL mutations in patient samples and found missense mutations in most cases of PV patients. When overexpressed in 32D cells co-expressing FLT3 mutations in CBL conferred a proliferation advantage in transduced cells. A study by Aranaz et al. (2012) confirmed these results and showed that the proliferative advantage is due to the hypersensitivity. A mutation in the CBL gene was detected in all iPSC clones used in this thesis (Table 21). Therefore, a possible hypersensitivity to IL3 due to the CBL mutation is transferred to all iPSC clone independent of JAK2V617F allele.

4.3.2 JAK2V617F confers enhanced expansion to CD34$^+$ cells

Results gained from JAK2V617F iPSC-derived hematopoietic cells showed a significant increase in CD34$^+$ CD31$^+$ HE cells in the first 6 days of hematopoietic differentiation (Figure 36 and Figure 37A). This was supported by a higher number of JAK2V617F$^+$ CD34$^+$ cells in the EB layer and a trend towards higher proliferation of JAK2V617F$^+$ CD34$^+$ cells (Figure 42C). This suggests that JAK2V617F also

confers an increased proliferation on the stem cell level. However, in literature there is a controversy about the possible enhancing capabilities of JAK2V617F in the hematopoietic lineage (Skoda, 2010).

To uncover the mechanism behind the increased HSC expansion studies with cell lines such as K562, HEL and BaF3 cells have been carried out (Walz et al. (2006), Wernig et al. (2008)). Walz et al. (2006) observed that JAK2V617F+ cells have an increased percentage of cells in S phase. Consequently, JAK2V617F cells grew. Wernig et al. (2008) found that the higher expansion of JAK2V617F+ cells is mediated due to higher PIM and cMyc expression. However, these studies were done with cell lines and not with primary cells. Results from JAK2 and JAK2V617F iPSC EB layer did not show any difference in cell cycle phases either for total cells or CD45+ cells (Figure 41).

Several studies in mouse models and also in isolated primary cells showed that JAK2V617F promoted the cell division of CD34+ cells (Lundberg et al. (2014), Fink et al. (2013), Kent et al. (2013), Hasan et al. (2013)). Moreover, these studies also provided results detailing an increased entering into the cell cycle and an increase in the percentages and total cell numbers of early (LSK and SLAM cells). This is in line with results obtained in this thesis as JAK2V617F+ CD34+ cells isolated from the EB layer showed an increased cell number after 12 days of proliferation in comparison to their JAK2 counterparts (Figure 42D) which would support the higher proliferative capacity of the most primitive hematopoietic cells. In contrast, other studies using mouse models and primary cells from PV, ET and MF patients merely showed an expansion of the late myeloid cells (MEP cells) and that JAK2V617F did not have any expansion of the stem cells pool (Anand et al. (2011), Mullally et al. (2010), James et al. (2008)). Notably, Anand et al. (2011) showed an expansion effect in primary MF patient cells and JAK2V617F homozygous samples suggesting that either additional mutations or the JAK2V617F allele burden influences the expansion of the HSC compartment.

Anand et al. (2011) suggested that the proliferative effect in JAK2V617F$^+$ cells may be attributed to additional mutations. In line with this statement several studies showed a synergy between JAK2V617F and additional mutations, such as loss of EZH2 and TET2 (Delhommeau et al. (2009), Moran-Crusio et al. (2011), Chen et al. (2015), Shimizu et al. (2016)). All studies showed that the loss of EZH2 or TET2 enhanced the oncogenic ability of JAK2V617F and expanded the HSC compartment. Notably, Chen et al. (2015) showed an expansion of the LT-HSC, ST-HSC and MPP compartment in the spleen independent of TET2 loss. However, TET2 deletion conferred a strong functional competitive advantage to JAK2V617F$^+$ HSC. As JAK2V617F clones contain a TET2 mutation it is tempting to say that this is the underlying cause for the higher explanation of CD34$^+$ cells (Figure 42D).

4.4 Evaluating the IFNα signaling pathway

4.4.1 IFNα response in JAK2 and JAK2V617F$^+$ iPSC-derived hematopoietic cells contrasts with other iPSC-derived cells

To understand the molecular mechanism of the IFNα signaling pathway iPSC derived hematopoietic cells from the supernatant fraction were treated with and without IFNα followed by gene expression analysis of IFNα target genes, like IRF7 and IRF9. Surprisingly, treatment of JAK2 and JAK2V617F iPSC-derived hematopoietic cells showed a poor response towards IFNα (Figure 45, Supplemental Figure 14). IFNα target genes, like IRF7 and IRF9 barely displayed an upregulation in the presence of IFNα. This is in contrast to the underlying patient PBMNC that showed as significant upregulation of IRF7 upon IFNα treatment (Figure 46).

A study by Kiladjian et al. (2010) showed that a hematological response was achieved in 80% of PV patients after IFNα therapy. However, due to an additional TET2 mutation PV patients showed a resistance towards IFNα treatment. As Table 21 showed both PV 1 JAK2V617F$^+$ iPSC clones have a mutation in the TET2 gene.

It is tempting to assume that the IFNα resistance in the JAK2V617F[+] iPSC derived hematopoietic cells is due to the TET2 mutation. However, JAK2_1 iPSC clone does not show a mutation in TET2 and still showed the same poor response in iPSC-derived cells (Figure 45). Moreover, the results in iPSC derived hematopoietic cells contrasts with several studies that showed a robust upregulation of IFNα target genes in iPSC and ESC derived cells. Studies by D'Angelo et al. (2016) and Wang et al. (2014b) differentiated mouse ESC into fibroblasts. Both studies found that though type I IFN response lacks behind primary cells it is still inducible in ESC derived cells. Moreover, undifferentiated mouse ESC were able to upregulate type I IFN target genes. This is in line with studies in human ESC and iPSC derived fibroblasts and hepatic cells (Drukker et al. (2002), Hong and Carmichael (2013), Irudayam et al. (2015), Schöbel et al. (2018)). All studies showed a robust IFN type I response by the upregulation of ISG, like IRF7, IRF9 and STAT1. Moreover, Irudayam et al. (2015) also showed that pSTAT1 levels are increased in ESC derived hepatic like cells upon IFNα treatment.

IFNα is used by the innate immune system as a mediator of the antiviral response of cells. Therefore, pre-treatment of cells with IFNα should stunt the replication of any given virus within the cells. Along those lines was a study done by Lafaille et al. (2012) who investigated the replication of the Herpes Simplex Virus (HSV-1) in cells of the central nervous system using human ESC and iPSC for neuronal differentiation. Lafaille et al. (2012) observed the antiviral effect of IFNα as HSV-1 could not replicate in IFNα pre-treated neuronal cells, thus confirming that iPSC and ESC derived cells respond to IFNα.

Finally, another study by Kaneko et al. (2016) differentiated iPSC into hepatic progenitors and tested IFNα responses via Western Blot. They showed that iPSC-derived hepatic cells have sufficient protein levels of STAT1 and show pSTAT1 protein levels upon IFNα treatment. These studies are in contrast to the JAK2 and JAK2V617F derived hematopoietic cells used in this thesis. Although gene expression of STAT1 is upregulated in response to IFNα (Figure 51A), JAK2 and JAK2V617F iPSC derived hematopoietic cells showed low to no pSTAT1 activation

in Western Blot analysis (Figure 52B – C). In human diseases, low STAT1 protein can be seen in some patients suffering from STAT1 deficiencies (Kong et al. (2010), Chapgier et al. (2009)). STAT1 deficiencies occur because of mutations in STAT1 gene, such as a premature STOP codon, which truncates STAT1 protein. However, these deficiencies have only been described in about 10 patients up to date. Furthermore, all cases have been reported in families and have been in children so far, thus the reported STAT1 deficiencies are in the germline. The used iPSC clones have been analyzed by NGS (Table 21). However, STAT1 mutations have not been included in the run as an acquired STAT1 deficiency due to reprogramming should be unlikely. Sendai viruses do not integrate into the genome, thus the possibility of mutagenesis during reprogramming should be very low.

4.4.2 IFNAR1 downregulated by various human cancers

For IFNα to activate gene expression IFNα has to bind to its receptor on the cell surface. Flow cytometric analyses of iPSC-derived hematopoietic cells from the supernatant showed a low percentage of IFNAR1$^+$ cells (Figure 47A, Figure 47C, Supplemental Figure 16A). Hence, only very few cells are able to activate the JAK/STAT pathway in response to IFNα and the possible upregulation of IRF7 and IRF9 might be diluted.

Several studies have investigated IFNAR1 and IFNAR2 expression in human cancers and cancer cell lines (Wagner et al. (2004), Booy et al. (2014)). Both studies showed a correlation between IFNAR1/IFNAR2 expression and IFNα anti-proliferative effect. However, IFNα response (measured by reduced cell growth) varied quite drastically over the tested cell lines that were responding to IFNα. Booy et al. (2014) showed 3 cell lines that were unresponsive to IFNα treatment although via Western Blot and RT-qPCR IFNAR1 and IFNAR2 were expressed. This is reminiscent of the results obtained with iPSC-derived hematopoietic cells in this

thesis as IFNAR1 and IFNAR2 have been detected in RT-qPCR (Figure 45, Supplemental Figure 14A), however low amounts have been on the cell surface of the cells (Figure 47A, Figure 47C, Supplemental Figure 16A).

A study by Katlinski et al. (2017) showed a downregulation of IFNAR1 in human colorectal cancers (CRC) and in CRC mouse models. They hypothesized that the lack of IFNAR1 has a role in the immune suppressive niche and is a poor prognosis for CRC patients. The application of a p38 inhibitor and protein kinase 2 (PKD2) inhibitor on tumors increased IFNAR1 expression, consequently the IFNα response in tumor cells. This is in line with a report by Zheng et al. (2011) and Bhattacharya et al. (2011). Zheng et al. (2011) showed that PKD2 directly phosphorylates IFNAR1 at Ser535, which marks the receptor subunit for degradation. Bhattacharya et al. (2011) showed that IFNAR1 was downregulated due to BcrAbl. The study showed that BcrAbl activates PKD2 which in turn accelerated the phosphorylation-dependent degradation of IFNAR1. Consequently, IFNα signaling was inhibited in BcrAbl+ cells. For future analyzes it might be worthwhile to investigate whether this mechanism also applies in JAK2V617F+ iPSC derived hematopoietic cells. However, this does not yet explain the poor response for JAK2 iPSC derived hematopoietic cells.

Another study that investigated IFNAR1 expression on the cell surface was performed by Ragimbeau et al. (2003). They found that IFNAR1 expression is controlled by the presence of TYK2. In the absence of TYK2 the mature IFNAR1 is barely expressed on the cell surface. IFNAR1 is confined in vesicles and able to reach cell surface. However, due to TYK2 absence IFNAR1 is constantly internalized. A forced expression of TYK2 enhanced the expression of IFNAR1 on cell surface and slowed down IFNAR1 degradation. To investigate whether this applies to JAK2 and JAK2V617F derived hematopoietic cells an expression analysis and stabilization of TYK2 might be beneficial for analyzing IFNα signaling pathway in these cells in the future. A study in a hepatocellular carcinoma cell line (HCC) combined 5-FU treatment with IFNα (Oie et al., 2006). It showed that 5-FU treatment induced IFNAR1 and IFNAR2 expression and cell growth is strongly inhibited. For

future analysis of the IFNα signaling pathway in iPSC-derived hematopoietic cells it might be beneficial to investigate whether IFNAR1 expression can be induced pharmacologically using a p38 or a PDK2 inhibitor.

5 Conclusion and Future Perspective

First, additionally to sole IRF8 knock-out or BcrAbl overexpression that had been done in literature, this thesis showed that the combination of IRF8 knock-out and BcrAbl overexpression enhances the expansion of total BcrAbl$^+$ BM cells and of Gr1$^+$ cells more drastically than BcrAbl overexpression alone. Additionally, lack of IRF8 resulted in an absence of Imatinib response in BcrAbl$^+$ BM cells. Surprisingly, lack of IRF8 has no negative effect on IFNα treatment as treatment of both IRF8$^{+/+}$ and IRF8$^{-/-}$ BM cells resulted in a reduction of BcrAbl$^+$ BM cells. Overexpression of human JAK2V617F in murine BM cells resulted in low transduction efficiency. Therefore, to study IFNα pathways in JAK2V617F$^+$ cells and compare it to BcrAbl$^+$ cells JAK2V617F transduction efficiencies have to be optimized. For this thesis IFNα pathways were studied in patient derived iPSC.

Second, this thesis showed that patient derived iPSC are a useful tool for disease modeling *in vitro*. Moreover, it was shown that the formed EB layer is a valuable source of CD34$^+$ stem cells and might be another useful tool to study the microenvironment during hematopoiesis. It was shown that JAK2V617F increases the formation and expansion of the most primitive hematopoietic stem cells *in vitro* iPSC differentiation. However, to study the IFNα signaling pathway it is not possible to use iPSC-derived CD45$^+$ committed progenitors from the supernatant fraction as these have low levels of IFNAR1 on their surface. For future analysis of the IFNα pathway it might be of value to investigate whether the few CD45$^+$ IFNAR1$^+$ cells within the supernatant cell fraction can be sorted followed by IFNα treatment and RT-qPCR. Another possible approach might be to sort the CD45$^+$ cells from the EB layer. As the EB layer contains a higher percentage of IFNAR1$^+$ cells there might be a higher cell number. A last approach would be to investigate the pharmacological activation of IFNAR1 expression during differentiation to increase the yield of IFNAR1$^+$ cells.

6 References

1) Adamson, J.W., Fialkow, P.J., Murphy, S., Prchal, J.F., and Steinmann, L. (1976). Polycythemia vera: stem-cell and probable clonal origin of the disease. New England Journal of Medicine *295*, 913-916.

2) Anand, S., Stedham, F., Beer, P., Gudgin, E., Ortmann, C.A., Bench, A., Erber, W., Green, A.R., and Huntly, B.J.P. (2011). Effects of the JAK2 mutation on the hematopoietic stem and progenitor compartment in human myeloproliferative neoplasms. Blood *118*, 177-181.

3) Aoi, T., Yae, K., Nakagawa, M., Ichisaka, T., Okita, K., Takahashi, K., Chiba, T., and Yamanaka, S. (2008). Generation of Pluripotent Stem Cells from Adult Mouse Liver and Stomach Cells. Science *321*, 699-702.

4) Aranaz, P., Hurtado, C., Erquiaga, I., Migueliz, I., Ormazabal, C., Cristobal, I., Garcia-Delgado, M., Novo, F.J., and Vizmanos, J.L. (2012). CBL mutations in myeloproliferative neoplasms are also found in the gene's proline-rich domain and in patients with the JAK2V617F. Haematologica *97*, 1234-1241.

5) Arber, D.A., Orazi, A., Hasserjian, R., Thiele, J., Borowitz, M.J., Le Beau, M.M., Bloomfield, C.D., Cazzola, M., and Vardiman, J.W. (2016). The 2016 revision to the World Health Organization classification of myeloid neoplasms and acute leukemia. Blood *127*, 2391-2405.

6) Asada, N., Takeishi, S., and Frenette, P.S. (2017). Complexity of bone marrow hematopoietic stem cell niche. International Journal of Hematology *106*, 45-54.

7) Asprer, J.S., and Lakshmipathy, U. (2015). Current methods and challenges in the comprehensive characterization of human pluripotent stem cells. Stem Cell Rev *11*, 357-372.

8) Badger, J.L., Cordero-Llana, O., Hartfield, E.M., and Wade-Martins, R. (2014). Parkinson's disease in a dish – using stem cells as a molecular tool. Neuropharmacology *76*, 88-96.

9) Barbany, G., Hoglund, M., Simonsson, B., and Swedish, C.M.L.G. (2002). Complete molecular remission in chronic myelogenous leukemia after imatinib therapy. In The New England journal of medicine (United States), pp. 539-540.

10) Barnes, D.J., Schultheis, B., Adedeji, S., and Melo, J.V. (2005). Dose-dependent effects of Bcr-Abl in cell line models of different stages of chronic myeloid leukemia. Oncogene *24*, 6432-6440.

11) Baum, C.M., Weissman, I.L., Tsukamoto, A.S., Buckle, A.M., and Peault, B. (1992). Isolation of a candidate human hematopoietic stem-cell

population. Proceedings of the National Academy of Sciences *89*, 2804-2808.

12) Beaudin, A.E., Boyer, S.W., Perez-Cunningham, J., Hernandez, G.E., Derderian, S.C., Jujjavarapu, C., Aaserude, E., MacKenzie, T., and Forsberg, E.C. (2016). A transient developmental hematopoietic stem cell gives rise to innate-like B and T cells. Cell Stem Cell *19*, 768-783.

13) Bellin, M., Marchetto, M.C., Gage, F.H., and Mummery, C.L. (2012). Induced pluripotent stem cells: the new patient? Nature Reviews Molecular Cell Biology *13*, 713.

14) Bhattacharya, S., Zheng, H., Tzimas, C., Carroll, M., Baker, D.P., and Fuchs, S.Y. (2011). Bcr-abl signals to desensitize chronic myeloid leukemia cells to IFNα via accelerating the degradation of its receptor. Blood *118*, 4179-4187.

15) Bjørn, M.E., de Stricker, K., Kjær, L., Ellemann, K., and Hasselbalch, H.C. (2014). Combination therapy with interferon and JAK1-2 inhibitor is feasible: proof of concept with rapid reduction in JAK2V617F-allele burden in polycythemia vera. Leukemia Research Reports *3*, 73-75.

16) Bocchia, M., Sicuranza, A., Abruzzese, E., Iurlo, A., Sirianni, S., Gozzini, A., Galimberti, S., Aprile, L., Martino, B., Pregno, P.*, et al.* (2018). Residual peripheral blood CD26(+) leukemic stem cells in chronic myeloid leukemia patients during TKI therapy and during treatment-free remission. Front Oncol *8*, 194.

17) Boisset, J.C., van Cappellen, W., Andrieu-Soler, C., Galjart, N., Dzierzak, E., and Robin, C. (2010). In vivo imaging of haematopoietic cells emerging from the mouse aortic endothelium. Nature *464*, 116-120.

18) Booy, S., van Eijck, C.H., Dogan, F., van Koetsveld, P.M., and Hofland, L.J. (2014). Influence of type-I Interferon receptor expression level on the response to type-I Interferons in human pancreatic cancer cells. J Cell Mol Med *18*, 492-502.

19) Bornstein, C., Winter, D., Barnett-Itzhaki, Z., David, E., Kadri, S., Garber, M., and Amit, I. (2014). A negative feedback loop of transcription factors specifies alternative dendritic cell chromatin States. Mol Cell *56*, 749-762.

20) Bradford, M.M. (1976). A rapid and sensitive method for the quantitation of microgram quantities of protein utilizing the principle of protein-dye binding. Analytical Biochemistry *72*, 248-254.

21) Brambrink, T., Foreman, R., Welstead, G.G., Lengner, C.J., Wernig, M., Suh, H., and Jaenisch, R. (2008). Sequential expression of pluripotency markers during direct reprogramming of mouse somatic cells. Cell Stem Cell *2*, 151-159.

22) Branford, S., Rudzki, Z., Walsh, S., Grigg, A., Arthur, C., Taylor, K., Herrmann, R., Lynch, K.P., and Hughes, T.P. (2002). High frequency of point mutations clustered within the adenosine triphosphate-binding

region of BCR/ABL in patients with chronic myeloid leukemia or Ph-positive acute lymphoblastic leukemia who develop imatinib (STI571) resistance. Blood *99*, 3472-3475.

23) Briggs, R., and King, T.J. (1952). Transplantation of living nuclei from blastula cells into enucleated frogs' eggs. Proceedings of the National Academy of Sciences of the United States of America *38*, 455-463.

24) Bunimovich-Mendrazitsky, S., Kronik, N., and Vainstein, V. (2018). Optimization of interferon–alpha and imatinib combination therapy for chronic myeloid leukemia: a modeling approach. Advanced Theory and Simulations *0*, 1800081.

25) Burchert, A., Cai, D., Hofbauer, L.C., Samuelsson, M.K.R., Slater, E.P., Duyster, J., Ritter, M., Hochhaus, A., Müller, R., Eilers, M.*, et al.* (2004). Interferon consensus sequence binding protein (ICSBP; IRF-8) antagonizes BCR/ABL and down-regulates bcl-2. Blood *103*, 3480-3489.

26) Campbell, P.J., Scott, L.M., Buck, G., Wheatley, K., East, C.L., Marsden, J.T., Duffy, A., Boyd, E.M., Bench, A.J., Scott, M.A.*, et al.* (2005). Definition of subtypes of essential thrombocythaemia and relation to polycythaemia vera based on JAK2 V617F mutation status: a prospective study. Lancet *366*, 1945-1953.

27) Carter, B.Z., Mak, P.Y., Mu, H., Zhou, H., Mak, D.H., Schober, W., Leverson, J.D., Zhang, B., Bhatia, R., Huang, X.*, et al.* (2016). Combined targeting of BCL-2 and BCR-ABL tyrosine kinase eradicates chronic myeloid leukemia stem cells. Science translational medicine *8*, 355ra117.

28) Challen, G.A., Boles, N., Lin, K.K., and Goodell, M.A. (2009). Mouse hematopoietic stem cell identification and analysis. Cytometry Part A : the journal of the International Society for Analytical Cytology *75*, 14-24.

29) Chan, E.M., Ratanasirintrawoot, S., Park, I.-H., Manos, P.D., Loh, Y.-H., Huo, H., Miller, J.D., Hartung, O., Rho, J., Ince, T.A.*, et al.* (2009). Live cell imaging distinguishes bona fide human iPS cells from partially reprogrammed cells. Nature Biotechnology *27*, 1033.

30) Chapgier, A., Kong, X.F., Boisson-Dupuis, S., Jouanguy, E., Averbuch, D., Feinberg, J., Zhang, S.Y., Bustamante, J., Vogt, G., Lejeune, J.*, et al.* (2009). A partial form of recessive STAT1 deficiency in humans. J Clin Invest *119*, 1502-1514.

31) Chauvistre, H., Kustermann, C., Rehage, N., Klisch, T., Mitzka, S., Felker, P., Rose-John, S., Zenke, M., and Sere, K.M. (2014). Dendritic cell development requires histone deacetylase activity. European journal of immunology *44*, 2478-2488.

32) Chen, E., Beer, P.A., Godfrey, A.L., Ortmann, C.A., Li, J., Costa-Pereira, A.P., Ingle, C.E., Dermitzakis, E.T., Campbell, P.J., and Green, A.R.

(2010). Distinct clinical phenotypes associated with JAK2V617F reflect differential STAT1 signaling. Cancer Cell *18*, 524-535.

33) Chen, E., and Mullally, A. (2014). How does JAK2V617F contribute to the pathogenesis of myeloproliferative neoplasms? Hematology Am Soc Hematol Educ Program *2014*, 268-276.

34) Chen, E., Schneider, R.K., Breyfogle, L.J., Rosen, E.A., Poveromo, L., Elf, S., Ko, A., Brumme, K., Levine, R., Ebert, B.L.*, et al.* (2015). Distinct effects of concomitant Jak2V617F expression and Tet2 loss in mice promote disease progression in myeloproliferative neoplasms. Blood *125*, 327-335.

35) Chen, Y. (2012). Calcium Phosphate Transfection of Eukaryotic Cells. Bio-protocol *2*, e86.

36) Chen, Z.Q., Lautenberger, J.A., Lyons, L.A., McKenzie, L., and O'Brien, S.J. (1999). A human genome map of comparative anchor tagged sequences. J Hered *90*, 477-484.

37) Choi, K.-D., Yu, J., Smuga-Otto, K., Salvagiotto, G., Rehrauer, W., Vodyanik, M., Thomson, J., and Slukvin, I. (2009). Hematopoietic and endothelial differentiation of human induced pluripotent stem cells. Stem cells (Dayton, Ohio) *27*, 559-567.

38) Chotinantakul, K., and Leeanansaksiri, W. (2012). Hematopoietic stem cell development, niches, and signaling pathways. Bone Marrow Research *2012*, 16.

39) Chungwen, W., John, J., and Iñaki, S. (2011). OMIP-003: Phenotypic analysis of human memory B cells. Cytometry Part A *79A*, 894-896.

40) Coluccia, A.M.L., Vacca, A., Duñach, M., Mologni, L., Redaelli, S., Bustos, V.H., Benati, D., Pinna, L.A., and Gambacorti-Passerini, C. (2007). Bcr-Abl stabilizes β-catenin in chronic myeloid leukemia through its tyrosine phosphorylation. The EMBO Journal *26*, 1456-1466.

41) Corbin, A.S., Agarwal, A., Loriaux, M., Cortes, J., Deininger, M.W., and Druker, B.J. (2011). Human chronic myeloid leukemia stem cells are insensitive to imatinib despite inhibition of BCR-ABL activity. The Journal of Clinical Investigation *121*, 396-409.

42) D'Angelo, W., Acharya, D., Wang, R., Wang, J., Gurung, C., Chen, B., Bai, F., and Guo, Y.-L. (2016). Development of antiviral innate immunity during in vitro differentiation of mouse embryonic stem cells. Stem Cells and Development *25*, 648-659.

43) Dahlin, J.S., Ding, Z., and Hallgren, J. (2015). Distinguishing mast cell progenitors from mature mast cells in mice. Stem Cells and Development *24*, 1703-1711.

44) Dai, C., Chung, I.J., and Krantz, S.B. (2005). Increased erythropoiesis in polycythemia vera is associated with increased erythroid progenitor proliferation and increased phosphorylation of Akt/PKB. Exp Hematol *33*, 152-158.

45) Daley, G.Q., Van Etten, R.A., and Baltimore, D. (1990). Induction of chronic myelogenous leukemia in mice by the P210bcr/abl gene of the Philadelphia chromosome. Science *247*, 824-830.

46) Dameshek, W. (1951). Some speculations on the myeloproliferative syndromes. Blood *6*, 372-375.

47) Danisz, K., and Blasiak, J. (2013). Role of anti-apoptotic pathways activated by BCR/ABL in the resistance of chronic myeloid leukemia cells to tyrosine kinase inhibitors. Acta biochimica Polonica *60*, 503-514.

48) Davis, R.L., Weintraub, H., and Lassar, A.B. (1987). Expression of a single transfected cDNA converts fibroblasts to myoblasts. Cell *51*, 987-1000.

49) de Groot, R.P., Raaijmakers, J.A.M., Lammers, J.-W.J., and Koenderman, L. (2000). STAT5-Dependent CyclinD1 and Bcl-xL Expression in Bcr-Abl-Transformed Cells. Molecular Cell Biology Research Communications *3*, 299-305.

50) De Los Angeles, A., Ferrari, F., Xi, R., Fujiwara, Y., Benvenisty, N., Deng, H., Hochedlinger, K., Jaenisch, R., Lee, S., Leitch, H.G.*, et al.* (2015). Hallmarks of pluripotency. Nature *525*, 469.

51) Deininger, M.W., Goldman, J.M., and Melo, J.V. (2000). The molecular biology of chronic myeloid leukemia. Blood *96*, 3343-3356.

52) Delhommeau, F., Dupont, S., Della Valle, V., James, C., Trannoy, S., Masse, A., Kosmider, O., Le Couedic, J.P., Robert, F., Alberdi, A.*, et al.* (2009). Mutation in TET2 in myeloid cancers. The New England journal of medicine *360*, 2289-2301.

53) Der, S.D., Zhou, A., Williams, B.R.G., and Silverman, R.H. (1998). Identification of genes differentially regulated by interferon α, β, or γ using oligonucleotide arrays. Proceedings of the National Academy of Sciences *95*, 15623-15628.

54) Deshpande, A., Reddy, M.M., Schade, G.O.M., Ray, A., Chowdary, T.K., Griffin, J.D., and Sattler, M. (2011). Kinase domain mutations confer resistance to novel inhibitors targeting JAK2V617F in myeloproliferative neoplasms. Leukemia *26*, 708.

55) DeVries, T.A., Kalkofen, R.L., Matassa, A.A., and Reyland, M.E. (2004). Protein kinase Cdelta regulates apoptosis via activation of STAT1. J Biol Chem *279*, 45603-45612.

56) Diaz-Blanco, E., Bruns, I., Neumann, F., Fischer, J.C., Graef, T., Rosskopf, M., Brors, B., Pechtel, S., Bork, S., Koch, A.*, et al.* (2007). Molecular signature of CD34+ hematopoietic stem and progenitor cells of patients with CML in chronic phase. Leukemia *21*, 494.

57) Dieterlen-Lievre, p.F. (1975). On the origin of haemopoietic stem cells in the avian embryo: an experimental approach. Journal of Embryology and Experimental Morphology *33*, 607-619.

58) Dimos, J.T., Rodolfa, K.T., Niakan, K.K., Weisenthal, L.M., Mitsumoto, H., Chung, W., Croft, G.F., Saphier, G., Leibel, R., Goland, R., *et al.* (2008). Induced pluripotent stem cells generated from patients with ALS can be differentiated into motor neurons. Science *321*, 1218-1221.

59) Ditadi, A., and Sturgeon, C.M. (2016). Directed differentiation of definitive hemogenic endothelium and hematopoietic progenitors from human pluripotent stem cells. Methods *101*, 65-72.

60) Ditadi, A., Sturgeon, C.M., and Keller, G. (2017). A view of human haematopoietic development from the Petri dish. Nat Rev Mol Cell Biol *18*, 56-67.

61) Dorn, I., Klich, K., Arauzo-Bravo, M.J., Radstaak, M., Santourlidis, S., Ghanjati, F., Radke, T.F., Psathaki, O.E., Hargus, G., Kramer, J., *et al.* (2015). Erythroid differentiation of human induced pluripotent stem cells is independent of donor cell type of origin. Haematologica *100*, 32-41.

62) Driggers, P.H., Ennist, D.L., Gleason, S.L., Mak, W.H., Marks, M.S., Levi, B.Z., Flanagan, J.R., Appella, E., and Ozato, K. (1990). An interferon gamma-regulated protein that binds the interferon-inducible enhancer element of major histocompatibility complex class I genes. Proc Natl Acad Sci U S A *87*, 3743-3747.

63) Drukker, M., Katz, G., Urbach, A., Schuldiner, M., Markel, G., Itskovitz-Eldor, J., Reubinoff, B., Mandelboim, O., and Benvenisty, N. (2002). Characterization of the expression of MHC proteins in human embryonic stem cells. Proceedings of the National Academy of Sciences *99*, 9864-9869.

64) Duek, A., Lundberg, P., Shimizu, T., Grisouard, J., Karow, A., Kubovcakova, L., Hao-Shen, H., Dirnhofer, S., and Skoda, R.C. (2014). Loss of Stat1 decreases megakaryopoiesis and favors erythropoiesis in a JAK2-V617F-driven mouse model of MPNs. Blood *123*, 3943-3950.

65) Dupont, S., Massé, A., James, C., Teyssandier, I., Lécluse, Y., Larbret, F., Ugo, V., Saulnier, P., Koscielny, S., Le Couédic, J.P., *et al.* (2007). The JAK2 617VF mutation triggers erythropoietin hypersensitivity and terminal erythroid amplification in primary cells from patients with polycythemia vera. Blood *110*, 1013-1021.

66) Durkin, M.E., Qian, X., Popescu, N.C., and Lowy, D.R. (2013). Isolation of Mouse Embryo Fibroblasts. Bio-protocol *3*, e908.

67) Edelson, B.T., Kc, W., Juang, R., Kohyama, M., Benoit, L.A., Klekotka, P.A., Moon, C., Albring, J.C., Ise, W., Michael, D.G., *et al.* (2010). Peripheral CD103+ dendritic cells form a unified subset developmentally related to CD8alpha+ conventional dendritic cells. J Exp Med *207*, 823-836.

68) Eilken, H.M., Nishikawa, S., and Schroeder, T. (2009). Continuous single-cell imaging of blood generation from haemogenic endothelium. Nature *457*, 896-900.

69) Eiring, A.M., Khorashad, J.S., Anderson, D.J., Yu, F., Redwine, H.M., Mason, C.C., Reynolds, K.R., Clair, P.M., Gantz, K.C., Zhang, T.Y.*, et al.* (2015). β-Catenin is required for intrinsic but not extrinsic BCR-ABL1 kinase-independent resistance to tyrosine kinase inhibitors in chronic myeloid leukemia. Leukemia *29*, 2328.

70) Elena, A., Marzia, D.R., Sara, G., Giuliana, R., Eleonora, R., Stefania, C., Claudia, B., Mario, P., Romano, D., and Antonello, D.P. (2018). Concise review: chronic myeloid leukemia: stem cell niche and response to pharmacologic treatment. STEM CELLS Translational Medicine *7*, 305-314.

71) Elias, J., and Hagop, K. (2018). Chronic myeloid leukemia: 2018 update on diagnosis, therapy and monitoring. American Journal of Hematology *93*, 442-459.

72) Elitt, M.S., Barbar, L., and Tesar, P.J. (2018). Drug screening for human genetic diseases using iPSC models. Human Molecular Genetics *27*, R89-R98.

73) England, J., and Loughna, S. (2013). Heavy and light roles: myosin in the morphogenesis of the heart. In Cell Mol Life Sci, pp. 1221-1239.

74) Essers, M.A., Offner, S., Blanco-Bose, W.E., Waibler, Z., Kalinke, U., Duchosal, M.A., and Trumpp, A. (2009). IFNalpha activates dormant haematopoietic stem cells in vivo. Nature *458*, 904-908.

75) Evans, M.J., and Kaufman, M.H. (1981). Establishment in culture of pluripotential cells from mouse embryos. Nature *292*, 154.

76) Faial, T., Bernardo, A.S., Mendjan, S., Diamanti, E., Ortmann, D., Gentsch, G.E., Mascetti, V.L., Trotter, M.W.B., Smith, J.C., and Pedersen, R.A. (2015). Brachyury and SMAD signalling collaboratively orchestrate distinct mesoderm and endoderm gene regulatory networks in differentiating human embryonic stem cells. Development.

77) Felker, P., Sere, K., Lin, Q., Becker, C., Hristov, M., Hieronymus, T., and Zenke, M. (2010). TGF-beta1 accelerates dendritic cell differentiation from common dendritic cell progenitors and directs subset specification toward conventional dendritic cells. Journal of immunology *185*, 5326-5335.

78) Fink, J., Kent, D., Li, J., Hawkins, E., Lo Celso, C., and Green, A. (2013). Homozygous JAK2V617F drives rapid hematopoietic stem cell proliferation and differentiation at the expense of self-renewal. Experimental Hematology *41*, S15.

79) Fish, E.N., Uddin, S., Korkmaz, M., Majchrzak, B., Druker, B.J., and Platanias, L.C. (1999). Activation of a CrkL-stat5 signaling complex by type I interferons. J Biol Chem *274*, 571-573.

80) Funakoshi-Tago, M., Sumi, K., Kasahara, T., and Tago, K. (2013). Critical roles of Myc-ODC axis in the cellular transformation induced by

myeloproliferative neoplasm-associated JAK2 V617F mutant. PLoS One *8*, e52844.

81) Fusaki, N., Ban, H., Nishiyama, A., Saeki, K., and Hasegawa, M. (2009). Efficient induction of transgene-free human pluripotent stem cells using a vector based on Sendai virus, an RNA virus that does not integrate into the host genome. Proceedings of the Japan Academy, Series B *85*, 348-362.

82) Gabriele, L., Phung, J., Fukumoto, J., Segal, D., Wang, I.-M., Giannakakou, P., Giese, N.A., Ozato, K., and Morse, H.C. (1999). Regulation of apoptosis in myeloid cells by interferon consensus sequence–binding protein. The Journal of Experimental Medicine *190*, 411-422.

83) Garcia-Manero, G., Faderl, S., O'Brien, S., Cortes, J., Talpaz, M., and Kantarjian, H.M. (2003). Chronic myelogenous leukemia: a review and update of therapeutic strategies. Cancer *98*, 437-457.

84) Garçon, L., Rivat, C., James, C., Lacout, C., Camara-Clayette, V., Ugo, V., Lecluse, Y., Bennaceur-Griscelli, A., and Vainchenker, W. (2006). Constitutive activation of STAT5 and Bcl-xL overexpression can induce endogenous erythroid colony formation in human primary cells. Blood *108*, 1551-1554.

85) Geissmann, F., Manz, M.G., Jung, S., Sieweke, M.H., Merad, M., and Ley, K. (2010). Development of monocytes, macrophages, and dendritic cells. Science *327*, 656-661.

86) Genethliou, N., Panayiotou, E., Panayi, H., Orford, M., Mean, R., Lapathitis, G., Gill, H., Raoof, S., Gasperi, R.D., Elder, G.*, et al.* (2009). SOX1 links the function of neural patterning and Notch signalling in the ventral spinal cord during the neuron-glial fate switch. Biochemical and Biophysical Research Communications *390*, 1114-1120.

87) Ghaffari, L.T., Starr, A., Nelson, A.T., and Sattler, R. (2018). Representing diversity in the dish: using patient-derived in vitro models to recreate the heterogeneity of neurological disease. Frontiers in Neuroscience *12*.

88) Godfrey, A.L., Chen, E., Pagano, F., Ortmann, C.A., Silber, Y., Bellosillo, B., Guglielmelli, P., Harrison, C.N., Reilly, J.T., Stegelmann, F.*, et al.* (2012). JAK2V617F homozygosity arises commonly and recurrently in PV and ET, but PV is characterized by expansion of a dominant homozygous subclone. Blood *120*, 2704-2707.

89) Goldman, J.M., and Melo, J.V. (2003). Chronic myeloid leukemia-- advances in biology and new approaches to treatment. The New England journal of medicine *349*, 1451-1464.

90) Gotta, V., Widmer, N., Decosterd, L.A., Chalandon, Y., Heim, D., Gregor, M., Benz, R., Leoncini-Franscini, L., Baerlocher, G.M., Duchosal, M.A.*, et al.* (2014). Clinical usefulness of therapeutic concentration monitoring

for imatinib dosage individualization: results from a randomized controlled trial. Cancer Chemother Pharmacol *74*, 1307-1319.

91) Graham, V., Khudyakov, J., Ellis, P., and Pevny, L. (2003). SOX2 functions to maintain neural progenitor identity. Neuron *39*, 749-765.

92) Grand, F.H., Hidalgo-Curtis, C.E., Ernst, T., Zoi, K., Zoi, C., McGuire, C., Kreil, S., Jones, A., Score, J., Metzgeroth, G.*, et al.* (2009). Frequent CBL mutations associated with 11q acquired uniparental disomy in myeloproliferative neoplasms. Blood *113*, 6182-6192.

93) Grisouard, J., Shimizu, T., Duek, A., Kubovcakova, L., Hao-Shen, H., Dirnhofer, S., and Skoda, R.C. (2015). Deletion of Stat3 in hematopoietic cells enhances thrombocytosis and shortens survival in a JAK2-V617F mouse model of MPN. Blood *125*, 2131-2140.

94) Grumbach, I.M., Mayer, I.A., Uddin, S., Lekmine, F., Majchrzak, B., Yamauchi, H., Fujita, S., Druker, B.J., Fish, E.N., and Platanias, L.C. (2001). Engagement of the CrkL adaptor in interferon alpha signalling in BCR-ABL-expressing cells. Brit J Haematol *112*, 327-336.

95) Grundschober, E., Hoelbl-Kovacic, A., Bhagwat, N., Kovacic, B., Scheicher, R., Eckelhart, E., Kollmann, K., Keller, M., Grebien, F., Wagner, K.U.*, et al.* (2014). Acceleration of Bcr-Abl+ leukemia induced by deletion of JAK2. Leukemia *28*, 1918.

96) Guibentif, C., Rönn, R.E., Böiers, C., Lang, S., Saxena, S., Soneji, S., Enver, T., Karlsson, G., and Woods, N.-B. (2017). Single-cell analysis identifies distinct stages of human endothelial-to-hematopoietic transition. Cell Reports *19*, 10-19.

97) Gurdon, J.B., Elsdale, T.R., and Fischberg, M. (1958). Sexually mature Individuals of xenopus laevis from the transplantation of single somatic nuclei. Nature *182*, 64.

98) Haas, S., Trumpp, A., and Milsom, M.D. (2018). Causes and consequences of hematopoietic stem cell heterogeneity. Cell Stem Cell *22*, 627-638.

99) Hambleton, S., Salem, S., Bustamante, J., Bigley, V., Boisson-Dupuis, S., Azevedo, J., Fortin, A., Haniffa, M., Ceron-Gutierrez, L., Bacon, C.M.*, et al.* (2011). IRF8 mutations and human dendritic-cell immunodeficiency. The New England journal of medicine *365*, 127-138.

100) Han, L., Schubert, C., Köhler, J., Schemionek, M., Isfort, S., Brümmendorf, T.H., Koschmieder, S., and Chatain, N. (2016). Calreticulin-mutant proteins induce megakaryocytic signaling to transform hematopoietic cells and undergo accelerated degradation and Golgi-mediated secretion. Journal of hematology & oncology *9*, 45-45.

101) Hanna, J., Wernig, M., Markoulaki, S., Sun, C.-W., Meissner, A., Cassady, J.P., Beard, C., Brambrink, T., Wu, L.-C., Townes, T.M.*, et al.*

(2007). Treatment of sickle cell anemia mouse model with iPS cells generated from autologous skin. Science *318*, 1920-1923.

102) Hao, S.X., and Ren, R. (2000). Expression of interferon consensus sequence binding protein (ICSBP) is downregulated in Bcr-Abl-induced murine chronic myelogenous leukemia-like disease, and forced coexpression of ICSBP inhibits Bcr-Abl-induced myeloproliferative disorder. Molecular and cellular biology *20*, 1149-1161.

103) Hara, T., Schwieger, M., Kazama, R., Okamoto, S., Minehata, K., Ziegler, M., Lohler, J., and Stocking, C. (2008). Acceleration of chronic myeloproliferation by enforced expression of Meis1 or Meis3 in Icsbp-deficient bone marrow cells. Oncogene *27*, 3865-3869.

104) Hasan, S., Lacout, C., Marty, C., Cuingnet, M., Solary, E., Vainchenker, W., and Villeval, J.L. (2013). JAK2(V617F) expression in mice amplifies early hematopoietic cells and gives them a competitive advantage that is hampered by IFN alpha. Blood *122*, 1464-1477.

105) Heine, A., Held, S.A., Daecke, S.N., Wallner, S., Yajnanarayana, S.P., Kurts, C., Wolf, D., and Brossart, P. (2013). The JAK-inhibitor ruxolitinib impairs dendritic cell function in vitro and in vivo. Blood *122*, 1192-1202.

106) Hiwase, D.K., Saunders, V.A., Nievergall, E., Ross, D.D., White, D.L., and Hughes, T.P. (2013). Dasatinib targets chronic myeloid leukemia-CD34(+) progenitors as effectively as it targets mature cells. Haematologica *98*, 896-900.

107) Hjort, E.E., Huang, W.Q., Hu, L.P., and Eklund, E.A. (2016). Bcr-abl regulates Stat5 through Shp2, the interferon consensus sequence binding protein (Icsbp/Irf8), growth arrest specific 2 (Gas2) and calpain. Oncotarget *7*, 77635-77650.

108) Hochedlinger, K., and Jaenisch, R. (2002). Nuclear transplantation: lessons from frogs and mice. Current Opinion in Cell Biology *14*, 741-748.

109) Hol, E.M., and Pekny, M. (2015). Glial fibrillary acidic protein (GFAP) and the astrocyte intermediate filament system in diseases of the central nervous system. Current Opinion in Cell Biology *32*, 121-130.

110) Holtschke, T., Löhler, J., Kanno, Y., Fehr, T., Giese, N., Rosenbauer, F., Lou, J., Knobeloch, K.-P., Gabriele, L., Waring, J.F.*, et al.* (1996). Immunodeficiency and chronic myelogenous leukemia-like syndrome in mice with a targeted mutation of the ICSBP gene. Cell *87*, 307-317.

111) Hong, X.X., and Carmichael, G.G. (2013). Innate immunity in pluripotent human cells: attenuated response to interferon-beta. J Biol Chem *288*, 16196-16205.

112) Hookham, M.B., Elliott, J., Suessmuth, Y., Staerk, J., Ward, A.C., Vainchenker, W., Percy, M.J., McMullin, M.F., Constantinescu, S.N., and Johnston, J.A. (2007). The myeloproliferative disorder-associated

JAK2 V617F mutant escapes negative regulation by suppressor of cytokine signaling 3. Blood *109*, 4924-4929.

113) Hou, P., Li, Y., Zhang, X., Liu, C., Guan, J., Li, H., Zhao, T., Ye, J., Yang, W., Liu, K.*, et al.* (2013). Pluripotent stem cells induced from mouse somatic cells by small-molecule compounds. Science *341*, 651-654.

114) Hsia, N., and Zon, L.I. (2005). Transcriptional regulation of hematopoietic stem cell development in zebrafish. Experimental Hematology *33*, 1007-1014.

115) Huang, W., Zhou, W., Saberwal, G., Konieczna, I., Horvath, E., Katsoulidis, E., Platanias, L.C., and Eklund, E.A. (2010). Interferon consensus sequence binding protein (ICSBP) decreases beta-catenin activity in myeloid cells by repressing GAS2 transcription. Molecular and cellular biology *30*, 4575-4594.

116) Huber, T.L., Kouskoff, V., Joerg Fehling, H., Palis, J., and Keller, G. (2004). Haemangioblast commitment is initiated in the primitive streak of the mouse embryo. Nature *432*, 625.

117) Inoue, K., Wakao, H., Ogonuki, N., Miki, H., Seino, K.-i., Nambu-Wakao, R., Noda, S., Miyoshi, H., Koseki, H., Taniguchi, M.*, et al.* (2005). Generation of cloned mice by direct nuclear transfer from natural killer T cells. Current Biology *15*, 1114-1118.

118) Irudayam, J.I., Contreras, D., Spurka, L., Subramanian, A., Allen, J., Ren, S., Kanagavel, V., Nguyen, Q., Ramaiah, A., Ramamoorthy, K.*, et al.* (2015). Characterization of Type I Interferon pathway during Hepatic Differentiation of Human Pluripotent Stem Cells and hepatitis C virus infection. Stem cell research *15*, 354-364.

119) Ishii, T., Xu, M., Zhao, Y., Hu, W.Y., Ciurea, S., Bruno, E., and Hoffman, R. (2007a). Recurrence of clonal hematopoiesis after discontinuing pegylated recombinant interferon-alpha 2a in a patient with polycythemia vera. Leukemia *21*, 373-374.

120) Ishii, T., Zhao, Y., Sozer, S., Shi, J., Zhang, W., Hoffman, R., and Xu, M. (2007b). Behavior of CD34+ cells isolated from patients with polycythemia vera in NOD/SCID mice. Experimental Hematology *35*, 1633-1640.

121) Itskovitz-Eldor, J., Schuldiner, M., Karsenti, D., Eden, A., Yanuka, O., Amit, M., Soreq, H., and Benvenisty, N. (2000). Differentiation of human embryonic stem cells into embryoid bodies compromising the three embryonic germ layers. Molecular medicine (Cambridge, Mass) *6*, 88-95.

122) Ivashkiv, L.B., and Donlin, L.T. (2014). Regulation of type I interferon responses. Nat Rev Immunol *14*, 36-49.

123) Iwasaki, H., and Akashi, K. (2007). Myeloid lineage commitment from the hematopoietic stem cell. Immunity *26*, 726-740.

124) Jabbour, E., Kantarjian, H., O'Brien, S., Shan, J., Quintas-Cardama, A., Faderl, S., Garcia-Manero, G., Ravandi, F., Rios, M.B., and Cortes, J. (2011). The achievement of an early complete cytogenetic response is a major determinant for outcome in patients with early chronic phase chronic myeloid leukemia treated with tyrosine kinase inhibitors. Blood *118*, 4541-4546; quiz 4759.

125) Jaffredo, T., Gautier, R., Eichmann, A., and Dieterlen-Lievre, F. (1998). Intraaortic hemopoietic cells are derived from endothelial cells during ontogeny. Development *125*, 4575-4583.

126) Jagannathan-Bogdan, M., and Zon, L.I. (2013). Hematopoiesis. Development *140*, 2463-2467.

127) James, C., Mazurier, F., Dupont, S., Chaligne, R., Lamrissi-Garcia, I., Tulliez, M., Lippert, E., Mahon, F.-X., Pasquet, J.-M., Etienne, G.*, et al.* (2008). The hematopoietic stem cell compartment of JAK2V617F-positive myeloproliferative disorders is a reflection of disease heterogeneity. Blood *112*, 2429-2438.

128) James, C., Ugo, V., Le Couedic, J.P., Staerk, J., Delhommeau, F., Lacout, C., Garcon, L., Raslova, H., Berger, R., Bennaceur-Griscelli, A.*, et al.* (2005). A unique clonal JAK2 mutation leading to constitutive signalling causes polycythaemia vera. Nature *434*, 1144-1148.

129) Jamieson, C.H., Gotlib, J., Durocher, J.A., Chao, M.P., Mariappan, M.R., Lay, M., Jones, C., Zehnder, J.L., Lilleberg, S.L., and Weissman, I.L. (2006). The JAK2 V617F mutation occurs in hematopoietic stem cells in polycythemia vera and predisposes toward erythroid differentiation. Proc Natl Acad Sci U S A *103*, 6224-6229.

130) Jones, A.V., Kreil, S., Zoi, K., Waghorn, K., Curtis, C., Zhang, L., Score, J., Seear, R., Chase, A.J., Grand, F.H.*, et al.* (2005). Widespread occurrence of the JAK2 V617F mutation in chronic myeloproliferative disorders. Blood *106*, 2162-2168.

131) Jones, E.A., Clement-Jones, M., James, O.F., and Wilson, D.I. (2001). Differences between human and mouse alpha-fetoprotein expression during early development. Journal of anatomy *198*, 555-559.

132) Junfeng, J., H., N.S., Vivek, S., Dante, N., Samer, H., Michelle, S., Quang, T., M., C.G., D., M.J., Andras, N.*, et al.* (2012). Elevated coding mutation rate during the reprogramming of human somatic cells into induced pluripotent stem cells. STEM CELLS *30*, 435-440.

133) Kaneko, S., Kakinuma, S., Asahina, Y., Kamiya, A., Miyoshi, M., Tsunoda, T., Nitta, S., Asano, Y., Nagata, H., Otani, S.*, et al.* (2016). Human induced pluripotent stem cell-derived hepatic cell lines as a new model for host interaction with hepatitis B virus. Scientific Reports *6*, 29358.

134) Kanno, Y., Levi, B.Z., Tamura, T., and Ozato, K. (2005). Immune cell-specific amplification of interferon signaling by the IRF-4/8-PU.1

complex. Journal of interferon & cytokine research : the official journal of the International Society for Interferon and Cytokine Research *25*, 770-779.

135) Kantarjian, H., Sawyers, C., Hochhaus, A., Guilhot, F., Schiffer, C., Gambacorti-Passerini, C., Niederwieser, D., Resta, D., Capdeville, R., Zoellner, U.*, et al.* (2002). Hematologic and cytogenetic responses to imatinib mesylate in chronic myelogenous leukemia. The New England journal of medicine *346*, 645-652.

136) Kantarjian, H.M., O'Brien, S., Cortes, J.E., Shan, J., Giles, F.J., Rios, M.B., Faderl, S.H., Wierda, W.G., Ferrajoli, A., Verstovsek, S.*, et al.* (2003). Complete cytogenetic and molecular responses to interferon-α-based therapy for chronic myelogenous leukemia are associated with excellent long-term prognosis. Cancer *97*, 1033-1041.

137) Karamitros, D., Stoilova, B., Aboukhalil, Z., Hamey, F., Reinisch, A., Samitsch, M., Quek, L., Otto, G., Repapi, E., Doondeea, J.*, et al.* (2018). Single-cell analysis reveals the continuum of human lympho-myeloid progenitor cells. Nature immunology *19*, 85-97.

138) Katlinski, K.V., Gui, J., Katlinskaya, Y.V., Ortiz, A., Chakraborty, R., Bhattacharya, S., Carbone, C.J., Beiting, D.P., Girondo, M.A., Peck, A.R.*, et al.* (2017). Inactivation of interferon receptor promotes the establishment of immune privileged tumor microenvironment. Cancer Cell *31*, 194-207.

139) Kelly, S.J. (1977). Studies of the developmental potential of 4- and 8-cell stage mouse blastomeres. Journal of Experimental Zoology *200*, 365-376.

140) Kennedy, M., Awong, G., Sturgeon, C.M., Ditadi, A., LaMotte-Mohs, R., Zuniga-Pflucker, J.C., and Keller, G. (2012). T lymphocyte potential marks the emergence of definitive hematopoietic progenitors in human pluripotent stem cell differentiation cultures. Cell Rep *2*, 1722-1735.

141) Kennedy, M., D'Souza, S.L., Lynch-Kattman, M., Schwantz, S., and Keller, G. (2007). Development of the hemangioblast defines the onset of hematopoiesis in human ES cell differentiation cultures. Blood *109*, 2679-2687.

142) Kennedy, M., Firpo, M., Choi, K., Wall, C., Robertson, S., Kabrun, N., and Keller, G. (1997). A common precursor for primitive erythropoiesis and definitive haematopoiesis. Nature *386*, 488-493.

143) Kent, D.G., Li, J., Tanna, H., Fink, J., Kirschner, K., Pask, D.C., Silber, Y., Hamilton, T.L., Sneade, R., Simons, B.D.*, et al.* (2013). Self-renewal of single mouse hematopoietic stem cells Is reduced by JAK2V617F without compromising progenitor cell expansion. PLOS Biology *11*, e1001576.

144) Kessel, K.U., Bluemke, A., Scholer, H.R., Zaehres, H., Schlenke, P., and Dorn, I. (2017). Emergence of CD43-expressing hematopoietic

progenitors from human induced pluripotent stem cells. Transfus Med Hemother *44*, 143-150.

145) Kiladjian, J.J., Cassinat, B., Turlure, P., Cambier, N., Roussel, M., Bellucci, S., Menot, M.L., Massonnet, G., Dutel, J.L., Ghomari, K.*, et al.* (2006). High molecular response rate of polycythemia vera patients treated with pegylated interferon alpha-2a. Blood *108*, 2037-2040.

146) Kiladjian, J.J., Giraudier, S., and Cassinat, B. (2016). Interferon-alpha for the therapy of myeloproliferative neoplasms: targeting the malignant clone. Leukemia *30*, 776-781.

147) Kiladjian, J.J., Masse, A., Cassinat, B., Mokrani, H., Teyssandier, I., le Couedic, J.P., Cambier, N., Almire, C., Pronier, E., Casadevall, N.*, et al.* (2010). Clonal analysis of erythroid progenitors suggests that pegylated interferon alpha-2a treatment targets JAK2V617F clones without affecting TET2 mutant cells. Leukemia *24*, 1519-1523.

148) Kissa, K., and Herbomel, P. (2010). Blood stem cells emerge from aortic endothelium by a novel type of cell transition. Nature *464*, 112-115.

149) Kohnken, R., Porcu, P., and Mishra, A. (2017). Overview of the use of murine models in leukemia and lymphoma research. Front Oncol *7*.

150) Kong, X.F., Ciancanelli, M., Al-Hajjar, S., Alsina, L., Zumwalt, T., Bustamante, J., Feinberg, J., Audry, M., Prando, C., Bryant, V.*, et al.* (2010). A novel form of human STAT1 deficiency impairing early but not late responses to interferons. Blood *116*, 5895-5906.

151) Kovarova, M. (2013). Isolation and characterization of mast cells in mouse models of allergic diseases. Methods in molecular biology (Clifton, NJ) *1032*, 109-119.

152) Kovarova, M., Latour, A.M., Chason, K.D., Tilley, S.L., and Koller, B.H. (2010). Human embryonic stem cells: a source of mast cells for the study of allergic and inflammatory diseases. Blood *115*, 3695-3703.

153) Kubo, A., Shinozaki, K., Shannon, J.M., Kouskoff, V., Kennedy, M., Woo, S., Fehling, H.J., and Keller, G. (2004). Development of definitive endoderm from embryonic stem cells in culture. Development *131*, 1651-1662.

154) Kujawski, L.A., and Talpaz, M. (2007). The role of interferon-alpha in the treatment of chronic myeloid leukemia. Cytokine & growth factor reviews *18*, 459-471.

155) Kumano, K., Arai, S., Hosoi, M., Taoka, K., Takayama, N., Otsu, M., Nagae, G., Ueda, K., Nakazaki, K., Kamikubo, Y.*, et al.* (2012). Generation of induced pluripotent stem cells from primary chronic myelogenous leukemia patient samples. Blood *119*, 6234-6242.

156) Kuo, F.C., and Dong, F. (2015). Next-generation sequencing-based panel testing for myeloid neoplasms. Current hematologic malignancy reports *10*, 104-111.

157) Kurotaki, D., Osato, N., Nishiyama, A., Yamamoto, M., Ban, T., Sato, H., Nakabayashi, J., Umehara, M., Miyake, N., Matsumoto, N.*, et al.* (2013). Essential role of the IRF8-KLF4 transcription factor cascade in murine monocyte differentiation. Blood *121*, 1839-1849.

158) Kurotaki, D., Yamamoto, M., Nishiyama, A., Uno, K., Ban, T., Ichino, M., Sasaki, H., Matsunaga, S., Yoshinari, M., Ryo, A.*, et al.* (2014). IRF8 inhibits C/EBPalpha activity to restrain mononuclear phagocyte progenitors from differentiating into neutrophils. Nat Commun *5*, 4978.

159) Lacaud, G., and Kouskoff, V. (2017). Hemangioblast, hemogenic endothelium, and primitive versus definitive hematopoiesis. Experimental Hematology *49*, 19-24.

160) Lachmann, N., Ackermann, M., Frenzel, E., Liebhaber, S., Brennig, S., Happle, C., Hoffmann, D., Klimenkova, O., Lüttge, D., Buchegger, T.*, et al.* (2015). Large-scale hematopoietic dfferentiation of human induced pluripotent stem cells provides granulocytes or macrophages for cell replacement therapies. Stem Cell Reports *4*, 282-296.

161) Lacout, C., Pisani, D.F., Tulliez, M., Gachelin, F.M., Vainchenker, W., and Villeval, J.L. (2006). JAK2V617F expression in murine hematopoietic cells leads to MPD mimicking human PV with secondary myelofibrosis. Blood *108*, 1652-1660.

162) Lafaille, F.G., Pessach, I.M., Zhang, S.-Y., Ciancanelli, M.J., Herman, M., Abhyankar, A., Ying, S.-W., Keros, S., Goldstein, P.A., Mostoslavsky, G.*, et al.* (2012). Impaired intrinsic immunity to HSV-1 in human iPSC-derived TLR3-deficient CNS cells. Nature *491*, 769.

163) Lam, E.Y.N., Hall, C.J., Crosier, P.S., Crosier, K.E., and Flores, M.V. (2010). Live imaging of Runx1 expression in the dorsal aorta tracks the emergence of blood progenitors from endothelial cells. Blood *116*, 909-914.

164) Landázuri, N., and Le Doux, J.M. (2006). Complexation with chondroitin sulfate C and Polybrene rapidly purifies retrovirus from inhibitors of transduction and substantially enhances gene transfer. Biotechnology and Bioengineering *93*, 146-158.

165) Lee, J., Zhou, Y.J., Ma, W., Zhang, W., Aljoufi, A., Luh, T., Lucero, K., Liang, D., Thomsen, M., Bhagat, G.*, et al.* (2017). Lineage specification of human dendritic cells is marked by IRF8 expression in hematopoietic stem cells and multipotent progenitors. Nature immunology *18*, 877.

166) Lee, M.S., Kantarjian, H., Talpaz, M., Freireich, E.J., Deisseroth, A., Trujillo, J.M., and Stass, S.A. (1992). Detection of minimal residual disease by polymerase chain reaction in Philadelphia chromosome-positive chronic myelogenous leukemia following interferon therapy. Blood *79*, 1920-1923.

167) Leung, A., Zulick, E., Skvir, N., Vanuytsel, K., Morrison, T.A., Naing, Z.H., Wang, Z., Dai, Y., Chui, D.H.K., Steinberg, M.H.*, et al.* (2018). Notch

and aryl hydrocarbon receptor signaling impact definitive hematopoiesis from human pluripotent stem cells. STEM CELLS *36*, 1004-1019.

168) Levine, R.L., Pardanani, A., Tefferi, A., and Gilliland, D.G. (2007). Role of JAK2 in the pathogenesis and therapy of myeloproliferative disorders. Nature reviews Cancer *7*, 673-683.

169) Levy, D.E., Kessler, D.S., Pine, R., and Darnell, J.E., Jr. (1989). Cytoplasmic activation of ISGF3, the positive regulator of interferon-alpha-stimulated transcription, reconstituted in vitro. Genes Dev *3*, 1362-1371.

170) Li, W., and Ding, S. (2010). Small molecules that modulate embryonic stem cell fate and somatic cell reprogramming. Trends in pharmacological sciences *31*, 36-45.

171) Li, Y., Brauer, P.M., Singh, J., Xhiku, S., Yoganathan, K., Zúñiga-Pflücker, J.C., and Anderson, M.K. (2017). Targeted disruption of TCF12 reveals HEB as essential in human mesodermal specification and hematopoiesis. Stem Cell Reports *9*, 779-795.

172) Lin, C.H.S., Kaushansky, K., and Zhan, H. (2016). JAK2V617F-mutant vascular niche contributes to JAK2V617F clonal expansion in myeloproliferative neoplasms. Blood Cells Mol Dis *62*, 42-48.

173) Lu, M., Zhang, W., Li, Y., Berenzon, D., Wang, X., Wang, J., Mascarenhas, J., Xu, M., and Hoffman, R. (2010). Interferon-alpha targets JAK2V617F-positive hematopoietic progenitor cells and acts through the p38 MAPK pathway. Exp Hematol *38*, 472-480.

174) Lu, X., Levine, R., Tong, W., Wernig, G., Pikman, Y., Zarnegar, S., Gilliland, D.G., and Lodish, H. (2005). Expression of a homodimeric type I cytokine receptor is required for JAK2V617F-mediated transformation. Proceedings of the National Academy of Sciences of the United States of America *102*, 18962-18967.

175) Ludwig, T.E., Bergendahl, V., Levenstein, M.E., Yu, J., Probasco, M.D., and Thomson, J.A. (2006). Feeder-independent culture of human embryonic stem cells. Nature Methods *3*, 637.

176) Lundberg, P., Takizawa, H., Kubovcakova, L., Guo, G., Hao-Shen, H., Dirnhofer, S., Orkin, S.H., Manz, M.G., and Skoda, R.C. (2014). Myeloproliferative neoplasms can be initiated from a single hematopoietic stem cell expressing JAK2-V617F. J Exp Med *211*, 2213-2230.

177) Manzella, L., Tirro, E., Pennisi, M.S., Massimino, M., Stella, S., Romano, C., Vitale, S.R., and Vigneri, P. (2016). Roles of interferon regulatory factors in chronic myeloid leukemia. Current cancer drug targets *16*, 594-605.

178) Massirer, K.B., Hirata, M.H., Silva, A.E.B., Ferraz, M.L.G., Nguyen, N.Y., and Hirata, R.D.C. (2004). Interferon-a receptor 1 mRNA expression in peripheral blood mononuclear cells is associated with response to

interferon-a therapy of patients with chronic hepatitis C. Brazilian Journal of Medical and Biological Research *37*, 643-647.

179) Mayer, I.A., Verma, A., Grumbach, I.M., Uddin, S., Lekmine, F., Ravandi, F., Majchrzak, B., Fujita, S., Fish, E.N., and Platanias, L.C. (2001). The p38 MAPK pathway mediates the growth inhibitory effects of interferon-alpha in BCR-ABL-expressing cells. Journal of Biological Chemistry *276*, 28570-28577.

180) Mazzella, G., Saracco, G., Festi, D., Rosina, F., Marchetto, S., Jaboli, F., Sostegni, R., Pezzoli, A., Azzaroli, F., Cancellieri, C.*, et al.* (1999). Long-term results with interferon therapy in chronic type B hepatitis: a prospective randomized trial. American Journal Of Gastroenterology *94*, 2246.

181) McGrath, Kathleen E., Frame, Jenna M., Fegan, Katherine H., Bowen, James R., Conway, Simon J., Catherman, Seana C., Kingsley, Paul D., Koniski, Anne D., and Palis, J. (2015). Distinct sources of hematopoietic progenitors emerge before HSCs and provide functional blood cells in the mammalian embryo. Cell Reports *11*, 1892-1904.

182) Medvinsky, A.L., Samoylina, N.L., Muller, A.M., and Dzierzak, E.A. (1993). An early pre-liver intraembryonic source of CFU-S in the developing mouse. Nature *364*, 64-67.

183) Moran-Crusio, K., Reavie, L., Shih, A., Abdel-Wahab, O., Ndiaye-Lobry, D., Lobry, C., Figueroa, Maria E., Vasanthakumar, A., Patel, J., Zhao, X.*, et al.* (2011). Tet2 loss leads to increased hematopoietic stem cell self-renewal and myeloid transformation. Cancer Cell *20*, 11-24.

184) Moreau, T., Evans, A.L., Vasquez, L., Tijssen, M.R., Yan, Y., Trotter, M.W., Howard, D., Colzani, M., Arumugam, M., Wu, W.H.*, et al.* (2016). Large-scale production of megakaryocytes from human pluripotent stem cells by chemically defined forward programming. Nat Commun *7*, 11208.

185) Moretti, A., Bellin, M., Welling, A., Jung, C.B., Lam, J.T., Bott-Flügel, L., Dorn, T., Goedel, A., Höhnke, C., Hofmann, F.*, et al.* (2010). Patient-specific induced pluripotent stem-cell models for long-QT syndrome. New England Journal of Medicine *363*, 1397-1409.

186) Mullally, A., Bruedigam, C., Poveromo, L., Heidel, F.H., Purdon, A., Vu, T., Austin, R., Heckl, D., Breyfogle, L.J., Kuhn, C.P.*, et al.* (2013). Depletion of Jak2V617F myeloproliferative neoplasm-propagating stem cells by interferon-alpha in a murine model of polycythemia vera. Blood *121*, 3692-3702.

187) Mullally, A., Lane, S.W., Ball, B., Megerdichian, C., Okabe, R., Al-Shahrour, F., Paktinat, M., Haydu, J.E., Housman, E., Lord, A.M.*, et al.* (2010). Physiological Jak2V617F expression causes a lethal myeloproliferative neoplasm with differential effects on hematopoietic stem and progenitor cells. Cancer Cell *17*, 584-596.

188) Neubauer, A.B., Dali, C., Lorenz, C.H., Magnus, K.R.S., Emily, P.S., Justus, D., Markus, R., Andreas, H., Rolf, M., Martin, E.*, et al.* (2004). Interferon consensus sequence binding protein (ICSBP; IRF-8) antagonizes BCR/ABL and down-regulates bcl-2.

189) Ng, A.P., and Alexander, W.S. (2017). Haematopoietic stem cells: past, present and future. Cell Death Discovery *3*, 17002.

190) Nguyen, K.B., Watford, W.T., Salomon, R., Hofmann, S.R., Pien, G.C., Morinobu, A., Gadina, M., O'Shea, J.J., and Biron, C.A. (2002). Critical role for STAT4 activation by type 1 interferons in the interferon-γ response to viral infection. Science *297*, 2063-2066.

191) Notta, F., Zandi, S., Takayama, N., Dobson, S., Gan, O.I., Wilson, G., Kaufmann, K.B., McLeod, J., Laurenti, E., Dunant, C.F.*, et al.* (2016). Distinct routes of lineage development reshape the human blood hierarchy across ontogeny. Science *351*.

192) Oberlin, E., Tavian, M., Blazsek, I., and Peault, B. (2002). Blood-forming potential of vascular endothelium in the human embryo. Development *129*, 4147-4157.

193) Oie, S., Ono, M., Yano, H., Maruyama, Y., Terada, T., Yamada, Y., Ueno, T., Kojiro, M., Hirano, K., and Kuwano, M. (2006). The up-regulation of type I interferon receptor gene plays a key role in hepatocellular carcinoma cells in the synergistic antiproliferative effect by 5-fluorouracil and interferon-alpha. Int J Oncol *29*, 1469-1478.

194) Okita, K., Ichisaka, T., and Yamanaka, S. (2007). Generation of germline-competent induced pluripotent stem cells. Nature *448*, 313.

195) Ortmann, C.A., Kent, D.G., Nangalia, J., Silber, Y., Wedge, D.C., Grinfeld, J., Baxter, E.J., Massie, C.E., Papaemmanuil, E., Menon, S.*, et al.* (2015). Effect of mutation order on myeloproliferative neoplasms. New England Journal of Medicine *372*, 601-612.

196) Palis, J., Chan, R.J., Koniski, A., Patel, R., Starr, M., and Yoder, M.C. (2001). Spatial and temporal emergence of high proliferative potential hematopoietic precursors during murine embryogenesis. Proceedings of the National Academy of Sciences *98*, 4528-4533.

197) Paredes, J., and Krown, S.E. (1991). Interferon-α therapy in patients with Kaposi's Sarcoma and the acquired immunodeficiency syndrome. International Journal of Immunopharmacology *13*, 77-81.

198) Pereira, C.-F., Chang, B., Gomes, A., Bernitz, J., Papatsenko, D., Niu, X., Swiers, G., Azzoni, E., de Bruijn, Marella F.T.R., Schaniel, C.*, et al.* (2016). Hematopoietic reprogramming in vitro informs in vivo identification of hemogenic precursors to definitive hematopoietic stem cells. Developmental Cell *36*, 525-539.

199) Pieri, L., Pancrazzi, A., Pacilli, A., Rabuzzi, C., Rotunno, G., Fanelli, T., Guglielmelli, P., Fjerza, R., Paoli, C., Verstovsek, S.*, et al.* (2015). JAK2 V617F complete molecular remission in polycythemia vera/essential

thrombocythemia patients treated with ruxolitinib. Blood *125*, 3352-3353.

200) Pietras, E.M., Lakshminarasimhan, R., Techner, J.M., Fong, S., Flach, J., Binnewies, M., and Passegue, E. (2014). Re-entry into quiescence protects hematopoietic stem cells from the killing effect of chronic exposure to type I interferons. J Exp Med *211*, 245-262.

201) Pinho, S., Marchand, T., Yang, E., Wei, Q., Nerlov, C., and Frenette, P.S. (2018). Lineage-biased hematopoietic stem cells are regulated by distinct niches. Developmental Cell *44*, 634-641.e634.

202) Platanias, L.C. (2005). Mechanisms of type-I- and type-II-interferon-mediated signalling. Nat Rev Immunol *5*, 375-386.

203) Platanias, L.C., Uddin, S., Bruno, E., Korkmaz, M., Ahmad, S., Alsayed, Y., Van Den Berg, D., Druker, B.J., Wickrema, A., and Hoffman, R. (1999). CrkL and CrkII participate in the generation of the growth inhibitory effects of interferons on primary hematopoietic progenitors. Exp Hematol *27*, 1315-1321.

204) Preudhomme, C., Guilhot, J., Nicolini, F.E., Guerci-Bresler, A., Rigal-Huguet, F., Maloisel, F., Coiteux, V., Gardembas, M., Berthou, C., Vekhoff, A.*, et al.* (2010). Imatinib plus peginterferon alfa-2a in chronic myeloid leukemia. New England Journal of Medicine *363*, 2511-2521.

205) Qin, J., Sontag, S., Lin, Q., Mitzka, S., Leisten, I., Schneider, R.K., Wang, X., Jauch, A., Peitz, M., Brüstle, O.*, et al.* (2014). Cell fusion enhances mesendodermal differentiation of human induced pluripotent stem cells. Stem cells and development *23*, 2875-2882.

206) Quintas-Cardama, A., Kantarjian, H., Manshouri, T., Luthra, R., Estrov, Z., Pierce, S., Richie, M.A., Borthakur, G., Konopleva, M., Cortes, J.*, et al.* (2009). Pegylated interferon alfa-2a yields high rates of hematologic and molecular response in patients with advanced essential thrombocythemia and polycythemia vera. J Clin Oncol *27*, 5418-5424.

207) Rafii, S., Kloss, C.C., Butler, J.M., Ginsberg, M., Gars, E., Lis, R., Zhan, Q., Josipovic, P., Ding, B.S., Xiang, J.*, et al.* (2013). Human ESC-derived hemogenic endothelial cells undergo distinct waves of endothelial to hematopoietic transition. Blood *121*, 770-780.

208) Ragimbeau, J., Dondi, E., Alcover, A., Eid, P., Uzé, G., and Pellegrini, S. (2003). The tyrosine kinase Tyk2 controls IFNAR1 cell surface expression. The EMBO Journal *22*, 537-547.

209) Rahman, N., Brauer, P.M., Ho, L., Usenko, T., Tewary, M., Zúñiga-Pflücker, J.C., and Zandstra, P.W. (2017). Engineering the haemogenic niche mitigates endogenous inhibitory signals and controls pluripotent stem cell-derived blood emergence. Nature Communications *8*, 15380.

210) Ren, R. (2005). Mechanisms of BCR-ABL in the pathogenesis of chronic myelogenous leukaemia. Nature reviews Cancer *5*, 172-183.

211) Roffi, L., Mels, G.C., Antonelli, G., Bellati, G., Panizzuti, F., Piperno, A., Pozzi, M., Ravizza, D., Angeli, G., Dianzani, F.*, et al.* (1995). Breakthrough during recombinant interferon alfa therapy in patients with chronic hepatitis C virus infection: Prevalence, etiology, and management. Hepatology *21*, 645-649.

212) Rosti, V., Villani, L., Riboni, R., Poletto, V., Bonetti, E., Tozzi, L., Bergamaschi, G., Catarsi, P., Dallera, E., Novara, F.*, et al.* (2013). Spleen endothelial cells from patients with myelofibrosis harbor the JAK2V617F mutation. Blood *121*, 360-368.

213) Rousselot, P., Huguet, F., Rea, D., Legros, L., Cayuela, J.M., Maarek, O., Blanchet, O., Marit, G., Gluckman, E., Reiffers, J.*, et al.* (2007). Imatinib mesylate discontinuation in patients with chronic myelogenous leukemia in complete molecular remission for more than 2 years. Blood *109*, 58-60.

214) Saliba, J., Hamidi, S., Lenglet, G., Langlois, T., Yin, J., Cabagnols, X., Secardin, L., Legrand, C., Galy, A., Opolon, P.*, et al.* (2013). Heterozygous and homozygous JAK2(V617F) states modeled by induced pluripotent stem cells from myeloproliferative neoplasm patients. PLoS One *8*, e74257.

215) Salvagiotto, G., Burton, S., Daigh, C.A., Rajesh, D., Slukvin, II, and Seay, N.J. (2011). A defined, feeder-free, serum-free system to generate in vitro hematopoietic progenitors and differentiated blood cells from hESCs and hiPSCs. PLoS One *6*, e17829.

216) Scheller, M., Schonheit, J., Zimmermann, K., Leser, U., Rosenbauer, F., and Leutz, A. (2013). Cross talk between Wnt/beta-catenin and Irf8 in leukemia progression and drug resistance. J Exp Med *210*, 2239-2256.

217) Schiavoni, G., Mattei, F., Sestili, P., Borghi, P., Venditti, M., Morse, H.C., 3rd, Belardelli, F., and Gabriele, L. (2002). ICSBP is essential for the development of mouse type I interferon-producing cells and for the generation and activation of CD8alpha(+) dendritic cells. J Exp Med *196*, 1415-1425.

218) Schmidt, M., Hochhaus, A., Nitsche, A., Hehlmann, R., and Neubauer, A. (2001). Expression of nuclear transcription factor interferon consensus sequence binding protein in chronic myeloid leukemia correlates with pretreatment risk features and cytogenetic response to interferon-alpha. Blood *97*, 3648-3650.

219) Schmidt, M., Nagel, S., Proba, J., Thiede, C., Ritter, M., Waring, J.F., Rosenbauer, F., Huhn, D., Wittig, B., Horak, I.*, et al.* (1998). Lack of interferon consensus sequence binding protein (ICSBP) transcripts in human myeloid leukemias. Blood *91*, 22-29.

220) Schmitt, C.E., Lizama, C.O., and Zovein, A.C. (2014). From transplantation to transgenics: mouse models of developmental hematopoiesis. Experimental Hematology *42*, 707-716.

221) Schöbel, A., Rösch, K., and Herker, E. (2018). Functional innate immunity restricts Hepatitis C Virus infection in induced pluripotent stem cell–derived hepatocytes. Scientific Reports *8*, 3893.

222) Schubert, C., Chatain, N., Braunschweig, T., Schemionek, M., Feldberg, K., Hoffmann, M., Dufva, O., Mustjoki, S., Brummendorf, T.H., and Koschmieder, S. (2017). The SCLtTAxBCR-ABL transgenic mouse model closely reflects the differential effects of dasatinib on normal and malignant hematopoiesis in chronic phase-CML patients. Oncotarget *8*, 34736-34749.

223) Schwieger, M., Lohler, J., Friel, J., Scheller, M., Horak, I., and Stocking, C. (2002). AML1-ETO inhibits maturation of multiple lymphohematopoietic lineages and induces myeloblast transformation in synergy with ICSBP deficiency. J Exp Med *196*, 1227-1240.

224) Seita, J., and Weissman, I.L. (2010). Hematopoietic stem cell: self-renewal versus differentiation. Wiley interdisciplinary reviews Systems biology and medicine *2*, 640-653.

225) Sharma, A., Yun, H., Jyotsana, N., Chaturvedi, A., Schwarzer, A., Yung, E., Lai, C.K., Kuchenbauer, F., Argiropoulos, B., Gorlich, K.*, et al.* (2015). Constitutive IRF8 expression inhibits AML by activation of repressed immune response signaling. Leukemia *29*, 157-168.

226) Shimizu, T., Kubovcakova, L., Nienhold, R., Zmajkovic, J., Meyer, S.C., Hao-Shen, H., Geier, F., Dirnhofer, S., Guglielmelli, P., Vannucchi, A.M.*, et al.* (2016). Loss of Ezh2 synergizes with JAK2-V617F in initiating myeloproliferative neoplasms and promoting myelofibrosis. J Exp Med *213*, 1479-1496.

227) Sichien, D., Scott, Charlotte L., Martens, L., Vanderkerken, M., Van Gassen, S., Plantinga, M., Joeris, T., De Prijck, S., Vanhoutte, L., Vanheerswynghels, M.*, et al.* (2016). IRF8 transcription factor controls survival and function of terminally differentiated conventional and plasmacytoid dendritic cells, respectively. Immunity *45*, 626-640.

228) Skoda, R.C. (2010). JAK2 impairs stem cell function? Blood *116*, 1392-1393.

229) Slukvin, II (2016). Generating human hematopoietic stem cells in vitro - exploring endothelial to hematopoietic transition as a portal for stemness acquisition. FEBS Lett *590*, 4126-4143.

230) Sommer, C.A., Sommer, A.G., Longmire, T.A., Christodoulou, C., Thomas, D.D., Gostissa, M., Alt, F.W., Murphy, G.J., Kotton, D.N., and Mostoslavsky, G. (2010). Excision of reprogramming transgenes improves the differentiation potential of iPS cells generated with a single excisable vector. Stem Cells *28*, 64-74.

231) Sommer, C.A., Stadtfeld, M., Murphy, G.J., Hochedlinger, K., Kotton, D.N., and Mostoslavsky, G. (2009). Induced pluripotent stem cell

generation using a single lentiviral stem cell cassette. STEM CELLS *27*, 543-549.

232) Sontag, S., Forster, M., Qin, J., Wanek, P., Mitzka, S., Schuler, H.M., Koschmieder, S., Rose-John, S., Sere, K., and Zenke, M. (2017a). Modelling IRF8 deficient human hematopoiesis and dendritic cell development with engineered iPS cells. Stem Cells *35*, 898-908.

233) Sontag, S., Förster, M., Seré, K., and Zenke, M. (2017b). Differentiation of human induced pluripotent stem cells (iPS cells) and embryonic stem cells (ES cells) into dendritic cell (DC) subsets. Bio-protocol *7*, e2419.

234) Sozer, S., Fiel, M.I., Schiano, T., Xu, M., Mascarenhas, J., and Hoffman, R. (2009). The presence of JAK2V617F mutation in the liver endothelial cells of patients with Budd-Chiari syndrome. Blood *113*, 5246-5249.

235) Stadtfeld, M., Nagaya, M., Utikal, J., Weir, G., and Hochedlinger, K. (2008). Induced pluripotent stem cells generated without viral integration. Science *322*, 945-949.

236) Stewart, C.L., Stuhlmann, H., Jähner, D., and Jaenisch, R. (1982). De novo methylation, expression, and infectivity of retroviral genomes introduced into embryonal carcinoma cells. Proceedings of the National Academy of Sciences *79*, 4098-4102.

237) Sturgeon, C.M., Ditadi, A., Awong, G., Kennedy, M., and Keller, G. (2014). Wnt signaling controls the specification of definitive and primitive hematopoiesis from human pluripotent stem cells. Nature Biotechnology *32*, 554.

238) Su, L., and David, M. (2000). Distinct mechanisms of STAT phosphorylation via the interferon-alpha/beta receptor - Selective inhibition of STAT3 and STAT5 by piceatannol. Journal of Biological Chemistry *275*, 12661-12666.

239) Swiers, G., Baumann, C., O'Rourke, J., Giannoulatou, E., Taylor, S., Joshi, A., Moignard, V., Pina, C., Bee, T., Kokkaliaris, K.D.*, et al.* (2013). Early dynamic fate changes in haemogenic endothelium characterized at the single-cell level. Nature Communications *4*, 2924.

240) Szabo, E., Rampalli, S., Risueno, R.M., Schnerch, A., Mitchell, R., Fiebig-Comyn, A., Levadoux-Martin, M., and Bhatia, M. (2010). Direct conversion of human fibroblasts to multilineage blood progenitors. Nature *468*, 521-526.

241) Takahashi, K., Tanabe, K., Ohnuki, M., Narita, M., Ichisaka, T., Tomoda, K., and Yamanaka, S. (2007). Induction of pluripotent stem cells from adult human fibroblasts by defined factors. Cell *131*, 861-872.

242) Takahashi, K., and Yamanaka, S. (2006). Induction of pluripotent stem cells from mouse embryonic and adult fibroblast cultures by defined factors. Cell *126*, 663-676.

243) Talpaz, M., Hehlmann, R., Quintás-Cardama, A., Mercer, J., and Cortes, J. (2013). Re-emergence of interferon-α in the treatment of chronic myeloid leukemia. Leukemia *27*, 803-812.

244) Talpaz, M., Kantarjian, H., Kurzrock, R., Trujillo, J.M., and Gutterman, J.U. (1991). Interferon-alpha produces sustained cytogenetic responses in chronic myelogenous leukemia. Philadelphia chromosome-positive patients. Annals of internal medicine *114*, 532-538.

245) Talpaz, M., Silver, R.T., Druker, B.J., Goldman, J.M., Gambacorti-Passerini, C., Guilhot, F., Schiffer, C.A., Fischer, T., Deininger, M.W., Lennard, A.L.*, et al.* (2002). Imatinib induces durable hematologic and cytogenetic responses in patients with accelerated phase chronic myeloid leukemia: results of a phase 2 study. Blood *99*, 1928-1937.

246) Tamura, T., Kurotaki, D., and Koizumi, S.-i. (2015). Regulation of myelopoiesis by the transcription factor IRF8. International Journal of Hematology *101*, 342-351.

247) Tefferi, A., and Barbui, T. (2017). Polycythemia vera and essential thrombocythemia: 2017 update on diagnosis, risk-stratification, and management. Am J Hematol *92*, 94-108.

248) Tefferi, A., and Vainchenker, W. (2011). Myeloproliferative neoplasms: molecular pathophysiology, essential clinical understanding, and treatment strategies. J Clin Oncol *29*, 573-582.

249) Tehranchi, R., Woll, P.S., Anderson, K., Buza-Vidas, N., Mizukami, T., Mead, A.J., Åstrand-Grundström, I., Strömbeck, B., Horvat, A., Ferry, H.*, et al.* (2010). Persistent malignant stem cells in del(5q) myelodysplasia in remission. New England Journal of Medicine *363*, 1025-1037.

250) Thomas, G.D., Hamers, A.A.J., Nakao, C., Marcovecchio, P., Taylor, A.M., McSkimming, C., Nguyen, A.T., McNamara, C.A., and Hedrick, C.C. (2017). Human blood monocyte subsets: a new gating strategy defined using cell surface markers identified by mass cytometry. Arteriosclerosis, thrombosis, and vascular biology *37*, 1548-1558.

251) Thomson, J.A., Itskovitz-Eldor, J., Shapiro, S.S., Waknitz, M.A., Swiergiel, J.J., Marshall, V.S., and Jones, J.M. (1998). Embryonic stem cell lines derived from human blastocysts. Science *282*, 1145-1147.

252) Tober, J., Koniski, A., McGrath, K.E., Vemishetti, R., Emerson, R., de Mesy-Bentley, K.K., Waugh, R., and Palis, J. (2007). The megakaryocyte lineage originates from hemangioblast precursors and is an integral component both of primitive and of definitive hematopoiesis. Blood *109*, 1433-1441.

253) Tran, T.H., Wang, X., Browne, C., Zhang, Y., Schinke, M., Izumo, S., and Burcin, M. (2009). Wnt3a-induced mesoderm formation and cardiomyogenesis in human embryonic stem cells. Stem Cells *27*, 1869-1878.

254) Trumpp, A., Essers, M., and Wilson, A. (2010). Awakening dormant haematopoietic stem cells. Nat Rev Immunol *10*, 201-209.

255) Tsujimura, H., Tamura, T., and Ozato, K. (2003). Cutting edge: IFN consensus sequence binding protein/IFN regulatory factor 8 drives the development of type I IFN-producing plasmacytoid dendritic cells. Journal of immunology *170*, 1131-1135.

256) Uddin, S., Yenush, L., Sun, X.J., Sweet, M.E., White, M.F., and Platanias, L.C. (1995). Interferon-alpha engages the insulin receptor substrate-1 to associate with the phosphatidylinositol 3'-kinase. J Biol Chem *270*, 15938-15941.

257) Vainchenker, W., and Constantinescu, S.N. (2013). JAK/STAT signaling in hematological malignancies. Oncogene *32*, 2601-2613.

258) van Dijk, E.L., Auger, H., Jaszczyszyn, Y., and Thermes, C. (2014). Ten years of next-generation sequencing technology. Trends in genetics : TIG *30*, 418-426.

259) Vannucchi, A.M., Guglielmelli, P., and Tefferi, A. (2009). Advances in understanding and management of myeloproliferative neoplasms. CA Cancer J Clin *59*, 171-191.

260) Vannucchi, A.M., Kiladjian, J.J., Griesshammer, M., Masszi, T., Durrant, S., Passamonti, F., Harrison, C.N., Pane, F., Zachee, P., Mesa, R.*, et al.* (2015). Ruxolitinib versus standard therapy for the treatment of polycythemia vera. New England Journal of Medicine *372*, 426-435.

261) Velazquez, L., Fellous, M., Stark, G.R., and Pellegrini, S. (1992). A protein tyrosine kinase in the interferon αβ signaling pathway. Cell *70*, 313-322.

262) Velten, L., Haas, S.F., Raffel, S., Blaszkiewicz, S., Islam, S., Hennig, B.P., Hirche, C., Lutz, C., Buss, E.C., Nowak, D.*, et al.* (2017). Human haematopoietic stem cell lineage commitment is a continuous process. Nature Cell Biology *19*, 271.

263) Verma, A., Deb, D.K., Sassano, A., Uddin, S., Varga, J., Wickrema, A., and Platanias, L.C. (2002). Activation of the p38 mitogen-activated protein kinase mediates the suppressive effects of type I interferons and transforming growth factor-beta on normal hematopoiesis. J Biol Chem *277*, 7726-7735.

264) Vestweber, D. (2008). VE-Cadherin. The Major Endothelial Adhesion Molecule Controlling Cellular Junctions and Blood Vessel Formation *28*, 223-232.

265) Waas, B., and Maillard, I. (2017). Fetal hematopoietic stem cells are making waves. Stem Cell Investigation *4.*

266) Wagner, T.C., Velichko, S., Chesney, S.K., Biroc, S., Harde, D., Vogel, D., and Croze, E. (2004). Interferon receptor expression regulates the antiproliferative effects of interferons on cancer cells and solid tumors. International Journal of Cancer *111*, 32-42.

267) Waight, J.D., Banik, D., Griffiths, E.A., Nemeth, M.J., and Abrams, S.I. (2014). Regulation of the interferon regulatory factor-8 (IRF-8) tumor suppressor gene by the signal transducer and activator of transcription 5 (STAT5) transcription factor in chronic myeloid leukemia. J Biol Chem *289*, 15642-15652.

268) Waight, J.D., Netherby, C., Hensen, M.L., Miller, A., Hu, Q., Liu, S., Bogner, P.N., Farren, M.R., Lee, K.P., Liu, K*., et al.* (2013). Myeloid-derived suppressor cell development is regulated by a STAT/IRF-8 axis. J Clin Invest *123*, 4464-4478.

269) Walz, C., Ahmed, W., Lazarides, K., Betancur, M., Patel, N., Hennighausen, L., Zaleskas, V.M., and Van Etten, R.A. (2012). Essential role for Stat5a/b in myeloproliferative neoplasms induced by BCR-ABL1 and JAK2V617F in mice. Blood *119*, 3550-3560.

270) Walz, C., Crowley, B.J., Hudon, H.E., Gramlich, J.L., Neuberg, D.S., Podar, K., Griffin, J.D., and Sattler, M. (2006). Activated Jak2 with the V617F point mutation promotes G1/S phase transition. J Biol Chem *281*, 18177-18183.

271) Wang, H., Yan, M., Sun, J., Jain, S., Yoshimi, R., Abolfath, S.M., Ozato, K., Coleman, W.G., Jr., Ng, A.P., Metcalf, D*., et al.* (2014a). A reporter mouse reveals lineage-specific and heterogeneous expression of IRF8 during lymphoid and myeloid cell differentiation. Journal of immunology *193*, 1766-1777.

272) Wang, R., Wang, J., Acharya, D., Paul, A.M., Bai, F., Huang, F., and Guo, Y.L. (2014b). Antiviral responses in mouse embryonic stem cells: differential development of cellular mechanisms in type I interferon production and response. J Biol Chem *289*, 25186-25198.

273) Watanabe, T., Hotta, C., Koizumi, S., Miyashita, K., Nakabayashi, J., Kurotaki, D., Sato, G.R., Yamamoto, M., Nakazawa, M., Fujita, H*., et al.* (2013). The transcription factor IRF8 counteracts BCR-ABL to rescue dendritic cell development in chronic myelogenous leukemia. Cancer research *73*, 6642-6653.

274) Weinstein, I.B. (2002). Cancer. Addiction to oncogenes--the Achilles heal of cancer. Science *297*, 63-64.

275) Wernig, G., Gonneville, J.R., Crowley, B.J., Rodrigues, M.S., Reddy, M.M., Hudon, H.E., Walz, C., Reiter, A., Podar, K., Royer, Y*., et al.* (2008). The Jak2V617F oncogene associated with myeloproliferative diseases requires a functional FERM domain for transformation and for expression of the Myc and Pim proto-oncogenes. Blood *111*, 3751-3759.

276) Wilkinson, D.G., Bhatt, S., and Herrmann, B.G. (1990). Expression pattern of the mouse T gene and its role in mesoderm formation. Nature *343*, 657.

277) Wilmut, I., Schnieke, A.E., McWhir, J., Kind, A.J., and Campbell, K.H.S. (1997). Viable offspring derived from fetal and adult mammalian cells. Nature *385*, 810.

278) Woltjen, K., Michael, I.P., Mohseni, P., Desai, R., Mileikovsky, M., Hämäläinen, R., Cowling, R., Wang, W., Liu, P., Gertsenstein, M.*, et al.* (2009). piggyBac transposition reprograms fibroblasts to induced pluripotent stem cells. Nature *458*, 766.

279) Yan, D., Jobe, F., Hutchison, R.E., and Mohi, G. (2015). Deletion of STAT3 enhances myeloid cell expansion and increases the severity of myeloproliferative neoplasms in Jak2V617F knock-in mice. Leukemia *29*, 2050-2061.

280) Yáñez, A., and Goodridge, H.S. (2016). Interferon regulatory factor 8 and the regulation of neutrophil, monocyte, and dendritic cell production. Current Opinion in Hematology *23*, 11-17.

281) Yang, C.T., Ma, R., Axton, R.A., Jackson, M., Taylor, A.H., Fidanza, A., Marenah, L., Frayne, J., Mountford, J.C., and Forrester, L.M. (2017). Activation of KLF1 Enhances the Differentiation and Maturation of Red Blood Cells from Human Pluripotent Stem Cells. Stem Cells *35*, 886-897.

282) Yang, L., Soonpaa, M.H., Adler, E.D., Roepke, T.K., Kattman, S.J., Kennedy, M., Henckaerts, E., Bonham, K., Abbott, G.W., Linden, R.M.*, et al.* (2008). Human cardiovascular progenitor cells develop from a KDR+ embryonic-stem-cell-derived population. Nature *453*, 524-528.

283) Yarilina, A., Park-Min, K.H., Antoniv, T., Hu, X., and Ivashkiv, L.B. (2008). TNF activates an IRF1-dependent autocrine loop leading to sustained expression of chemokines and STAT1-dependent type I interferon-response genes. Nature immunology *9*, 378-387.

284) Ye, Z., Liu, C.F., Lanikova, L., Dowey, S.N., He, C., Huang, X., Brodsky, R.A., Spivak, J.L., Prchal, J.T., and Cheng, L. (2014). Differential sensitivity to JAK inhibitory drugs by isogenic human erythroblasts and hematopoietic progenitors generated from patient-specific induced pluripotent stem cells. Stem Cells *32*, 269-278.

285) Yoder, M.C. (2014). Inducing definitive hematopoiesis in a dish. Nature Biotechnology *32*, 539.

286) Yokota, A., Hirai, H., Sato, A., Kamio, N., Hayashi, Y., Miura, Y., Kimura, S., and Maekawa, T. (2017). IFN-α upregulates the expression of C/EBPβ and induces myeloid differentiation and exhaustion of CD34+ CML stem cells. Blood *130*, 2863-2863.

287) Yoshida, Y., and Yamanaka, S. (2017). Induced pluripotent stem cells 10 Years Later: for cardiac applications. Circ Res *120*, 1958-1968.

288) Yu, J., Vodyanik, M.A., Smuga-Otto, K., Antosiewicz-Bourget, J., Frane, J.L., Tian, S., Nie, J., Jonsdottir, G.A., Ruotti, V., Stewart, R.*, et al.*

(2007). Induced pluripotent stem cell Lines derived from human somatic cells. Science *318*, 1917-1920.

289) Zaleskas, V.M., Krause, D.S., Lazarides, K., Patel, N., Hu, Y., Li, S., and Van Etten, R.A. (2006). Molecular pathogenesis and therapy of polycythemia induced in mice by JAK2 V617F. PLoS One *1*, e18.

290) Zambidis, E.T., Peault, B., Park, T.S., Bunz, F., and Civin, C.I. (2005). Hematopoietic differentiation of human embryonic stem cells progresses through sequential hematoendothelial, primitive, and definitive stages resembling human yolk sac development. Blood *106*, 860-870.

291) Zanjani, E.D., Lutton, J.D., Hoffman, R., and Wasserman, L.R. (1977). Erythroid colony formation by polycythemia vera bone marrow in vitro. Dependence on erythropoietin. The Journal of clinical investigation *59*, 841-848.

292) Zhan, H., Lin, C.H.S., Segal, Y., and Kaushansky, K. (2018). The JAK2V617F-bearing vascular niche promotes clonal expansion in myeloproliferative neoplasms. Leukemia *32*, 462-469.

293) Zhang, B., Ho, Yin W., Huang, Q., Maeda, T., Lin, A., Lee, S.-u., Hair, A., Holyoake, Tessa L., Huettner, C., and Bhatia, R. (2012). Altered microenvironmental regulation of leukemic and normal stem cells in chronic myelogenous leukemia. Cancer Cell *21*, 577-592.

294) Zhao, F., Shi, Y., Huang, Y., Zhan, Y., Zhou, L., Li, Y., Wan, Y., Li, H., Huang, H., Ruan, H.*, et al.* (2018). IRF8 regulates the progression of myeloproliferative neoplasm-like syndrome via Mertk signaling in zebrafish. Leukemia *32*, 149-158.

295) Zhao, R., Xing, S., Li, Z., Fu, X., Li, Q., Krantz, S.B., and Zhao, Z.J. (2005). Identification of an acquired JAK2 mutation in polycythemia vera. J Biol Chem *280*, 22788-22792.

296) Zheng, H., Qian, J., Varghese, B., Baker, D.P., and Fuchs, S. (2011). Ligand-stimulated downregulation of the alpha interferon receptor: role of protein kinase D2. Molecular and cellular biology *31*, 710-720.

297) Zhu, H., Lai, Y.-S., Li, Y., Blum, R.H., and Kaufman, D.S. (2018). Concise review: human pluripotent stem cells to produce cell-based cancer immunotherapy. STEM CELLS *36*, 134-145.

298) Zhu, Y., Pan, L., Hong, M., Liu, W., Qiao, C., Li, J., and Qian, S. (2016). The combination therapy of imatinib and dasatinib achieves long-term molecular response in two imatinib-resistant and dasatinibintolerant patients with advanced chronic myeloid leukemia. Journal of biomedical research *30*, 525-528.

299) Zovein, A.C., Hofmann, J.J., Lynch, M., French, W.J., Turlo, K.A., Yang, Y., Becker, M.S., Zanetta, L., Dejana, E., Gasson, J.C.*, et al.* (2008). Fate tracing reveals the endothelial origin of hematopoietic stem cells. Cell Stem Cell *3*, 625-636.

7   Appendix

7.1   Abbreviations

7AAD	7-Aminoactinomycin D
(Hyp.)IL6	(Hyper) interleukin 6
AFP	Alpha-Fetoprotein
bFGF	Basic fibroblast growth factor
BrdU	Bromodeoxyuridine
BFU-E	Burst forming unit – erythroid
BM	Bone marrow
BMP4	Bone morphogenetic protein 4
CD	Cluster of differentiation
CFU-E	Colony forming unit – erythroid
CFU-G	Colony forming unit – granulocyte
CFU-GEMM	Colony forming unit – granulocyte, erythrocyte, macrophage, megakaryocyte
CFU-GM	Colony forming unit – granulocyte, macrophage
CFU-M	Colony forming unit – macrophage
CFSE	Carboxyfluorescein succinimidyl ester
KIT	Stem cell factor receptor
Ctrl	Control
EB	Embryoid body
EHT	Endothelial-to-hematopoietic transition

EPO	Erythropoietin
FcεR	FcEpsilon Receptor
FLT3L	FMS-like tyrosine kinase 3 ligand
FSC – A	Forward scatter – Area
FSC – W	Forward scatter – Width
GFAP	Glial fibrillary acidic protein
GFP	Green fluorescent protein
H&E staining	Hematoxylin & Eosin staining
HLA (-DR)	Human leukocyte antigen (-DR)
HSPC	Hematopoietic stem and progenitor cell(s)
IFNAR	Interferon α Receptor
IFNα	Interferon α
IGF1	Insulin-like growth factor 1
IgG	Immunoglobulin G
IgM	Immunoglobulin M
IL3	Interleukin 3
iPSC	Induced pluripotent stem cell(s)
iPSC-HPC	iPSC-derived hematopoietic progenitor cell(s)
IRF1	Interferon regulatory factor 1
IRF7	Interferon regulatory factor 7
IRF8	Interferon regulatory factor 8
JAK2	Janus kinase 2
MACS	Magnetic activated cell sorting

MET	Mesenchymal-to-epithelial transition
MFI	Mean fluorescence intensity
Myh6	Myosin heavy chain 6
PBMNC	Peripheral blood mononuclear cells
RT-qPCR	Reverse transcription – quantitative polymerase chain reaction
SCF	Stem cell factor
SDS-PAGE	Sodium dodecyl sulfate polyacrylamide gel electrophoresis
SSC – A	Side scatter – Area
SSC – W	Side scatter – Width
STAT1	Signal transducer and activator of transcription 1
STAT2	Signal transducer and activator of transcription 2
T	Brachyury
TKI	Tyrosine kinase inhibitor
TPO	Thrombopoietin
VEGF	Vascular endothelial growth factor
VE-cad	Vascular endothelial cadherin
WT	Wild type

7.2 Supplemental Figures

7.2.1 Supplemental Figures for retrovirally transfected murine BM cells
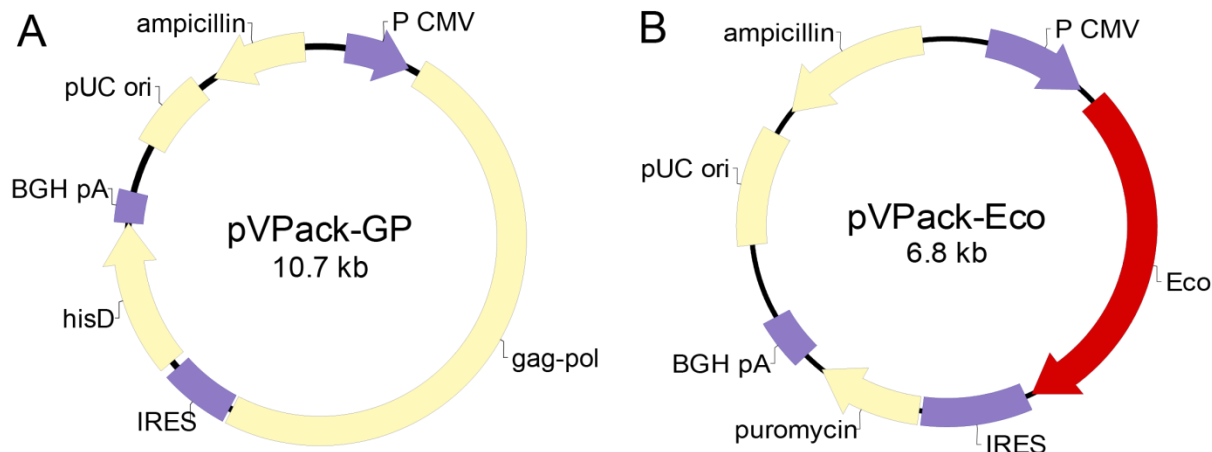
Supplemental Figure 1. Vector maps of packaging vectors

(A) The packaging vector pVPack-GP encodes genes for gag and pol. (B) The packaging vector pVpackEco encodes the eco gene. Both vectors have are under the control of the CMV promotor and have an ampicillin resistance. The Retroviral genes are separated from the ampicillin resistance by an IRES sequence. Vector maps were taken from agilent homepage.
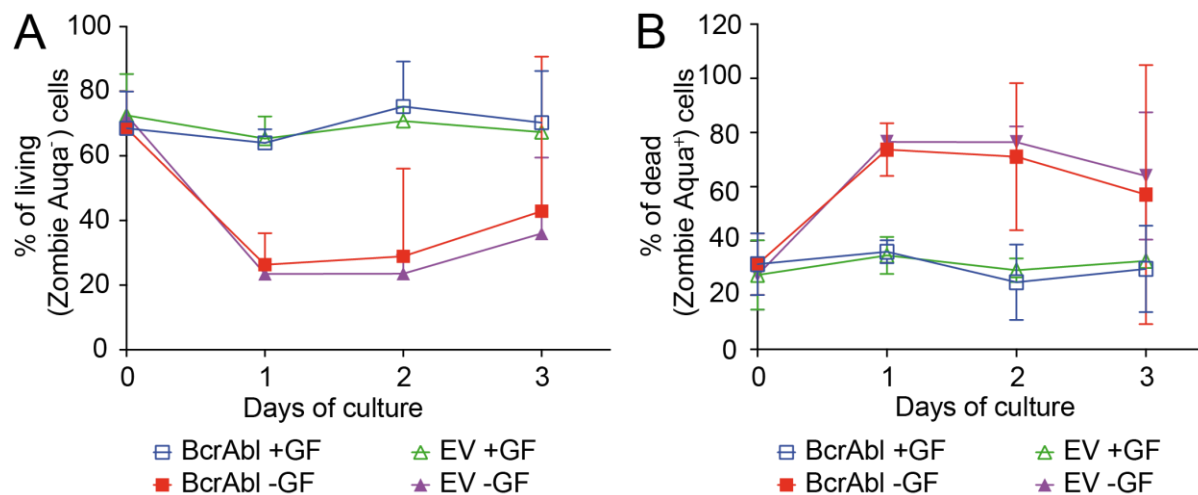
Supplemental Figure 2. Living BcrAbl$^+$ cells increase only after 2 days of cytokine withdrawal

Murine BM cells were transduced with BcrAbl or empty vector. Cultures were split in half and cultured with and without cytokines. Medium was refreshed every 24h. Samples for flow cytometry were taken every day. To quantify dead cells via flow cytometry cells were stained with Zombie Aqua as described in Materials and Methods. (A) The percentage of living (Zombie Aqua$^-$) cells is shown. (B) The percentage of dead (Zombie Aqua$^+$) cells is shown. Data represent means ± standard deviation (n = 3).
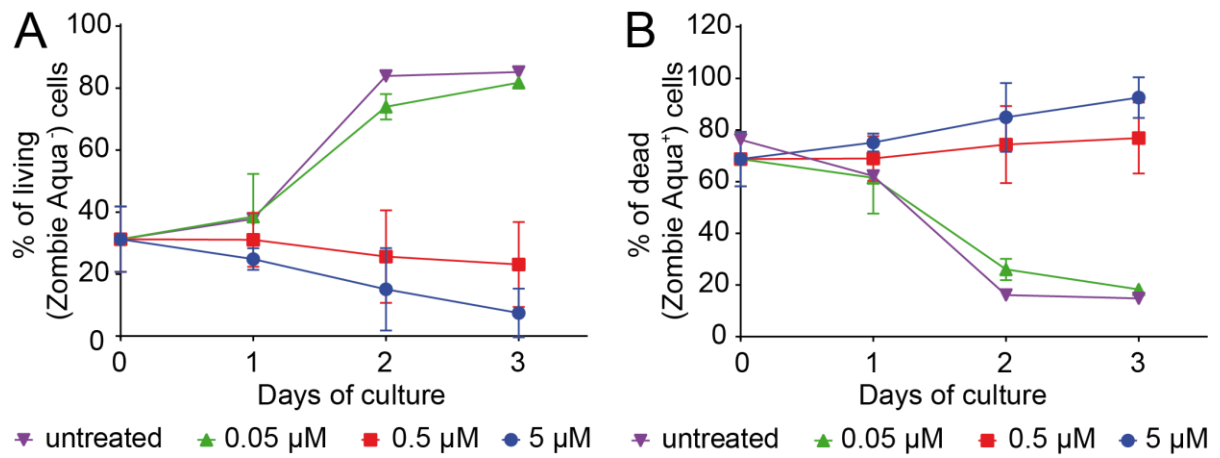
Supplemental Figure 3. Dose response of BcrAbl+ cells to Imatinib

Murine BM cells were transduced with BcrAbl. Cells were split and cultured with increasing Imatinib concentrations for 4 days as shown in Figure 21. Medium and Imatinib was refreshed and analyzed with flow cytometry every 24h. To this end, cells were stained with Zombie Aqua to quantify dead cells. (A) Living cells (Zombie Aqua⁻) cells are shown. (B) Dead (Zombie Aqua⁺) cells are shown. Data represent means ± standard deviation (n = 3).

A

untreated

d0

0.5 µM Imatinib

d1   d2

Flow cytometry and cell count

10² U/ml IFNα

d0

10³ U/ml IFNα

10⁴ U/ml IFNα

d1   d2

Flow cytometry and cell count

B

% of BcrAbl⁺ cells

IFNα	-	-	10²	10³	10⁴
Imatinib	-	0.5	-	-	-

C

# of BcrAbl⁺ cells

IFNα	-	-	10²	10³	10⁴
Imatinib	-	0.5	-	-	-
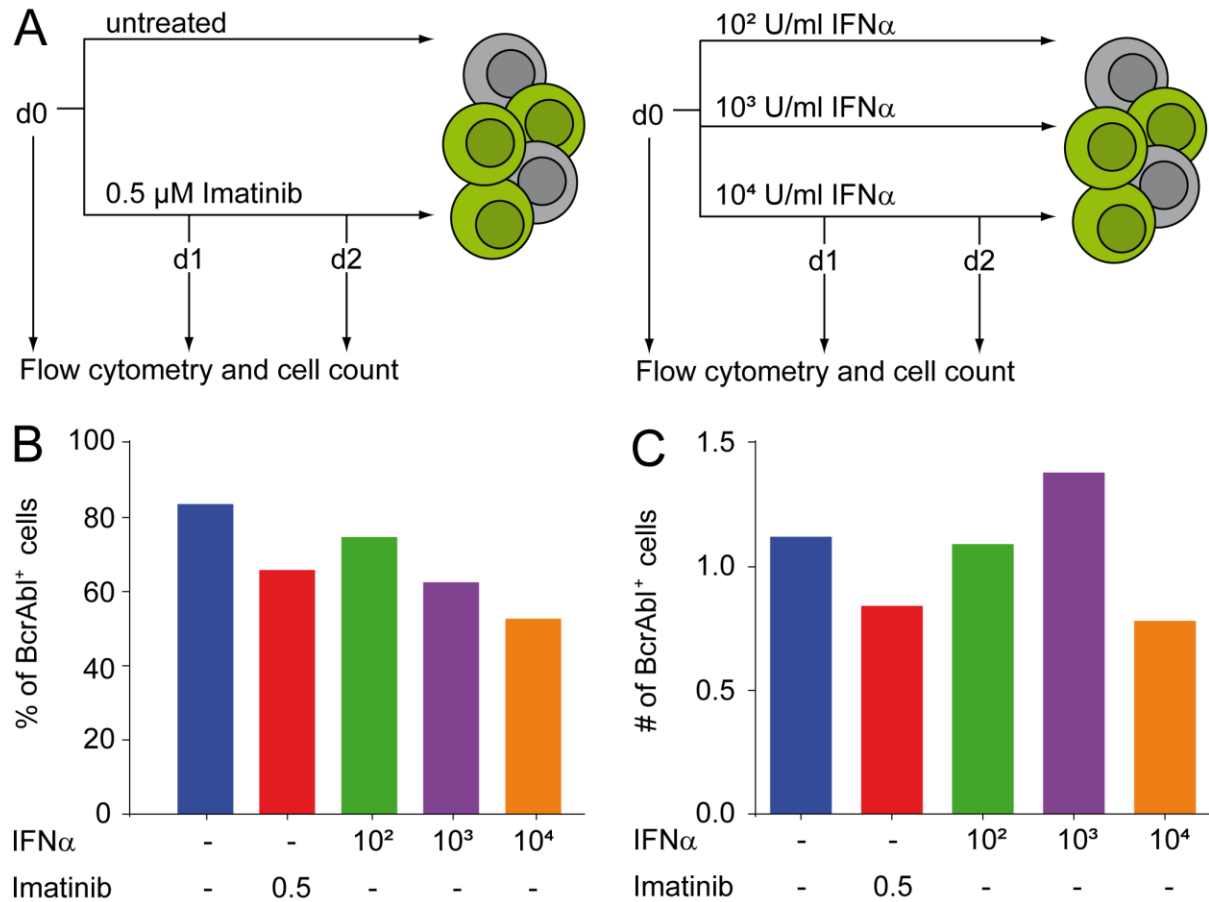
Supplemental Figure 4. IFNα inhibits BcrAbl+ BM cells only slightly

Primary murine BM cells were isolated and transduced with BcrAbl as shown in Figure 21A. (A – left panel) Cells were left untreated or treated with 0.5 µM Imatinib alone as control. Cell counts on day 0 and on day 2 were taken with an electronic cell counter. (A – right panel) Cells were treated with 10^2, 10^3 and 10^4 U/ml IFNα for another 2 days. Percentage of BcrAbl⁺ cells were analyzed via flow cytometry by measuring GFP expression. (B) The percentage of BcrAbl⁺ cells on day 2 of culture is shown. (C) The number of BcrAbl⁺ cells was determined by multiplying the cell count with the amount of GFP⁺ cells. Next, the number was normalized to the day 0 of treatment (n =1).

A

0 µM Imatinib

d0

0.15 µM Imatinib

0.3 µM Imatinb

0.5 µM Imatinib

d1   d2   d3

Flow cytometry and cell count

B   d0 of treatment

55.6%   65.5%

Zombie Aqua   GFP

C   0 µM Imatinib

89.0%   93.8%

Zombie Aqua   GFP

0.3 µM Imatinib

83.4%   93.9%

Zombie Aqua   GFP

0.15 µM Imatinib

85.3%   94.5%

Zombie Aqua   GFP

0.5 µM Imatinib

80.7%   93.1%

Zombie Aqua   GFP

D

% of BcrAbl⁺ cells

100
90
80
70
60
0   1   2   3   4
Days of culture

▼ 0 µM   ◆ 0.15 µM   ● 0.3 µM   ■ 0.5 µM

E

# of BcrAbl⁺ cells (x106)

8
6
4
2
0
0   1   2   3   4
Days of culture

** *   * *   * **

▼ 0 µM   ◆ 0.15 µM   ● 0.3 µM   ■ 0.5 µM

Supplemental Figure 5. Refinement of Imatinib concentration to 0.3 µM

BM cells were isolated and cultured as showed in Results Figure 5A. (A) Cells were treated with 0.15 µM, 0.3 µM and 0.5 µM Imatinib of left untreated for 4 days. Cells were counted daily via an electronic cell counter. Samples for flow cytometry were taken daily. During Imatinib treatment, cells were cultured under cytokine withdrawal. (B

– E) BcrAbl+ cells were analyzed for their GFP expression by flow cytometry daily. (B) Shown is the flow cytometry analysis on day 0 of treatment. (C) Shown are representative flow cytometry analyses per Imatinib concentration on day 4 of treatment. (D) The percentages of BcrAbl+ cells per treatment and over time is shown (n = 3). (E) The number of BcrAbl+ cells over time and per treatment is shown. BcrAbl+ cell number was calculated by multiplying the percentages of BcrAbl+ cells in D with the cell number obtained from the electronic cell counter.

7.2.2 Gating strategies for flow cytometry analysis for mouse BM cells
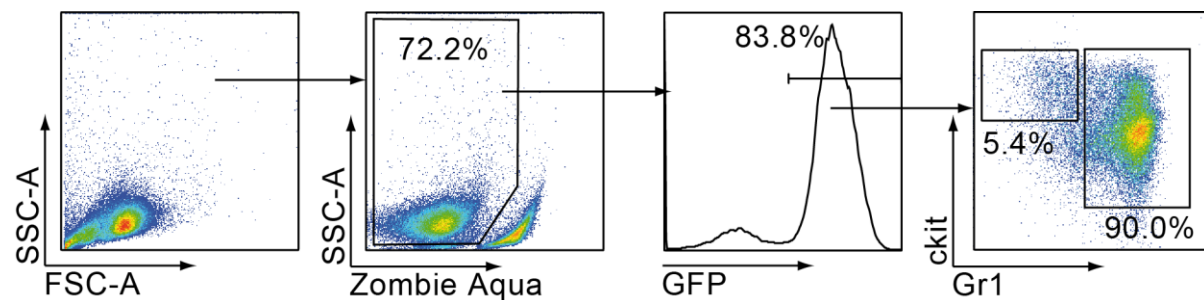
Supplemental Figure 6. Gating strategy for IRF8+/+ and IRF8–/– BM cells transduced with BcrAbl

IRF8+/+ and IRF8–/– BM cells were transduced retrovirally with BcrAbl followed by TKI and/or IFNα treatment for 4 days. The gating strategy for all experiments with murine BM cells is show. The shown data is taken from untreated murine IRF8+/+ cells on day 1 of culture.

7.2.3 Supplemental figures for the hematopoietic differentiation of iPSC
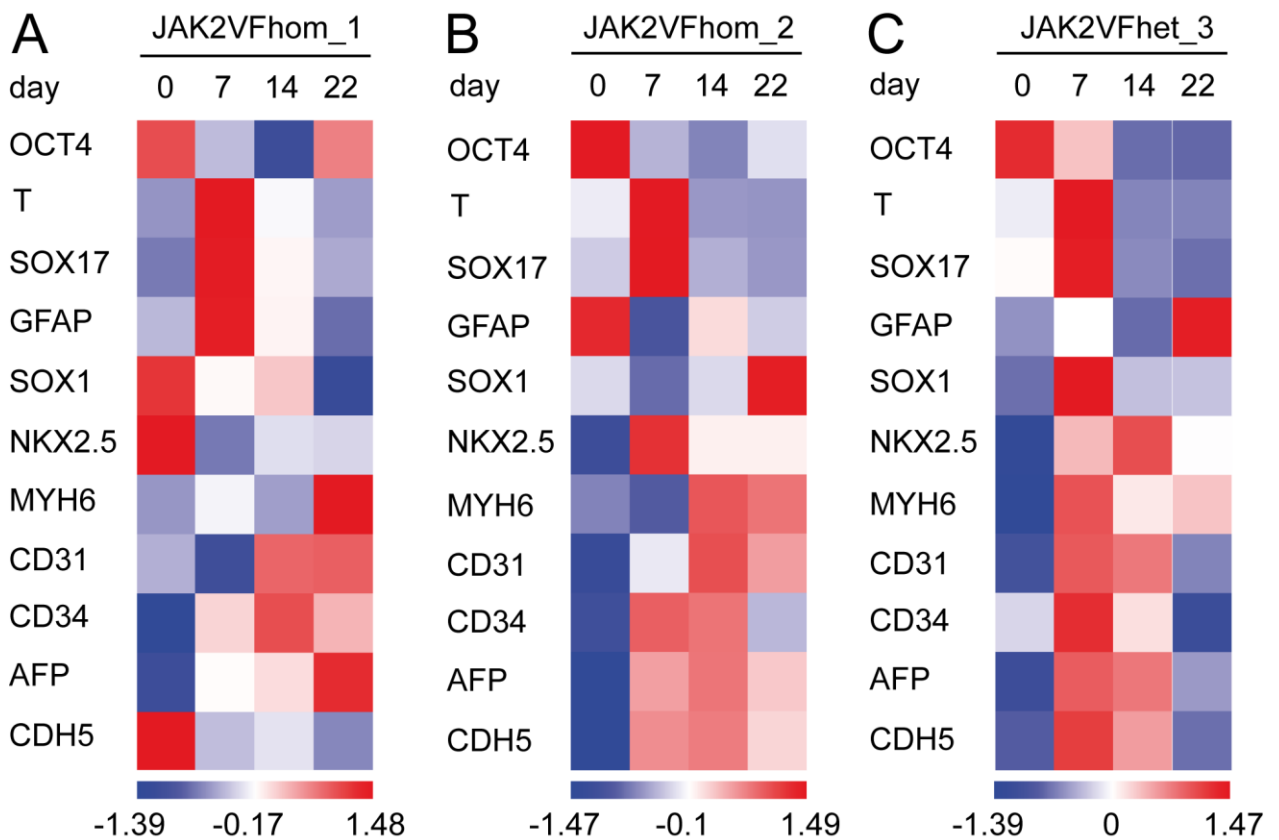
Supplemental Figure 7. iPSC clones from PV patient 2 and 3 have 3 germ layer differentiation potential

iPSC clones of (A) PV2 and (B – C) PV3 were induced to differentiate into all three germ layers. In short, iPSC clones were harvested by Collagenase IV treatment for 1h at 37°C. After, MEF depletion for 10 min EB were washed once with KO-DMEM. EB were resuspended in KO-DMEM supplemented with 10 % FCS, 1 % L-Glutamine, 1 % Penicillin/Streptomycin, 1 % minimal non-essential amino acids and 0.2 % β-mercaptoethanol and seeded onto ULA plates followed by culturing for 7 days. Finally, EB were seeded onto gelatin-coated TCP and cultured for another 7 to 14 days. On day 0 (undifferentiated iPSC), 7, 14 and 22 samples were harvested and RNA was isolated. RT-qPCR was performed. OCT4 and T were used as pluripotency marker; CD31, CD34, CDH5, NKX2.5 and MYH6 were used as mesodermal markers; SOX1 and GFAP were used as ectodermal marker; SOX17 and AFP were used as endodermal markers. Data is shown in a heatmap format. Z-Score represents expression levels: red, high expression; blue, low expression.
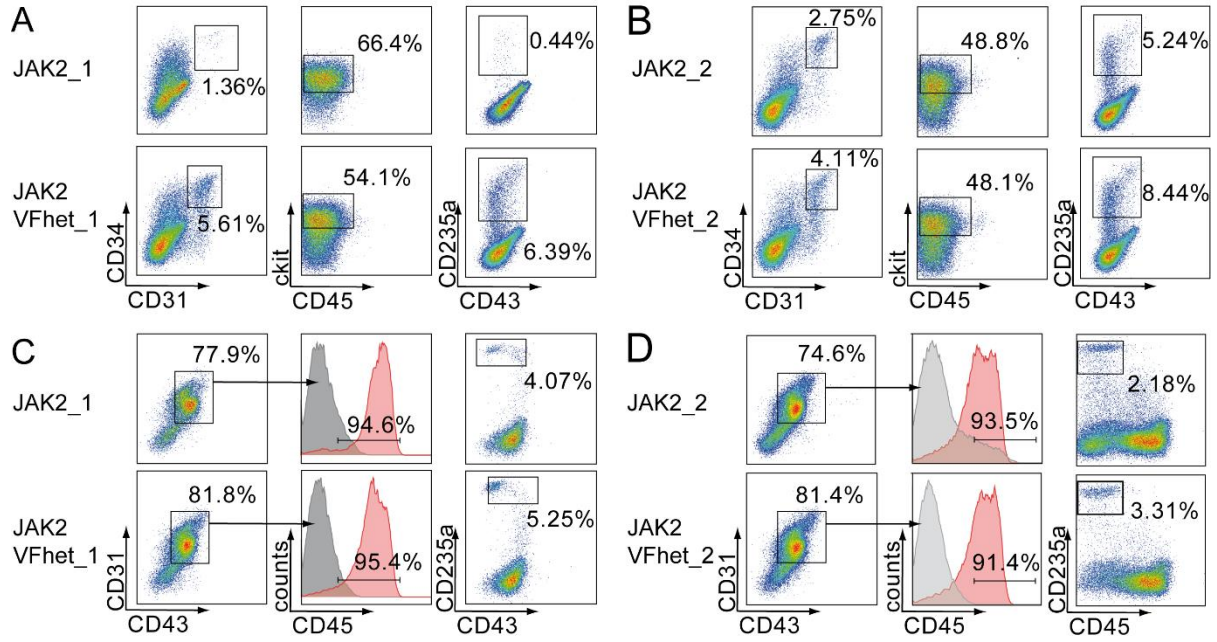
Supplemental Figure 8. JAK2V617F mutation has a minor effect during hematopoietic differentiation of iPSC

JAK2 and JAK2V617F iPSC were induced to differentiate into hematopoietic cells according to Figure 34. Scheme hematopoietic differentiation of patient derived iPSC. Cells were stained with antibodies for CD34, CD31, CD45, CD43, ckit and CD235a as described in Materials and Methods and analyzed by flow cytometry on (A – B) day 6 and (C – D) day 18. Shown is the representative flow cytometry analyses for (A + C) JAK2_1 and JAK2VFhet_1 and (B + D) JAK2_2 and JAK2VFhet_2. Grey histograms in the overlays show the signal for isotype stained sample.
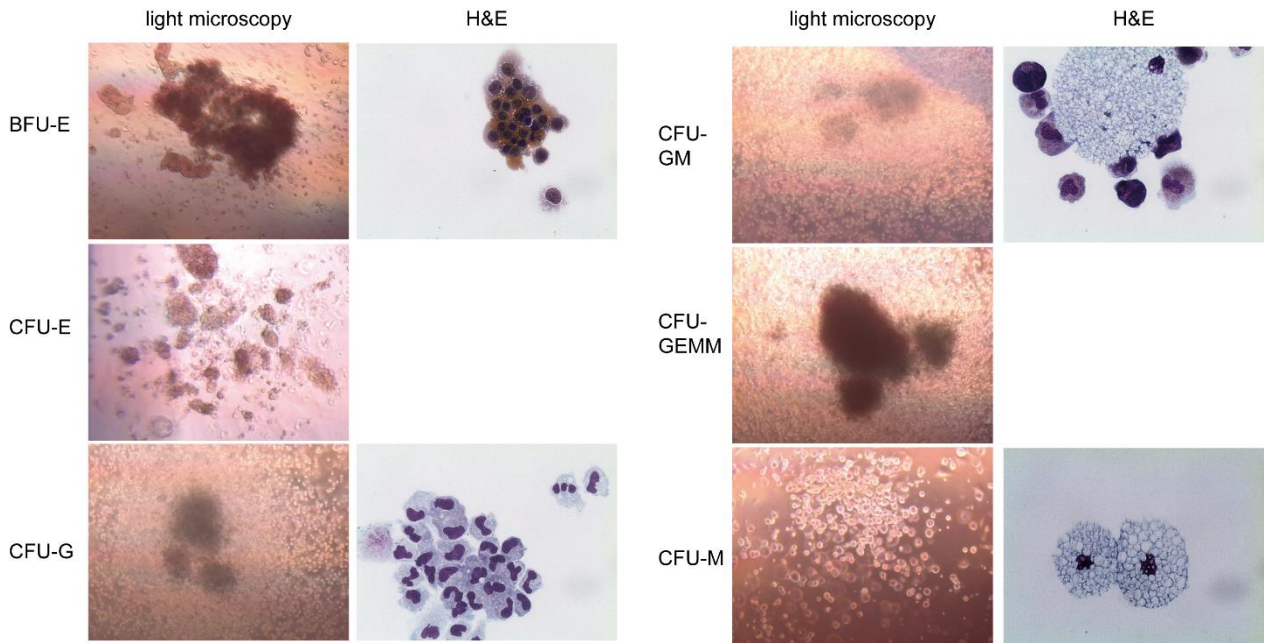
Supplemental Figure 9. CFU assay of iPSC-derived hematopoietic cells

JAK2 and JAK2VFhet iPSC-derived cells were harvested from the supernatant fraction on day 18 of differentiation. 20.000 to 40.000 cells were seeded in semisolid medium according to manufacturer's protocol. Colonies were scored and photographed with a light microscope after 14 days of incubation at 37°C. Individual colonies were picked, spun onto a glass slide and stained with DiffQuick. H&E staining of picked colonies was analyzed with a Leica DMRX microscope and the Leica Application Software suite v3.1.0.
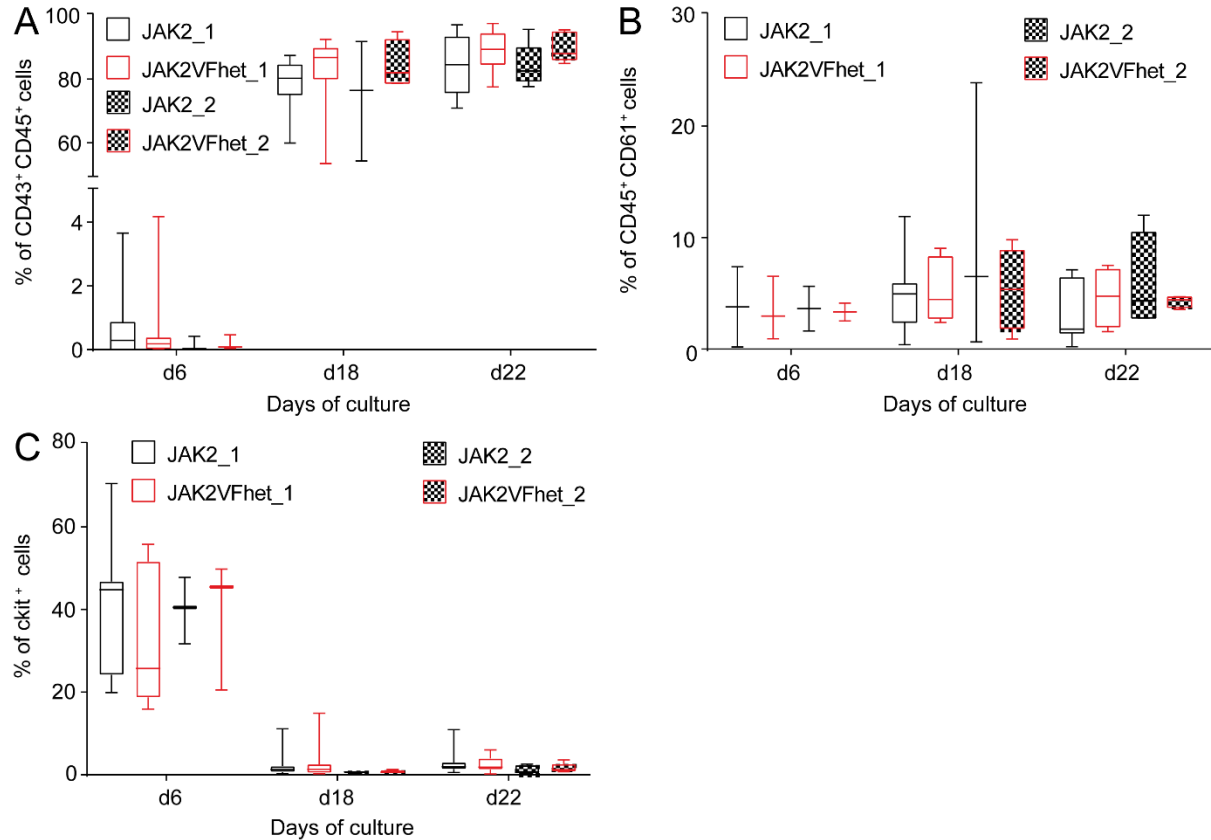
Supplemental Figure 10. JAK2V617F has no influence on the formation of mature myeloid cells, ckit+ cells or megakaryocytes

JAK2 and JAK2V617F iPSC clones of PV1 were differentiated into hematopoietic cells as shown in Figure 34. On day 6 of differentiation EB were harvested, digested with Accutase. From day 14 of differentiation onwards suspension cells were harvested every 4 days. Cells were stained with antibodies against CD45, CD43, CD31, CD34, ckit, CD61, CD66b and CD235a followed by flow cytometry analysis. Shown is the flow cytometry analysis for (A) CD45+ CD43+ mature hematopoietic cells, (B) CD45+ CD61+ megakaryocytes and (C) ckit+ cells for multiple independent experiments (n = 5-11).
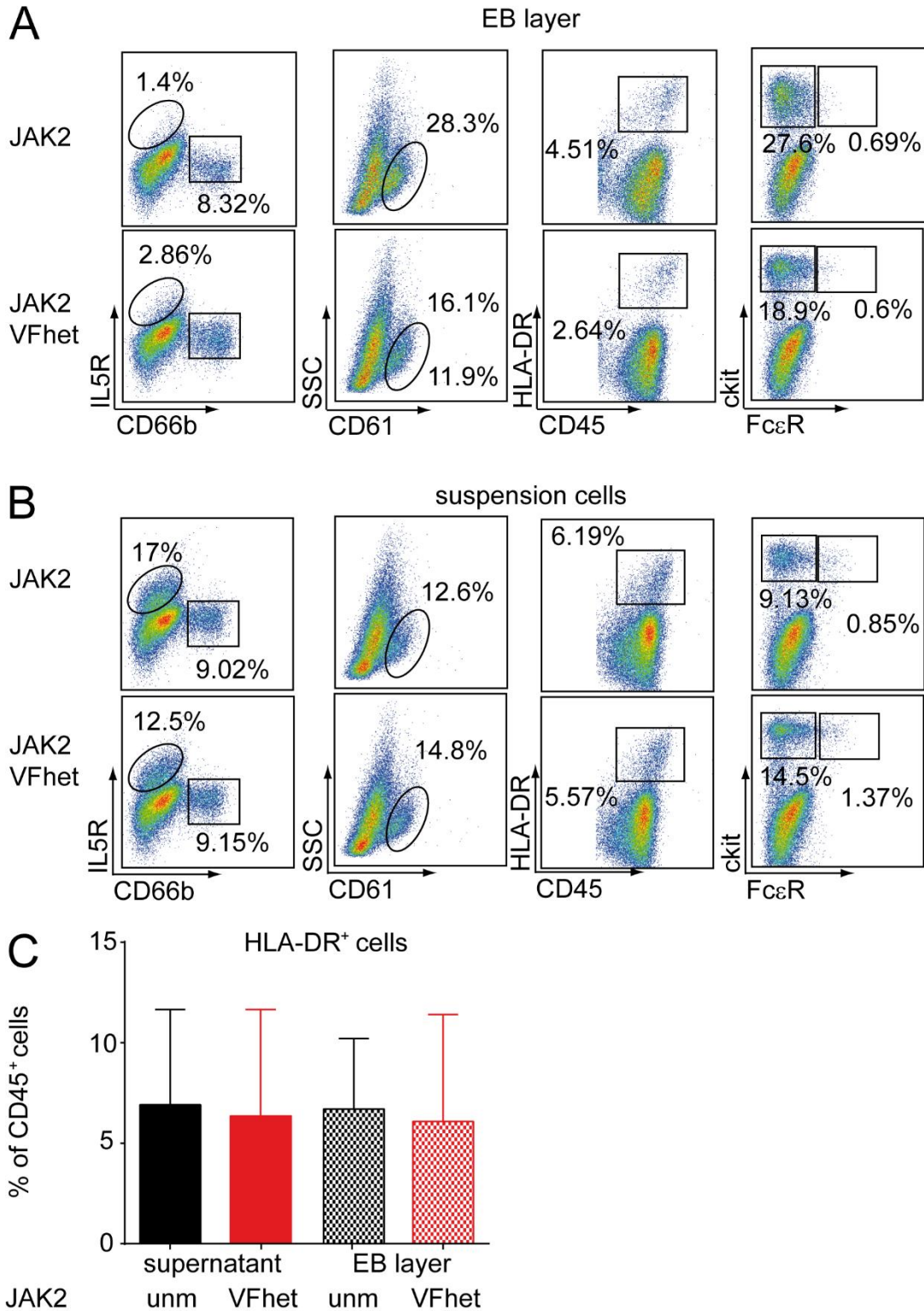
Supplemental Figure 11. JAK2V617F does not confer a bias towards a myeloid lineage due to JAK2V617F

PV1 iPSC clones were subjected to hematopoietic differentiation for 49 days. Medium changes were done every 4-5 days. On day 49 of differentiation, suspension cells were harvested whereas the EB layer was collected, treated for 20 min with Accutase and thoroughly resuspended. Cells were stained with antibodies against

myeloid lineage markers. (A – B) Flow cytometry analyses of (A) supernatant fraction and (B) EB layer for JAK2_2 and JAK2V617F_2 is shown as an example. Myeloid cells were gated according to gating strategy in Supplemental Figure 20. Gating strategy undirected hematopoietic differentiation of iPSC. (C) Summary of HLA-DR$^+$ cells during differentiation. Data is summarized per genotype (JAK2 vs JAK2VFhet) of PV1 iPSC clones and represents means + standard deviation (n = 3). Unm, unmutated; VFhet, JAK2V617F heterozygous.
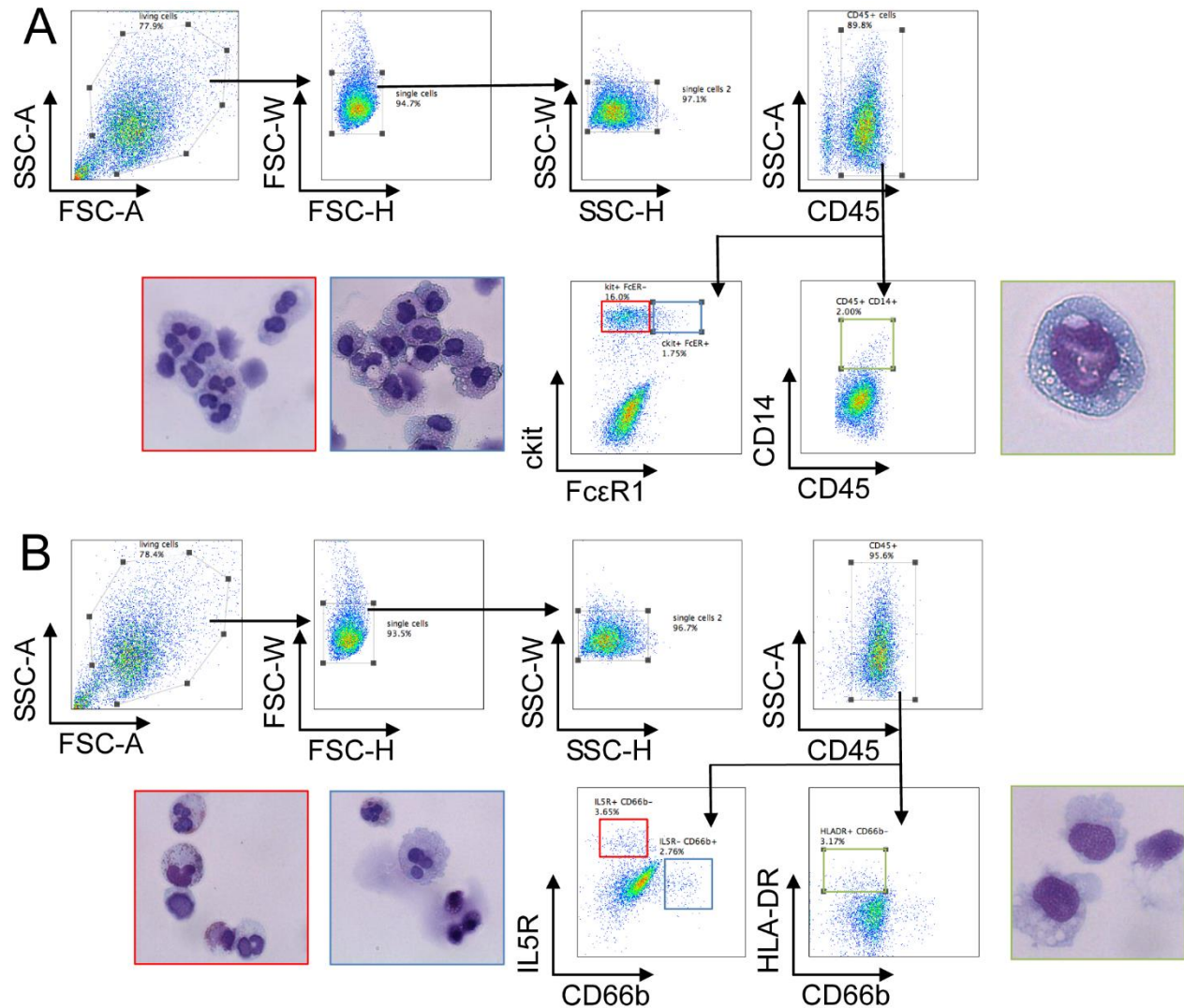
Supplemental Figure 12. Phenotypical analyses of iPSC-derived myeloid cells

JAK2 and JAK2617F iPSC clones of PV1 were differentiated into hematopoietic cells as described in Figure 34. On day 60 of differentiation EB layers were digested with Accutase for 20 min followed by thoroughly resuspending with KO-DMEM. Next, cells were passed through a 40 µM cell strainer and stained with CD45, ckit, CD14, IL5R, CD66b and HLA-DR specific antibodies. Myeloid cell populations were sorted with a FACS Aria device. Sorted cells were spun on glass slides and stained with H&E. Cells for JAK2 and JAK2VFhet were pooled. (A) Shown are the gating strategy and cytospin images for immature mast cells (red), mature mast cells (blue) and monocytes (green). (B) Shown is the gaiting and cytospin images for neutrophils (red), eosinophils (blue) and DC (green).
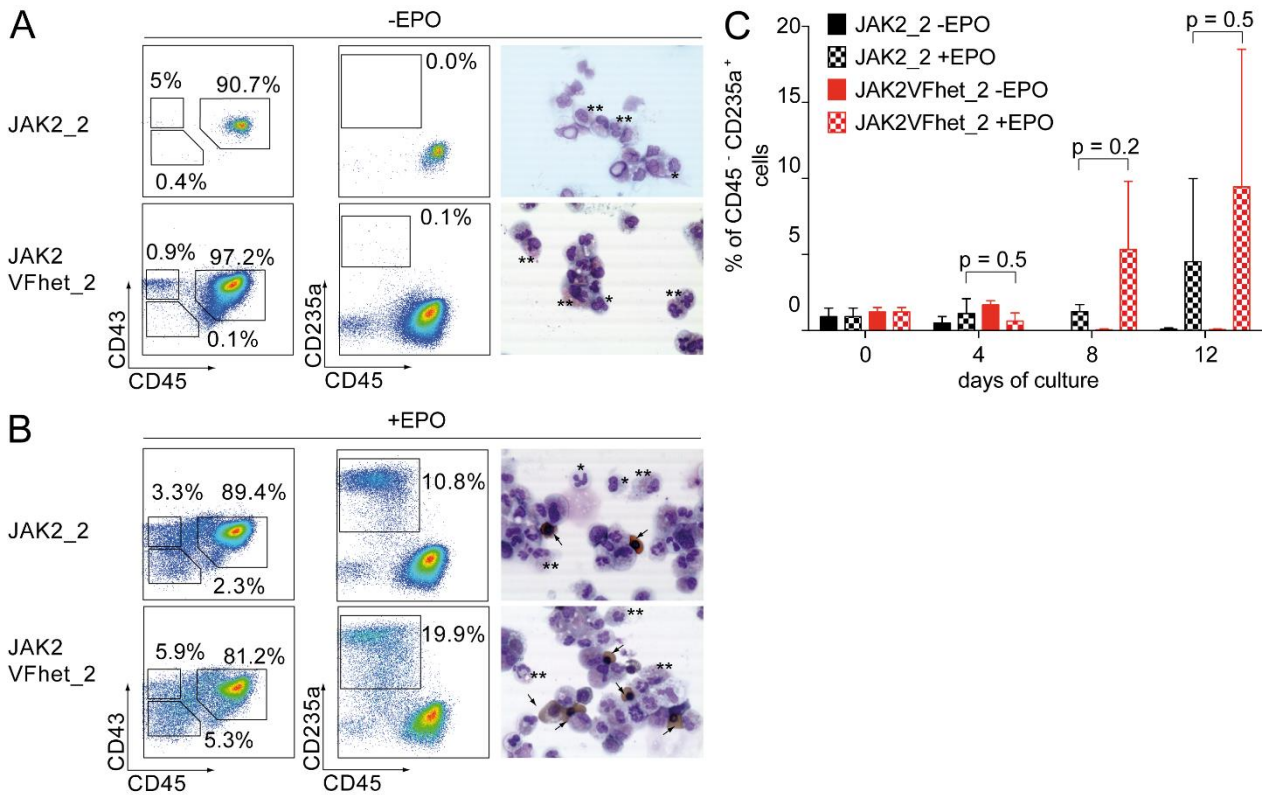
Supplemental Figure 13. JAK2V617F expression confers hypersensitivity to EPO and results in higher RBC population compared to JAK2

JAK2 and JAK2V617F iPSC were differentiated into hematopoietic cells according to Figure 34. On day 22 of hematopoietic differentiation, cells of the supernatant fraction were harvested and cultured (A) without and (B) with EPO (0.2 U/ml EPO) to induced red blood cell differentiation. Flow cytometry analyses were performed on day 0, 4, 8 and 12 of red blood cell differentiation. (A – B) Left and middle panel show a representative flow cytometry analysis of JAK2_2 and JAK2VFhet_2 on day 12 of differentiation with and without addition of EPO (A and B, respectively). (Right panel) Cells were spun onto a glass slide and stained with neutral benzidine/DiffQuik. Arrows indicate normoblasts. Asterisks indicated neutrophils (*) and eosinophils (**). (C) Red blood cells shown in A and B were quantified. The percentage of CD45$^-$ CD235a$^+$ cells over time is shown for JAK2_2 and JAK2VFhet_2. Data represent means ± standard deviation (n = 3).
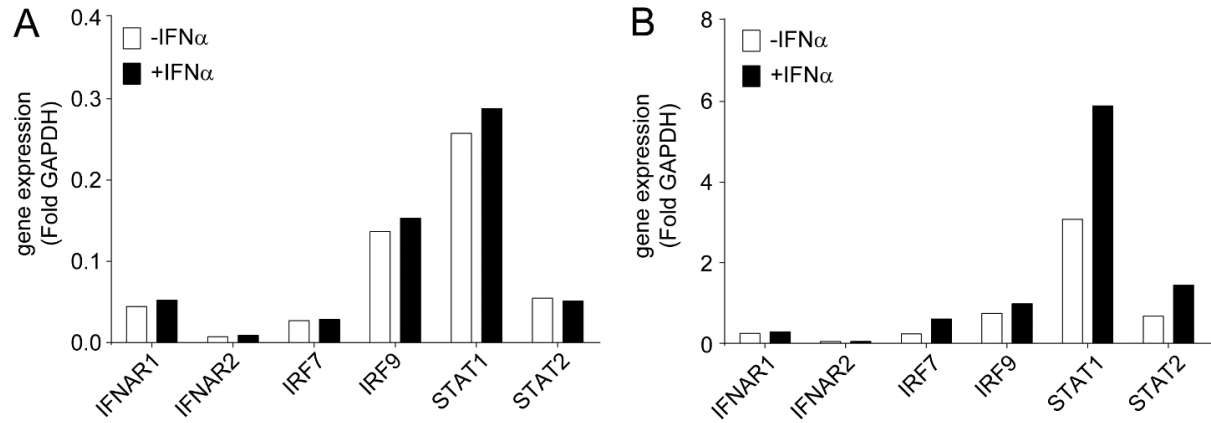
Supplemental Figure 14. iPSC-derived hematopoietic cells of PV2 and PV3 do not upregulate IFNα target genes

(A – B) iPSC-derived hematopoietic cells of PV2 and PV3 were harvested on day 18 of differentiation and were cultured without cytokines in the presence or absence of IFNα (200 U/ml) for 4h. RNA was isolated and RT-qPCR for the indicated genes was performed (C) Gene expression in the absence and presence of IFNα for JAK2VFhom_1 is shown (n = 1). (D) Gene expression in the absence and presence of IFNα for JAK2V617F/V617F_2 is shown (n = 1).
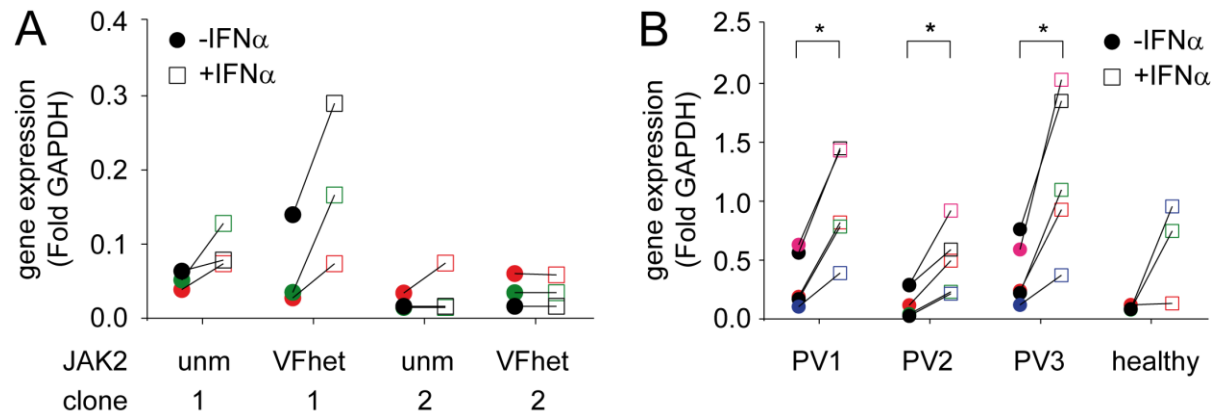
Supplemental Figure 15. STAT2 gene expression in iPSC-derived hematopoietic cells and patient PBMNC

 (A) iPSC were differentiated into hematopoietic cells according to Figure 34. Supernatant cells were harvested on day 18 of differentiation. Cells were washed two times and put back into culture. Cells were cultured as described in chapter 2.2.1.17 without growth factors in the presence or absence of IFNα (200 U/ml) for 4h. Afterwards, cells were collected, RNA isolated and cDNA synthesis followed by RT-qPCR was performed. GAPDH was used for normalization (n = 3). (B) Patient PBMNC were thawed and treated with IFNα as described in A (n = 5). Colors represent independent experiments the data was obtained from. Student's t-test was used to test for significant expression changes. Unm, unmutated; VFhet, JAK2V617F heterozygous.
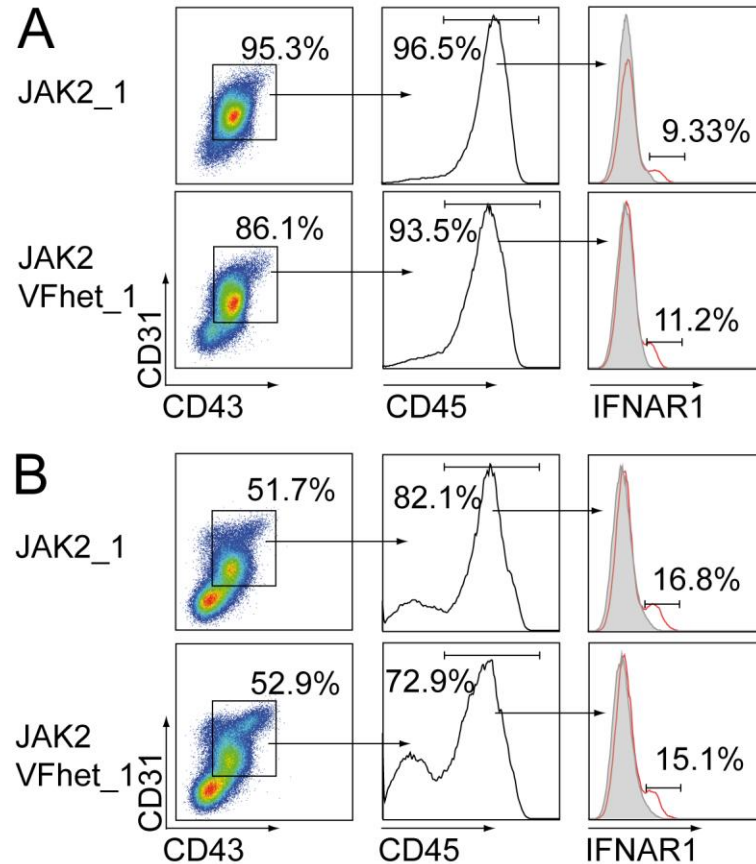
Supplemental Figure 16. iPSC-derived hematopoietic progenitor cells of supernatant fraction express low levels of IFNAR1

JAK2 and JAK2V617F iPSC of PV1 were induced to differentiate into hematopoietic cells as shown in Figure 34. On day 18 of differentiation cells from the supernatant fraction were harvested by washing them off of the EB layer. EB layer was harvested and digested with Accutase to obtain single cells. Cells from both fractions were stained with IFNAR1 specific antibodies. Additionally, cells were stained with CD45, CD34, CD31, CD43 and CD235a specific antibodies followed by flow cytometry analyses. Shown are the flow cytometry analyses of (A) supernatant cells and (B) cells from the EB layer for JAK2_1 and JAK2VFhet_1.
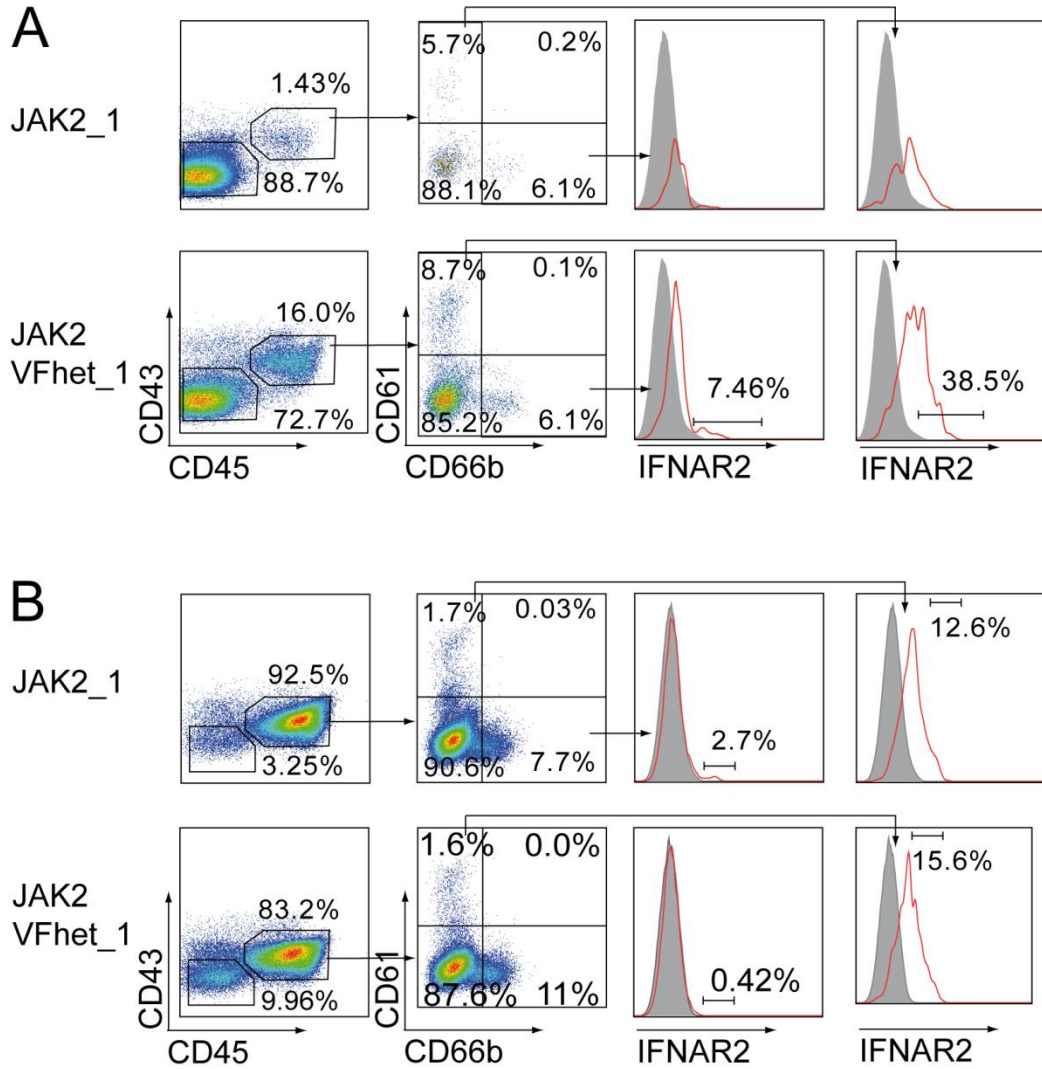
Supplemental Figure 17. IFNAR2 expression on CD66b$^+$ and CD61$^+$ cells

JAK2 and JAK2V617F iPSC were induced to differentiate into hematopoietic cells according to Figure 34. On day 18 of differentiation cells from the supernatant fraction were harvested by washing them off of the EB layer. EB layer was digested with Accutase to obtain single cells. (A) Cells from the EB layer and (B) supernatant fraction were stained with IFNAR1 and IFNAR2 specific antibodies. Furthermore, cells were stained with CD43, CD34, CD45, CD66b, CD61 and CD235a specific antibodies followed by flow cytometry analyses. Shown is a representative analysis for JAK2_1 and JAK2VFhet_1. Gating strategy was done according to Supplemental Figure 23A.
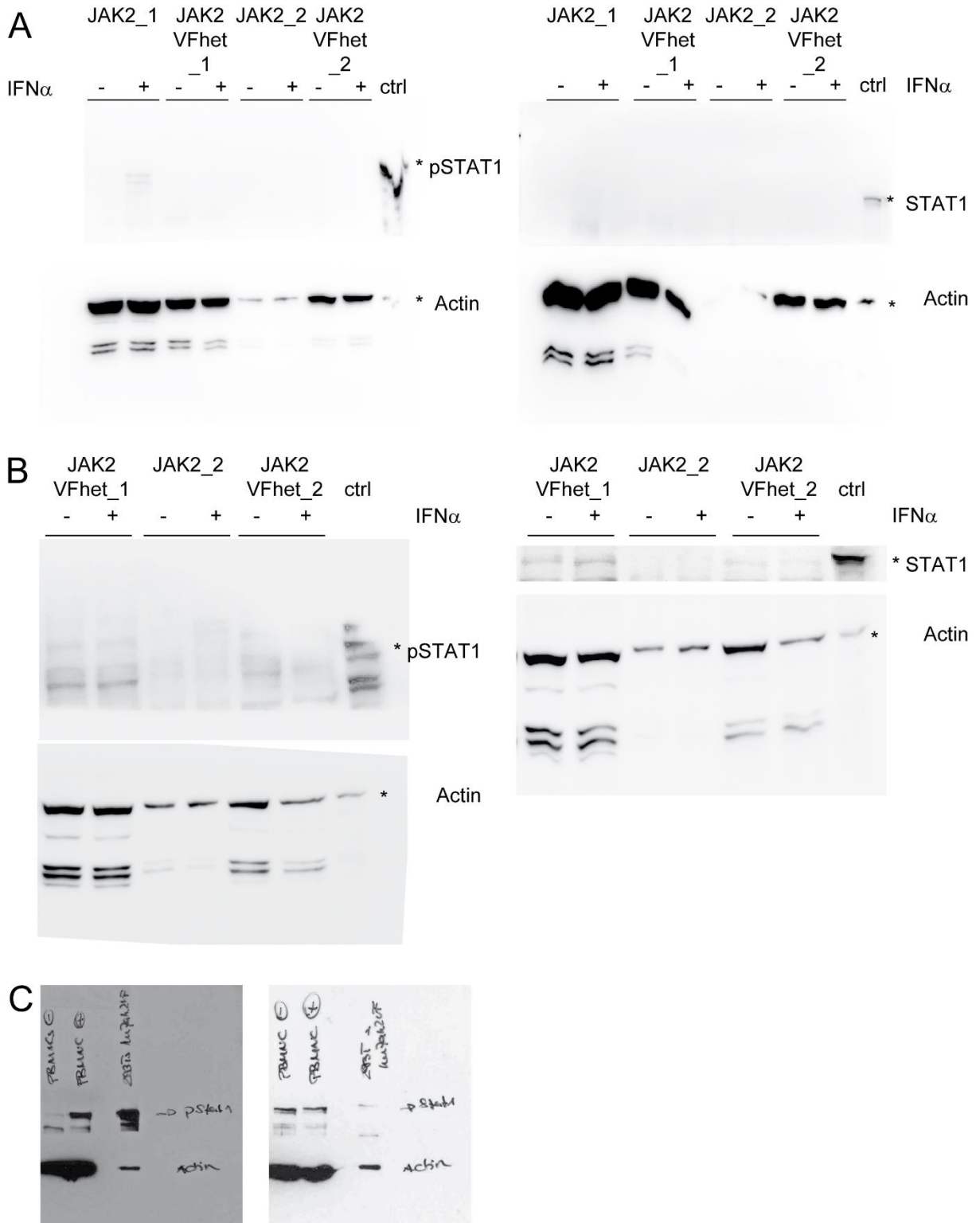
Supplemental Figure 18. STAT1 and pSTAT1 expression by iPSC derived hematopoietic cells and PBMNC

(A – B) iPSC-derived hematopoietic suspension cells were harvested on day 26 to day 34 of hematopoietic differentiation. Cells were cultured in RPMI without cytokines for 4 h followed by IFNα stimulation (2000 U/ml) for 30 min. Afterwards protein lysates were prepared. SDS-PAGE and Western Blot was done as described (chapter

2.2.2.7). To this end, 40µg protein was loaded onto 10% SDS gels. SDS-PAGE ran at 25 mA for 2h. Blotting onto nitrocellulose membranes was done at 80 mA for 2h. Nitrocellulose membranes were probed with antibodies against STAT1, pSTAT1 and Actin. STAT1 and pSTAT1 were detected on different membranes. The membranes were not stripped. As control (ctrl) protein lysates from HEK293T overexpressing huJAK2V617F was used. Shown are the whole membranes. (C) Healthy PBMNC were isolated with density gradient centrifugation from fresh blood. Cells were processed as in A and B.

7.2.4 Gating strategies for flow cytometry analysis for hematopoietic iPSC differentiation
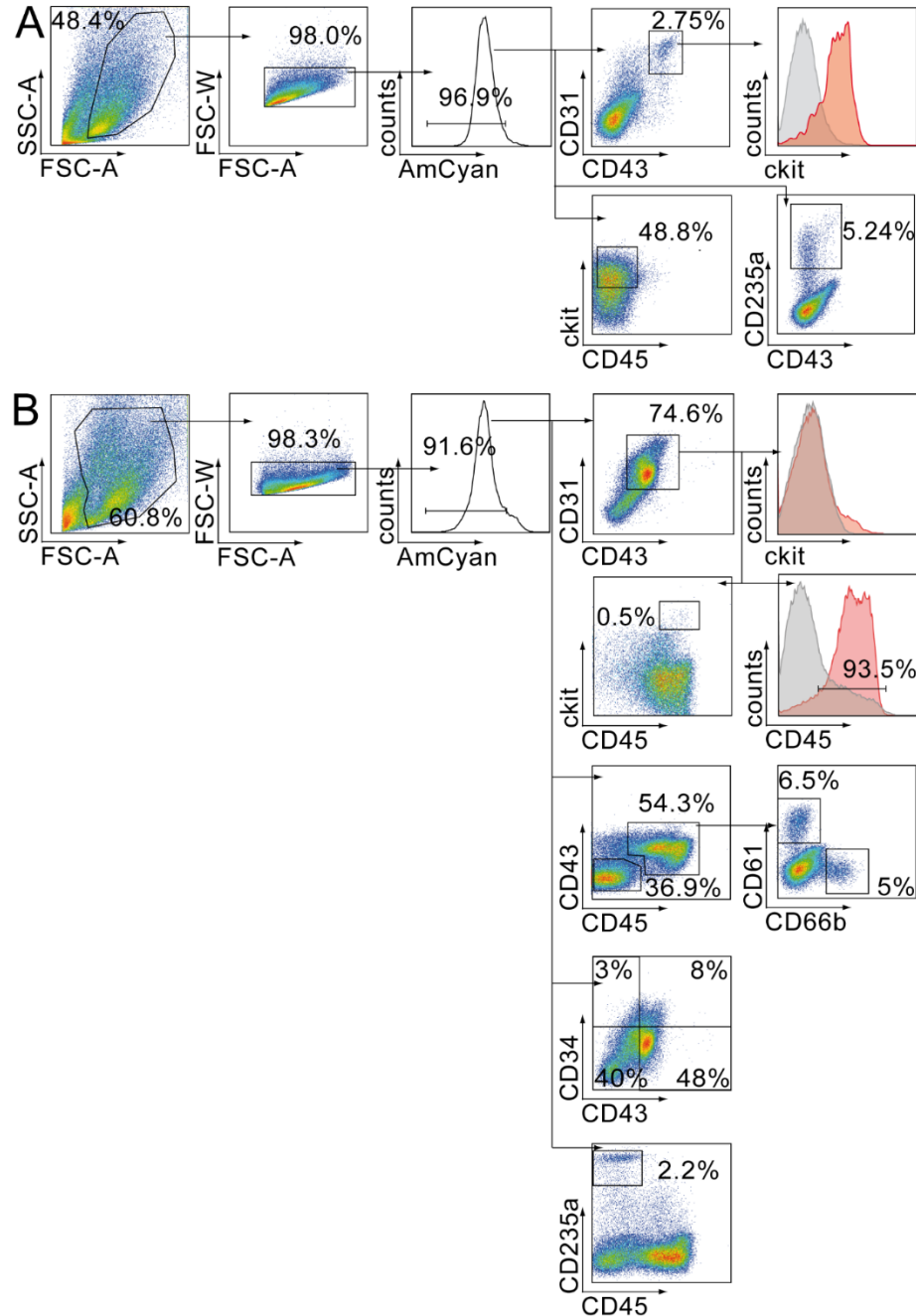
Supplemental Figure 19. Gating strategy hematopoietic differentiation iPSC

JAK2 iPSC were differentiated into hematopoietic cells according to Figure 34. The gating strategy used for cell analysis during hematopoietic differentiation is shown for JAKWT_2. (A) On day 6 of differentiation EB were harvested and dissociated with Accutase. Cells were stained with CD34, CD43, CD45, ckit, CD31 and CD235a

specific antibodies for 30 min. Cells were analyzed with flow cytometry. (B) On day 18 of differentiation supernatant cells were harvested. Cells were stained with antibodies as in A. Additionally, cells were stained with CD61 and CD66b followed by flow cytometry analysis.
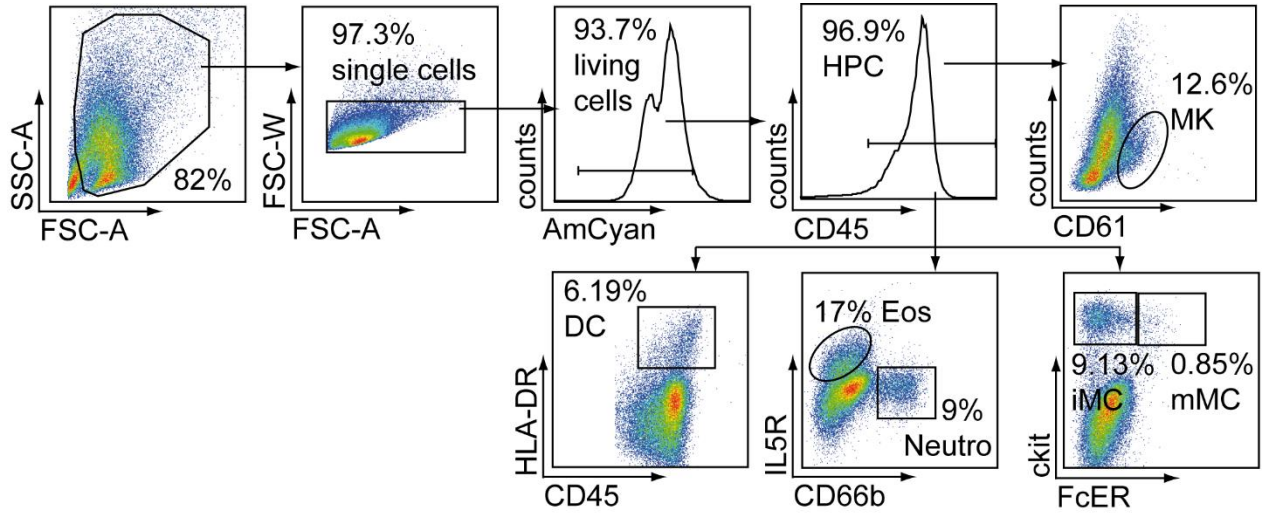
Supplemental Figure 20. Gating strategy undirected hematopoietic differentiation of iPSC

JAK2 iPSC were differentiated for 49 days. Supernatant cells were harvested by washing EB layer with medium. EB layer was harvested by digestion with Accutase. Cells were stained for surface marker expression and analyzed by flow cytometry immediately afterwards. Gating of supernatant fraction and the EB layer is shown with the gating strategy of supernatant cells for JAK2_2. HPC, hematopoietic progenitor cell; DC, dendritic cells; MK, megakaryocytes; Eos, eosinophil; neutro, neutrophil; iMC, immature mast cell; mMC, mature mast cell.
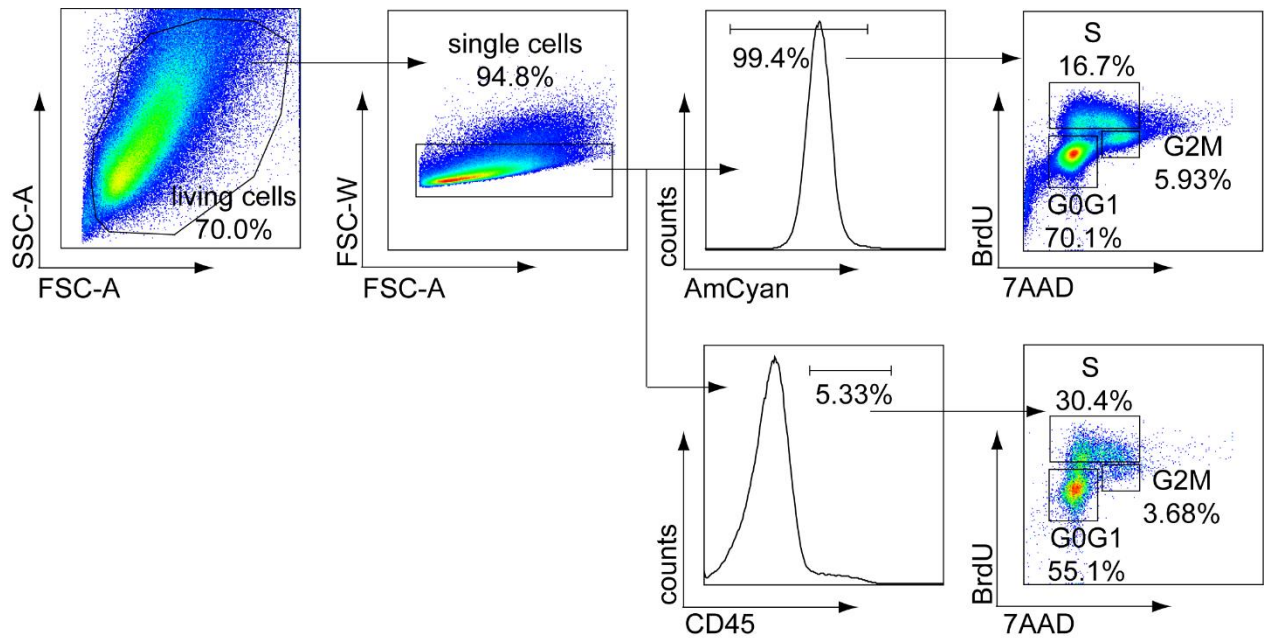
Supplemental Figure 21. Gating strategy for BrdU/7AAD staining

iPSC clones were subjected to hematopoietic differentiation as described in chapter 2.2.1.10. On day 14 of differentiation EB layer was harvested by digestion with Accutase for 20 min. Accutase was diluted with KO-DMEM. Cell suspension was transferred in a Falcon tube followed by vigorous resuspension to detach more cells from the partially digested EB layer. Cells were passed over a 40 µm cell strainer. Afterwards, 1.5×10^6 cells/ml were seeded into 6 well plates and were pulsed with or without BrdU (10 µM) for 1h. EB layer cells were stained for flow cytometry with CD45 prior to intracellular staining for BrdU. Fixation and Permeabilization for BrdU staining was done as described in chapter 2.2.1.13.2. Afterwards, cells were stained with antibodies against BrdU incorporation. Finally, cells were stained with 7AAD to analyze cell cycle.
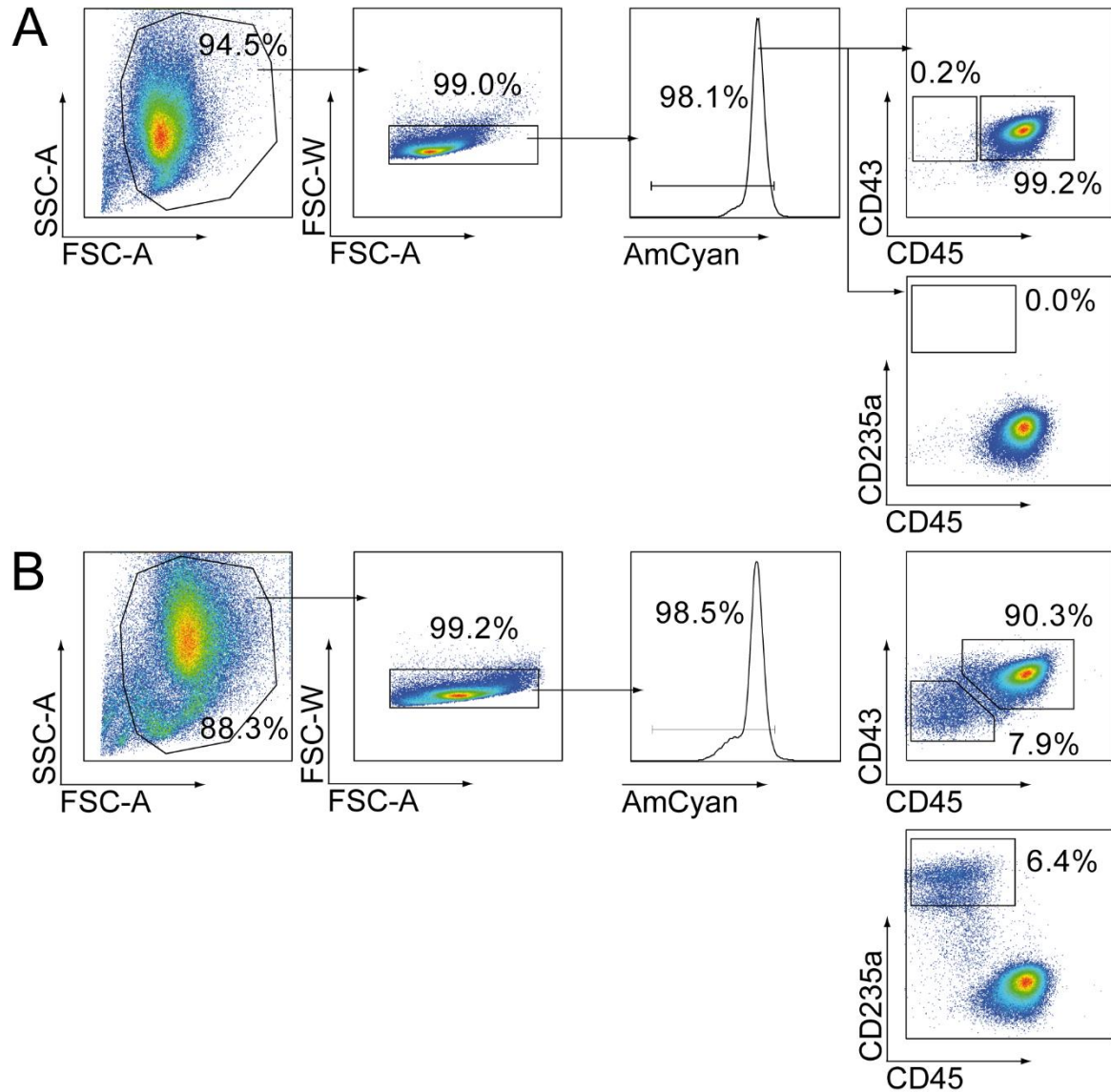
Supplemental Figure 22. Gating strategy for RBC differentiation of iPSC-derived hematopoietic cells

JAK2V617F were differentiated into hematopoietic cells as shown in Figure 34 for JAK2VFhet_1. On day 22 of differentiation, cells of the supernatant fraction were harvested. For red blood cell differentiation supernatant cells were washed once and cultured in StemPro34. 0.2 U/ml EPO, 100 ng/ml SCF and 30 ng/ml IL-3 were added during culture. As control cells were cultured without EPO. On day 8 of culture SCF and EPO were used (see Figure 18, chapter 2.2.1.11). Cells were analyzed by flow cytometry on day 0, 4, 8 and 12 of red blood cell differentiation. To this end, cells were stained with CD45, CD43 and CD235a specific antibodies. Shown is the gating strategy on day 12 of red blood cell differentiation for the culture (A) without EPO and (B) with EPO.
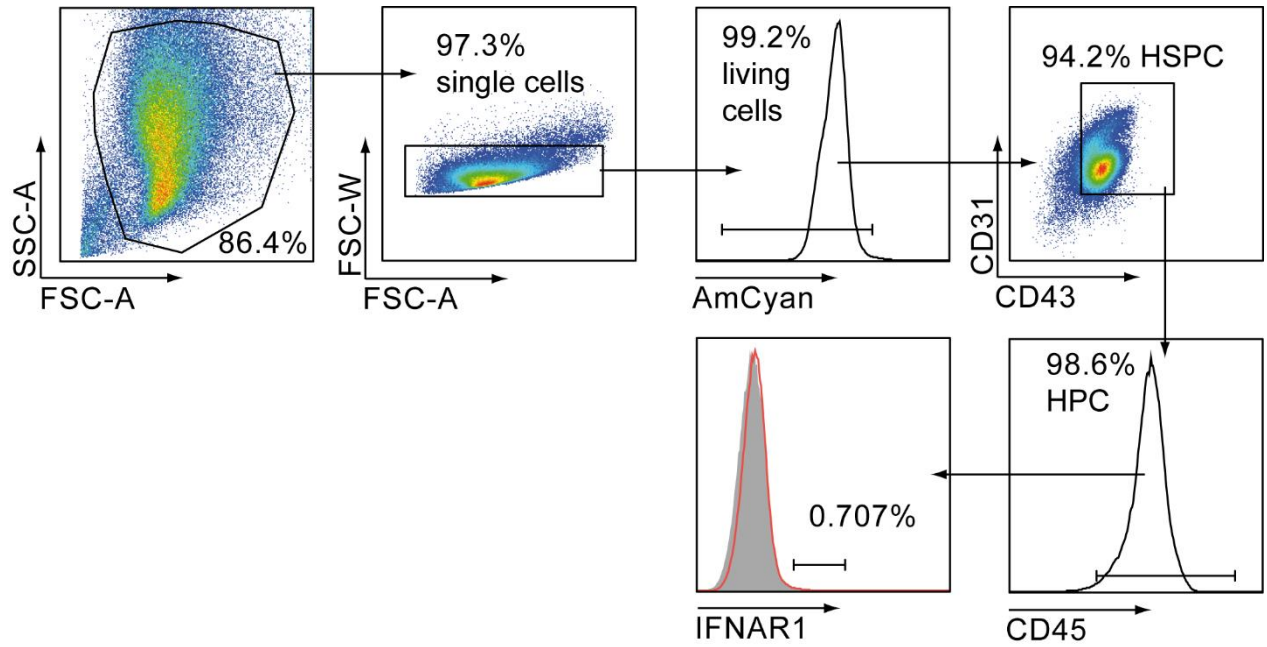
Supplemental Figure 23. Gating strategy for flow cytometric analysis of IFNAR1

iPSC were differentiated into hematopoietic cells as described in chapter 2.2.1.10. Supernatant cells were washed off the EB layer. EB layer was digested with Accutase and thoroughly resuspended to make a single cell suspension. Cells were stained with CD45, CD43, CD31 and IFNAR1 specific antibodies and analyzed with flow cytometry. Shown is the gating strategy for IFNAR1 analysis on day 18 of differentiation for JAK2_2.

7.3   Supplemental Tables

Supplemental Table 1. Cytokines and supplements used in hematopoietic differentiation of iPSC

Reagent	Supplier	Catalog #	Stock concentration	Dilution Factor
bFGF	Peprotech	100-18B	100 µg/ml	10000
BMP4	Miltenyi	130-098-786	25 µg/ml	3000
FLT3L	Peprotech	300-19	25 µg/ml	2500
hyper-IL6	gift from Dr. Rose-John		Batch dep.	Batch dep.
IGF1	Sigma	100-11	40 µg/ml	1600
IL-3	Miltenyi	130-094-193	150 µg/ml	5000
L-Ascorbic acid (LAA)	Sigma	A4403	50 mg/ml	1000
SCF	Selfmade		100 µg/ml	100
TPO	Miltenyi	130-094-013	20 µg/ml	1000
VEGF	Peprotech	100-20	100 µg/ml	10000

Supplemental Table 2. Media used in cell culture

Reagent	Supplier	Catalog #
DMEM	Gibco	41965-039
RPMI 1640	Gibco	11875-093
KO-DMEM	Gibco	10829-018
KO-Serum Replacement	Gibco	10828028
StemPro34	Thermo Scientific	10639-11
StemSpan^{TM} SFEM	Stemcell Technologies	09650
iPSbrew	Miltenyi	130-104-368
DPBS	Gibco	14190-094

Supplemental Table 3. Media supplements used in cell culture

Reagent	Supplier	Catalog #	Stock concentration	Dilution Factor
FCS	Gibco	Different LOT numbers used	-	10
FCS	LONZA		-	5
L-Glutamine	Thermo Scientific	25030	200 mM	100
Monothio-glycerol (MTG)	Sigma	M1753	100 mM	250
Penicillin/ Streptomycin	Thermo Scientific	15140	10000 U/ml	100
β-Mer-captoethanol	Gibco	31350-010	50 mM	1000

Supplemental Table 4. Human primers for RT-qPCR of undirected differentiation of iPSC

Target		Sequence (5' > 3)	Reference
OCT4	Forward	GGGGGTTCTATTTGGGAAGGTA	Tran et al. (2009)
	Reverse	ACCCACTTCTGCAGCAAGGG	
NKX2.5	Forward	ACCTCAACAGCTCCCTGACTCT	Yang et al. (2008)
	Reverse	ATAATCGCCGCCACAAACTCTCC	
CD31	Forward	GAGTCCTGCTGACCCTTCTG	Zambidis et al. (2005)
	Reverse	ATTTTGCACCGTCCAGTCC	
CD34	Forward	TGGACCGCGCTTTGCT	Zambidis et al. (2005)
	Reverse	CCCTGGGTAGGTAACTCTGGG	
MYH6	Forward	AAGCTCAAGAACGCCTAC	Chen et al. (1999)
	Reverse	CATTCTTTCCTCCTTCTCC	
VeCadherin	Forward	TGGAGAAGTGGCATCAGTCAACAG	Kennedy et

	Reverse	TCTACAATCCCTTGCAGTGTGAG	al. (2007)
T	Forward	CAGTGGCAGTCTCAGGTTAAGAAGGA	Yang et al. (2008)
	Reverse	CGCTACTGCAGGTGTGAGCAA	
SOX1	Forward	CCTGTGTGTACCCTGGAGTTTCTGT	Yang et al. (2008)
	Reverse	TGCACGAAGCACCTGCAATAAGATG	
GFAP	Forward	AGGAGGAGGTTCGGGAACTC	Sontag et al. (2017a)
	Reverse	CGCCATTGCCTCATACTGC	
AFP	Forward	GCCAAGCTCAGGGTGTAG	Sontag et al. (2017a)
	Reverse	CAATGACAGCCTCAAGTTGT	
SOX17	Forward	AGGAAATCCTCAGACTCCTGGGTT	Yang et al. (2008)
	Reverse	CCCAAACTGTTCAAGTGGCAGACA	

Supplemental Table 5. Primer sequences for JAK2V617F allele specific PCR adapted from (Jones et al., 2005)

Primer	Sequence 5' to 3'
JAK2 forward primer	TCCTCAGAACGTTGATGGCAG
JAK2 reverse primer	ATTGCTTTCCTTTTTCACAAGAT
JAK2 WT Primer	GCATTTGGTTTTAAATTATGGAGTATATG
JAK2V617F primer	GTTTTACTTACTCTCGTCTCCACAAAA

Supplemental Table 6. Human primers used for RT-qPCR of IFNα target genes

Primer	Sequence 5' to 3'	Reference
huIFNAR1_tQ_F	TCGCAAAGCTCAGATTGGTCCTC	Hong and Carmichael (2013)
huIFNAR1_tQ_R	ACCATCCAAAGCCCACATAACAC	
huIFNAR2_tQ_F	AGCACCATAGTGACACTGAAATGG	Hong and Carmichael (2013)
huIFNAR2_tQ_R	GAGACCTTGCCTCAAGACTTTGG	
IRF7_tQ_F	TGTGCTGGCGAGAAGGC	
IRF7_tQ_R	TGGAGTCCAGCATGTGTGTG	
IRF9_tQ_F	TTCTTCAAGGCCTGGGCAAT	

IRF9_tQ_R	CCTGGTGGCAGCAACTGATA	
STAT1_tQ_F	TGTATGCCATCCTCGAGAGC	
STAT1_tQ_R	AGACATCCTGCCACCTTGTG	
STAT2_tQ_F	CCGGGACATTCAGCCCTTTT	
STAT2_tQ_R	CTCATGTTGCTGGCTCTCCA	
GAPDH_tQ_F	GAAGGTGAAGGTCGGAGTC	Szabo et al. (2010)
GAPDH_tQ_R	GAAGATGGTGATGGGATTTC	

Supplemental Table 7. RIPA and lysis buffer for protein extraction

Buffer	**Reagent**	**Amount**
RIPA buffer	Tris-HCL, pH 7.4	50 mM
	NP-40	1 %
	SDS	0.1 %
	Sodiumdeoxycholate	0.625 g
	NaCl	150 mM
	EGTA	0.475 g
Lysis buffer	RPIA buffer	747 µl
	500 mM NaF	100 µl
	200 mM Na_3Vo_4	10 µl
	7x complete mini	143 µl

Supplemental Table 8. Buffer composition SDS-Page

Buffer	**Reagent**	**Amount**
Running buffer	Tris	25 mM
	Glycine (pH 8.3)	250 mM
	SDS	0.1 %
Transfer buffer (1L)	Tris	5.8 g
	Glycine	29 g
	Methanol	200 ml

	Distilled water	Filled up to 1 L
TBS buffer (10x)	NaCl	80 g
(pH 7.4)	KCl	2 g
	Trizma base	30 g
	Distilled water	1 L
TBS-T buffer (1x)	TBS buffer (10x) (pH 7.4)	100 ml
	Distilled water	900 ml
	Tween-20%	1 ml
Ponceau S Solution	Ponceau	0.5 g
	Acetic acid	25 ml
	Distilled water	475 ml

List of Figures

List of Supplemental Figures

List of Tables

List of Supplemental Tables

Acknowledgements

First, I would like to thank you Prof. Dr. Martin Zenke and Prof. Dr. Steffen Koschmieder for letting me work on this interesting project and supervising me in my PhD thesis and giving constructive feedback. Also I would like to say thank you to Prof. Dr. Martin Zenke, Prof. Dr. Steffen Koschmieder and Prof. Dr. Geraldine Zimmer-Bensch for agreeing to be my examiners and reading this PhD thesis. Also I want to thank Prof. Dr. Gabriele Pradel for agreeing to be the 4th examiner for my PhD defense on such short notice.

Second, I would like to thank Dr. Kristin Seré for guiding me along this journey and through this time, for having always ideas when something did not work out and for proof-reading my thesis multiple times. Thank you for your patience.

Thank you also to the iPSC team, Dr. Stephanie Sontag, Malrun Förster, Dr. Marcelo Szymanski and Lijuan Han. A big thank you goes to Steffi for teaching me about the iPSC culture and always answering my questions. Thank you to Marlun, Marcelo and Han for stepping in for medium changes on weekends when I was not able to do it myself. Thank you all for making the weekends in the lab not so lonely and boring, picking me up when my mood was not the best and something did not go as planned. Thank you to Saskia, Gülcan and Carmen for the technical advice when it came to FACS, Western Blot, transductions or cloning. Also a big thank you goes to the rest of the cell biology lab!

I would like to thank the whole lab at the Med IV, especially Julia Czech, Oliver Herrmann, Kristina Feldberg and Dr. Claudia Schubert that I was able to use your antibodies and your RT-qPCR primers. A major thanks goes to Kristina Feldberg and her expertise for the allele specific PCR. I know there were many iPSC clones to test. Thank you!!

Als Letztes will ich meinen Eltern und meiner Schwester danken. Sie haben mich immer unterstützt und mir Auszeiten gegeben wenn es sehr stressig war. Ihr wart mein Ruhepol. Tausend Dank!

Eidesstattliche Erklärung

Ich versichere hiermit an Eides statt, dass ich die vorliegende Arbeit mit dem Titel

„**Modeling MPN Pathogenesis and the IFNα Signaling Pathway in Murine Bone Marrow Cells and Patient Derived iPS Cells**"

selbstständig und unter ausschließlicher Verwendung der angegebenen Literatur und Hilfsmittel erstellt habe. Die Arbeit wurde in gleicher oder ähnlicher Form bisher weder einer anderen Prüfungsbehörde vorgelegt noch veröffentlicht. Ich habe die Grundsätze zur Sicherung guter wissenschaftlicher Praxis der RWTH zur Kenntnis genommen und eingehalten.

Aachen, den

_____

Caroline Küstermann